LOOKING BEYOND

CILIA IN RENAL CILIOPATHIES

GISELA SLAATS

LOOKING BEYOND CILIA IN RENAL CILIOPATHIES

ISBN: 978-94-6295-284-3

Cover design:	Joan Slaats and Wendy Schoneveld
Design & Lay out:	Wendy Schoneveld I www.wenzid.nl
Printed by:	Proefschriftmaken.nl II Uitgeverij BOXPress
Published by:	Uitgeverij BOXPress, 's-Hertogenbosch

The research described in this thesis was financially supported by the European Community's Seventh Framework Programme FP7/2009 under grant agreement no: 241955, Syscilia.

Publication of this thesis was financially supported by the Dutch Kidney Foundation. Additional financial support for the publication of this thesis was given by AM-Pharma B.V., ChipSoft B.V., Fresenius Medical Care B.V. and ZEISS.

LOOKING BEYOND
CILIA IN RENAL CILIOPATHIES

VERDER KIJKEN DAN
CILIA IN RENALE CILIOPATHIEËN
(met een samenvatting in het Nederlands)

PROEFSCHRIFT

ter verkrijging van de graad van doctor aan de Universiteit Utrecht
op gezag van de rector magnificus, prof. dr. G.J. van der Zwaan,
ingevolge het besluit van het college voor promoties
in het openbaar te verdedigen
op donderdag 17 september 2015 des middags te 12.45 uur

door

Gisela Gijsbertje Gerretje Slaats

geboren op 4 juli 1985 te Geldrop

Promotoren: Prof. dr. M.C. Verhaar
Prof. dr. V.V.A.M. Knoers

Copromotor: Dr. R.H. Giles

CONTENTS

PART THREE
FUTURE PERSPECTIVES

APPENDICES

ABBREVIATIONS

53BP1	P53 binding protein 1
ACEi	Angiotensin converting enzyme inhibitors
ADPKD	Autosomal dominant polycystic kidney disease
ADR	Adriamycin
APH	Aphidicolin
AQP2	Aquaporin 2
ARB	Angiotensin II receptor blockers
ARL13B	ADP-ribosylation factor-like protein 13B
ARPKD	Autosomal recessive polycystic kidney disease
ATM	Ataxia-Telangiectasia mutated
ATR	Ataxia-Telangiectasia and RAD3-related protein
ATRIP	ATR interacting protein
BBS	Bardet Biedl syndrome
BrdU	Bromodeoxyuridine
cAMP	Cyclic adenosine monophosphate
CCD	Cortical collecting duct
CDK	Cyclin-dependent kinase
CED	Cranioectodermal dysplasia
CEP164	Centrosomal protein 164 kDa
CEP290	Centrosomal protein 290 kDa
CHD	Congenital heart disease
CHK1/2	Checkpoint kinase 1/2
CIN	Chromosome instability
CKD	Chronic kidney disease
CLCN4	Chloride channel, voltage-gated 4
CldU	Chlorodeoxyuridine
CS	Centriolar satellite
CTGF	Connective tissue growth factor
DCT	Distal convoluted tubule
DDR	DNA damage response
DNA-PKcs	DNA-dependent protein kinase, catalytic subunit
DSB	Double strand break
EAST	Epilepsy, ataxia, sensorineural deafness, tubulopathy
ECM	Extracellular matrix
EGF	Epidermal growth factor
EMT	Epithelial-to-mesenchymal transition
EndoMT	Endothelial-to-mesenchymal transition

ESRD	End-stage renal disease
EVC	Ellis van Creveld syndrome
FACS	Fluorescence-activated cell sorting
FAN1	FANCD2/FANCI-associated nuclease 1
FSGS	Focal segmental glomerulosclerosis
FUCCI	Fluorescent ubiquitination-based cell cycle indicator
GFR	Glomerular filtration rate
H2AX	Histone 2A, family member X
HDAC	Histone deacetylase
Hh	Hedgehog
Hpf	Hours post fertilization
HRP	Horseradish peroxidase
ID	Intellectual disability
IdU	Iododeoxyuridine
IF	Immunofluorescence
IFT	Intraflagellar transport
IMCD3	Inner medullary collecting duct 3
INPP5E	Inositol polyphosphate-5-phosphatase E
IP	Inositol polyphosphate
iPSC	Induced pluripotent stem cell
JATD	Jeune Asphyxiating Thoracic Dystrophy
JLNS	Jervell and Lange-Nielsen syndrome
JS/JBTS	Joubert syndrome
KCNF1	Potassium channel, voltage-gated, subfamily F, member 1
KCNJ10	Potassium channel, inwardly rectifying, subfamily J, member 10
KCNQ1	Potassium channel, voltage-gated, kqt-like subfamily, member 1
kDa	kilodalton
LCA	Leber congenital amaurosis
LQTS	Long QT syndrome
MEF	Mouse embryonic fibroblast
MKS	Meckel-Grüber syndrome
MO	Morpholino oligonucleotide
MRI	Magnetic resonance imaging
MRN	MRE11 (meiotic recombination 11) RAD50 NBS1 (Nijmegen breakage syndrome)
MT	Microtubule
MTOC	Microtubule organizing centre
mTOR	mammalian target of rapamycin
MTS	Molar tooth sign

NDI	Nephrogenic diabetes insipidus
NEK8	NIMA (never in mitosis gene A)-related kinase 8
NPHP	Nephronophthisis
NPHP-RC	Nephronophthisis-related ciliopathies
OFD1	Oro-facial-digital type 1
OMIM	Online mendelian inheritance in man
ORC1	Origin recognition complex subunit 1
PC1	Polycystin-1
PCM1	Pericentriolar material 1
PCNT	Pericentrin
PCP	Planar cell polarity
PDGF	Platelet-derived growth factor
PKD1/2	Polycystic kidney disease 1/2
PKHD1	Polycystic kidney and hepatic disease 1
PLK4	Polo-like kinase 4
PTCH	Patched
RP1	Retinitis pigmentosa protein 1
RPE	Retinal pigment epithelium
RPGR	Retinitis pigmentosa GTPase regulator
RPGRIP1	Retinitis pigmentosa GTPase regulator interacting protein 1
RRT	Renal replacement therapy
SAS4	Spindle assembly defective-4
SDCCAG8	Serologically defined colon cancer antigen 8
SEM	Standard error of mean
siRNA	Small interfering RNA
SLS	Senior-Løken syndrome
SMO	Smoothened
SRP	Short Rib Polydactyly
SUFU	Suppressor of fused
TAZ	Transcriptional coactivator with PDZ-binding domain
TGF-β	Transforming growth factor beta
TIP60	Tat-interactive protein 60
TLR-4	Toll-like receptor 4
TZ	Transition zone
UREC	Urine-derived epithelial cell
USH	Usher syndrome
UUO	Unilateral ureteral obstruction
UV	Ultraviolet
Wnt	Wingless-Int

WT	Wild-type
YAP	Yes-associated protein
γH2AX	phosphorylated histone 2A, family member X
ZNF423	Zinc finger protein 423

CHAPTER 1

Introduction and outline

INTRODUCTION

Cilium biology

Organ tissue is arranged in polarized sheets or tubules; cells oriented with an apical side towards the lumen. Cells that have exited the cell cycle will anchor their mother centriole to the apical plasma membrane where vesicles will deliver membrane and the ciliary axoneme, a collection of nine microtubule doublets with or without a central pair (9+0 or 9+2), will begin to emerge (Figure 1) (1). Multiple hypotheses have been formulated regarding the origin of the cilium. One hypothesis proposes that the cilium evolved from an enveloped RNA virus with a primitive basal body core (2). The existence of centrosomal RNA and the sequence similarity of centriolar proteins with retrovirusses provide evidence for this hypothesis (4). There are two classes of mammalian cilia, which are functionally and structurally different. The motile cilium has a 9+2 axonemal microtubule organisation and motile cilia are often present in clusters which in general generate fluid flow, although the sperm's flagella is an example of a singular motile cilium on a cell intended for cell propulsion (5). Immotile cilia, also referred to as primary or sensory cilia which are studied in this thesis, have a 9+0 axonemal pattern (lacking the central pair; Figure 1) projecting from most cells used to sense their anatomical environment (6). In general, primary cilia transduce signals from extracellular stimuli to a cellular response that regulates proliferation, differentiation, transcription, migration, polarity and tissue morphology (7) in a tissue-specific manner (8). Developmental and pathological pathways of cellular signalling linked to primary cilia include, but are not limited to, canonical and non-canonical Wnt-, Hedgehog (Hh), and Hippo signalling (9), which are briefly described later in this introduction. Cilia membrane proteins enter the cilium via lateral transport (10), which is regulated by the transition zone (discussed below). However, cargo transport along the axoneme is facilitated by intraflagellar transport (IFT) proteins connected to kinesin and dynein motors (Figure 1) (11,12). There are two IFT complexes; IFT complex A directs retrograde transport from the ciliary tip to the base, and IFT complex B governs anterograde transport to the ciliary tip (13).

Ciliogenesis and the cell cycle

The ciliary axoneme is anchored at the plasma membrane by a modified centrosome, which is called the basal body. Centrosomes consist of both the mother and daughter centriole together with a pericentriolar matrix, and form the microtubule organization center (MTOC) (14) (Figure 1). The mother centriole is converted to the basal body by vesicle docking at the distal end (15). The mother centriole not only initiates microtubule outgrowth for cilium formation, but the duplicated mother centriole also forms a spindle pole body during the mitotic phase of the cell cycle. It ensures proper division of the duplicate genome between two daughter cells (Figure 2). However, centrosomes are not essential for cell cycle progression (16), and centrioles are not essential for mammalian

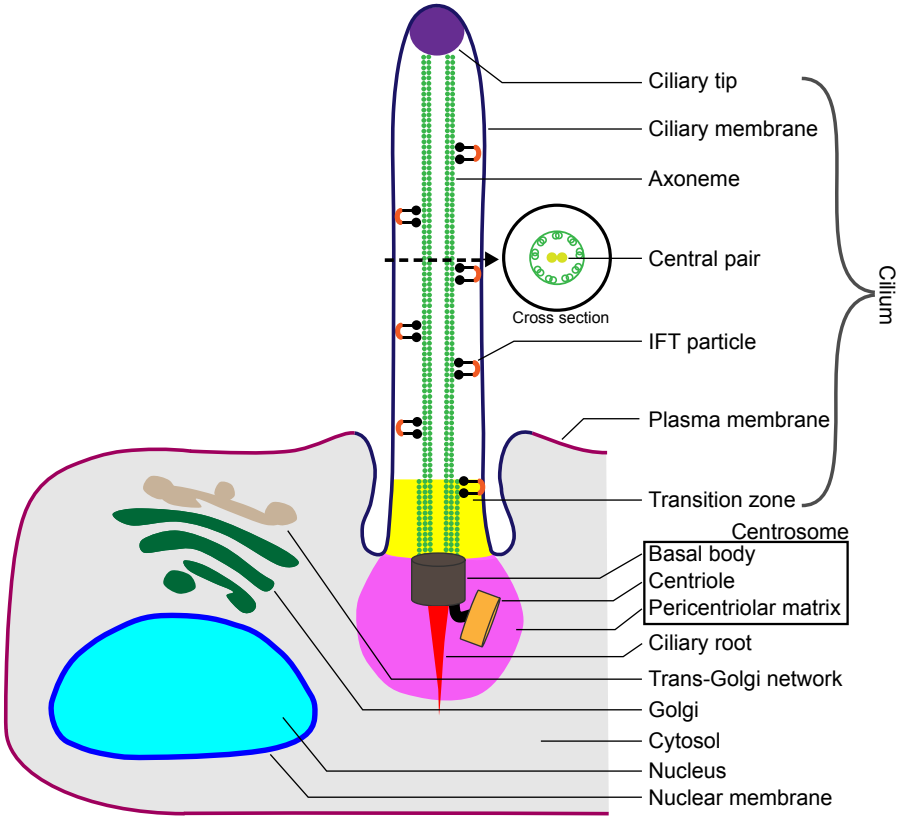

Figure 1. Schematic overview of ciliary components
The schematic depiction of the eukaryotic cilium and its components, and other cellular compartments, based on van Dam *et al.* (3) (authors hold copyright).

development until mid-gestation (17). Because of the dual function of the mother centriole, ciliogenesis and cell cycle are always linked processes. Cilia are present during the G0- (quiescent) or G1-phase of the cell cycle. Resorption of the cilium starts in most cell types before entering S-phase (Figure 2). Terminally differentiated cells do not divide and typically have one or more cilia (18,19).

The regulation of ciliary length is connected to the cell cycle as well. Centrosomal protein Ndel negatively regulates ciliary length resulting in accelerated cell cycle entry (20). IFT88 overexpression in non-ciliated cells blocks G1/S transition and depletion induces cell cycle progression (21). Consequently, epithelial cell hyperproliferation in several tissues was observed in orpk (*Ift88* mutant) mice (22). Additionally, the balance between assembly and disassembly at the ciliary tip controls cilium length. Equal assembly and disassembly rates are assumed to be responsible for identical cilium length (23). How ciliary length and cell cycle progression are exactly connected remains to be investigated. The transition zone

plays an important role in the import and export of ciliary proteins required for ciliary assembly and disassembly.

Localization of ciliary proteins

How is the access of proteins into the cilium regulated? The transition zone (TZ) is thought to have an important role in the size-dependent exclusion barrier of cytoplasmic proteins into the cilium and restricted membrane protein transport between ciliary and non-ciliary membrane proteins (Figure 1) (24,25). The TZ is characterized by Y-links at the base of the cilium that connect the ciliary membrane and microtubule doublets, and Y-links organize a ciliary necklace (26). Transition fibers at the TZ, probably derived from the distal appendages of the mother centriole, link the basal body to the plasma membrane (27). The transition fibers are thought to form the ciliary pores (11), which has a size-excluding gate of 60 nm, comparable with nuclear pores (28). Several Joubert syndrome and Meckel-Grüber syndrome proteins, which are responsible for cilia assembly and trafficking, and for example Septin-2, localize to the TZ and regulate axonemal membrane composition, by forming a diffusion barrier and ciliary gate at the TZ (29,30). This implicates that TZ dysfunction can contribute to ciliopathy (see section below) development.

Many gene products have multiple localizations, and do not exclusively localize to the cilium (3). PKD2 localizes to the endoplasmic reticulum (31), IFT20 and TMEM216 localize to the Golgi (32,33), nephrocystin localizes to adherens junctions (34), and TRIM32 localizes to

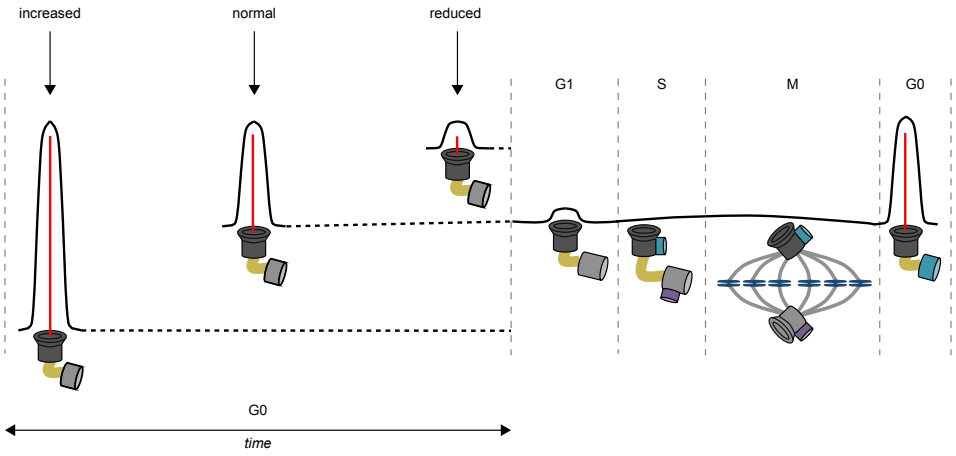

Figure 2. Centrosomes during the cell cycle
A schematic depiction of the centrosome during the cell cycle. Cilia provide a physical block for cell cycle progression by claiming the mother centriole. Disassembly of the primary cilium is required to liberate the centrosome and allow duplication during S-phase and subsequent formation of the mitotic spindle during chromosomal segregation. Furthermore, ciliary length controls cell cycle entry. Figure from Basten and Giles (authors hold copyright) (9).

the intermediate filaments (35) for example. In this thesis we are particularly interested in ciliopathy proteins and their nuclear function. Similar mechanisms regulate ciliary and nuclear import (36), and import into both compartments is regulated by pore exclusion. Many kinases and phosphates critical for DNA damage signalling regulation localize to the centrosome and nucleus, including Ataxia-Telangiectasia and RAD3-related (ATR) (37), Ataxia-Telangiectasia mutated (ATM), ATR interacting protein (ATRIP), CHK1, CHK2, and DNA-dependent protein kinase, catalytic subunit (DNA-PKcs) (38-41). Furthermore, cyclin-dependent kinase 1 (CDK1) (42), CDK3, and Cyclin A localize to the nucleus and to the centrosome as well (43). Centrosomes may coordinate multiple signalling networks that involve the DNA damage checkpoint proteins, either for regulating cell cycle progression or the DNA damage response (42). For example, replication stress response influences cell cycle progression by regulating the intra-S phase checkpoint to avoid stalled replication forks from reversing (44). DNA damage checkpoint proteins may control the formation of gamma-tubulin and/or the kinetics of microtubule formation at the centrosomes, and thereby couple them to the DNA damage response (38). DNA damage signalling and replication stress are discussed in more detail later in this chapter.

Further evidence linking nuclear and ciliary/centrosomal functions can be found in proteins mutated in the human renal ciliopathy nephronophthisis (NPHP; OMIM 256100): Never in mitosis A-related kinase 8 (NEK8; NPHP9) and Centrosomal protein 164 (CEP164; NPHP15) each interact with ATR and ATRIP, as well as CHK1 or ATM, respectively, at the DNA (45,46). Zinc Finger protein 423 (ZNF423; NPHP14) is a DNA binding transcription factor, which interacts with Centrosomal protein 290 (CEP290; NPHP6) (47). Moreover, DNA damage associated centrosomal proteins CEP164, ZNF423 and SDCCAG8 colocalize with SC35, TIP60 and phosphorylated CHK1 in the nucleus (47). Another cilia protein Oral-Facial-Digital type I (OFD1) localizes to both the nucleus and the cilium and forms a complex with TIP60 and RUVBL1 in the chromatin remodelling complex (48). It is not known whether the same pool of proteins shuttle between the ciliary and nuclear compartments of the cell, or how the two compartments communicate.

Centriolar satellites

Centriolar satellites (CSs) are small peri-centrosomal granules, containing pericentriolar material 1 (PCM1), which are involved in transport to and from the centrosome. Dynein transports the CSs towards the minus-ends of microtubules to the centrosome (49,50). CS factors such as C2CD3 (mutations in this gene cause OFD (51)) facilitate the recruitment of distal appendage proteins including TTKB2, CEP164, IFT88 and IFT52 (52). Centriole distal appendages promote membrane docking, which is required for cilia initiation (53,54). Satellite proteins Cep131 and Cdc13 are not only important for ciliogenesis, but additionally maintain genome stability (55,56). Several ciliopathy proteins, OFD1, BBS4, CEP290, and C2CD3 are CS components (51,57,58), and upon cellular stress, a subset of CS factors

including CEP131, PCM1, and CEP290 is removed from the CS (59). Cells arrested in S-phase show supernumerary centrosomes and nuclear centrin accumulation, which is dependent on CDK2 and CHK1, suggesting a link between CS and centrosome over-duplication (60,61). Furthermore, CSs are implicated in neurogenesis (62), regularly affected in so-called ciliopathies.

Ciliopathies

Primary cilia play an important role in the healthy functioning of different organs. Taking into account the complexity of ciliogenesis and the essential role of primary cilia in signal transduction in a large variety of tissues and organ systems, including eye, kidney, liver, brain and bone, numerous diseases have been linked to abnormal cilium function. Of the ciliopathies (Table 1), kidney cysts are one of the more common phenotypes (63).

Table 1. Phenotypes of ciliopathies (9,63,69,158)

		Phenotype											
Ciliopathy	**Abbreviation**	**Retinitis pigmentosa**	**Renal cystis disease**	**Situs inversus**	**Intellectual disability / developmental delay**	**Hypoplasia of corpus callosum**	**Dandy-Walker malformation**	**Posterior encephalocele**	**Hepatic disease**	**Polydactyly**	**Craniofacial abnormality**	**Bone malformation**	**Hearing loss / Deafness**
Leber Congenital Amaurosis	LCA	•			•				•				
Nephronophthisis	NPHP		•										
Senior-Løken Syndrome	SLS	•	•										
Joubert syndrome	JBTS	•	•	•	•	•	•		•	•	•		
Bardet Biedl Syndrome	BBS	•	•	•	•	•	•		•	•	•		•
Meckel-Grüber Syndrome	MKS		•	•		•	•	•	•	•	•		
Oro-facial-digital syndrome	OFD		•		•	•			•	•	•		•
Cranioectodermal Dysplasia	CED	•	•			•				•	•	•	
Short Rib Polydactyly	SRP	•	•						•	•	•	•	
Jeune Asphyxiating Thoracic Dystrophy	JATD	•	•						•	•	•	•	
Usher Syndrome	USH	•											•
Ellis van Creveld syndrome	EVC				•		•			•	•	•	

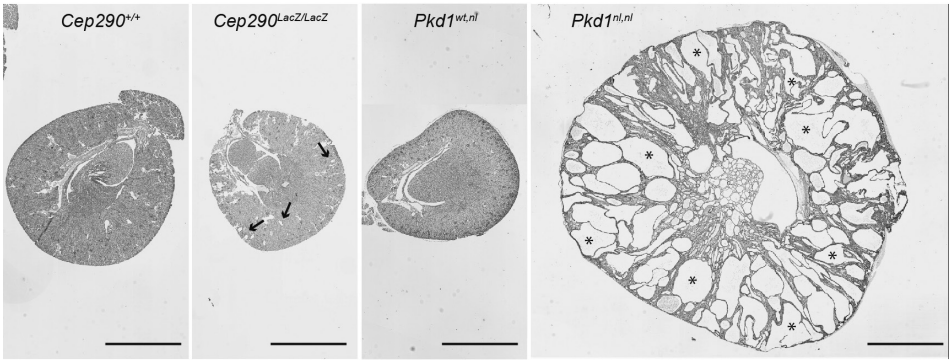

Figure 3. Renal phenotypic differences among mouse models of NPHP and ADPKD
Cep290$^{LacZ/LacZ}$ genetrap mice have slightly smaller kidney size and display small cysts at the corticomedullary junction as indicated by arrows compared to their wildtype (+/+) littermates (71). In contrast, Pkd1$^{nl/nl}$ mice have many large cysts (*), and enlarged kidneys (72). All kidneys are from 4 week old mice (scale bar is 2 mm).

While almost every ciliopathy disease entity is individually rare, collectively they are common (1 in 300-400 individuals) (64,65). Revealing new cilia genes provides improved understanding of this organelle and helps genetic diagnosis of ciliopathy patients (66,67). To date the list of ciliopathies is still growing; the definition of "ciliopathy" is as follows: "a genetic disease, where proteins localizing at the cilium or associated complexes and pathways are disturbed and give rise to classical core features associated with ciliopathies. Ciliary perturbation is not limited to cilia structure, but also function". This makes careful classification and diagnosis on phenotypic, genotypic and finally on physiological grounds challenging but nonetheless important (63).
Apart from displaying phenotypic variability, the ciliopathies also feature extensive genetic and allelic heterogeneity. Mutations in distinct genes can underlie the same phenotype, while on the other hand mutations in one gene can give rise to a plethora of phenotypes of different severity. *CEP290* is a good example of a gene responsible for six distinct ciliopathies characterized by phenotypes of different severity, such as retinal degeneration, nervous system disorders, polydactyly, and renal ciliopathies including nephronophthisis (NPHP) (Figure 3). No clear genotype-phenotype correlation could be established (68). The systems biology and genetics underlying ciliopathies are complex, and mutational load is probably an important contributor to genotype-phenotype correlation (69). In this next section a selection of the classic ciliopathies is discussed.

Autosomal dominant polycystic kidney disease
The most common form of polycystic kidney disease is autosomal dominant polycystic kidney disease (ADPKD). ADPKD affects 1:400-1:1000 persons worldwide (70), making one of the most common genetic diseases known to man (73). ADPKD is caused by

mutations in *PKD1* in 85% of all patients (OMIM 173900) (74), with mutations in *PKD2* accounting for the remaining 15% (OMIM 613095) (75). In *C. elegans* both ADPKD orthologues were observed to localize to cilia (76). Polycystin-1 and Polycystin-2 localize together at the primary cilium membrane, acting as a calcium channel to facilitate mechanosensation. Cyst development after loss of polycystins is not yet entirely understood, but most researchers agree that it involves more than loss of primary cilia function alone (77,78). It is thought that ADPKD occurs as a result of calcium-mediated ciliary flow sensation defects resulting in enhanced Wnt-signalling (79-81). Defective planar cell polarity (PCP) among the epithelial cells of the collecting ducts and convoluted tubules in the kidney caused by ciliary dysfunction is believed to be the underlying mechanism of cystogenesis in PKD (Figure 4) (82,83). Mutations in the ADPKD genes cause epithelial cells of the renal tubules to form progressive cysts and bilaterally enlarged kidneys (Figure 3); fluid filled cyst cause loss of functional tissue (84). Extra-renal manifestations include cysts in other organs including the liver, the seminal vesicle (which is derived from the renal mesonephros), the pancreas, the arachnoid membrane, and the spinal meningeal sac, as well as connective tissue abnormalities (85) and cardiovascular manifestations (86). Intracranial aneurysms affect 10% of ADPKD patients; it is not known whether ciliary dysfunction in endothelial cells contributes to this serious condition, however it is linked to chromosomal aneuploidy and chromosomal instability (87,88).

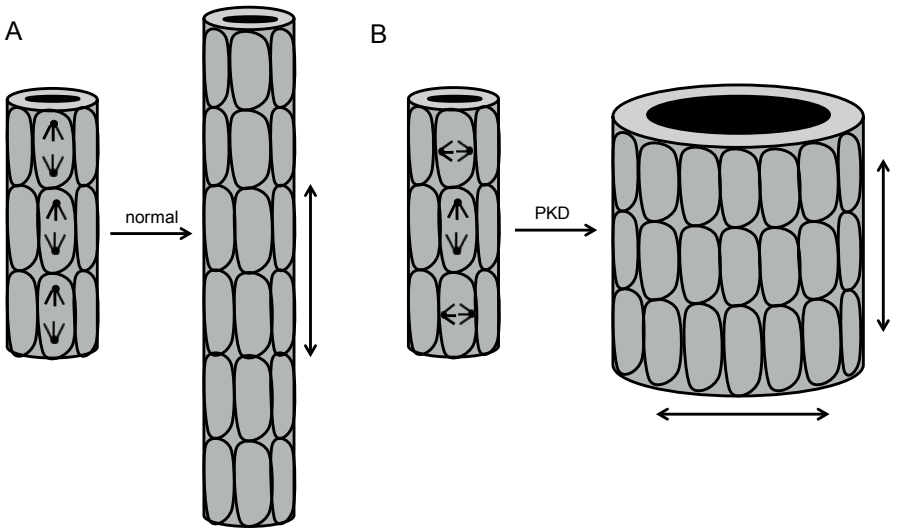

Figure 4. Planar cell polarity defects in PKD
(A) Kidney tubules elongate by cell division oriented along the longitudinal axes. Planar cell polarity (PCP) determines the orientation of cell division of the epithelial cells. **(B)** Disrupted PCP causes misoriented cell division and increased tubular diameter which, eventually, can lead to cyst formation.

Nephronophthisis and other autosomal recessive polycystic kidney diseases

Polycystic kidney and hepatic disease 1 (PKHD1) leads to autosomal recessive polycystic kidney disease (ARPKD) and has an incidence of about 1:20,000 (OMIM 263200) (89,90). Another leading cause of cystic kidney disease in children and young adults is NPHP (91,92). The first time juvenile NPHP was described was in 1951 (93). NPHP gene products localize to the primary cilium-centrosome complex (67,94), of which INVS (NPHP2) was the first linked to primary cilium function (91). Roughly fifty percent of all NPHP cases can be diagnosed by inactivating mutations in nineteen genes. Approximately 20% of all NPHP patients have mutations in *NPHP1* (95). NPHP demonstrates excessive renal interstitial fibrosis and (not always) corticomedullary cysts (Figure 3) which replace normal tissue (92). The NPHP phenotype presents in three forms, depending on the time of onset of end-stage renal disease: infantile, juvenile and adolescent. The occurrence of NPHP is estimated to be 1 in 50,000 - 900,000 births, although this number will almost certainly increase as more young adults with renal failure are being sequenced (66,96,97). NPHP presents variably with degeneration of the retina, kidney, brain, bone and liver (98,99) and is closely related to other ciliopathies: NPHP-related ciliopathies (NPHP-RC) such as Joubert Syndrome (JBTS; OMIM 213300) and Meckel-Grüber syndrome (MKS; OMIM 249000) (Table 1).

Disease spectrum of NPHP-related renal ciliopathies Joubert syndrome, Meckel-Grüber syndrome and other ciliopathies

The renal phenotype is different among the NPHP-RC syndromes, regarding presentation of cysts and/or fibrosis and dysplasia. To date, the literature mainly emphasizes renal cysts as phenotype for NPHP. NPHP-RC phenotypes range from mild to severe, depending on different organs affected and the level of tissue degeneration. Senior-Løken syndrome (SLS; OMIM 266900) is characterized by NPHP and retinitis pigmentosa, which causes vision impairment. Besides the retinal-renal abnormalities, an important contributor to JBTS development is brain malformation. Brain imaging of JBTS patients almost always reveals the molar tooth sign (MTS; Figure 5).

Developmental characteristics such as polydactyly and situs inversus can be observed among JBTS patients. Bardet Biedl syndrome (BBS; OMIM 615993) and Oro-facial-digital syndrome (OFD; OMIM 311200) include craniofacial abnormalities and obesity, with polydactyly being more prominent. The most severely affected are patients diagnosed with MKS, who die *in utero* or neonatally. Jeune Asphyxiating Thoracic Dystrophy (JATD; OMIM 208500), Short Rib Polydactyly (SRP; OMIM 613091), Cranioectodermal Dysplasia (CED; OMIM 218330), also known as Sensenbrenner, are ciliopathies with additional skeletal defects, being present in Ellis van Creveld syndrome (EVC; OMIM 225500) as well. However, EVC is rarely associated with NPHP (100). Furthermore, in ciliopathies like Usher syndrome (OMIM 276900) deafness and blindness are major features (Table 1) (63,69,101).

The clinical and genetic overlap of different ciliopathies suggest that some ciliopathies might be one disease, but are divided into different subtypes depending on clinical manifestations.

Fibrosis and EMT

Fibrosis is an important characteristic of NPHP. Organ fibrosis is a deregulated form of tissue repair triggered by chronic epithelial injury (102). Until now, there is no known mechanism to explain how loss of NPHP genes leads to rapid development of fibrosis. Loss of stem cells in early developmental stages could lead to loss of regeneration capacity and result in the fibrotic phenotype (103). Fibrosis originates mainly from myofibroblasts, which are derived from different cell origins. Data from different groups have revealed different models of the fibroblast progenitor cells, leading to controversy in this field. The total pool of myofibroblasts during renal fibrosis is derived from bone marrow-derived fibroblasts, tubular epithelial cells, endothelial cells, pericytes and interstitial fibroblasts. The nonproliferating myofibroblasts could be derived through differentiation from endothelial-to-mesenchymal transition (EndoMT) and epithelial-to-mesenchymal transition (EMT) as well (104). The primary cilium is lost during EMT, nevertheless, it is required for the initiation of the transition. In the pro-fibrotic tissue environment EMT and cilium loss are thought to require two triggers, which are disassembly of cellular contacts and TGFβ exposure (105). Molecular mechanisms of EMT are reviewed by Lamouille and collegues

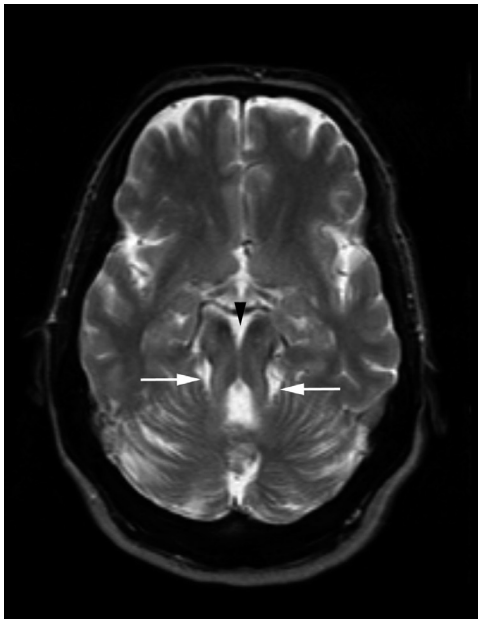

Figure 5. Brain phenotype characteristic of Joubert syndrome: the molar tooth sign
Brain image (MRI axial T2 SE image) of the molar tooth sign (MTS) in a JBTS patient. Deepened interpeduncular fossa of the mesencephalon (black arrowhead) and abnormally oriented and thickened superior cerebellar peduncles (white arrows) shape the MTS. (Courtesy of H. Kroes)

(106), including cilia signalling modules, such as canonical Wnt, Hh and Notch signalling (discussed in this chapter), as potential regulators of EMT. Furthermore, crosstalk between these pathways regulating EMT will accelerate the transition (106). Cells that have undergone EMT acquire resistance to apoptosis (programmed cell death) and senescence (107). Apoptosis is persistent in ADPKD and NPHP (108). A balance between cell proliferation and apoptosis is essential for normal growth and differentiation of the kidney. Formation of renal cysts is associated with enhanced apoptosis, since inactivation of anti-apoptosis protein BCL-2 causes renal cysts in knockout mice and BCL-2 overexpression prevents cyst formation (109,110). Another direct cause of apoptosis is loss of centrosomes; a recent study shows that spindle assembly defective-4 (SAS4) (CPAP/CENPJ) depleted mouse embryos lack centrioles and centrosomes and lack primary cilia and cilia-dependent signalling. Despite the absence of centrosomes, bipolar spindle formation, chromosome segregation, cell-cycle profile, and DNA damage response are normal in the mutants. Unlike mutants that lack cilia, most cells in acentriolar embryos activate a p53-dependent apoptotic pathway. Mammalian centrioles promote the efficient and rapid assembly of the mitotic spindle and a short delay in prometaphase activates a checkpoint that leads to p53-dependent cell death *in vivo* (111). Both apoptosis and fibrosis are cellular processes contributing to the renal phenotypes in ciliopathies. In the next section, ciliary signalling pathways are discussed that are potentially upstream of cellular deregulation.

Ciliary signalling

Not all ciliopathies are caused by disruption of the ciliary structure. For example, loss of *SDCCAG8* (*NPHP10*) causes cell polarity defects in 3D renal cell culture, however, primary cilia are intact (112). Disturbance of ciliary signalling is an important contributor to ciliopathy development. Here, we briefly discuss some ciliary signalling pathways important for ciliary function.

Canonical Wnt, Platelet-derived growth factor, and Notch signalling

In the canonical (β-catenin–dependent) Wingless-Int (Wnt) pathway, Wnt ligand binds to a Frizzled receptor and produces, via stabilization and accumulation of β-catenin, nuclear transcription of Wnt target genes (113). Wnt signaling controls many cellular processes, including cell proliferation and cell-fate determination (114), and abnormal activation of canonical Wnt signalling leads, among others, to tumor formation (115). Notch signalling regulates left-right asymmetry determination (116) and cell fate (117). Furthermore, platelet-derived growth factor (PDGF) signalling is regulated through the primary cilium in fibroblasts (118) and influences cell migration, proliferation and survival (119).

Hedgehog signalling

Hedgehog (Hh) signaling can be initiated by three ligands; Sonic-Hh (Shh), Indian-Hh (Ihh)

and Desert-Hh. The best-characterized member in vertebrates is Shh (120). The Hh signaling pathway is required for normal organ development, patterning, and cell signaling. In the absence of Hh ligand, Patched (PTCH) blocks the activation of Smoothened (SMO), and three Gli transcription factors are processed into smaller repressor forms (GliR). In the presence of Hh binding to PTCH, SMO transports into the cilium, blocking suppressor of fused (SUFU) function and leading to an increase in Gli in its activator form (GliA). Target-gene expression is thus finely balanced by the ratio of GliA and GliR (121-123).

Hippo signalling

The Hippo pathway (Salvador-Warts-Hippo), named after the core component Hippo kinase, might explain how disturbed ciliary signalling can result in renal cyst growth, by promoting nuclear Yes-associated protein (YAP) accumulation. A crosstalk between Hippo- and canonical and non-canonical Wnt-signaling possibly plays a role in cyst development (124,125). The Hippo pathway promotes fibrosis development as well, by functionally interacting with the TGFβ pathway and regulating connective tissue growth factor (CTGF) (126). Studies have shown that NEK8 (NPHP9) has a role in Hippo signalling by promoting the nuclear delivery and activation of transcriptional coactivator with PDZ-binding domain (TAZ) (127). Additionally, NPHP4 negatively regulates the Hippo pathway by interaction with the kinase Lats1 and inhibited Lats1-mediated phosphorylation of YAP and TAZ, leading to derepression of these protooncogenic transcriptional regulators and mediating cell proliferation (125). *Yap* knockout mice are embryonically lethal (128), but *Taz* knockout mice are viable and acquire NPHP-like renal disease (129). Histological examination of human PKD sections demonstrates nuclear translocation of YAP and TAZ (130).

Phosphatidylinositol signalling

Phosphatidylinositol signalling was linked to ciliopathies when mutations in inositol polyphosphate-5-phosphatase E (*INPP5E)* were found to cause JBTS (131). A number of receptor-mediated pathways that involve G-protein-coupled and cytokine receptors as well as receptor tyrosine kinases require inositol signalling. Receptor stimulation leads to soluble inositol polyphosphate (IP) production (132). The IP signalling cascade is linked to cilium motility and maintenance (133). Indeed, *INPP5E* mutant fibroblasts have an increased cilium destabilization rate upon serum stimulation, suggesting cilium stability requires IP signalling (131). The IP signalling cascade is connected to ciliary mammalian target of rapamycin (mTOR) signalling as well.

mTOR signalling

Ciliary mTOR signalling is upregulated in ADPKD (134), and is of interest as a therapeutic target. mTOR signalling inhibition by sirolimus is tested in clinical trials, but does not bring glomerular filtration rate (GFR) completely back to normal (135). mTOR signalling is

upregulated, and was found to cause the cyst development in the conditional *Ofd1* KO mouse model, with renal-specific *Ofd1* inactivation. In this model, primary cilia initially form and then disappear after the progression of renal cysts. The absence of primary cilia is a result rather than the primary origin of the kidney cysts (136).

DNA damage response signalling

Another signalling pathway upstream of cilia loss has recently been identified; DNA damage response (DDR) signalling, which is activated in *Nphp15* depleted cells (47). Interestingly, DDR is not a receptor-mediated signal transduction pathway like many ciliary signalling pathways as described above; nevertheless, this nuclear signalling has been linked to ciliopathies (45,47,137). Chapters 5, 6 and 7 of this thesis describe further evidence for this hypothesis.

Endogenous or exogenous factors can induce nuclear DNA damage. The DNA damage response is a complex, multi-faceted response. The earliest double strand break (DSB)-induced events involve the MRE11 (meiotic recombination 11), RAD50, NBS1 (Nijmegen breakage syndrome) (MRN) complex (138). The MRN complex promotes ATM activation (139), and ATM phosphorylates H2AX (γH2AX) (140), which recruits repair and cell cycle checkpoint factors at the site of damage, for example tumor suppressor P53 binding protein 1 (53BP1) (141). Another downstream effector of ATM is checkpoint 2 (CHK2), which is important for DNA damage checkpoint regulation (142). Furthermore ATR can be activated upon DNA breaks mediated by the damage sensing RAD9-HUS1-RAD1 (9-1-1) complex. Phosphorylation of the downstream kinase checkpoint 1 (CHK1) mediates cell cycle arrest, and slows down origin firing during DNA replication (143). Checkpoint proteins regulate WEE1, CDC25 and P53 to inactivate cyclindependent kinases (CDKs) (142). DNA damage signalling also induces DNA repair, and when damage is beyond repair, apoptosis. The complex downstream signalling of ATM and ATR includes crosstalk between those signalling pathways as well, however a simplified model is described here.

Syndromes associated with DNA damage response genes are characterized by intellectual disability (ID) and growth retardation, microcephaly, dysmorphic facial features and skeletal abnormalities (144). Furthermore, DDR genes are associated with progeroid syndromes as well (145). For example, mutations in *ATR*, *ATRIP* and *PCNT* cause Seckel syndrome (OMIM 210600) with impaired DNA damage signalling (146,147), which shares phenotypic characteristics with ciliopathies like intrauterine growth retardation, dwarfism, microcephaly and ID and the Joubert-associated molar tooth sign. Meier-Gorlin syndrome (OMIM 224690) is related to Seckel syndrome from a clinical perspective, conferring microcephaly, primordial dwarfism, very small ears, and skeletal abnormalities. Meier-Gorlin syndrome is caused by defects in proteins required for DNA replication origin licencing and cilia formation (148).

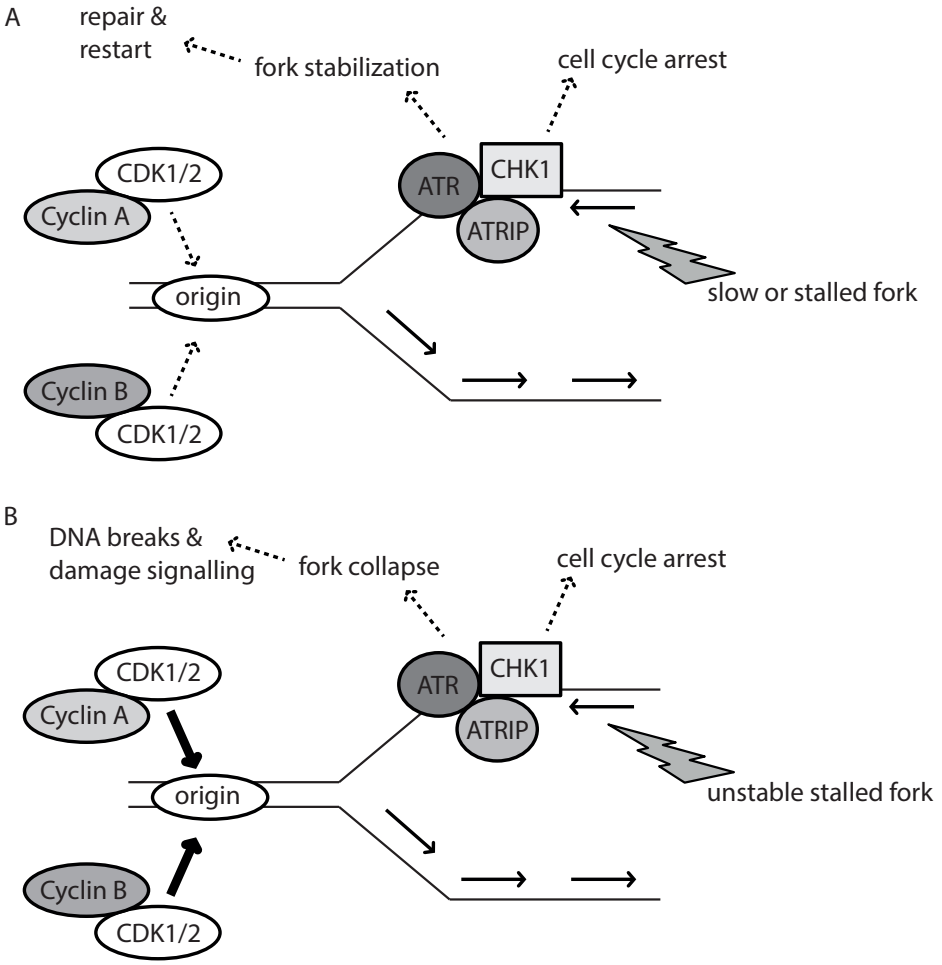

Figure 6. Cells with replication stress rely on the ATR/CHK1 pathway for survival during NPHP
(A) Schematic (simplified) overview of ATR-mediated replication stress response. Slow replication fork progression or stalled forks cause replication stress. Forks need to be stabilized and repaired, before DNA replication can restart. During repair the cell cycle is arrested after phosphorylation of CHK1. To compensate for slow DNA replication, cells can fire dormant origins, which is stimulated by Cyclin A- or Cyclin B-associated CDK activity. **(B)** Enhanced Cyclin A- or Cyclin B-associated CDK activity results in firing of a lot of origins which leads to replication stress (45). Replication forks are stalled, but unstable. Unstable forks can collapse and cause DNA breaks. DNA breaks cause DNA damage response signalling to promote repair, but when damage is beyond repair, cells undergo apoptosis.

Replication stress

DNA damage response signalling can be initiated by replication stress, which is mainly ATR-mediated. Replication stress is defined as the slowing or stalling of the replication fork progression and/or DNA synthesis and forms a problem for cell survival and genome stability (Figure 6A) (149). One source of replication stress is stalled replication forks, which

become unstable and can collapse, leading to double-strand break formation and chromosomal rearrangements (Figure 6B) (149). Thus, cells must rapidly stabilize stalled fork (150) and initiate a pathway to restart and complete DNA replication (Figure 6A) (151). *NEK8* (*NPHP9*) depletion has been shown to cause replication stress and concomitant DNA breaks by enhancing CDK activity, which results in decreased fork speed, shorter inter-origin distance and fork asymmetry (Figure 6B) (45). The cell has several mechanisms to bypass replication stress and allow restart of replication, for example DNA damage tolerance pathway (152) or firing of dormant origins (153). However, firing of dormant origins could lead to DNA damage breaks if there is a shortage of nucleotide resources. Limited availability of these resources can slow down fork progression as well (154). Furthermore, misincorporation of ribonucleotides can result in replication stress (155). In early stages of cyst development, hyperproliferation could cause replication stress in sensitized cells by overconsumption of resources like nucleotides and replication factors (156). Catastrophic replication stress might result in the increased apoptosis observed in both models of ADPKD and NPHP (72,157).

Scope and chapter outline of thesis

The aim of this thesis is to investigate the molecular mechanisms underlying NPHP-RCs. In **Chapter 1**, ciliary structure and function are introduced and the connection to disease is described.

The first part of this thesis describes novel insights in ciliopathies. **Chapter 2** describes how ciliated cells can be non-invasively isolated from urine or spontaneously shed milk teeth and how these cells can be applied in bio-medical research. In **Chapter 3** a set of hits (*Kcnf1, Kcnj10, Kcnq10, Clcn4*) of the genome wide screen of the Syscilia consortium is validated. siRNA knockdown of these 4 ion channels reduces cilia frequency. We extend functional studies of these four ion channels and their effects on renal cilia; where possible linking human disease alleles with this novel function. In **Chapter 4**, it is described how loss of *MKS1* due to mutation causes ciliary INPP5E mislocalization in JBTS patient fibroblasts.

The second part of this thesis describes the connection between DNA damage signalling and renal ciliopathies. In **Chapter 5** the characterization of the *Sdccag8 (Nphp10)* gene-trap mouse line is described. This mouse model of human NPHP type 10 shows renal cysts and fibrosis and increased DNA damage signalling. Replication stress, underlying DNA damage accumulation in renal *Cep290* gene-trap mice cells is investigated in **Chapter 6.** Loss of CEP290 function is a common cause of NPNP-related ciliopathies, demonstrating the relevance of replication stress for the disease etiology. In **Chapter 7** the potential downstream effects of DNA damage and cilia defects on cell behaviour after loss of *Cep164* are illustrated. Disturbed cell cycle, apoptosis and EMT are investigated, which are hypothesized to contribute to the fibrosis phenotype of NPHP.

The final part of this thesis summarizes and discusses the findings in this thesis and gives an outlook for future studies. **Chapter 8** is a review describing opportunities for treating cysts and/or fibrosis in NPHP. Low-dose paclitaxel treatment is discussed as one possible therapeutic worth re-investigating. **Chapter 9** summarizes the state-off-the-art findings regarding replication stress and concomitant DNA damage signalling in NPHP-RC, including effects on the cell cycle and cilia. A general discussion on the studies performed in this thesis is described in **Chapter 10**.

REFERENCES

1. Kobayashi T, Dynlacht BD. Regulating the transition from centriole to basal body. *The Journal of cell biology.* 2011;193(3):435-444.
2. Satir P, Guerra C, Bell AJ. Evolution and persistence of the cilium. *Cell motility and the cytoskeleton.* 2007;64(12):906-913.
3. van Dam TJ, Wheway G, Slaats GG, Group SS, Huynen MA, Giles RH. The SYSCILIA gold standard (SCGSv1) of known ciliary components and its applications within a systems biology consortium. *Cilia.* 2013;2(1):7.
4. Alliegro MC, Satir P. Origin of the cilium: novel approaches to examine a centriolar evolution hypothesis. *Methods in cell biology.* 2009;94:53-64.
5. Afzelius BA, Eliasson R. Male and female infertility problems in the immotile-cilia syndrome. *European journal of respiratory diseases. Supplement.* 1983;127:144-147.
6. Satir P, Christensen ST. Structure and function of mammalian cilia. *Histochemistry and cell biology.* 2008;129(6):687-693.
7. Oh EC, Katsanis N. Cilia in vertebrate development and disease. *Development.* 2012;139(3):443-448.
8. D'Angelo A, Franco B. The primary cilium in different tissues-lessons from patients and animal models. *Pediatric nephrology.* 2011;26(5):655-662.
9. Basten SG, Giles RH. Functional aspects of primary cilia in signaling, cell cycle and tumorigenesis. *Cilia.* 2013;2(1):6.
10. Milenkovic L, Scott MP, Rohatgi R. Lateral transport of Smoothened from the plasma membrane to the membrane of the cilium. *The Journal of cell biology.* 2009;187(3):365-374.
11. Rosenbaum JL, Witman GB. Intraflagellar transport. *Nature reviews. Molecular cell biology.* 2002;3(11):813-825.
12. Verhey KJ, Dishinger J, Kee HL. Kinesin motors and primary cilia. *Biochemical Society transactions.* 2011;39(5):1120-1125.
13. Pedersen LB, Rosenbaum JL. Intraflagellar transport (IFT) role in ciliary assembly, resorption and signalling. *Current topics in developmental biology.* 2008;85:23-61.
14. Luders J, Stearns T. Microtubule-organizing centres: a re-evaluation. *Nature reviews. Molecular cell biology.* 2007;8(2):161-167.
15. Schmidt KN, Kuhns S, Neuner A, Hub B, Zentgraf H, Pereira G. Cep164 mediates vesicular docking to the mother centriole during early steps of ciliogenesis. *The Journal of cell biology.* 2012;199(7):1083-1101.
16. Uetake Y, Loncarek J, Nordberg JJ, et al. Cell cycle progression and de novo centriole assembly after centrosomal removal in untransformed human cells. *The Journal of cell biology.* 2007;176(2):173-182.
17. David A, Liu F, Tibelius A, et al. Lack of centrioles and primary cilia in STIL(-/-) mouse embryos. *Cell cycle.* 2014;13(18):2859-2868.
18. Santos N, Reiter JF. Building it up and taking it down: the regulation of vertebrate ciliogenesis. *Developmental dynamics : an official publication of the American Association of Anatomists.* 2008;237(8):1972-1981.
19. Nigg EA, Stearns T. The centrosome cycle: Centriole biogenesis, duplication and inherent asymmetries. *Nature cell biology.* 2011;13(10):1154-1160.
20. Kim S, Zaghloul NA, Bubenshchikova E, et al. Nde1-mediated inhibition of ciliogenesis affects cell cycle re-entry. *Nature cell biology.* 2011;13(4):351-360.
21. Robert A, Margall-Ducos G, Guidotti JE, et al. The intraflagellar transport component IFT88/polaris is a centrosomal protein regulating G1-S transition in non-ciliated cells. *Journal of cell science.* 2007;120(Pt 4):628-637.
22. Zhang Q, Davenport JR, Croyle MJ, Haycraft CJ, Yoder BK. Disruption of IFT results in both exocrine and endocrine abnormalities in the pancreas of Tg737(orpk) mutant mice. *Laboratory investigation; a journal of technical methods and pathology.* 2005;85(1):45-64.
23. Marshall WF, Rosenbaum JL. Intraflagellar transport balances continuous turnover of outer doublet microtubules: implications for flagellar length control. *The Journal of cell biology.* 2001;155(3):405-414.
24. Kee HL, Dishinger JF, Blasius TL, Liu CJ, Margolis B, Verhey KJ. A size-exclusion permeability barrier and nucleoporins characterize a ciliary pore complex that regulates transport into cilia. *Nature cell biology.* 2012;14(4):431-437.
25. Chih B, Liu P, Chinn Y, et al. A ciliopathy complex at the transition zone protects the cilia as a privileged membrane domain. *Nature cell biology.* 2012;14(1):61-72.
26. Reiter JF, Blacque OE, Leroux MR. The base of the cilium: roles for transition fibres and the transition zone in ciliary formation, maintenance and compartmentalization. *EMBO reports.* 2012;13(7):608-618.
27. Rohatgi R, Snell WJ. The ciliary membrane. *Current opinion in cell biology.* 2010;22(4):541-546.

28. Anderson RG. The three-dimensional structure of the basal body from the rhesus monkey oviduct. *The Journal of cell biology.* 1972;54(2):246-265.
29. Hu Q, Milenkovic L, Jin H, et al. A septin diffusion barrier at the base of the primary cilium maintains ciliary membrane protein distribution. *Science.* 2010;329(5990):436-439.
30. Garcia-Gonzalo FR, Corbit KC, Sirerol-Piquer MS, et al. A transition zone complex regulates mammalian ciliogenesis and ciliary membrane composition. *Nat Genet.* 2011;43(8):776-784.
31. Cai Y, Maeda Y, Cedzich A, et al. Identification and characterization of polycystin-2, the PKD2 gene product. *The Journal of biological chemistry.* 1999;274(40):28557-28565.
32. Follit JA, Tuft RA, Fogarty KE, Pazour GJ. The intraflagellar transport protein IFT20 is associated with the Golgi complex and is required for cilia assembly. *Molecular biology of the cell.* 2006;17(9):3781-3792.
33. Lee JH, Silhavy JL, Lee JE, et al. Evolutionarily assembled cis-regulatory module at a human ciliopathy locus. *Science.* 2012;335(6071):966-969.
34. Donaldson JC, Dempsey PJ, Reddy S, Bouton AH, Coffey RJ, Hanks SK. Crk-associated substrate p130(Cas) interacts with nephrocystin and both proteins localize to cell-cell contacts of polarized epithelial cells. *Experimental cell research.* 2000;256(1):168-178.
35. Chiang AP, Beck JS, Yen HJ, et al. Homozygosity mapping with SNP arrays identifies TRIM32, an E3 ubiquitin ligase, as a Bardet-Biedl syndrome gene (BBS11). *Proceedings of the National Academy of Sciences of the United States of America.* 2006;103(16):6287-6292.
36. Dishinger JF, Kee HL, Jenkins PM, et al. Ciliary entry of the kinesin-2 motor KIF17 is regulated by importin-beta2 and RanGTP. *Nature cell biology.* 2010;12(7):703-710.
37. Valdes-Sanchez L, De la Cerda B, Diaz-Corrales FJ, et al. ATR localizes to the photoreceptor connecting cilium and deficiency leads to severe photoreceptor degeneration in mice. *Human molecular genetics.* 2013;22(8):1507-1515.
38. Zhang S, Hemmerich P, Grosse F. Centrosomal localization of DNA damage checkpoint proteins. *Journal of cellular biochemistry.* 2007;101(2):451-465.
39. Kramer A, Mailand N, Lukas C, et al. Centrosome-associated Chk1 prevents premature activation of cyclin-B-Cdk1 kinase. *Nature cell biology.* 2004;6(9):884-891.
40. Oricchio E, Saladino C, Iacovelli S, Soddu S, Cundari E. ATM is activated by default in mitosis, localizes at centrosomes and monitors mitotic spindle integrity. *Cell cycle.* 2006;5(1):88-92.
41. Tsvetkov L, Xu X, Li J, Stern DF. Polo-like kinase 1 and Chk2 interact and co-localize to centrosomes and the midbody. *The Journal of biological chemistry.* 2003;278(10):8468-8475.
42. Fletcher L, Muschel RJ. The centrosome and the DNA damage induced checkpoint. *Cancer letters.* 2006;243(1):1-8.
43. Diener DR, Lupetti P, Rosenbaum JL. Proteomic analysis of isolated ciliary transition zones reveals the presence of ESCRT proteins. *Current biology : CB.* 2015;25(3):379-384.
44. Hu J, Sun L, Shen F, et al. The intra-S phase checkpoint targets Dna2 to prevent stalled replication forks from reversing. *Cell.* 2012;149(6):1221-1232.
45. Choi HJ, Lin JR, Vannier JB, et al. NEK8 links the ATR-regulated replication stress response and S phase CDK activity to renal ciliopathies. *Molecular cell.* 2013;51(4):423-439.
46. Sivasubramaniam S, Sun X, Pan YR, Wang S, Lee EY. Cep164 is a mediator protein required for the maintenance of genomic stability through modulation of MDC1, RPA, and CHK1. *Genes & development.* 2008;22(5):587-600.
47. Chaki M, Airik R, Ghosh AK, et al. Exome capture reveals ZNF423 and CEP164 mutations, linking renal ciliopathies to DNA damage response signaling. *Cell.* 2012;150(3):533-548.
48. Giorgio G, Alfieri M, Prattichizzo C, Zullo A, Cairo S, Franco B. Functional characterization of the OFD1 protein reveals a nuclear localization and physical interaction with subunits of a chromatin remodeling complex. *Molecular biology of the cell.* 2007;18(11):4397-4404.
49. Kubo A, Sasaki H, Yuba-Kubo A, Tsukita S, Shiina N. Centriolar satellites: molecular characterization, ATP-dependent movement toward centrioles and possible involvement in ciliogenesis. *The Journal of cell biology.* 1999;147(5):969-980.
50. Dammermann A, Merdes A. Assembly of centrosomal proteins and microtubule organization depends on PCM-1. *The Journal of cell biology.* 2002;159(2):255-266.
51. Thauvin-Robinet C, Lee JS, Lopez E, et al. The oral-facial-digital syndrome gene C2CD3 encodes a positive regulator of centriole elongation. *Nature genetics.* 2014;46(8):905-911.
52. Ye X, Zeng H, Ning G, Reiter JF, Liu A. C2cd3 is critical for centriolar distal appendage assembly and ciliary vesicle docking in mammals. *Proceedings of the National Academy of Sciences of the United States of America.* 2014;111(6):2164-2169.
53. Tanos BE, Yang HJ, Soni R, et al. Centriole distal appendages promote membrane docking, leading to cilia initiation. *Genes & development.* 2013;27(2):163-168.

54. Graser S, Stierhof YD, Lavoie SB, et al. Cep164, a novel centriole appendage protein required for primary cilium formation. *The Journal of cell biology.* 2007;179(2):321-330.
55. Staples CJ, Myers KN, Beveridge RD, et al. The centriolar satellite protein Cep131 is important for genome stability. *Journal of cell science.* 2012;125(Pt 20):4770-4779.
56. Staples CJ, Myers KN, Beveridge RD, et al. Ccdc13 is a novel human centriolar satellite protein required for ciliogenesis and genome stability. *Journal of cell science.* 2014;127(Pt 13):2910-2919.
57. Lopes CA, Prosser SL, Romio L, et al. Centriolar satellites are assembly points for proteins implicated in human ciliopathies, including oral-facial-digital syndrome 1. *Journal of cell science.* 2011;124(Pt 4):600-612.
58. Kim J, Krishnaswami SR, Gleeson JG. CEP290 interacts with the centriolar satellite component PCM-1 and is required for Rab8 localization to the primary cilium. *Human molecular genetics.* 2008;17(23):3796-3805.
59. Villumsen BH, Danielsen JR, Povlsen L, et al. A new cellular stress response that triggers centriolar satellite reorganization and ciliogenesis. *The EMBO journal.* 2013;32(23):3029-3040.
60. Prosser SL, Straatman KR, Fry AM. Molecular dissection of the centrosome overduplication pathway in S-phase-arrested cells. *Molecular and cellular biology.* 2009;29(7):1760-1773.
61. Loffler H, Fechter A, Liu FY, Poppelreuther S, Kramer A. DNA damage-induced centrosome amplification occurs via excessive formation of centriolar satellites. *Oncogene.* 2013;32(24):2963-2972.
62. Ge X, Frank CL, Calderon de Anda F, Tsai LH. Hook3 interacts with PCM1 to regulate pericentriolar material assembly and the timing of neurogenesis. *Neuron.* 2010;65(2):191-203.
63. Baker K, Beales PL. Making sense of cilia in disease: the human ciliopathies. *American journal of medical genetics. Part C, Seminars in medical genetics.* 2009;151C(4):281-295.
64. Waters AM, Beales PL. Ciliopathies: an expanding disease spectrum. *Pediatric nephrology.* 2011;26(7):1039-1056.
65. Hildebrandt F, Benzing T, Katsanis N. Ciliopathies. *The New England journal of medicine.* 2011;364(16):1533-1543.
66. Renkema KY, Stokman MF, Giles RH, Knoers NV. Next-generation sequencing for research and diagnostics in kidney disease. *Nature reviews. Nephrology.* 2014;10(8):433-444.
67. Sang L, Miller JJ, Corbit KC, et al. Mapping the NPHP-JBTS-MKS protein network reveals ciliopathy disease genes and pathways. *Cell.* 2011;145(4):513-528.
68. Coppieters F, Lefever S, Leroy BP, De Baere E. CEP290, a gene with many faces: mutation overview and presentation of CEP290base. *Human mutation.* 2010;31(10):1097-1108.
69. Davis EE, Katsanis N. The ciliopathies: a transitional model into systems biology of human genetic disease. *Current opinion in genetics & development.* 2012;22(3):290-303.
70. Torres VE, Harris PC. Autosomal dominant polycystic kidney disease: the last 3 years. *Kidney international.* 2009;76(2):149-168.
71. Hynes AM, Giles RH, Srivastava S, et al. Murine Joubert syndrome reveals Hedgehog signaling defects as a potential therapeutic target for nephronophthisis. *Proceedings of the National Academy of Sciences of the United States of America.* 2014;111(27):9893-9898.
72. Happe H, van der Wal AM, Salvatori DC, et al. Cyst expansion and regression in a mouse model of polycystic kidney disease. *Kidney international.* 2013;83(6):1099-1108.
73. Wilson PD. Polycystic kidney disease. *The New England journal of medicine.* 2004;350(2):151-164.
74. The polycystic kidney disease 1 gene encodes a 14 kb transcript and lies within a duplicated region on chromosome 16. The European Polycystic Kidney Disease Consortium. *Cell.* 1994;77(6):881-894.
75. Mochizuki T, Wu G, Hayashi T, et al. PKD2, a gene for polycystic kidney disease that encodes an integral membrane protein. *Science.* 1996;272(5266):1339-1342.
76. Barr MM, DeModena J, Braun D, Nguyen CQ, Hall DH, Sternberg PW. The Caenorhabditis elegans autosomal dominant polycystic kidney disease gene homologs lov-1 and pkd-2 act in the same pathway. *Current biology : CB.* 2001;11(17):1341-1346.
77. Piontek K, Menezes LF, Garcia-Gonzalez MA, Huso DL, Germino GG. A critical developmental switch defines the kinetics of kidney cyst formation after loss of Pkd1. *Nature medicine.* 2007;13(12):1490-1495.
78. Ma M, Tian X, Igarashi P, Pazour GJ, Somlo S. Loss of cilia suppresses cyst growth in genetic models of autosomal dominant polycystic kidney disease. *Nature genetics.* 2013;45(9):1004-1012.
79. Nauli SM, Alenghat FJ, Luo Y, et al. Polycystins 1 and 2 mediate mechanosensation in the primary cilium of kidney cells. *Nature genetics.* 2003;33(2):129-137.
80. Low SH, Vasanth S, Larson CH, et al. Polycystin-1, STAT6, and P100 function in a pathway that transduces ciliary mechanosensation and is activated in polycystic kidney disease. *Developmental cell.* 2006;10(1):57-69.
81. Abdul-Majeed S, Nauli SM. Calcium-mediated mechanisms of cystic expansion. *Biochimica et biophysica acta.* 2011;1812(10):1281-1290.

82. Fischer E, Legue E, Doyen A, et al. Defective planar cell polarity in polycystic kidney disease. *Nature genetics.* 2006;38(1):21-23.
83. Simons M, Walz G. Polycystic kidney disease: cell division without a c(l)ue? *Kidney international.* 2006;70(5):854-864.
84. Yoder BK, Hou X, Guay-Woodford LM. The polycystic kidney disease proteins, polycystin-1, polycystin-2, polaris, and cystin, are co-localized in renal cilia. *Journal of the American Society of Nephrology : JASN.* 2002;13(10):2508-2516.
85. Pirson Y. Extrarenal manifestations of autosomal dominant polycystic kidney disease. *Advances in chronic kidney disease.* 2010;17(2):173-180.
86. Handa SP. Cardiovascular manifestations of autosomal dominant polycystic kidney disease in young adults. *Clinical and investigative medicine. Medecine clinique et experimentale.* 2006;29(6):339-346.
87. Aboualaiwi WA, Muntean BS, Ratnam S, et al. Survivin-induced abnormal ploidy contributes to cystic kidney and aneurysm formation. *Circulation.* 2014;129(6):660-672.
88. AbouAlaiwi WA, Rodriguez I, Nauli SM. Spectral karyotyping to study chromosome abnormalities in humans and mice with polycystic kidney disease. *Journal of visualized experiments : JoVE.* 2012(60).
89. Harris PC, Torres VE. Polycystic kidney disease. *Annual review of medicine.* 2009;60:321-337.
90. Hoyer PF. Clinical manifestations of autosomal recessive polycystic kidney disease. *Current opinion in pediatrics.* 2015;27(2):186-192.
91. Otto EA, Schermer B, Obara T, et al. Mutations in INVS encoding inversin cause nephronophthisis type 2, linking renal cystic disease to the function of primary cilia and left-right axis determination. *Nature genetics.* 2003;34(4):413-420.
92. Hildebrandt F, Zhou W. Nephronophthisis-associated ciliopathies. *Journal of the American Society of Nephrology : JASN.* 2007;18(6):1855-1871.
93. Fanconi G, Hanhart E, von AA, Uhlinger E, Dolivo G, Prader A. [Familial, juvenile nephronophthisis (idiopathic parenchymal contracted kidney)]. *Helvetica paediatrica acta.* 1951;6(1):1-49.
94. Hildebrandt F, Otto E. Cilia and centrosomes: a unifying pathogenic concept for cystic kidney disease? *Nature reviews. Genetics.* 2005;6(12):928-940.
95. Halbritter J, Porath JD, Diaz KA, et al. Identification of 99 novel mutations in a worldwide cohort of 1,056 patients with a nephronophthisis-related ciliopathy. *Human genetics.* 2013;132(8):865-884.
96. Ala-Mello S, Koskimies O, Rapola J, Kaariainen H. Nephronophthisis in Finland: epidemiology and comparison of genetically classified subgroups. *European journal of human genetics : EJHG.* 1999;7(2):205-211.
97. Waldherr R, Lennert T, Weber HP, Fodisch HJ, Scharer K. The nephronophthisis complex. A clinicopathologic study in children. *Virchows Archiv. A, Pathological anatomy and histology.* 1982;394(3):235-254.
98. Mainzer F, Saldino RM, Ozonoff MB, Minagi H. Familial nephropathy associatdd with retinitis pigmentosa, cerebellar ataxia and skeletal abnormalities. *The American journal of medicine.* 1970;49(4):556-562.
99. Boichis H, Passwell J, David R, Miller H. Congenital hepatic fibrosis and nephronophthisis. A family study. *The Quarterly journal of medicine.* 1973;42(165):221-233.
100. Moudgil A, Bagga A, Kamil ES, et al. Nephronophthisis associated with Ellis-van Creveld syndrome. *Pediatric nephrology.* 1998;12(1):20-22.
101. Tobin JL, Beales PL. The nonmotile ciliopathies. *Genetics in medicine : official journal of the American College of Medical Genetics.* 2009;11(6):386-402.
102. Wynn TA, Ramalingam TR. Mechanisms of fibrosis: therapeutic translation for fibrotic disease. *Nature medicine.* 2012;18(7):1028-1040.
103. Ruzankina Y, Pinzon-Guzman C, Asare A, et al. Deletion of the developmentally essential gene ATR in adult mice leads to age-related phenotypes and stem cell loss. *Cell stem cell.* 2007;1(1):113-126.
104. Falke LL, Gholizadeh S, Goldschmeding R, Kok RJ, Nguyen TQ. Diverse origins of the myofibroblast-implications for kidney fibrosis. *Nature reviews. Nephrology.* 2015;11(4):233-244.
105. Rozycki M, Lodyga M, Lam J, et al. The fate of the primary cilium during myofibroblast transition. *Molecular biology of the cell.* 2014;25(5):643-657.
106. Lamouille S, Xu J, Derynck R. Molecular mechanisms of epithelial-mesenchymal transition. *Nature reviews. Molecular cell biology.* 2014;15(3):178-196.
107. Thiery JP, Acloque H, Huang RY, Nieto MA. Epithelial-mesenchymal transitions in development and disease. *Cell.* 2009;139(5):871-890.
108. Woo D. Apoptosis and loss of renal tissue in polycystic kidney diseases. *The New England journal of medicine.* 1995;333(1):18-25.
109. Veis DJ, Sorenson CM, Shutter JR, Korsmeyer SJ. Bcl-2-deficient mice demonstrate fulminant lymphoid apoptosis, polycystic kidneys, and hypopigmented hair. *Cell.* 1993;75(2):229-240.
110. Lin HH, Yang TP, Jiang ST, Yang HY, Tang MJ. Bcl-2 overexpression prevents apoptosis-induced Madin-Darby canine kidney simple epithelial cyst formation. *Kidney international.* 1999;55(1):168-178.

111. Bazzi H, Anderson KV. Acentriolar mitosis activates a p53-dependent apoptosis pathway in the mouse embryo. *Proceedings of the National Academy of Sciences of the United States of America.* 2014;111(15):E1491-1500.
112. Otto EA, Hurd TW, Airik R, et al. Candidate exome capture identifies mutation of SDCCAG8 as the cause of a retinal-renal ciliopathy. *Nat Genet.* 2010;42(10):840-850.
113. Logan CY, Nusse R. The Wnt signaling pathway in development and disease. *Annual review of cell and developmental biology.* 2004;20:781-810.
114. Angers S, Moon RT. Proximal events in Wnt signal transduction. *Nature reviews. Molecular cell biology.* 2009;10(7):468-477.
115. Giles RH, van Es JH, Clevers H. Caught up in a Wnt storm: Wnt signaling in cancer. *Biochimica et biophysica acta.* 2003;1653(1):1-24.
116. Lopes SS, Lourenco R, Pacheco L, Moreno N, Kreiling J, Saude L. Notch signalling regulates left-right asymmetry through ciliary length control. *Development.* 2010;137(21):3625-3632.
117. Tsao PN, Vasconcelos M, Izvolsky KI, Qian J, Lu J, Cardoso WV. Notch signaling controls the balance of ciliated and secretory cell fates in developing airways. *Development.* 2009;136(13):2297-2307.
118. Schneider L, Clement CA, Teilmann SC, et al. PDGFRalphaalpha signaling is regulated through the primary cilium in fibroblasts. *Current biology : CB.* 2005;15(20):1861-1866.
119. Hoch RV, Soriano P. Roles of PDGF in animal development. *Development.* 2003;130(20):4769-4784.
120. Tasouri E, Tucker KL. Primary cilia and organogenesis: is Hedgehog the only sculptor? *Cell and tissue research.* 2011;345(1):21-40.
121. Rohatgi R, Milenkovic L, Scott MP. Patched1 regulates hedgehog signaling at the primary cilium. *Science.* 2007;317(5836):372-376.
122. Goetz SC, Anderson KV. The primary cilium: a signalling centre during vertebrate development. *Nature reviews. Genetics.* 2010;11(5):331-344.
123. Wong SY, Reiter JF. The primary cilium at the crossroads of mammalian hedgehog signaling. *Current topics in developmental biology.* 2008;85:225-260.
124. Happe H, de Heer E, Peters DJ. Polycystic kidney disease: the complexity of planar cell polarity and signaling during tissue regeneration and cyst formation. *Biochimica et biophysica acta.* 2011;1812(10):1249-1255.
125. Habbig S, Bartram MP, Muller RU, et al. NPHP4, a cilia-associated protein, negatively regulates the Hippo pathway. *The Journal of cell biology.* 2011;193(4):633-642.
126. Fujii M, Toyoda T, Nakanishi H, et al. TGF-beta synergizes with defects in the Hippo pathway to stimulate human malignant mesothelioma growth. *The Journal of experimental medicine.* 2012;209(3):479-494.
127. Habbig S, Bartram MP, Sagmuller JG, et al. The ciliopathy disease protein NPHP9 promotes nuclear delivery and activation of the oncogenic transcriptional regulator TAZ. *Human molecular genetics.* 2012;21(26):5528-5538.
128. Morin-Kensicki EM, Boone BN, Howell M, et al. Defects in yolk sac vasculogenesis, chorioallantoic fusion, and embryonic axis elongation in mice with targeted disruption of Yap65. *Molecular and cellular biology.* 2006;26(1):77-87.
129. Makita R, Uchijima Y, Nishiyama K, et al. Multiple renal cysts, urinary concentration defects, and pulmonary emphysematous changes in mice lacking TAZ. *American journal of physiology. Renal physiology.* 2008;294(3):F542-553.
130. Happe H, van der Wal AM, Leonhard WN, et al. Altered Hippo signalling in polycystic kidney disease. *The Journal of pathology.* 2011;224(1):133-142.
131. Bielas SL, Silhavy JL, Brancati F, et al. Mutations in INPP5E, encoding inositol polyphosphate-5-phosphatase E, link phosphatidyl inositol signaling to the ciliopathies. *Nat Genet.* 2009;41(9):1032-1036.
132. Irvine RF. 20 years of Ins(1,4,5)P3, and 40 years before. *Nature reviews. Molecular cell biology.* 2003;4(7):586-590.
133. Hatayama M, Mikoshiba K, Aruga J. IP3 signaling is required for cilia formation and left-right body axis determination in Xenopus embryos. *Biochemical and biophysical research communications.* 2011;410(3):520-524.
134. Ibraghimov-Beskrovnaya O, Natoli TA. mTOR signaling in polycystic kidney disease. *Trends in molecular medicine.* 2011;17(11):625-633.
135. Liu YM, Shao YQ, He Q. Sirolimus for treatment of autosomal-dominant polycystic kidney disease: a meta-analysis of randomized controlled trials. *Transplantation proceedings.* 2014;46(1):66-74.
136. Zullo A, Iaconis D, Barra A, et al. Kidney-specific inactivation of Ofd1 leads to renal cystic disease associated with upregulation of the mTOR pathway. *Human molecular genetics.* 2010;19(14):2792-2803.
137. Airik R, Slaats GG, Guo Z, et al. Renal-retinal ciliopathy gene Sdccag8 regulates DNA damage response signaling. *Journal of the American Society of Nephrology : JASN.* 2014;25(11):2573-2583.

138. Rupnik A, Grenon M, Lowndes N. The MRN complex. *Current biology : CB.* 2008;18(11):R455-457.
139. Paull TT, Lee JH. The Mre11/Rad50/Nbs1 complex and its role as a DNA double-strand break sensor for ATM. *Cell cycle.* 2005;4(6):737-740.
140. Rogakou EP, Pilch DR, Orr AH, Ivanova VS, Bonner WM. DNA double-stranded breaks induce histone H2AX phosphorylation on serine 139. *The Journal of biological chemistry.* 1998;273(10):5858-5868.
141. Petrini JH, Stracker TH. The cellular response to DNA double-strand breaks: defining the sensors and mediators. *Trends in cell biology.* 2003;13(9):458-462.
142. Niida H, Nakanishi M. DNA damage checkpoints in mammals. *Mutagenesis.* 2006;21(1):3-9.
143. Cimprich KA, Cortez D. ATR: an essential regulator of genome integrity. *Nature reviews. Molecular cell biology.* 2008;9(8):616-627.
144. O'Driscoll M, Jeggo PA. The role of double-strand break repair - insights from human genetics. *Nature reviews. Genetics.* 2006;7(1):45-54.
145. Kipling D, Davis T, Ostler EL, Faragher RG. What can progeroid syndromes tell us about human aging? *Science.* 2004;305(5689):1426-1431.
146. Ogi T, Walker S, Stiff T, et al. Identification of the first ATRIP-deficient patient and novel mutations in ATR define a clinical spectrum for ATR-ATRIP Seckel Syndrome. *PLoS genetics.* 2012;8(11):e1002945.
147. Griffith E, Walker S, Martin CA, et al. Mutations in pericentrin cause Seckel syndrome with defective ATR-dependent DNA damage signaling. *Nature genetics.* 2008;40(2):232-236.
148. Stiff T, Alagoz M, Alcantara D, et al. Deficiency in origin licensing proteins impairs cilia formation: implications for the aetiology of Meier-Gorlin syndrome. *PLoS genetics.* 2013;9(3):e1003360.
149. Zeman MK, Cimprich KA. Causes and consequences of replication stress. *Nature cell biology.* 2014;16(1):2-9.
150. Couch FB, Bansbach CE, Driscoll R, et al. ATR phosphorylates SMARCAL1 to prevent replication fork collapse. *Genes & development.* 2013;27(14):1610-1623.
151. Duursma AM, Cimprich KA. Checkpoint recovery after DNA damage: a rolling stop for CDKs. *EMBO reports.* 2010;11(6):411-412.
152. Mailand N, Gibbs-Seymour I, Bekker-Jensen S. Regulation of PCNA-protein interactions for genome stability. *Nature reviews. Molecular cell biology.* 2013;14(5):269-282.
153. Ge XQ, Jackson DA, Blow JJ. Dormant origins licensed by excess Mcm2-7 are required for human cells to survive replicative stress. *Genes & development.* 2007;21(24):3331-3341.
154. Poli J, Tsaponina O, Crabbe L, et al. dNTP pools determine fork progression and origin usage under replication stress. *The EMBO journal.* 2012;31(4):883-894.
155. Dalgaard JZ. Causes and consequences of ribonucleotide incorporation into nuclear DNA. *Trends in genetics : TIG.* 2012;28(12):592-597.
156. Nadasdy T, Laszik Z, Lajoie G, Blick KE, Wheeler DE, Silva FG. Proliferative activity of cyst epithelium in human renal cystic diseases. *Journal of the American Society of Nephrology : JASN.* 1995;5(7):1462-1468.
157. Attanasio M, Uhlenhaut NH, Sousa VH, et al. Loss of GLIS2 causes nephronophthisis in humans and mice by increased apoptosis and fibrosis. *Nature genetics.* 2007;39(8):1018-1024.
158. Badano JL, Mitsuma N, Beales PL, Katsanis N. The ciliopathies: an emerging class of human genetic disorders. *Annual review of genomics and human genetics.* 2006;7:125-148.

PART ONE

New insights in ciliopathies

CHAPTER 2

Non-invasive sources of cells with primary cilia from pediatric and adult patients

Cilia, 4:8 (2015)

Henry Ajzenberg*, Gisela G. Slaats*, Marijn F. Stokman, Heleen H. Arts, Ive Logister, Hester Y. Kroes, Kirsten Y. Renkema, Mieke M. van Haelst, Paulien A. Terhal, Iris A. Van Rooij, Mandy G. Keijzer-Veen, Nine V. Knoers, Marc R. Lilien, Michael A. Jewett, and Rachel H. Giles

* These authors contributed equally

ABSTRACT

Background

Ciliopathies give rise to a multitude of organ-specific pathologies; obtaining relevant primary patient material is useful for both diagnostics and research. However, acquisition of primary ciliated cells from patients, particularly pediatric patients, presents multiple difficulties. Biopsies and blood samples are invasive and patients (and their parents) may be reluctant to travel to medical centers, especially for research purposes. We sought to develop non-invasive methods of obtaining viable and ciliated primary cells from ciliopathy patients which could be obtained in the home environment.

Findings

We introduce two methods for the non-invasive acquisition of primary ciliated cells. In one approach, we collected spontaneously shed deciduous (milk) teeth from children. Fibroblast-like cells were observed after approximately 2 weeks of culture of fragmented teeth. Secondly, urine samples were collected from children or adults. Cellular content was isolated and after approximately 1 week renal epithelial cells were observed. Both urine and tooth-derived cells ciliate and express ciliary proteins visible with immunofluorescence. Urine-derived renal epithelial cells (URECs) are amenable to 3D culturing, siRNA knockdown, and *ex vivo* drug testing.

Conclusions

As evidence continues to accumulate showing that the primary cilium has a central role in development and disease, the need for readily available and ciliated patient cells will increase. Here, we introduce two methods for the non-invasive acquisition of cells with primary cilia. We believe that these cells can be used for further *ex vivo* study of ciliopathies and in the future, for personalized medicine.

Findings

Primary cells and ciliopathies

When cilia formation or function is perturbed, any of several dozen associated diseases, collectively known as ciliopathies, can occur. While each ciliopathy disease entity is individually rare, collectively they are common (1 in 300-400 individuals) (1). These genetically heterogeneous diseases can involve one or more organ features, ranging from mild to perinatal lethal phenotypes. Given the wide-ranging function attributed to cilia, it is not surprising that defects in these organelles give rise to a multitude of organ-specific functional defects and pathologies. The different ciliopathies related to non-motile cilia dysfunction often affect renal tissue and are typically diagnosed during childhood (1,2).

For clinical purposes including diagnosis and intervention, primary patient material is of vital importance. Obtaining patient material from pediatric ciliopathy patients via blood samples or skin biopsies can be traumatic for the patients and their parents/caregivers. Furthermore, patients and parents are often reluctant to travel to a medical centre to donate material purely for research. Despite these difficulties, primary ciliated cells from patients are extremely useful in researching ciliopathies and obtaining them may one day be an important part of routine clinical practice. We sought a child-friendly solution to derive valuable patient material that would normally be discarded, without causing the patient any physical or emotional discomfort. Here, we describe our experience (1) isolating renal epithelial cells from regular urine samples, called urine-derived renal epithelial cells (URECs), and (2) harvesting fibroblasts from spontaneously shed deciduous teeth; both cell types have a primary cilium.

Urine-derived epithelial cells

Isolation and expansion

Renal epithelial cells are regularly sloughed off of the renal tubule into the urine. These cells can be collected from the urine and specifically cultured to support proliferation of renal epithelial cells, while suppressing the growth of other cell types present in the urine (e.g. transitional and squamous cells) (3). Urine was collected from patients and controls within the AGORA study protocol (Aetiologic research into Genetic and Occupational/environmental Risk factors for Anomalies in children; http://www.agoraproject.nl/). The study protocol was approved by the regional Committee on Research Involving Human Subjects, and the parents submitted written informed consent for participation.

Approximately 25-150 ml of mid-stream urine is collected inside of a sterile container. The samples may be processed immediately or stored at 4°C for up to 4 hours, which allows transporting samples to a laboratory facility, as urine collection can be done in- or outside of a medical center, e.g. at the home of the patient. We regularly collect urine samples at the home of patients, because parents are more likely to approve participation in research, and then we transport the samples on ice or cold packs.

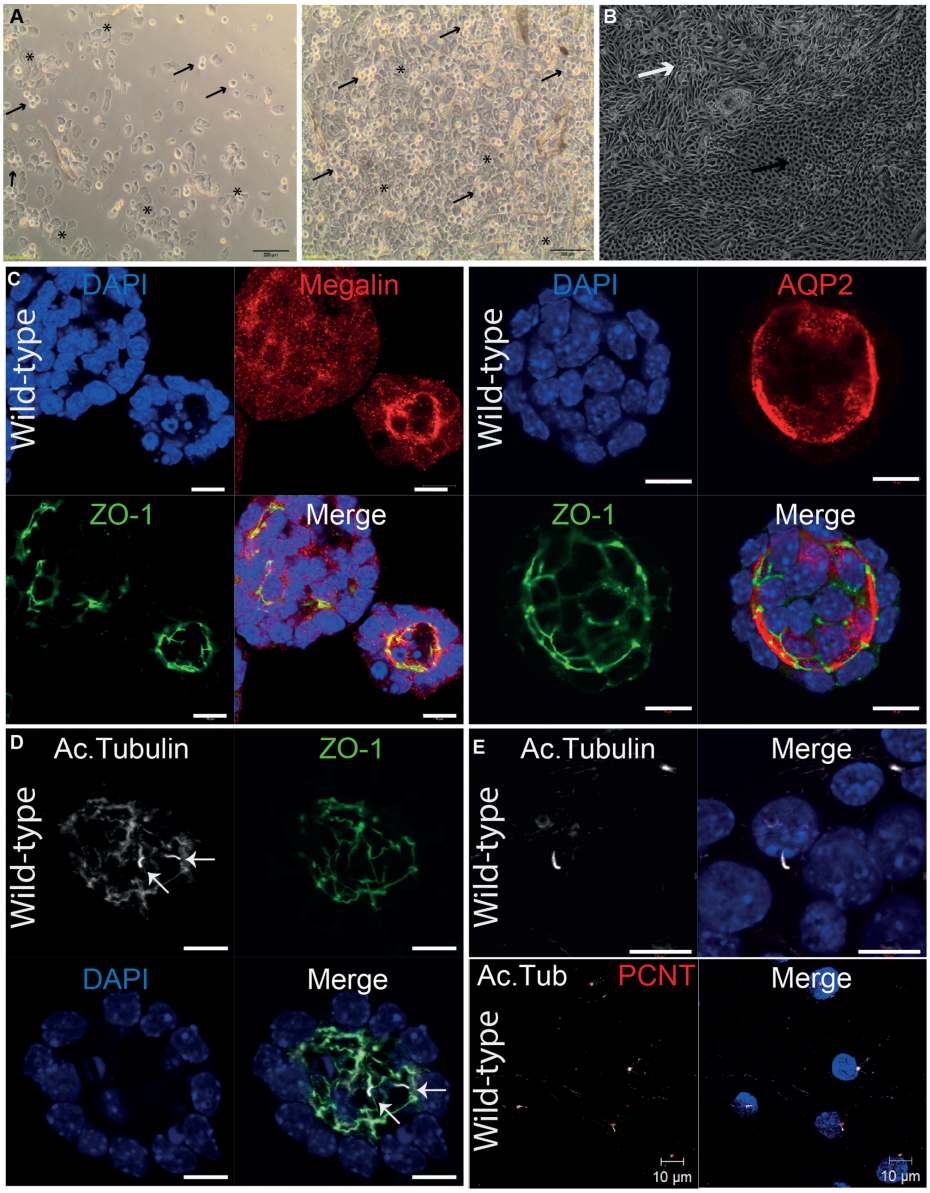

Figure 1. Cultures and images of URECs in 2D and 3D conditions
(A) Urine sample 24 hours after collection at 4x magnification. Asterisks indicated squamous cells and black arrows indicate transitional cells. Scale bar 200µm. Note that renal epithelial cells are not apparent. **(B)** Renal epithelial cells in culture 12 days after collection at 4x magnification. Note that there are two morphologically distinct types of renal epithelial cells, marked with a white or black arrow. Scale bar 200µm. **(C)** Wild-type UREC 3D spheroids. Megalin indicates that cells composing spheroids can be derived from the proximal tubule, while AQP2 was used as a marker for collecting duct cells. Nucleus (DAPI, blue); Megalin and AQP2 (red); and ZO-1 (green). Scale bar 10 µm. **(D)** Wild-type UREC 3D spheroids. Cilia are indicated with white arrows. Nucleus (DAPI, blue); Ac. Tubulin (white); and ZO-1 (green). Scale bar 10 µm. **(E)** Wild-type URECs in 2D monolayer. Nucleus (DAPI, blue); Ac. Tubulin (white); Pericentrin (PCNT, red). Scale bar 10 µm.

Through a series of centrifugation and washing steps, cellular material is isolated and plated on a 24-well plate using renal epithelial growth medium, and incubated at 37˚C. Initially, several cell types (squamous and transitional cells) are present and no URECs are visible (Figure 1A). Primary medium, which is used to enhance initial adherence and survival, is added for 3 days. After day 3 renal epithelial proliferation medium, which selectively supports renal epithelial proliferation, is used and changed daily. Early UREC colonies become visible 3-15 days after sample collecting and cell isolation. Cells are ready for passaging at 80-90% confluence around 9-20 days from collection (Figure 1B).

Analysis and current applications

One advantage of URECs is that they can grow in 3D culture to develop spheroids, which are physiologically relevant models of the renal epithelium. After 3-5 days in matrigel, fully formed spheroids develop apicobasal polarity, ciliate, and form complete lumens (Figure 1C), although we do not observe as many clear lumens as we see in mouse inner medullary collecting duct cells (4). Such characteristics make these UREC spheroids an excellent approximation of *in vivo* renal epithelial conditions. The matrigel can be subsequently dissolved and spheroids fixed.

We show that URECs from healthy controls are made up of a mean of 35% (range 30-40%, n=2) megalin-positive proximal tubule cells and 57.5% (range 50-70%, n=4) aquaporin 2 (AQP2)-positive collecting duct cells (Figure 1C). We have demonstrated that whereas URECs from healthy individuals ciliate well in both monolayer (mean 54% ciliated, range 52-56%, n=2; Figure 1E) and 3D culture (mean 58.2% ciliated, range 44-72%, n=4; Figure 1D), URECs from Joubert syndrome ciliopathy patients did not (mean 29% ciliated, range 25-33%, n=2) (5). The proportion of ciliated cells is obtained by examining at least 100 nuclei per sample. To date, we have isolated renal epithelial cells from n=50 healthy donors and n=20 from ciliopathy patients. However, several of these samples have become contaminated with bacteria or fungi and several samples have failed to deliver viable cells. While cultured renal epithelial cells have been extensively used in spheroid models to test gene variants, the use of human URECs in kidney and ciliopathy research offers patient-specific information and the potential to screen for pharmaceutical intervention. For example, we recently showed that URECs from a Joubert syndrome patient with a *CEP290* mutation were grown in spheroids and partially rescued by treatment with a Hedgehog agonist, confirming involvement of the Hedgehog pathway in nephronophthisis in Joubert syndrome (5). Furthermore, we have observed that these cells grow in a monolayer (Figure 1E), are amenable to siRNA knockdown (not shown), and can be used for immunofluorescence on cover slips.

Tooth-derived fibroblast-like cells

Isolation and expansion

An alternative non-invasive source of ciliated cells from pediatric ciliopathy patients is spontaneously shed deciduous (milk/baby) teeth shed between the ages of 5 to 14 years. Within 24 hours of spontaneous loss of the tooth, the tooth should be kept moist and cool (ideally 4°C) and transported to the laboratory facility. The PBS-washed enamel casing is

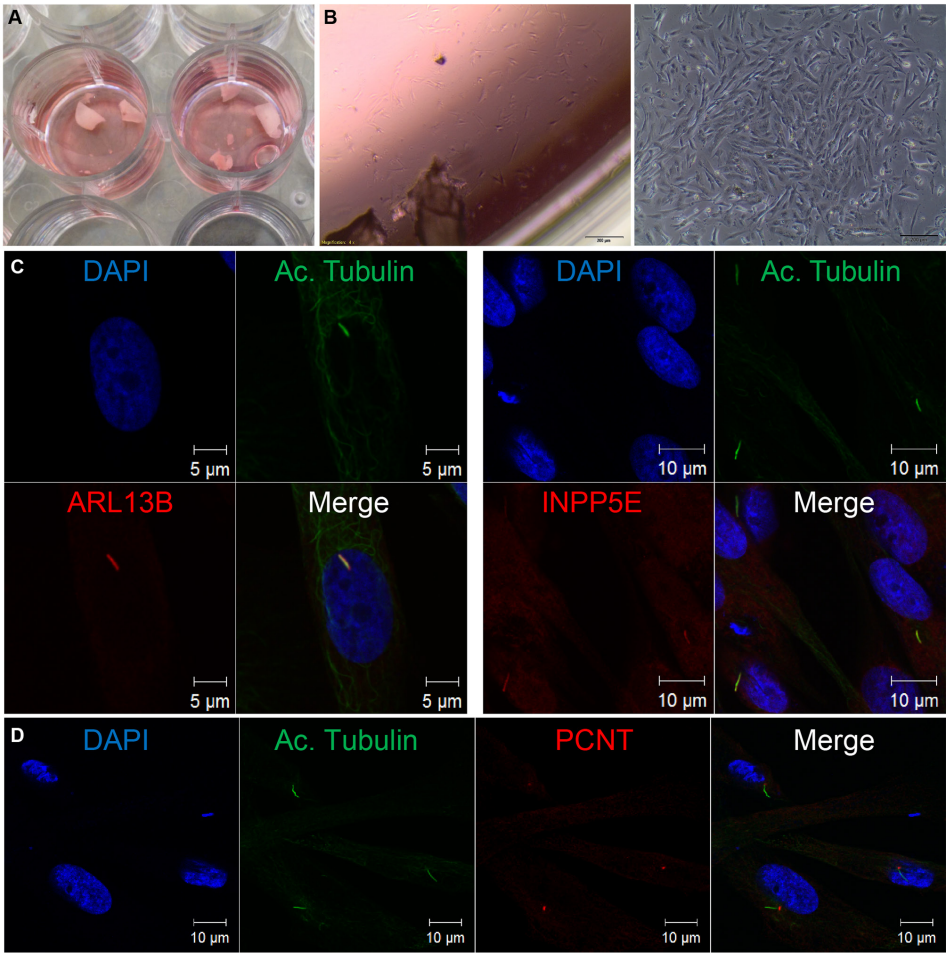

Figure 2. Cultures of cells derived from deciduous teeth
(A) Tooth fragments are taken into culture in a 12-well plate under standard fibroblast cell culture conditions. **(B)** Fibroblast-like cells were observed in the culture plate after approximately two weeks (left) and expanded ~1 week (right) at 4x magnification. Scale bar 200µm. **(C)** Immunofluorescence imaging of fibroblast-like cells from healthy donors (n=3) show 25-51% ciliation after 24 hours serum starvation. Cells from one donor are shown here. Nucleus (DAPI, blue); ARL13B and INPP5E (red); Ac. Tubulin (green). Scale bar 5 or 10 µm. **(D)**. Imaging of fibroblast-like cells from a healthy donor showing cilia and centrosome. Nucleus (DAPI, blue); Ac. Tubulin (green); pericentrin (PCNT; red). Scale bar 10 µm.

then crushed by a hammer in semi-sterile conditions. Tooth fragments are taken into culture under standard fibroblast cell culture conditions and incubated at 37˚C in a 12-well plate in Dulbecco's Modified Eagle Medium. (Figure 2A). Fibroblast-like cells were observed in the culture plate after approximately two weeks. These cells can be frozen and thawed for later use using standard cell culture protocols (Figure 2B). Teeth were collected from children within the AGORA study protocol approved by the regional Committee on Research Involving Human Subjects. Parents submitted written informed consent for participation.

Analysis and current applications

We show that after 24 hours of serum starvation a mean of 41.3% (range 25-51% ciliation, n=3, Figure 2) of the fibroblast-like cells from the tooth of healthy donors ciliate. Common ciliary markers are expressed, such as ADP-ribosylation factor-like protein 13B (ARL13B), Inositol polyphosphate-5-phosphatases E (INPP5E) (Figure 2C) which are associated with Joubert syndrome, as well as centrosome marker pericentrin (PCNT) (Figure 2D), thus indicating that these cells are an excellent model for investigating ciliary disorders, e.g. Joubert syndrome. To date, we have isolated n=10 healthy fibroblast-like tooth-derived cells; isolation of patient fibroblast-like tooth-derived cells is in progress.

Discarded milk teeth are a child-friendly source of patient material to study ciliopathies or other diseases. The tooth-derived cells can be used for diverse research applications including genomic, epigenetic, or metabolic analysis. Although the timing of the tooth being shed is difficult to plan, the use of milk teeth as a source of material for research is an attractive low-stress option that should be discussed with the parents.

DISCUSSION

Thus far, we have had promising results in using both tooth and urine-derived primary ciliated cells for the investigation of human ciliopathies. The usefulness of these methods lies in their non-invasive nature. With these techniques, the pain and inconvenience associated with obtaining blood samples and skin biopsies need not limit the availability of patient material. Although we have used these cells for investigating ciliopathies, they may also be used in other areas where primary cells are needed. Furthermore, their collection and expansion are relatively simple techniques that can be performed by an individual with basic laboratory experience and no specialized equipment.

A common difficulty with the isolation and expansion of primary cells is contamination due to semi-sterile collection, and we have found our techniques to be no exception. Fungal and/or bacterial infections may appear several days after plating. Minimizing the risk of contamination in both cell types involves performing all work in a sterile laminar flow hood and treating prophylactically with antibiotics and antifungal agents in the media. For URECs,

ensure that urine is carefully collected mid-stream. The tooth-derived cells require approximately 4 weeks of culturing, from the point of collection until sufficient cells are present for experimentation and freezing. This length of time in culture is not ideal for cilinical purposes and also increases the risk of contamination. Another limitation of both techniques is that processing must occur within a specific time frame (4 hours for URECs and 24 hours for tooth cells). For a more detailed discussion of UREC types seen in culture, see Dorrenhaus et al. (6).

Conclusion

As evidence continues to accumulate showing that the primary cilium has a central role in development and disease, the need for readily available and ciliated patient cells will increase. Here, we introduce two methods for the non-invasive acquisition of primary patient cells that ciliate well. We believe that these cells can be utilized for further *ex vivo* study of ciliopathies, drug testing, DNA mutation analysis, metabolomics, functional testing, and may be used as sources for the generation of inducible pluripotent stem cells.

Acknowledgements

We thank the urine and tooth donors and their parents for their participation in the studies. We thank members of the Giles/Knoers labs for weekend cell culturing, and Ernie Bongers for study support. We thank the Cell Microscopy Center at the UMC Utrecht for providing expert services. We acknowledge support from the European Community's Seventh Framework Programme FP7/2009 under grant agreement no: 241955 SYSCILIA, and 305608, and EURENOMICS, and Veni-91613008 from The Netherlands Organisation for Scientific Research, and support from the Dutch Kidney Foundation Consortium CP11.18 "KOUNCIL".

REFERENCES

1. Waters AM, Beales PL. Ciliopathies: an expanding disease spectrum. *Pediatr Nephrol.* 2011;26(7):1039-1056.
2. Hildebrandt F, Benzing T, Katsanis N. Ciliopathies. *N Engl J Med.* 2011;364(16):1533-1543.
3. Zhou T, Benda C, Dunzinger S, et al. Generation of human induced pluripotent stem cells from urine samples. *Nat Protoc.* 2012;7(12):2080-2089.
4. Giles RH, Ajzenberg H, Jackson PK. 3D spheroid model of mIMCD3 cells for studying ciliopathies and renal epithelial disorders. *Nat Protoc.* 2014;9(12):2725-2731.
5. Hynes AM, Giles RH, Srivastava S, et al. Murine Joubert syndrome reveals Hedgehog signaling defects as a potential therapeutic target for nephronophthisis. *Proc Natl Acad Sci U S A.* 2014;111(27):9893-9898.
6. Dorrenhaus A, Muller JI, Golka K, Jedrusik P, Schulze H, Follmann W. Cultures of exfoliated epithelial cells from different locations of the human urinary tract and the renal tubular system. *Arch Toxicol.* 2000;74(10):618-626.

CHAPTER 3

Screen-based identification and validation of four novel ion channels as regulators of renal ciliogenesis

Manuscript submitted

Gisela G. Slaats*, Gabrielle Wheway*, Veronica Foletto, Katarzyna Szymanska,
Bas W.M. van Balkom, Ive Logister, Krista den Ouden, Mandy G. Keijzer-Veen, Marc R. Lilien,
Nine V. Knoers, Colin A. Johnson, Rachel H. Giles

* These authors contributed equally

ABSTRACT

Polycystic kidney disease, the most common renal ciliopathy, is caused by calcium ion channel dysfunction in the cilium. To investigate the contribution of ion channels to ciliogenesis in collecting duct cells of the kidney, we carried out an siRNA-based reverse genetics screen of all ion channels in the mouse genome in murine inner medullary collecting duct cells. This screen revealed four candidate cilia ion channel genes: *Kcnq1*, *Kcnj10*, *Kcnf1* and *Clcn4*. We show that these four ion channels localize to primary cilia and renal tubules. We further report that human *KCNQ1* disease alleles, associated with Long QT syndrome, regulate renal ciliogenesis; KCNQ1-p.R518X, -p.A178T and -p.K362R could not rescue ciliogenesis after *Kcnq1* siRNA-mediated depletion in contrast to wild-type KCNQ1 and benign KCNQ1-p.R518Q. Our data suggest that these four ion channels have a novel role in renal ciliogenesis, with potential implication as genetic contributors to ciliopathy pathophysiology. The new functional roles of a subset of ion channels provide new insights into the disease pathogenesis of channelopathies and may suggest future therapeutic approaches.

INTRODUCTION

Primary cilia, also referred to as immotile or sensory cilia, project from most cells and function to sense their anatomical/physiological environment (1). In general, primary cilia transduce signals from extracellular stimuli to a cellular response that regulates proliferation, differentiation, transcription, migration, polarity and tissue morphology (2) in a tissue-specific manner (3). Developmental and pathological pathways of cellular signalling linked to primary cilia include, but are not limited to, canonical and non-canonical Wnt-, Hedgehog-, and Hippo signalling (4).

Primary cilia play an important role in the development and healthy physiology of many different organs, including eye, kidney, liver, brain and bone. Reflecting the complexity of ciliogenesis and the essential role of primary cilia in signal transduction in a large variety of tissues and organ systems, numerous diseases have been linked to abnormal cilium function (5). Of the so-called ciliopathies, kidney cysts are one of the more frequent phenotypes (5), and polycystic kidney diseases collectively represent one of the most common genetic diseases known to mankind (6). Besides cilia, ion channels also have critical roles in the renal epithelium, regulating sodium, potassium, and magnesium homeostasis, as well as the control of water reabsorption in the collecting duct (7). To study the roles of ion channels further, we systematically interrogated the contribution of all ion channels to ciliogenesis or maintenance of primary cilia in collecting duct cells of the kidney. An siRNA-based reverse genetics screen of all ion channels in the mouse genome in murine inner medullary collecting duct (mIMCD3) cells, revealed four ion channels with a significant effect on ciliogenesis, but not on cell number: *Kcnq1* (potassium channel, voltage-gated, kqt-like subfamily, member 1)*, Kcnj10* (potassium channel, inwardly rectifying, subfamily J, member 10)*, Kcnf1 (*potassium channel, voltage-gated, subfamily F, member 1*)* and *Clcn4* (chloride channel, voltage-gated 4*)*. We took all of these candidates forward for validation and further functional analysis. Human disease alleles of *KCNJ10* and *KCNQ1* were tested in 3D spheroids to examine their effects on ciliogenesis. By elucidating the role of these ion channels in primary cilia and disease, we offer new insights into disease pathogenesis of channelopathies and opportunities for potential improvements to disease management.

RESULTS

Reverse genetics screen

To investigate the potential roles of ion channels on renal ciliogenesis, we performed an siRNA-based reverse genetics screen of all ion channels in the mouse genome in mouse inner medullary collecting duct cells (mIMCD3 cells). This screen represents 340 ion channels across the mouse genome (Table S1). The effect of siRNA knockdown on

ciliogenesis was assessed by calculating the percentage of cells with a single cilium, with the statistical significance of this effect assessed by calculating *z* scores (z_{cilia}). *z* scores were also calculated for the effect of the knockdown on cell number (z_{cell}), to exclude effects of cell proliferation or apoptosis on ciliogenesis, since these could be due to non-specific secondary processes (8) (Figure S1). Based on this analysis, we identified four ion channels that had a significant negative effect on ciliogenesis but not on cell number: *Kcnq1* (potassium channel, voltage-gated, kqt-like subfamily, member 1), *Kcnj10* (potassium channel, inwardly rectifying, subfamily J, member 10), *Kcnf1 (*potassium channel, voltage-gated, subfamily F, member 1*)* and *Clcn4* (chloride channel, voltage-gated 4) (Table S1, Figure S1).

Validation

All four ion channels localize to the primary cilium and are required for ciliogenesis

To validate the effect of knockdowns of *Clcn4, Kcnf1, Kcnq1* and *Kcnj10* on ciliogenesis we repeated the siRNA knockdowns in mIMCD3 cells, followed by immunofluorescence (IF) staining of cilia using acetylated α-tubulin antibody and analysis by confocal microscopy. We tested ON-TARGETplus SMARTpool siRNA knockdown efficiency of *Clcn4, Kcnf1, Kcnq1* and *Kcnj10* at the mRNA level by RT-qPCR, and found all siRNAs to reduce transcript levels compared to cells transfected with non-targeting control siRNA (siControl) (Figure S2A). Knockdown of each of the four genes resulted in a lower percentage of ciliated cells compared to cells transfected with control siRNA (**p<0.01 and ***p<0.001, n=3) (Figure 1A). Additionally, we tested the effect of siRNA-mediated depletion of *Clcn4, Kcnf1, Kcnq1* and *Kcnj10* on ciliation in 3D spheroids, a commonly used to model renal ciliopathies (9). 3D spheroids transfected with siRNAs to deplete cellular levels of any of these four ion channels manifest significantly lower cilia frequency compared to non-targeting siRNA-treated control cells. Reduction of cilia levels is comparable to *Ift88* siRNA knockdown, a well-accepted regulator of ciliogenesis used here as a positive control (8,10) (Figure 1B) (*p<0.05, **p<0.01 and ***p<0.001, n=3). Cell cycle phase distribution analysis showed unchanged cell numbers in G1-, S-, and G2-phase of the cell cycle after siRNA-mediated depletion of *Clcn4, Kcnq1* and *Kcnj10* compared to siControl, excluding any possible cell cycle effect on the observed loss of cilia (Figure S2B).

Immunofluorescence staining using specific antibodies to each of these ion channels shows that endogenous Clcn4, Kcnf1, Kcnq1 and Kcnj10 proteins localize to primary cilia (axoneme or ciliary base) of mIMCD3 cells (Figure 1C), in addition to the previously described localizations of these channels at the endosomal membrane for CLCN4 (11), or basolateral membrane for KCNQ1 and KCNJ10 (12,13). Additionally, histology of rat paraffin-embedded kidney sections demonstrates localization of the ion channels to renal tubules (Figure S3). Furthermore, we examined overexpression of wild-type (WT) human CLCN4-GFP, KCNJ10-GFP and KCNQ1 in 3D spheroids of mIMCD3 cells (9). CLCN4-GFP and KCNJ10-GFP protein

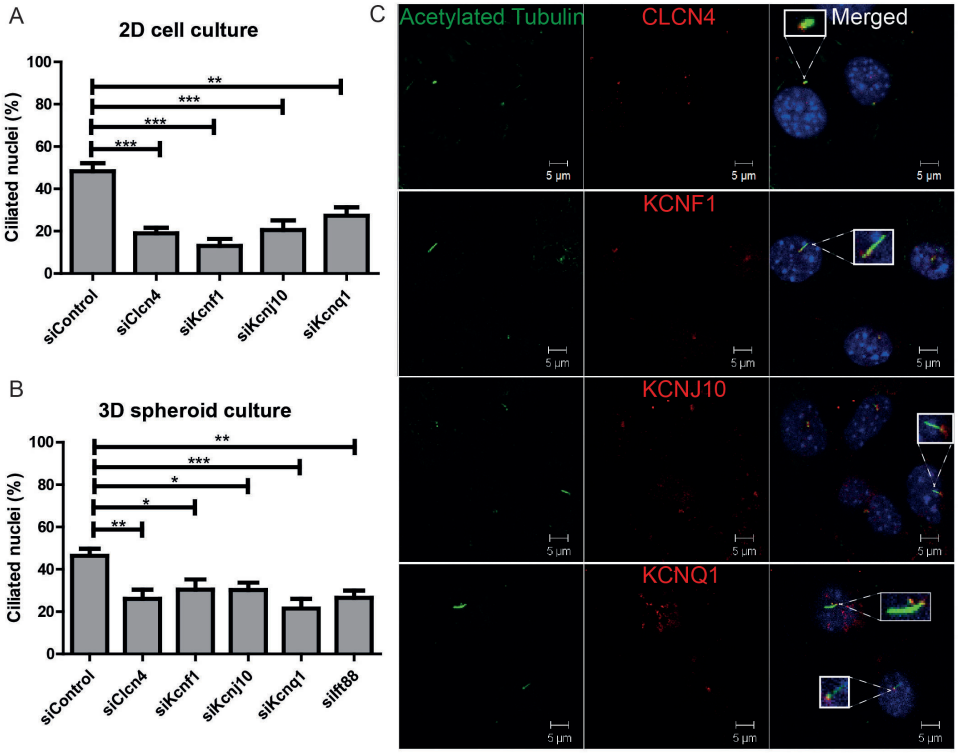

Figure 1. CLCN4, KCNF1, KCNJ10 and KCNQ1 localize to primary cilia and regulate primary cilia
(**A**) Quantification (%) of ciliated mIMCD3 cells shows loss of cilia after siRNA-mediated depletion for *Clcn4, Kcnf1, Kcnj10* or *Kcnq1*. >250 cells were scored per condition (**p<0.01 and ***p<0.001, n=3, mean and s.e.m., One-way ANOVA, Dunnett's). (**B**) Quantification (%) of cilia in 3D spheroids shows loss of cilia in spheroids depleted for *Clcn4, Kcnf1, Kcnj10, Kcnq1* or *Ift88*. 25 spheroids were scored per condition (*p<0.05, **p<0.01 and ***p<0.001, n=3, mean and s.e.m., One-way ANOVA, Dunnett's). (**C**) Immunostaining of mIMCD3 cells for cilia (Acetylated Tubulin, green) and the different ion channels CLCN4, KCNF1, KCNJ10 and KCNQ1 (red) with DAPI counterstaining (blue) shows localization of all four ion channels to primary cilia (magnified inserts). Scale bar 5 µm.

localized to primary cilia (white arrows) (Figure 2A), validating localization of endogenous ion channels observed at primary cilia (Figure 1C). Overexpression of the human WT protein in 3D spheroids rescued loss of cilia after siRNA knockdown of endogenous *Clcn4, Kcnj10 and Kcnq1* (Figure 2B; **p<0.01, ***p<0.001, n=3). In addition to GFP-tagged overexpression of WT CLCN4 and KCNJ10 (Figure 2A), western blot confirmed overexpression of WT KCNJ10 (Figure S2C) and KCNQ1 (Figure S2D).

As human mutations have been identified in *KCNQ1* and *KCNJ10* patients with inherited disease that have some features overlapping with ciliopathy phenotypes, we further tested whether patient mutations may affect the ability of the overexpressed proteins to rescue ciliogenesis defect after *Kcnq1* and *Kcnj10* knockdown.

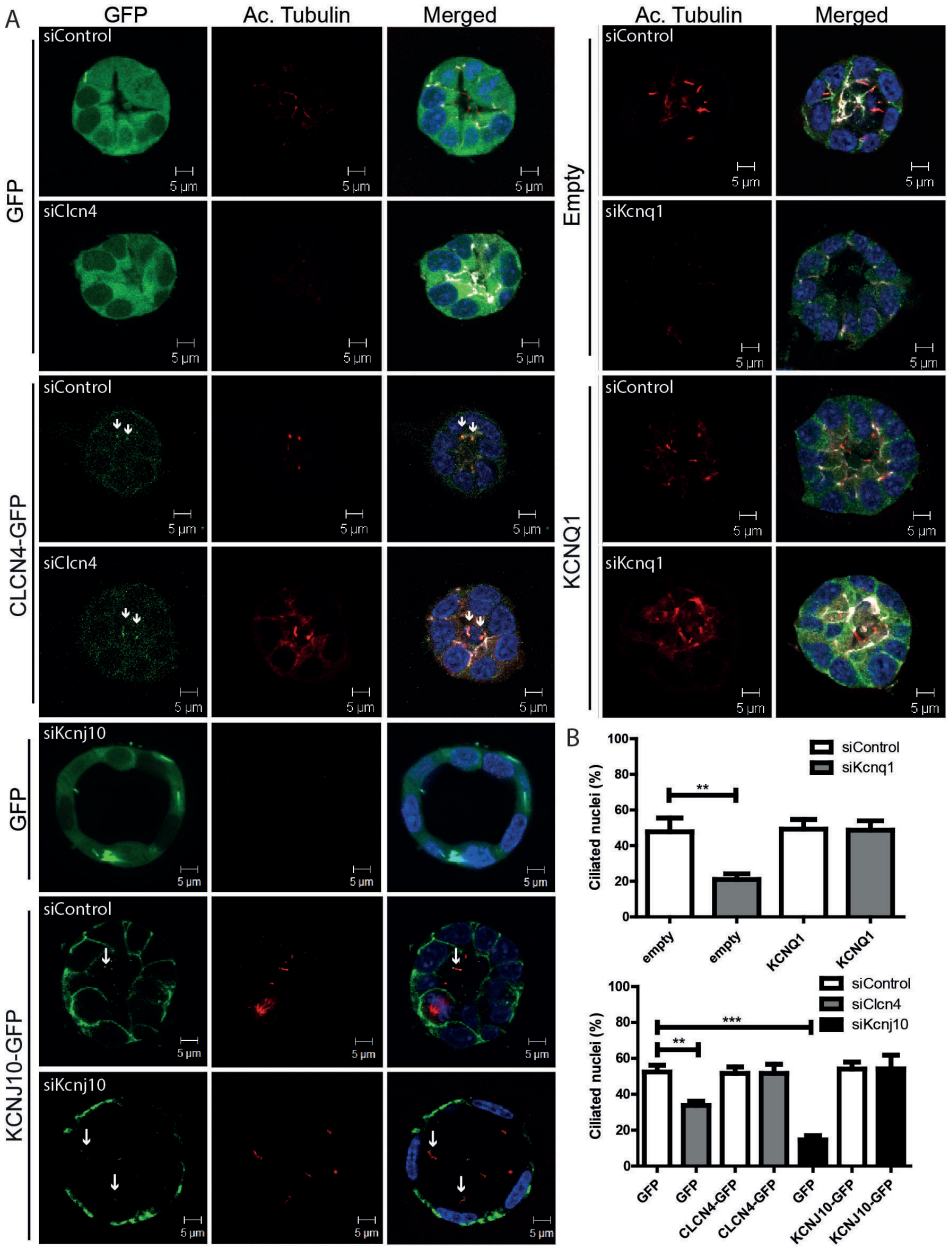

Figure 2. Ciliation in 3D spheroids with wild-type CLCN4-GFP, KCNJ10-GFP and KCNQ1
(**A**) Immunostaining of spheroids of mIMCD3 cells for cilia (Acetylated tubulin, red), tight junctions (ZO-1, white), with DAPI counterstaining (blue) shows loss of cilia after *Clcn4, Kcnj10* and *Kcnq1* siRNA transfection, and rescue of ciliation by overexpression of wild-type CLCN4-GFP, KCNJ10-GPF or KCNQ1. White arrows indicate localization of CLCN4-GFP and KCNJ10-GFP to primary cilia. In KCNQ1 spheroids adherens junctions (β-catenin, green) are stained as well. Scale bar 5 µm. (**B**) Quantification of ciliary frequency in spheroids shows loss of cilia in spheroids depleted for *Kcnq1* (**p<0.01), *Clcn4* (**p<0.01),

and *Kcnj10* (***p<0.001), and restoration of ciliary frequency was obtained upon transfection with wild-type KCNQ1, CLCN4-GFP, and KCNJ10-GFP respectively. 20 spheroids were scored per condition (n=3, mean and s.e.m., Two-way ANOVA, Bonferroni).

KCNJ10 EAST syndrome alleles

Mutations in *KCNJ10* have been associated with Epilepsy, Ataxia, Sensorineural deafness, and (Gitelman-like) Tubulopathy (EAST syndrome, alternatively named SESAME syndrome), an autosomal recessive disease (MIM 612780) occasionally featuring seizures and mental retardation. To test the effect of EAST syndrome-associated human mutations on KCNJ10 function in primary cilia, we examined the ability of wild-type (WT) and two mutant *KCNJ10* alleles to rescue the ciliogenesis defect seen in 3D spheroids after *Kcnj10* siRNA knockdown. A previous study performed patch clamp assays on a series of *KCNJ10* mutant alleles to quantify the effect of the missense mutation on ion channel function, showing many of them to be hypomorphic (14). The alleles we tested comprise: KCNJ10-c.194G>C/p.R65P (20% retained function), and KCNJ10- c.418T>C/p.C140R (total loss of function), normalized to KCNJ10-WT (100% function). All *KCNJ10* alleles were transfected into mIMCD3 cells and 24 hours later cells were transfected with non-targeting control siRNA or *Kcnj10* siRNAs that did not target the human KCNJ10 constructs. KCNJ10-WT rescued loss of primary cilia after *Kcnj10* knockdown (***p<0.001, n=3), as well as KCNJ10-p.R65P and p.C140R (***p<0.001 and **p<0.01 respectively) (Figure 3A, C), indicating completely retained function of these alleles with regard to ciliogenesis. In addition, similar to the WT protein, both mutated proteins localize to the cilium (white arrows; Figure 3A). No differences were found in cells transfected with any KCNJ10 construct and control siRNA (Figure 3B). Western blot assessed expression of the two missense mutant proteins, and validated expression of all constructs (70 kDa; Figure S2C). We conclude that loss-of-function of KCNJ10 is unlikely to affect primary cilia of EAST syndrome patients, and that the ciliary and ion channel functions of KCNJ10 are independent of each other.

KCNQ1 alleles associated with Long QT syndrome

Genetic variants of *KCNQ1* are known to cause Long QT syndrome (LQTS; MIM 192500), an inherited disease predominantly affecting heart function, as the KCNQ1 ion channel is required for the normal repolarization stage of the cardiac action potential (15,16). The autosomal dominant form of the condition is also known as Romano-Ward syndrome (MIM 192500). The autosomal recessive variant is known as Jervell and Lange-Nielsen syndrome (JLNS; MIM 220400), with congenital sensorineural hearing loss as an additional phenotypic feature (17). *KCNQ1* variants are also associated with familial Atrial Fibrillation 3 (MIM 607554) (18), Short QT syndrome 2 (MIM 609621) (19) and imprinting defects of *KCNQ1* results in Beckwith-Wiedemann syndrome, a congenital overgrowth syndrome

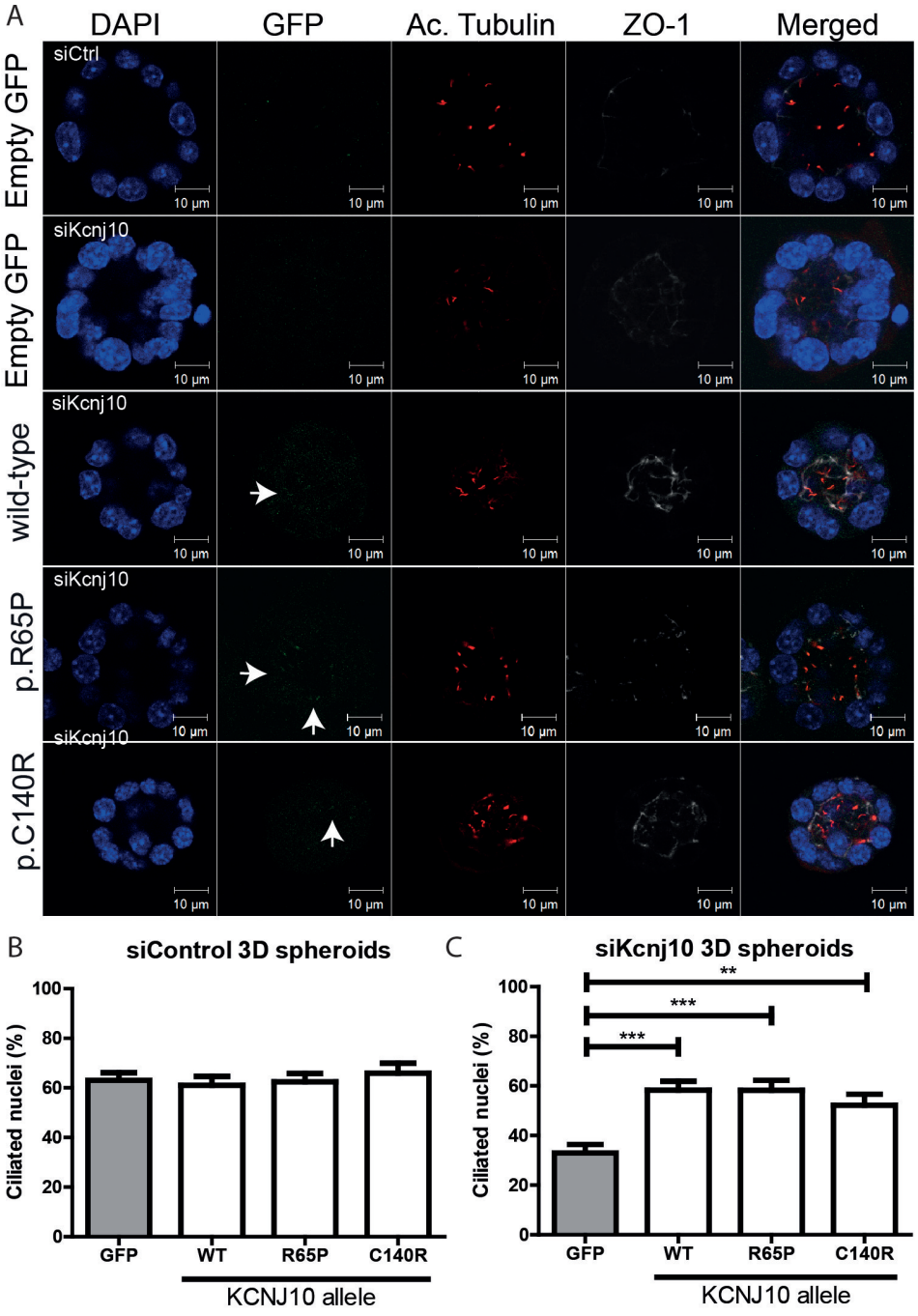

Figure 3. 3D spheroids of KCNJ10 EAST syndrome-associated alleles
(**A**) Immunostaining of spheroids of mIMCD3 cells for cilia (Acetylated tubulin, red) and tight junctions (ZO-1, white), with DAPI counterstaining (blue) shows loss of cilia after *Kcnj10* siRNA transfection, and rescue

of ciliation by wild-type (WT) and p.R65P and p.C140R KCNJ10-GFP (white arrows indicate localization at cilia). Scale bar 10 µm. (**B-C**) Quantification of ciliary frequency in spheroids shows loss of cilia in spheroids depleted for *Kcnj10* (***p<0.001), and restoration of ciliary frequency was obtained upon transfection with WT KCNJ10 (***p<0.001). Overexpression of variant KCNJ10 did not affect ciliation in siControl transfected cells. In siKcnj10 transfected cells, overexpression of KCNJ10 p.R65P and p.C140R rescues ciliation as well (***p<0.001, **p<0.01), 20 spheroids were scored per condition (n=3, mean and s.e.m., One-way ANOVA, Dunnett's).

which often involves kidney abnormalities (MIM 130650) (20). Furthermore, renal patients might develop acquired LQTS, which is enhanced by potassium channel inhibiting medication for their kidney disease (21).

To further investigate the potential role of KCNQ1 in renal primary cilia formation we examined whether patient alleles associated with LQTS perturb ciliogenesis in renal cells. We generated expression plasmids engineered with human variants associated with Long QT syndrome KCNQ1-c.1553G>A/p.R518Q (benign variant) (22), truncating allele KCNQ1-c.1552C>T/p.R518X (23), KCNQ1-c.532G>A/p.A178T (22,24,25), and KCNQ1-c.1085A>G/p.K362R (also associated with JLNS) (22,26). All *KCNQ1* alleles were transfected into mIMCD3 cells and 24 hours later cells were transfected with non-targeting control siRNA or *Kcnq1* siRNA (not targeting human KCNQ1). Both KCNQ1-WT and KCNQ1-p.R518Q rescued loss of primary cilia after *Kcnq1* knockdown (***p<0.001, n=3) (Figure 4A, C), indicating retained function of these alleles. In contrast, -p.R518X, -p.A178T and -p.K362R did not rescue the loss of cilia phenotype after *Kcnq1* knockdown, indicating that these alleles may play a pathogenic role in the kidney of human patients (Figure 4A, C). No differences were found in cells transfected with any KCNQ1 constructs and control siRNA, excluding a role for dominant negative action (Figure 4B). Additionally, we observed increased aberrant mitotic spindle orientation in cells depleted of *Kcnq1* compared to siControl-transfected cells (white arrows). Overexpression of WT or mutant KCNQ1-p.R518Q partly rescues aberrant mitotic spindle orientation, but, KCNQ1 alleles -p.R518X, -p.A178T and -p.K362R did not rescue spindle orientation (*p<0.05, ***p<0.001, n=3) (Figure 4D). Aberrant mitotic spindle orientation could possibly be caused by polarization defects. Western blot of overexpression of KCNQ1 and mutant alleles show expression of all constructs at 70 kDa, except for the truncated allele KCNQ1-p.R518X (predicted ~55 kDa). KCNQ1-p.A178T has lower expression levels, which might explain why no rescue is observed upon overexpression of this mutant (Figure S2D).

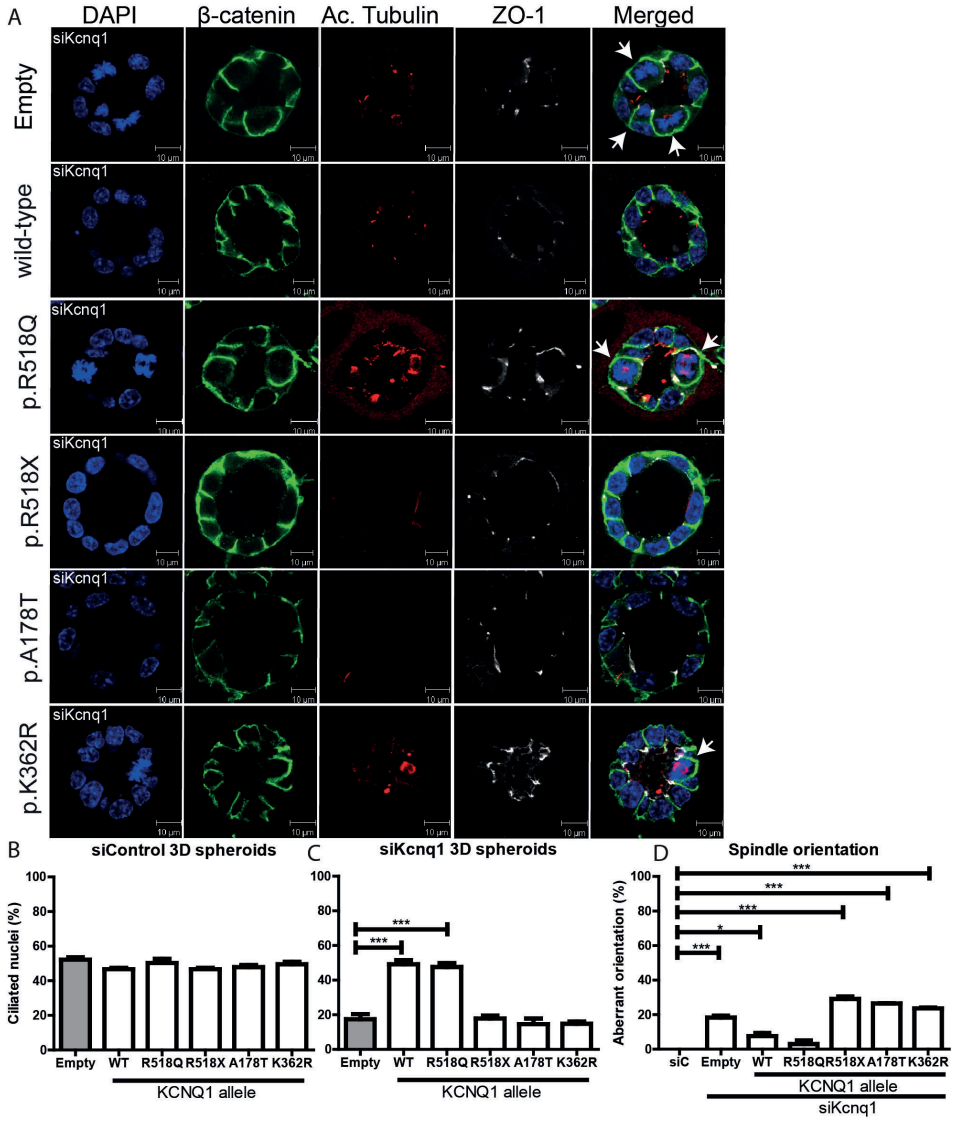

Figure 4. Long QT syndrome-associated KCNQ1 mutant alleles in 3D spheroids
(**A**) Immunostaining of spheroids of mIMCD3 cells for cilia (Acetylated tubulin, red), tight junctions (ZO-1, white), and adherens junctions (β-catenin, green) with DAPI counterstaining (blue) shows loss of cilia after *Kcnq1* siRNA transfection, and rescue of ciliation by wild-type (WT) and p.R518Q KCNQ1. No rescue of cilia is observed after overexpression of p.R518X, p.A178T and p.K362R KCNQ1. Scale bar 10 µm. (**B-C**) Quantification of ciliary frequency in spheroids shows loss of cilia in spheroids depleted for *Kcnq1* (***p<0.001), and restoration of ciliary frequency was obtained upon transfection with WT KCNQ1 (***p<0.001). Overexpression of variant KCNQ1 did not affect ciliation in siControl transfected cells. In siKcnq1 transfected cells, overexpression of KCNQ1 p.R518Q rescues ciliation as well (***p<0.001), but p.R518X, p.A178T and p.K362R KCNQ1 do not restore cilia. 20 spheroids were scored per condition (n=3, mean and s.e.m., One-way ANOVA, Dunnett's). (**D**) Aberrant spindle formation was observed in cells siRNA depleted for *Kcnq1* and overexpressing KCNQ1 mutant alleles (white arrows panel A). 20 spheroids were scored per condition (*p<0.05, ***p<0.001, n=3, mean and s.e.m., One-way ANOVA, Dunnett's).

DISCUSSION

We describe an unbiased siRNA knockdown screen of ion channels in a mouse ciliated cell line, and identified three potassium and one chloride channel that are implicated in ciliogenesis without affecting cell number. Further work shows for the first time that these ion channels localize to renal primary cilia *in vivo* and are required for ciliogenesis in 2D and 3D models of renal cilia. The ciliogenesis defect seen in 3D spheroids after knockdown of these ion channels can be rescued by exogenous overexpression of the WT human ion channels, which are not targeted by the mouse siRNA. However, overexpression of mutated versions of KCNQ1 failed to rescue the ciliogenesis defect after knockdown, suggesting that these mutations affect protein structure or function in such a way that is crucial to the formation of renal primary cilia. These *KCNQ1* mutations are found in patients with inherited diseases encompassing ciliopathy-like phenotypes including congenital heart disease and sensorineural hearing loss. The characterisation of the function of this ion channel in primary cilia, with an additional role in ciliogenesis, provides novel insights into disease pathogenesis in these patients.

Mutations in a range of cilia proteins lead to a suite of diseases known as the ciliopathies. Proteins mutated in ciliopathies include structural proteins and proteins involved in ciliary signalling (27), including ion channels. For example, *PKD1* and *PKD2*, which encode the polycystins that heterodimerize to form a calcium ion channel, are mutated in polycystic kidney disease (PKD) (28). Mutations in *PKD1* or *PKD2* can cause loss of cilia, or alternatively, can lead to disturbed ciliary signalling without affecting cilium structure (29,30). Our findings suggest that damaging mutations in *KCNQ1*, *KCNJ10*, *KCNF1* and *CLCN4* could cause similar defects in cilia structure and cilia signaling, but also that mutations affecting the ion channel function may not affect the cilia (e.g. *KCNJ10*). These findings not only suggest a possible role for primary cilia in the pathophysiology of conditions associated with LQTS, but they offer new insights into the general importance of ion channels and ion signalling in ciliopathies. Identification of four novel ion channels as being localized to primary cilia and being required for ciliogenesis supports previously published data showing that the length of the ciliary structure is regulated by ion current, and ion channel stimulation can result in cilia-generated signalling (31). Our data suggest that disturbance of ion balance by loss of the ion channel KCNQ1 results in ciliopathy phenotypes *in vitro*. On the other hand, our data suggest that KCNF1 and CLCN4 may be novel candidates in human ciliopathies. However, *KCNJ10*-associated EAST syndrome does not apparently involve ciliogenesis defects.

The relation of ion channels to disease, particularly heart disease, has been appreciated for over two decades (32), but the role of ciliary ion channels in this disease process is not entirely understood. Whilst the general importance of primary cilia at the embryonic node is understood to regulate normal heart laterality (33), the role of ciliary ion channels in this

process has not been examined. Recently, a central role for cilia in congenital heart disease (CHD) was identified by a recessive forward genetic screen in mice, and it could be inferred that, to some extent, ion channels in cilia may account for such phenotypes (34). Whole-exome sequencing in this study revealed that of 61 genes mutated in CHD, 34 encoded cilia-related proteins and, 16 encoded proteins involved in cilia signalling (34). In addition to this, a number of ciliopathies, including Ellis van Creveld syndrome (MIM 225500) and Alström syndrome (MIM 203800), can include CHD in their phenotypic spectrum (5). Together these findings suggest that ciliary ion channels are important for normal heart development and function, and that *KCNQ1*-associated heart disease might involve cilia dysfunction as well.

Although highly speculative, our findings suggest that long QT patients with *KCNQ1* mutations might possibly harbor a subclinical renal phenotype (most likely a mild nephronophthisis): acquiring renal sonograms and/or urine concentration data from patients with *KCNQ1* mutations would be an interesting follow-up to this study. Additionally, analyzing whole exome sequencing data from patient cohorts with end-stage renal disease or renal ciliopathies may uncover enrichment for *KCNQ1* variants or mutations. Interestingly, in patients with renal failure, hypertension and many other factors can contribute to consequent cardiovascular burden and acquired LQTS (21). Our data might likewise point to the dysfunction of cilia as one of the factors contributing to acquired LQTS.

Ciliopathies are defined as genetic diseases, involving defects in proteins localizing to the cilium or associated complexes and pathways. Ciliary perturbation is not limited to cilia structure, but also function, including signalling through ion channels. This makes careful classification and diagnosis on phenotypic, genotypic and finally on physiological grounds challenging but nonetheless important (5). Ciliopathies cover a wide range of genotypes and phenotypes, and the list of ciliopathies is ever expanding. Our data elucidating the function of four novel primary cilia ion channels suggest that KCNQ1 could be implicated in renal ciliopathies, but, in contrast, KCNJ10 seems not. Furthermore, KCNF1 and CLCN4 could be unidentified genetic causes of ciliopathies involving renal defects. These new insights into the pathophysiological disease mechanisms of patients with KCNQ1 mutations will inspire future research concerning therapeutic approaches, and molecular genetic screening of ion channel genes in ciliopathy patients.

MATERIAL AND METHODS

Cell culture

Mouse inner medullary collecting duct (mIMCD3) cells were cultured as previously described (35).

Reverse genetics visual screen

The reverse genetics visual screen was performed as described previously (8). In brief, pools of four Dharmacon siGENOME small interfering RNAs (siRNAs) were used to silence gene expression of 340 mouse ion channel genes in mIMCD3 cells (Table S1). siRNAs were dispensed into 96-well optical bottom View Plates (Perkin Elmer) using the Bravo liquid handling platform, Lipofectamine RNAiMAX (Life Technologies) in suspension in OptiMEM was added to the wells FluidX dispenser and after 20 minutes cells in a suspension of OptiMEM were added to the wells, also using a FluidX dispenser. All knockdowns were performed in duplicate to produce two independent replicates. Cells were fixed in methanol and immunostained with acetylated alpha tubulin antibody, DAPI and TOTO3 72 hours post-transfection and imaged within 48 hours of immunostaining. Images from 6 fields of view per well were captured from 3 focal planes using a x20 air objective lens on a PerkinElmer Operetta automated imaging platform. siRNA pools targeting *Ift88*, *Mks1* and *Rpgrip1l* were used as positive controls for an effect on ciliogenesis (not shown). *Plk1* was used as a positive control for effect on cell number and as a measure of the efficiency of transfection. Non-targeting siRNAs and siRNA targeting human *MLNR* (which does not target any mouse gene) were used as negative controls.

Antibodies and reagents

Antibodies used are rabbit anti-CLCN4 (Abcam Ab 105144), rabbit anti-KCNF1 (Bioss bs12173R), rabbit anti-KCNQ1 (Alomone labs APC-022), rabbit anti-KCNJ10 (Alomone labs APC-035), mouse anti-acetylated tubulin (Sigma T6793) and mouse anti-β-actin (AC-15 Sigma A5441), rat anti-ZO-1 (Santa Cruz), rabbit anti-β-catenin (BD Bioscience).

Plasmid DNA transfection was performed with Lipofectamine2000 (Invitrogen, 11668-019), according to the supplier's protocol. Opti-MEM (Invitrogen, 31985-062) was used to dilute the plasmids KCNJ10::C-GFP (Origene RG213543), KCNQ1 and CLCN4::N-GFP, or mutant alleles.

Lipofectamine RNAimax (Invitrogen, 13778-075) was used for siRNA transfection, according to the supplier's protocol. Opti-MEM (Invitrogen, 31985-062) was used to dilute the ON-TARGETplus siRNA SMARTpools (Thermo Scientific Dharmacon):

Non-targeting pool UGGUUUACAUGUCGACUAA/ UGGUUUACAUGUUGUGUGA/ UGGUUUACAUGUUUUCUGA/ UGGUUUACAUGUUUUCCUA (D-001810-10),

mouse Ift88 CGGAGAAUGUUGAAUGUUU/ GCUUGGAGCUUAUUACAUU/

CGUCAGCUCUCACUAAUAA/ GUAGCUAGCUGCUUUAGAA (L-050417-00), mouse Kcnq1 GCAGCGCGGUGGUCAAGAA/ GAUAGGAGGCCAGACCAUU/ GGAAGUGUUUCGUGUACCA/ GAUGAGUCCUGGAGAGAAG (L-046886-00), mouse Clcn4-2 GAGCUAAUCUUGGCUAUAA/ GGAAAUGGACUCUUCUAAU/ UAGAGGAGGUCAGUUACUA/ UGACUCGGCCUGUGGAUGA (L-062747-00), mouse Kcnf1 GCGAAGACAUUGAGAUCGU/ ACACAGCGAUACCUUCAUU/ CAAGCGCAGUUUCAAGGAA/ UGAUGGAGCUGACCAACGU (L-056002-00) and mouse Kcnj10 GCACAUUGCUGACAAACGU/ GAAAUCUUCAUCACAGGUA/ GCAAUGGCGCUACAAGCUU/ GCAAAUACAUAGCUGACUU (L-042680-00) to 20 nM.

RT-qPCR

RNA was isolated, cDNA was synthesized, and RT-qPCR analysis was performed as previously described (35). The mouse primer sequences (Sigma) used and concomitant annealing temperatures are: Kcnq1 Fw 5′-CAAAGACCGTGGCAGTAAC Rv 5′-CCTTCATTGCTGGCTACAAC (55°C), Kcnf1 Fw 5′-CGTGGCAGGCGAAGACATT Rv 5′-CCCCCGCCAAACAGTTGAT (60°C), Kcnj10 Fw 5′-CCAGGTCAAATGTATTTAG Rv 5′-CAAGAGATGCATCCAGTTTATTTAG (61°C), Clcn4 Fw 5′-GCGTCTCATCGGGTTTGC Rv 5′-TTGCCACAATGCCCTCTTG (55°C), Rpl27 Fw 5′-CGCCCTCCTTTCCTTTCTGC Rv 5′- GGTGCCATCGTCAATGTTCTTC (53°C). The ΔΔCT method was used for statistical analysis to determine gene expression levels.

In vitro mutagenesis

KCNJ10 mutations were introduced through site-directed mutagenesis. Presence of the mutation in the plasmid was verified by Sanger sequencing (all primers are available upon request).

Immunofluorescence

For immunostaining, mIMCD3 cells were grown on coverslips and fixed for 5 minutes in ice cold methanol and blocked 60 minutes in 1% BSA. Primary antibody incubations (mouse anti-acetylated tubulin 1:20.000, rabbit anti-CLCN4/KCNF1/KCNQ1/KCNJ10 1:200) were performed at 4°C overnight in block. Goat anti-mouse 488/rabbit 568 Alexa secondary antibody (Invitrogen, dilution 1:500) and Hoechst333 incubations were performed for 2 hours at RT. Coverslips were mounted in Fluormount G (Cell Lab, Beckman Coulter). Confocal imaging was performed using Zeiss Confocal laser microscope and images were processed with the ZEN 2012 software. 3D spheroids matrigel assays with mIMCD3 cells were performed as previously described (9).

Western blot

Protein lysates were prepared using RIPA lysis buffer. To correct for protein content BCA protein assay (Pierce) was performed. β-actin (1:15000) was used as loading control in combination with Coomassie Blue staining. After SDS-PAGE separation and transfer, the PVDF membranes were blocked in 5% dried skim milk in TBS with 0.5% Tween. The primary antibodies rabbit anti-CLCN4 (1:500), rabbit anti-KCNQ1 (1:300), rabbit anti-KCNF1 (1:500), rabbit anti-KCNJ10 (1:500), rabbit anti-GFP (1:1000) were incubated overnight at 4°C. The secondary swine anti-rabbit and rabbit anti-mouse antibodies which are HRP conjugated (DAKO, dilution 1:2000) were incubated for 1 hour at RT. The ECL Chemiluminescent Peroxidase Substrate kit (Sigma, CPS1120-1KT) was used for development. Scans of the blots were made with the BioRad ChemiDoc XRS+ device with Image Lab software 4.0.

Histology

Kidney tissue sections of healthy Lewis rats embedded in paraffin were deparaffinized and incubated at 100°C in Citrate/HCL buffer for 15 minutes (Citrate/HCL was skipped for rabbit anti-KCNF1 staining). Sections were blocked using peroxidase block for 15 minutes followed by 5% normal goat serum (NGS) block for 30 minutes. The sections were stained with rabbit anti-KCNJ10, rabbit anti-KCNQ1 (1:200), rabbit anti-CLCN4 (1:300) and rabbit-anti-KCNF1 (1:50) in 1% NGS 1 hour at RT. Finally, BrightVision Poly HRP goat anti-rabbit IgG (Immunologic, DPVR55HRP) was incubated for 30 minutes RT. NovaRED substrate kit for Peroxidase (Vector, SK-4800) was used and counterstained with hematoxylin. Photos were made using a 40x objective.

FACS

To quantify cell cycle phase distribution, cells were incubated with 10 μM BrdU for 30 minutes and fixed in ice cold 70% EtOH. Samples were stained for FACS analysis with BrdU mouse mAb Alexa Fluor 647 conjugate (1:200; Invitrogen) in 0.1% BSA-PBS-T for 1 hour on ice, and DAPI in PBS. 10,000 events were measured with a BD FACSCanto II flow cytometer and analyzed using BD FACSDiva Software.

Statistics

The effect of siRNA knockdown on ciliogenesis in the screen was assessed by calculating the percentage of cells with a single cilium, with the statistical significance of this effect assessed by calculating *z* scores (z_{cilia}). *z* scores were also calculated for the effect of the knockdown on cell number (z_{cell}), to enable the exclusion of any effects of cell proliferation or apoptosis on ciliogenesis since these could be due to non-specific secondary processes. We considered a siRNA to have a significant effect on ciliogenesis if $z_{cilia} < -2$ but $z_{cell} \geq -2$ in both independent experimental replicates.

In the follow-up experiments, *p*-values were calculated of normally distributed data sets using a two-tailed Student's t test, or One-way ANOVA with Dunnett's post-hoc test, or Two-way ANOVA with Bonferroni post-hoc tests. Statistical analyses represent the mean of at least three independent experiments; error bars represent standard error of mean (s.e.m.) or otherwise indicated.

Acknowledgements

This work was supported by the European Union FP7/2009 Consortium "SYSCILIA" [grant number 241955 to RHG, CAJ]; the Dutch Kidney Foundation "KOUNCIL" [CP11.18 to NVK, ML, RHG]; and by the Medical Research Council [MR/M000532/1 to CAJ].

We thank Sebastiaan Noordegraaf voor RT-qPCR, Glenn van de Hoek and Ka Man Wu for *in vitro* mutagenesis, Jaap Joles for rat kidney sections, as well as Oliver Blacque (Dublin) and Joost Hoenderop (Nijmegen) for experiments not included in the manuscript.

The Cell Microscopy Center and the Flow Cytometry Core Facility at the UMC Utrecht provided expert services. CLCN4 pcDNA6.2-N-GFP was a kind gift from Erica Davis (Duke University), and wild-type and variant KCNQ1 plasmids were a kind gift from Marcel van der Heyden and Paul de Bakker (Utrecht University).

REFERENCES

1. Satir P, Christensen ST. Structure and function of mammalian cilia. *Histochemistry and cell biology.* 2008;129(6):687-693.
2. Oh EC, Katsanis N. Cilia in vertebrate development and disease. *Development.* 2012;139(3):443-448.
3. D'Angelo A, Franco B. The primary cilium in different tissues-lessons from patients and animal models. *Pediatric nephrology.* 2011;26(5):655-662.
4. Basten SG, Giles RH. Functional aspects of primary cilia in signaling, cell cycle and tumorigenesis. *Cilia.* 2013;2(1):6.
5. Baker K, Beales PL. Making sense of cilia in disease: the human ciliopathies. *American journal of medical genetics. Part C, Seminars in medical genetics.* 2009;151C(4):281-295.
6. Wilson PD. Polycystic kidney disease. *The New England journal of medicine.* 2004;350(2):151-164.
7. Loudon KW, Fry AC. The renal channelopathies. *Annals of clinical biochemistry.* 2014;51(Pt 4):441-458.
8. Wheway G, Schmidts, M., Mans, D. A., Szymanska, K., Nguyen, T. T., Racher, H., Phelps, I. G., Toedt, G., Kennedy, J., Wunderlich, K. A., et. al. An siRNA-based functional genomics screen for the identification of regulators of ciliogenesis and ciliopathy genes. *Nat Cell Biol.* 2015;(in press).
9. Giles RH, Ajzenberg H, Jackson PK. 3D spheroid model of mIMCD3 cells for studying ciliopathies and renal epithelial disorders. *Nature protocols.* 2014;9(12):2725-2731.
10. Pazour GJ, Dickert BL, Vucica Y, et al. Chlamydomonas IFT88 and its mouse homologue, polycystic kidney disease gene tg737, are required for assembly of cilia and flagella. *The Journal of cell biology.* 2000;151(3):709-718.
11. Scheel O, Zdebik AA, Lourdel S, Jentsch TJ. Voltage-dependent electrogenic chloride/proton exchange by endosomal CLC proteins. *Nature.* 2005;436(7049):424-427.
12. Jespersen T, Rasmussen HB, Grunnet M, et al. Basolateral localisation of KCNQ1 potassium channels in MDCK cells: molecular identification of an N-terminal targeting motif. *Journal of cell science.* 2004;117(Pt 19):4517-4526.
13. Reichold M, Zdebik AA, Lieberer E, et al. KCNJ10 gene mutations causing EAST syndrome (epilepsy, ataxia, sensorineural deafness, and tubulopathy) disrupt channel function. *Proceedings of the National Academy of Sciences of the United States of America.* 2010;107(32):14490-14495.
14. Parrock S, Hussain S, Issler N, et al. KCNJ10 mutations display differential sensitivity to heteromerisation with KCNJ16. *Nephron. Physiology.* 2013;123(3-4):7-14.
15. Wang Q, Curran ME, Splawski I, et al. Positional cloning of a novel potassium channel gene: KVLQT1 mutations cause cardiac arrhythmias. *Nature genetics.* 1996;12(1):17-23.
16. Sanguinetti MC, Curran ME, Zou A, et al. Coassembly of K(V)LQT1 and minK (IsK) proteins to form cardiac I(Ks) potassium channel. *Nature.* 1996;384(6604):80-83.
17. Neyroud N, Tesson F, Denjoy I, et al. A novel mutation in the potassium channel gene KVLQT1 causes the Jervell and Lange-Nielsen cardioauditory syndrome. *Nature genetics.* 1997;15(2):186-189.
18. Chen YH, Xu SJ, Bendahhou S, et al. KCNQ1 gain-of-function mutation in familial atrial fibrillation. *Science.* 2003;299(5604):251-254.
19. Bellocq C, van Ginneken AC, Bezzina CR, et al. Mutation in the KCNQ1 gene leading to the short QT-interval syndrome. *Circulation.* 2004;109(20):2394-2397.
20. Lee MP, Hu RJ, Johnson LA, Feinberg AP. Human KVLQT1 gene shows tissue-specific imprinting and encompasses Beckwith-Wiedemann syndrome chromosomal rearrangements. *Nature genetics.* 1997;15(2):181-185.
21. Gussak I, Gussak HM. Sudden cardiac death in nephrology: focus on acquired long QT syndrome. *Nephrology, dialysis, transplantation : official publication of the European Dialysis and Transplant Association - European Renal Association.* 2007;22(1):12-14.
22. Kapplinger JD, Tester DJ, Salisbury BA, et al. Spectrum and prevalence of mutations from the first 2,500 consecutive unrelated patients referred for the FAMILION long QT syndrome genetic test. *Heart rhythm : the official journal of the Heart Rhythm Society.* 2009;6(9):1297-1303.
23. Stattin EL, Bostrom IM, Winbo A, et al. Founder mutations characterise the mutation panorama in 200 Swedish index cases referred for Long QT syndrome genetic testing. *BMC cardiovascular disorders.* 2012;12:95.
24. Tanaka T, Nagai R, Tomoike H, et al. Four novel KVLQT1 and four novel HERG mutations in familial long-QT syndrome. *Circulation.* 1997;95(3):565-567.
25. Refsgaard L, Holst AG, Sadjadieh G, Haunso S, Nielsen JB, Olesen MS. High prevalence of genetic variants previously associated with LQT syndrome in new exome data. *European journal of human genetics : EJHG.* 2012;20(8):905-908.
26. Tester DJ, Will ML, Haglund CM, Ackerman MJ. Compendium of cardiac channel mutations in 541 consecutive unrelated patients referred for long QT syndrome genetic testing. *Heart rhythm : the official journal of the Heart Rhythm Society.* 2005;2(5):507-517.

27. Sang L, Miller JJ, Corbit KC, et al. Mapping the NPHP-JBTS-MKS protein network reveals ciliopathy disease genes and pathways. *Cell.* 2011;145(4):513-528.
28. Barr MM, DeModena J, Braun D, Nguyen CQ, Hall DH, Sternberg PW. The Caenorhabditis elegans autosomal dominant polycystic kidney disease gene homologs lov-1 and pkd-2 act in the same pathway. *Current biology : CB.* 2001;11(17):1341-1346.
29. Nauli SM, Alenghat FJ, Luo Y, et al. Polycystins 1 and 2 mediate mechanosensation in the primary cilium of kidney cells. *Nature genetics.* 2003;33(2):129-137.
30. Low SH, Vasanth S, Larson CH, et al. Polycystin-1, STAT6, and P100 function in a pathway that transduces ciliary mechanosensation and is activated in polycystic kidney disease. *Developmental cell.* 2006;10(1):57-69.
31. Ludington WB, Ishikawa H, Serebrenik YV, et al. A systematic comparison of mathematical models for inherent measurement of ciliary length: how a cell can measure length and volume. *Biophysical journal.* 2015;108(6):1361-1379.
32. Ackerman MJ, Clapham DE. Ion channels--basic science and clinical disease. *The New England journal of medicine.* 1997;336(22):1575-1586.
33. Slough J, Cooney L, Brueckner M. Monocilia in the embryonic mouse heart suggest a direct role for cilia in cardiac morphogenesis. *Developmental dynamics : an official publication of the American Association of Anatomists.* 2008;237(9):2304-2314.
34. Li Y, Klena NT, Gabriel GC, et al. Global genetic analysis in mice unveils central role for cilia in congenital heart disease. *Nature.* 2015;521(7553):520-524.
35. Slaats GG, Ghosh AK, Falke LL, et al. Nephronophthisis-associated CEP164 regulates cell cycle progression, apoptosis and epithelial-to-mesenchymal transition. *PLoS genetics.* 2014;10(10):e1004594.

SUPPLEMENTAL FIGURES

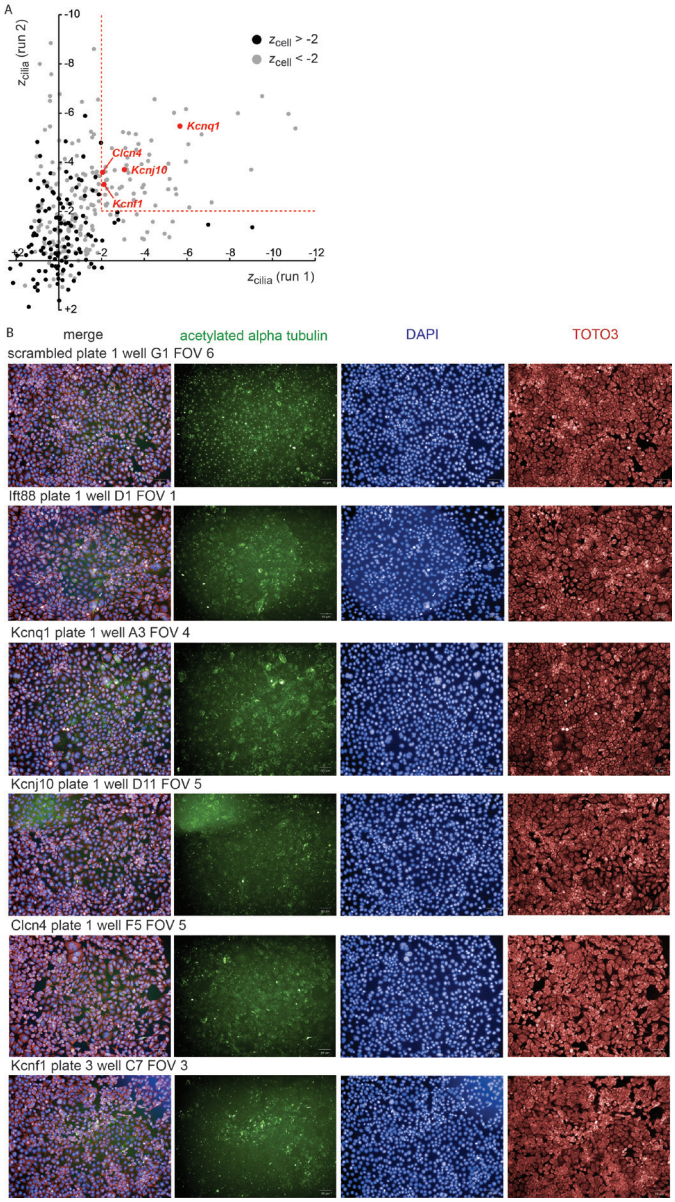

Supplemental 1. Scatter-plot and images of the siRNA-based ion channels screen
(**A**) Scatter-plot of *z*-scores from both runs of the screen. The cut-offs of *z* cilia <-2 for both run 1 and run 2 are shown with dotted red lines. Grey and black points discriminate between *z* cell >-2 or <-2 (grey means exclusion). (**B**) Representative images of the negative control (scrambled), the positive control (*Ift88*) and the four ion channel candidate genes. Immunostaining of mIMCD3 cells for cilia (acetylated α-tubulin, green) and TOTO3 (red), with DAPI counterstaining (blue) shows loss of cilia after *Ift88, Kcnj10, Kcnq1, Kcnf1* and *Clcn4* siRNA transfection.

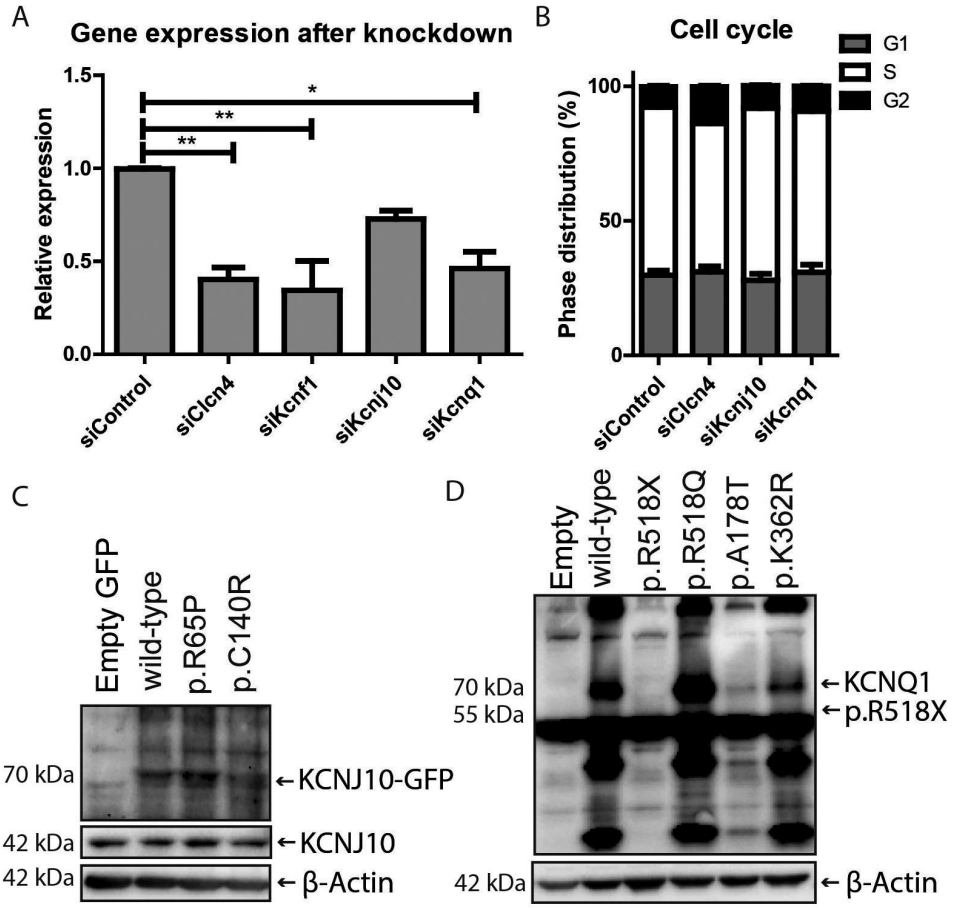

Supplemental 2. siRNA efficiency and Western blot of overexpression of KCNJ10-GFP and KCNQ1 variant alleles

(**A**) Gene expression analyzed by RT-qPCR (reference gene *Rpl27*) of the four ion channels measured in mIMCD3 cells after siRNA transfection targeting *Clcn4, Kcnf1, Kcnj10* or *Kcnq1*. Gene expression is normalized to siControl transfected cells, set to 1 (*p<0.05 and **p<0.01, n=3, mean and s.e.m., One-way ANOVA, Dunnett's). (**B**) Cell cycle distribution measurement of unsynchronized mIMCD3 cells after siRNA transfection targeting *Clcn4, Kcnj10* or *Kcnq1* reveals unchanged cell populations in G1- (grey), S- (white), or G2-phase (black). (10,000 events measured in duplicate; n=3). (**C**) Immunoblot for KCNJ10 (42 kDa) in IMCD3 lysates transfected with wild-type KCNJ10-GFP and mutant alleles (70 kDa). β-actin is used as loading control (42 kDa). (**D**) Immunoblot for KCNQ1 in IMCD3 lysates transfected with wild-type KCNQ1 and mutant alleles (70 kDa). No KCNQ1-p.R518X is expressed (~55 kDa). β-actin (42 kDa) is used as loading control.

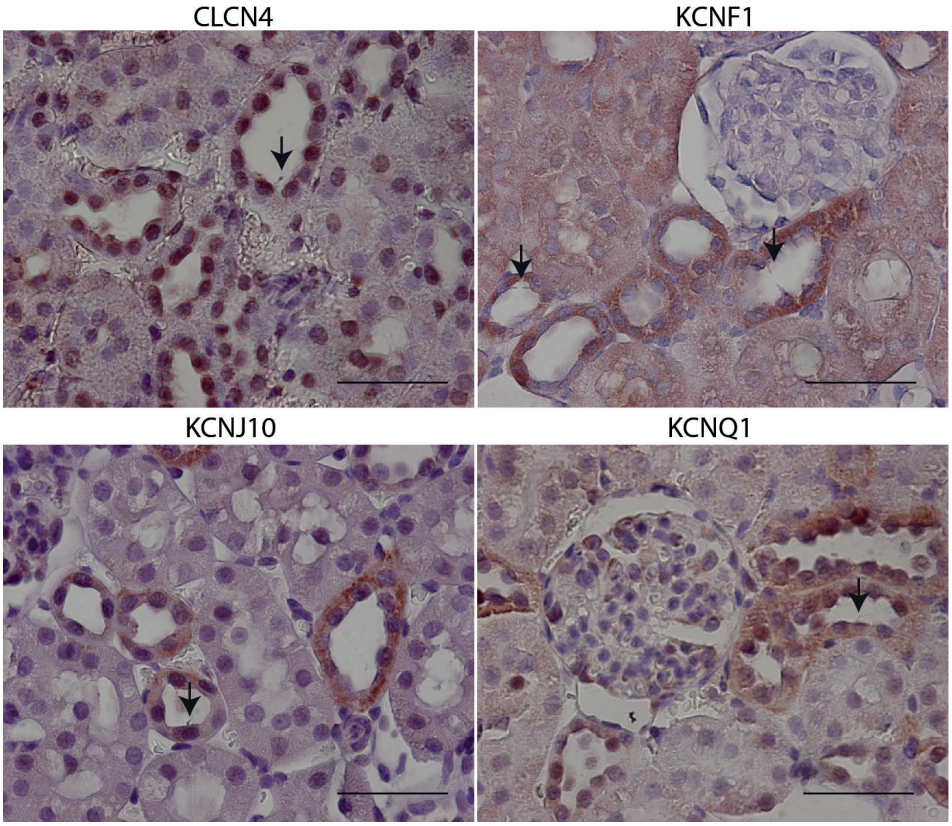

Supplemental 3. Localization and expression of ion channels in the kidney
Rat paraffin-embedded healthy kidney sections were stained (immunohistochemistry) for the four ion channels CLCN4, KCNF1, KCNJ10 and KCNF1. Endogenous protein expression localizes to tubules (brown). Arrows indicate cilia at apical site of tubules. Scale bar 50 µm.

SUPPLEMENTAL TABLE

Table S1. Ion channel z scores. siRNA-based reverse genetics screen of 340 ion channels in the mouse genome in mIMCD3 cells. *z* scores (z_{cilia} and z_{cell}) for both experimental runs performed are presented. http://www.syscilia.org/Giles/

CHAPTER 4

MKS1 regulates ciliary INPP5E levels in Joubert syndrome

Manuscript submitted

Gisela G. Slaats*, Christine R. Isabella*, Hester Y. Kroes*, Jennifer C. Dempsey, Hendrik Gremmels, Glen R. Monroe, Karen J. Duran, Jonathan Adkins, Sairam A. Kumar, Dana M. Knutzen, Nine V. Knoers, Nancy J. Mendelsohn, David Neubauer, Sotiria D. Mastroyianni, Julie Vogt, Lisa Worgan, Natalya Karp, Sarah Bowdin, Ian A. Glass, Melissa A. Parisi, Edgar A. Otto, Colin A. Johnson, Friedhelm Hildebrandt, Gijs van Haaften, Rachel H. Giles#*, Dan Doherty#*

* These authors contributed equally
and # these authors also contributed equally

ABSTRACT

Background

Joubert syndrome (JS) is a recessive ciliopathy characterized by a distinctive brain malformation "the molar tooth sign". Mutations in at least 24 genes cause JS, and ten of these genes are also mutated in fetuses with Meckel syndrome (MKS).

Methods

Cilia of fibroblasts from individuals with *MKS1*-related JS are examined. Furthermore, JS-associated *MKS1* variants are tested in 3D spheroid rescue assays.

Results

We confirm the reported allelism by identifying *MKS1* mutations (eight of them previously unreported) in nine individuals with JS. A minority of the individuals with *MKS1*-related JS have MKS features such as cystic dysplastic kidneys and polydactyly. In contrast to the truncating *MKS1* mutations associated with MKS, all of the individuals with *MKS1*-related JS carry at least one non-truncating mutation. We demonstrate that fibroblasts from individuals with *MKS1*-related JS make normal or fewer cilia than control fibroblasts, their cilia are more variable in length than controls, and show impaired ciliary localization of ARL13B and INPP5E. Additionally, *MKS1* mutant alleles affect cilia in 3D spheroids.

Conclusions

MKS1 functions in the transition zone at the base of the cilium to regulate ciliary protein content. Mutations in *INPP5E* also cause JS, but instead of being a component of the transition zone, INPP5E localizes to the cilium and requires the function of ARL13B, another JS-related protein, for its localization. Our findings in patient fibroblasts support the notion that loss of INPP5E function, due to either mutation or mislocalization, is a key mechanism underlying JS, downstream of MKS1 and ARL13B function.

INTRODUCTION

Human ciliopathies embody a rapidly growing group of disorders characterized by dysfunction of the primary cilium, a membrane-bound bundle of microtubules that projects from the apical surface of most cells (1). In addition to transducing chemo-, mechano- and/or light-sensation depending on the cell type, primary cilia mediate among others sonic hedgehog, Wnt, Hippo, PDGFα and G-protein coupled receptor signaling. Dysfunction of primary cilia results in a spectrum of phenotypes including central nervous system malformations, retinal dystrophy, cystic renal disease, and hepatic fibrosis (2).

Joubert syndrome (JS; MIM# 213300) and Meckel syndrome (MKS; MIM# 249000) are two recessive ciliopathies with overlapping phenotypic features. The defining feature of JS is the molar tooth sign (MTS) on brain magnetic resonance imaging (MRI): cerebellar vermis hypoplasia, thick, elongated and horizontally-oriented superior cerebellar peduncles, and a deep interpeduncular fossa (3). Clinically, JS is characterized by cognitive impairment, hypotonia, ataxia, abnormal eye movements, and episodic apnea and/or tachypnea in the neonatal period (4). Variable additional features have been observed, including other central nervous system anomalies (agenesis of the corpus callosum, polymicrogyria, heterotopia and occipital encephalocele), chorioretinal coloboma, retinal dystrophy, cystic renal disease, hepatic fibrosis, and polydactyly (5-16).

MKS is characterized by a posterior fossa brain malformation (typically occipital encephalocele), cystic renal disease, congenital hepatic fibrosis (e.g. ductal plate malformation), and postaxial polydactyly (17 18). Phenotypic variability is also present, and other characteristics can include microphthalmia, situs inversus, skeletal abnormalities and Dandy-Walker malformation (19 20). Whereas individuals with JS typically survive beyond infancy, MKS is usually lethal in the fetal or neonatal period.

To date, mutations in at least 24 genes have been shown to cause JS, including *NPHP1*, *AHI1, CEP290, RPGRIP1L*, *TMEM67*, *ARL13B*, *CC2D2A*, *INPP5E*, *OFD1*, *TMEM216*, *TCTN1*, *TCTN2*, *KIF7*, *TMEM237, CEP41, TMEM138*, *TMEM231*, *C5ORF42*, *TCTN3, IFT172, PDE6D, MKS1* and *CSPP1, B9D1* (21-23). Mutations in at least 12 genes have been shown to cause MKS, including *MKS1*, *TMEM216* (*MKS2*), *TMEM67* (*MKS3*), *CEP290* (*MKS4*), *RPGRIP1L* (*MKS5*), *CC2D2A* (*MKS6*), *NPHP3 (MKS7)*, *TCTN2* (*MKS8), B9D1 (MKS9)*, *B9D2 (MKS10), TMEM231 (MKS11),* and *TCTN3* (23). Different mutations in at least ten of these genes, can cause either JS or MKS, supporting the notion that JS and MKS represent mild and severe presentations of the same biological disorder. Due to the genetic overlap between JS and MKS (22 24 25), we evaluated a large cohort of individuals with JS for mutations in *MKS1*.

Most of the proteins encoded by genes involved in JS and MKS localize to a structure at the proximal part of the cilium called the transition zone (TZ) (25 26). The TZ anchors the cilium to the plasma membrane, and both restricts and facilitates the movement of proteins

in and out of the cilium (26 27). A few of the JS genes, among others *ARL13B* (28), *INPP5E* (29), *CSPP1* (30) and *IFT172* (31), encode proteins that localize to the cilium. Ciliary localization of ARL13B depends on TZ function, while ciliary localization of INPP5E depends on ARL13B, CEP164 and PDE6D function (32-34). Therefore, INPP5E dysfunction (due to mutation or mislocalization) is likely to be key to the JS disease mechanism.
Similar to a recent report of two individuals with JS with biallelic *MKS1* mutations (22), we identify mutations in *MKS1* as the cause of JS in nine families, supporting the notion of genetic overlap between JS and MKS. These mutations (eight of them previously unreported) are associated with variable defects in cilium length and number in patient fibroblasts, but a consistent decrease in ciliary localization of INPP5E and ARL13B, confirming *in vivo* and *in vitro* studies showing that MKS1-dependent INPP5E localization, likely through effects on ARL13B localization, is a central molecular defect underlying JS development.

RESULTS

Mutations in *MKS1* cause Joubert syndrome

We sequenced all coding exons of *MKS1* including at least 10 base pairs of flanking intronic sequence in a cohort of 435 individuals with JS from 371 families using next generation targeted sequencing methods (36). Individuals with known causes were not excluded. We identified *MKS1* mutations in nine families (Table 1 and Figure 1M). In contrast to previously published mutations identified in fetuses with MKS, most of the mutations in our cohort are not predicted to truncate the protein. All of the single nucleotide changes were identified in <0.02% of a large number of adults without congenital malformations sequenced as part of the NHBLI Exome Sequencing Project (ESP). Since insertion-deletion variants are not reliably included in the ESP data set, we evaluated 182 neurologically normal controls (Coriell panels NDPT020 and NDPT090 - http://ccr.coriell.org), none of whom carried the c.1115_1117delCCT variant. In addition, none of the nine individuals with *MKS1* mutations had biallelic rare, deleterious variants in the following genes known to be associated with JS: *NPHP1*, *AHI1, CEP290, RPGRIP1L*, *TMEM67*, *ARL13B*, *CC2D2A*, *INPP5E*, *OFD1*, *TMEM216*, *TCTN1*, *TCTN2*, *KIF7*, *TMEM237, CEP41, TMEM138*, *TMEM231*, *C5ORF42, IFT172, TCTN3, B9D1, C2CD3* and *CSPP1*.

Individuals with *MKS1*-related Joubert syndrome rarely have features of Meckel syndrome

All individuals with *MKS1* mutations have characteristic brain imaging findings of JS (Figure 1A-L). In addition to the MTS, individuals with JS can have brain abnormalities such as ventriculomegaly, heterotopia, agenesis of the corpus callosum and occipital encephalocele (15 40).

Table 1. *MKS1* mutations in individuals with Joubert syndrome (mutations in bold have not been previously reported)

Subject	Origin	cDNA change NM_017777.3	Protein change	Controls	P2[1]	Age (yr)	MTS	OE	Ret	Col	Kid	Liv	PD	Other
JBTS-10	Mixed N. European	c.417G>A **c.1208C>T**	p.F88_E139del[2] **p.S403L**	1/8246 0/8486	NA 1.0/1.0[3]	15	+	-	+	-[4]	-	-	-	Bilateral ptosis, cryptorchidism, clinodactyly
UW031-3	India	**c.1528dupC** **c.1528dupC**	**p.R510Pfs*81** **p.R510Pfs*81**	NA	NA	12	+	-	-	-	-	-	-	Sleep apnea treated by T&A
UW090-3	Turkey	c.262-37_179del c.262-37_179del	p.F88_E139del p.F88_E139del	NA	NA									
UW091-3	Pakistan	**c.55G>T** **c.55G>T**	**p.D19Y** **p.D19Y**	0/7590	1.0/1.0[3]	26	+	-	-[5]	-	+	+	-	OMA, deceased
UW092-3	Greece	**c.381delC** c.1115_1117delCCT	**p.Y128Tfs*17** p.S372del	NA 0/170	NA NA	12	+	-	-	-	-	-	-	Ptosis, functions 1 grade behind in school
UW093-3	Serbia	c.1115_1117delCCT c.1115_1117delCCT	p.S372del p.S372del	0/170	NA	6	+	-	-	-	-	-	-	Strabismus
UW150-3	Slovenia	**c.1589-2A>T** **c.1589-2A>T**	**splice** **splice**	0/8230	NA	11	+	-	-	+	-	-	-	Seizures, wheelchair-bound
JBTS-153	Greece Trinidad	c.1115_1117delCCT **c.950G>A**	p.S372del **p.G317E**	0/170 0/8314	NA 1.0[3]	4	+	-	+[6]	-[7]	+[8]	+[9]	+[10]	Critical aortic stenosis, bicuspid aortic valve, ASD, left 3rd nerve palsy, strabismus, left ptosis, vertical tali
JBTS-3504	The Netherlands	**c.157dupG** **c.625C>T**	**p.D53Gfs*6** **p.P218S**	0/8310 0/8484	NA 1.0[3]	14	+	-	-	-	-	-	-	OMA, tachypnea/ apnea), autism, tumor cordis[11]

ASD: Atrial Septal Defect; Col: coloboma; Kid: kidney disease; Liv: liver fibrosis; MTS: molar tooth sign; NA: Not Applicable, ND: Not Documented, OE: occipital encephalocele; OMA: oculomotor apraxia. PD: polydactyly; Ret: retinal dystrophy; T & A, tonsillectomy and adenoidectomy.
[1]PolyPhen-2 scores (HumDiv/HumVar); [2]Based on RT-PCR data in Consugar et al. 2007; [3]Probably damaging; [4]left optic pit; [5]thin retinal pigment epithelium and "choroidal pattern" on optical computed tomography; [6]abnormal electroretinogram; [7]large left optic disc; [8]echogenic kidneys on ultrasound; [9]mildly increased liver echogenicity and mildly enlarged spleen on ultrasound, mildly elevated gamma-glutamyl transpeptidase; [10]bilateral postaxial; [11]small tumor in myocardium of right ventricle, no functional consequences.

However, the only other brain imaging abnormality we observed in these individuals was an interpeduncular heterotopia in JBTS-153. Clinically, the affected individuals are indistinguishable from individuals with JS due to other genetic causes but strikingly different from fetuses with MKS (Table 1). Only one individual has polydactyly, another has coloboma, and two have kidney and liver disease, while none has other common features of MKS

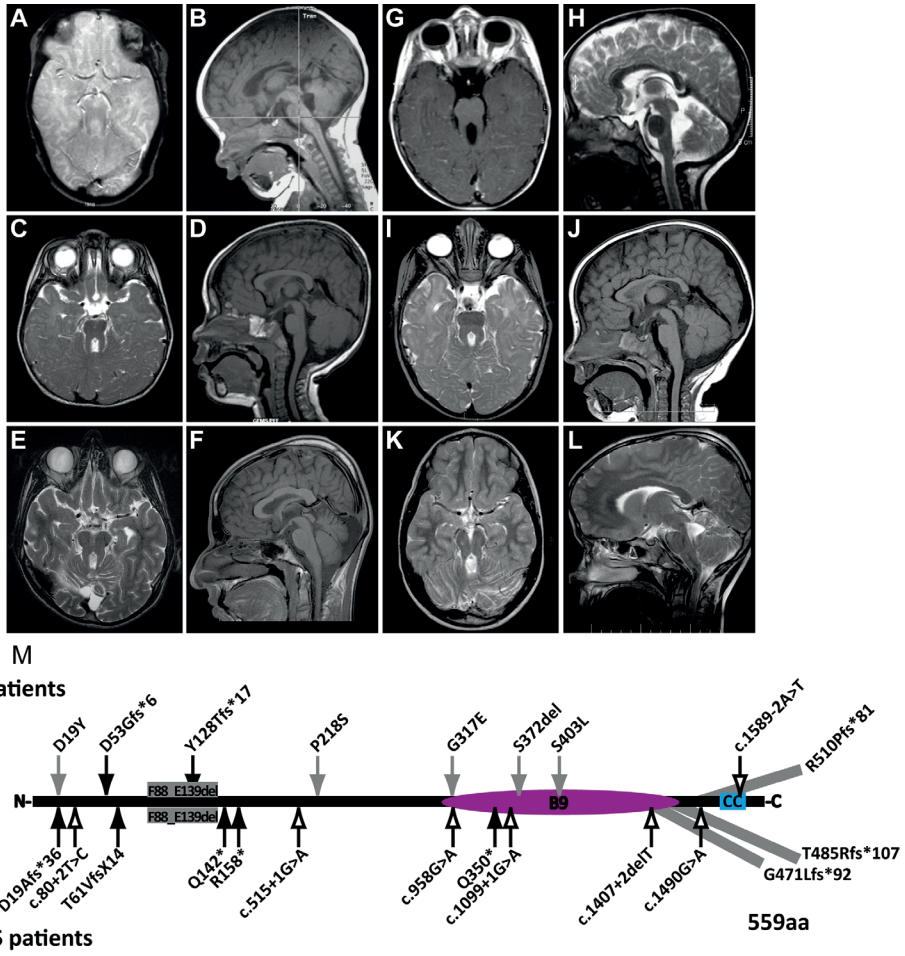

Figure 1. MRI findings and mutations in individuals with *MKS1*-related Joubert syndrome
(A-L) All affected individuals had classic imaging findings of JS including cerebellar vermis hypoplasia, and thick, horizontally-oriented superior cerebellar peduncles. (A-B) is JBTS-10, (C-D) is UW031-3, (E-F) is UW091-3, (G-H) is UW092-3, (I-J) is UW093-3, (K-L) is JBTS-3504 (A, C, E, I, K) are T2-weighted axial views, (G) is a T1-weighted axial view, (B, D, F, J) are T1-weighted sagittal views, (H, L) are T2-weighted sagittal views; **(M)** *MKS1* mutations in individuals with JS and MKS based on sequence NM_017777.3. p.G471Lfs*92 extends the protein by 4 amino acids; p.Thr485Argfs*107 extends the protein by 33 amino acids; p.R510Pfs*81 extends protein by 40 amino acids; MKS1 protein (559 aa). Black arrows, truncating mutations; Gray arrows, non-truncating mutations; Outline arrows, splice site mutations. CC, coiled-coil; B9, B9-domain.

(encephalocele, cleft palate, or skeletal dysplasia). One individual died at 26 years of age, while the other individuals are still alive, ranging from 4 to 15 years of age, which is in contrast to individuals with MKS who usually die *in utero* or neonatally.

Cilium length in fibroblasts from individuals with *MKS1*-related JS tends to be longer and more variable than controls

To determine the cellular effects of the *MKS1* mutations, we evaluated cilium number and length in primary skin fibroblasts from three of the affected individuals (JBTS-10, JBTS-153, and JBTS-3504), a single fetus with MKS (MKS-158; Table S1 Subject: Khaddour '07:562), as well as the carrier parents of JBTS-3504 (Parent-3229 and Parent-1753) and healthy, non-carrier controls (Ctrl-10 and Ctrl-117, and Fetal Ctrl-26153), using acetylated α-tubulin antibody to mark the ciliary axoneme and γ-tubulin antibody to mark the basal body (Figure 2A, S2). To control for *MKS1*-specific effects, we also used fibroblast lines from JS patients with biallelic *ARL13B* (ARL13B-277) [28) and *INPP5E* (INPP5E-171) (38) mutations (See Material and Methods; Cell culture section). Typically, 70-90% of control fibroblasts have cilia after 48 hours of serum starvation (Figure 2B). In contrast, JBTS-10 fibroblasts were only 52.7% ciliated ($p<0.05$), and MKS-158 fibroblasts were 24,5% ciliated ($p<0.001$), while ciliation of fibroblasts from the other patients and the parents of JBTS-3504 was not statistically different from the controls. Cilium length is also consistent in controls, typically measuring ~3 μm (range 0.2-7.6 μm), based on both acetylated α-tubulin and ARL13B antibody staining (Figure 2A). The median length (L) was significantly longer in fibroblasts from JBTS-10 and JBTS-3504 (~4μm; $p<0.001$). Additionally, all of the affected JBTS fibroblasts made cilia >8μm, which are longer than the cilia of control fibroblasts, demonstrating higher ciliary length variance (σ^2; $p<0,001$; Figure 2C). MKS-158 fibroblasts have more variance in ciliary length compared to Fetal Ctrl-26153 as well ($p<0.001$).

Functional effects of *MKS1* mutations on primary cilia

Truncating presumed null-allele mutations in *MKS1* result in the severe Meckel syndrome. To address the functional significance of several of the non-truncating *MKS1* variants identified in individuals with JS, we used a 3D mouse IMCD3 (Inner Medullary Collecting Duct 3) cell culture assay previously used to model ciliopathies (39). We validated the siRNA knockdown of *Mks1* by RT-qPCR, western blot and immunofluorescence (Suppl Figure 1A-D). In IMCD3 cells grown as a monolayer, *Mks1* knockdown results in decreased ciliation ($p<0.004$; Suppl Figure 1B). Next, IMCD3 cells were transfected with control or *Mks1* siRNA in conditions promoting 3D spheroid growth. Immunostaining the spheroids for cilia, tight junctions and adherens junctions revealed that ciliation was reduced >50% upon MKS1 depletion ($p<0.0003$; Figure 3A-B). No gross architectural differences of spheroids were found. Rescue experiments were performed by reconstituting MKS1-depleted IMCD3 cells with wild-type and patient-based mutant expression constructs of human *MKS1*,

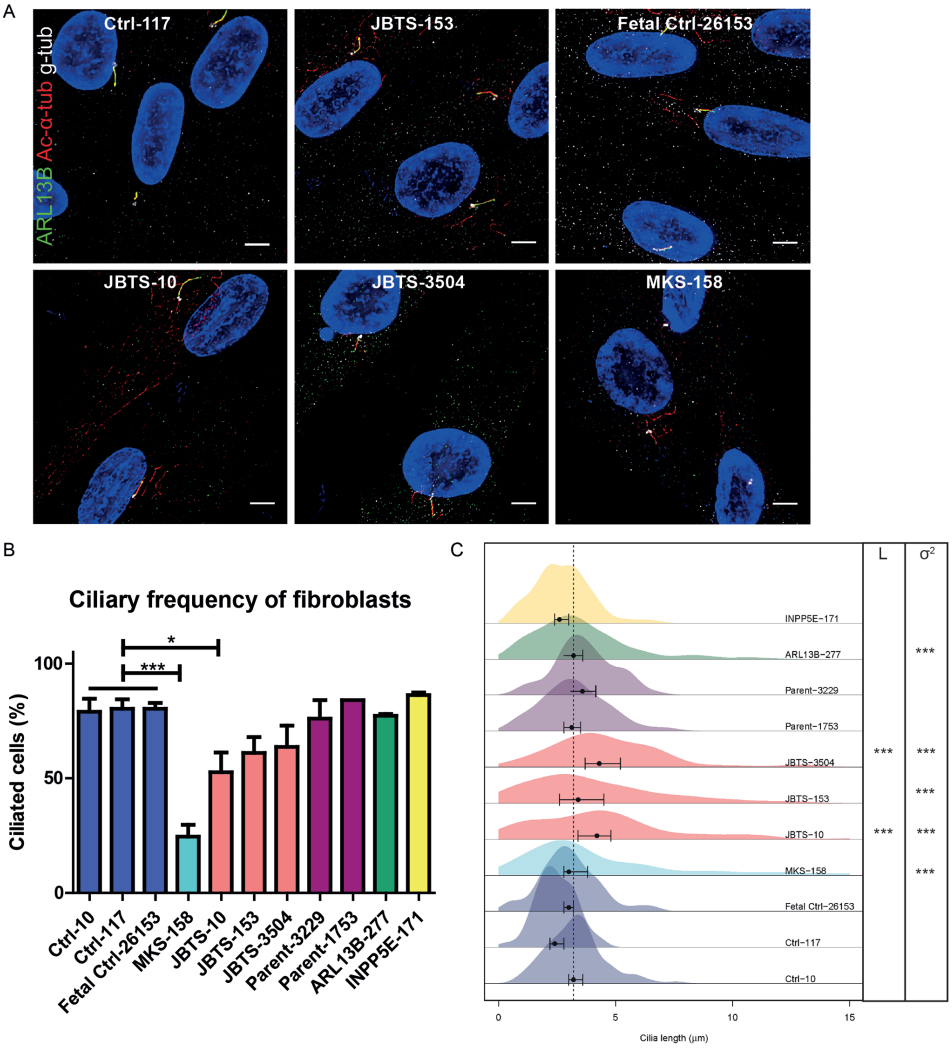

Figure 2. Fibroblasts from individuals with *MKS1*-related Joubert syndrome display primary cilia defects

(A) Immunostaining of fibroblasts derived from skin biopsies of JBTS-10, JBTS-153, JBTS-3504, MKS-158, and controls. ARL13B (green), gamma tubulin (g-tub; white) and cilia (acetylated tubulin, red; scalebar 5 µm). Brightness and contrast were identically adjusted across photos for visualization purposes; original data is in Figure S2. **(B)** Quantification of cilia frequency (mean and SEM) in fibroblasts from controls (Ctrl-10, Ctrl-117, Fetal Ctrl-26153), three individuals with JS (JBTS-10, JBTS-153 and JBTS-3504), the carrier parents of JBTS-3504 (Parent-3229 and Parent-1753), one fetus with *MKS1*-related MKS (MKS-158), and ARL13B (ARL13B-277) and INPP5E (INPP5E-171) mutants. * indicates $p<0.05$, *** $p<0.001$ (One-way ANOVA). **(C)** Kernel density plots depicting distribution of cilia length (x-axis) in fibroblasts obtained from individuals with different *MKS1* mutations and controls (y-axis). Points and error bars represent medians and 99% confidence intervals respectively. JBTS-10 and JBTS-3504 have longer (L) cilia than the controls Ctrl-10 and Ctrl-117. *** indicates $p<0.001$ (Kruskal-Wallis test). Variance (σ^2) in ciliary length was different between Fetal Ctrl-26153 and MKS-158, and between Ctrl-10 and Ctrl-117 compared to JBTS-10, JBTS-153, JBTS-3504 and ARL13B-277. *** indicates $p<0.001$ (F-test). Number of cells scored 100-300 in 2 batches.

which is not targeted by the mouse siRNA against *Mks1* (Figure S1G). The ciliation defect caused by si*Mks1* was completely rescued by wild-type (WT) MKS1 or MKS1-p.S403L ($p<0.01$) and partly rescued by MKS1-p.P218S ($p<0.06$) (Figure 3B). A potential dominant negative effect on ciliary frequency was observed after transfection with MKS1-p.D19Y ($p<0.001$; Figure 3A). Expression of the alleles (in a shorter human isoform of MKS1 construct; full-length was not available) was validated by western blot (Figure 3C), and shows different migration from the endogenous full-length mouse MKS1 protein.

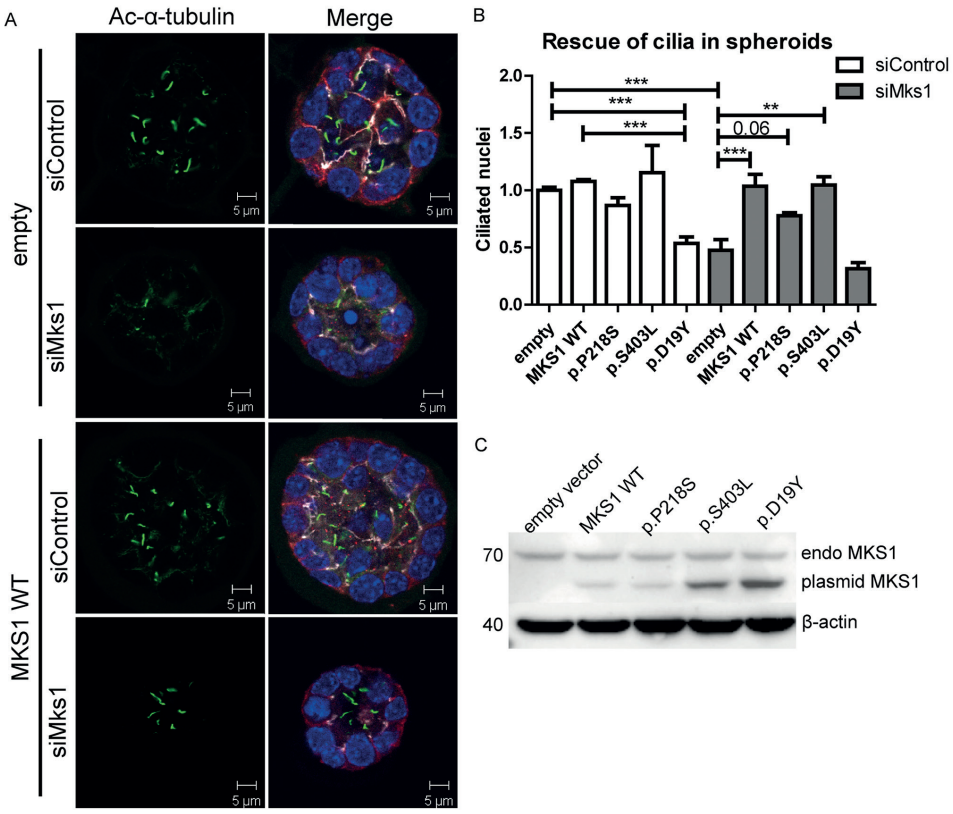

Figure 3. *Mks1* knockdown impairs ciliogenesis in 3D spheroid culture of IMCD3 cells
(A) Immunostaining of spheroids for cilia (acetylated tubulin, green), tight junctions (ZO1, white), and adherens junctions (β-catenin, red) with DAPI counterstaining (blue) shows loss of cilia after *Mks1* siRNA transfection, and rescue by MKS1-WT. **(B)** Quantification of ciliary frequency in spheroids shows significant differences between control spheroids and spheroids depleted for MKS1 (indicates $p<0.0003$), and a potential dominant negative effect of transfection with MKS1-p.D19Y ($p<0.001$). Complete rescue of ciliary frequency was obtained upon transfection with MKS1-WT or MKS1-p.S403L ($p<0.01$), and a partial rescue upon transfection with MKS1-p.P218S ($p<0.06$). 50 spheroids were scored per condition. Error bars represent SEM (n = 3 experiments), **(C)** Immunoblot for MKS1 in IMCD3 lysates (siControl) transfected with different MKS1 alleles. Upper band indicates equal endogenous levels of MKS1 in IMCD3 cells. Lower band indicates different MKS1 alleles (not full-length human MKS1 construct). β-actin is used as loading control.

Despite transfection with equal amounts of DNA, expression differed across the mutant constructs, whereas endogenous MKS1 expression and β-actin levels were equal.

ARL13B and INPP5E distribution is altered in fibroblasts from individuals with *MKS1*-related JS

While most of the proteins associated with JS localize to the TZ, where they seem to be involved in the TZ's gate keeping function, several (ARL13B (28), INPP5E (29), CSPP1 (30), and IFT172 (31)) localize to the cilium. ARL13B is required for ciliary localization of INPP5E, which supports the developing hypothesis that mislocalization of ARL13B and INPP5E is a key part of the mechanism underlying JS (25 28 29 33).

To test whether this hypothesis is correct in MKS1-mutated JS, we evaluated INPP5E localization in JBTS-10, JBTS-153, JBTS-3504 and MKS-158, and found that INPP5E is markedly reduced in the cilium in all four lines ($p<0.001$; Figure 4 A, C, S3). Consistent with the known requirement for MKS1 function for ARL13B localization, ARL13B is also decreased in the cilium ($p<0.001$; Figure 4B, 2A, S2). IMCD3 cells transfected with si*Mks1* show a similar decrease in ciliary ARL13B and INPP5E, supporting the notion that this effect is MKS1 dependent (Supplemental Figure 1E). Of note, decreased ciliary ARL13B and INPP5E are unlikely to be due to decreased expression since the total amounts of ARL13B and INPP5E protein are equal in whole cell lysates from siControl and si*Mks*-transfected IMCD3 cells (Figure S1F).

INPP5E localization is ARL13B-dependent, while ARL13B localization is not INPP5E-dependent

We extended the INPP5E mislocalization or dysfunction in JS patients measuring ciliary ARL13B and INPP5E in fibroblasts from JS patients ARL13B-277 and INPP5E-171. Both ARL13B and INPP5E were decreased in cilia of ARL13B-277 ($p<0.001$; Figure 5A-D, S2, S3). In contrast, only INPP5E was decreased in the cilia of INPP5E-171 ($p<0.001$; Figure 5A-D, S2, S3). These observations in patient fibroblasts indicate that INPP5E localization is downstream of both MKS1 and ARL13B function and combined with the fact the INPP5E mutations cause JS, support this hypothesis that INPP5E dysfunction may be central in JS (Figure 5E) (25 29 33).

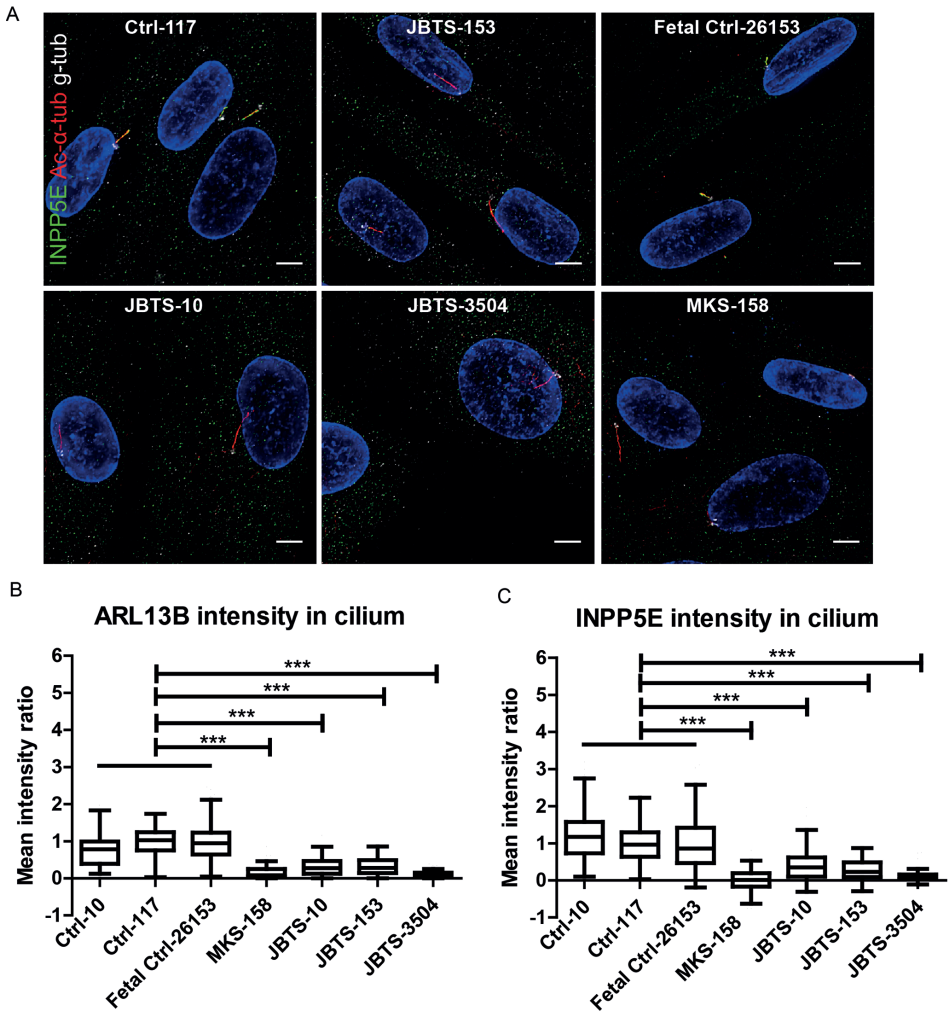

Figure 4. Reduced ciliary ARL13B and INPP5E in fibroblasts from individuals with *MKS1*-related Joubert syndrome

(A) Immunostaining of fibroblasts derived from skin biopsies of JBTS-10, JBTS-153, JBTS-3504, MKS-158, and controls. INPP5E (green), gamma tubulin (g-tub; white) and cilia (acetylated tubulin, red; scalebar 5 µm). Brightness and contrast were identically adjusted across photos for visualization purposes; original data is in Figure S3. **(B)** *MKS1*-mutant fibroblasts have less ARL13B in the cilium than control cells (Tukey whiskers). *** indicates p<0.001 (Kruskal-Wallis test). **(C)** *MKS1*-mutant fibroblasts have less INPP5E in the cilium than control cells (Tukey whiskers). *** indicates p<0.001 (Kruskal-Wallis test). Axonemal fluorescence intensity was calculated by subtracting cytoplasmic background from cilium signal and normalizing to Ctrl-117 intensity to be able to combine batches (n = 50-150 cilia in 2 batches).

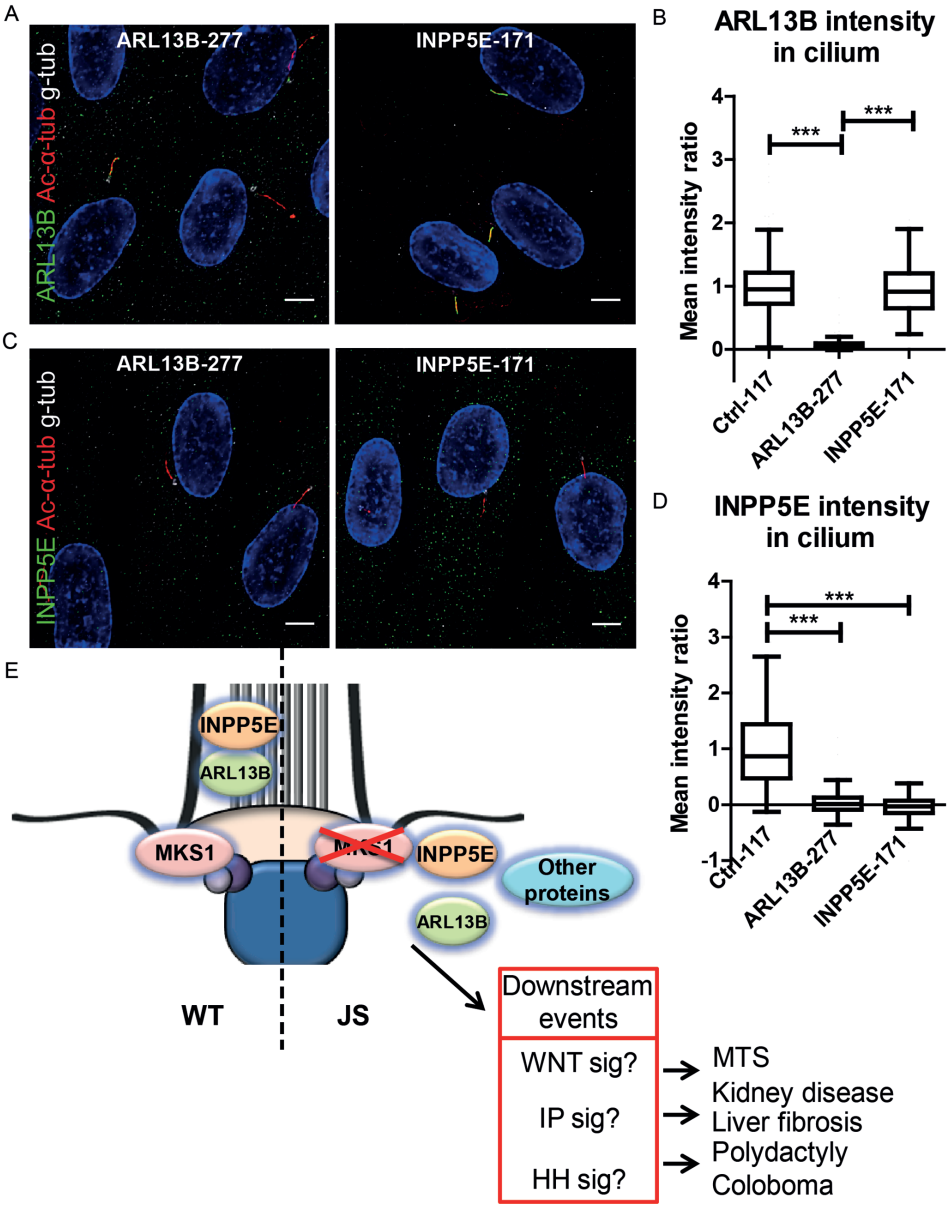

Figure 5. Reduced ciliary ARL13B and INPP5E in fibroblasts from individuals with *ARL13B*- and *INPP5E*-related Joubert syndrome.
(A) Immunostaining of fibroblasts derived from skin biopsies of ARL13B-277 and INPP5E-171. ARL13B (green), gamma tubulin (g-tub; white) and cilia (acetylated tubulin, red; scalebar 5 µm). Brightness and contrast were identically adjusted across photos for visualization purposes; original data is in Figure S2. **(B)** Only ARL13B-277 fibroblasts have less ARL13B in the cilium than control (Tukey whiskers). *** indicates $p<0.001$ (Kruskal-Wallis test, $n > 100$ cilia in 2 batches). **(C)** Immunostaining of fibroblasts derived from skin biopsies of ARL13B-277 and INPP5E-171. INPP5E (green), gamma tubulin (white) and cilia (acetylated tubulin, red; scalebar 5 µm). Brightness and contrast were identically adjusted across photos

for visualization purposes; original data is in Figure S3. (**D**) Both mutant fibroblasts have less INPP5E in the cilium than control (Tukey whiskers). *** indicates p<0.001 (Kruskal-Wallis test, n > 100 cilia in 2 batches). Axonemal fluorescence intensity was calculated by subtracting cytoplasmic background from cilium signal and normalizing to Ctrl-117 intensity. Ctrl-117 images are included in Figure 2A (Figure S2) for ARL13B and 4A (Figure S3) for INPP5E. **(E)** Schematic overview of the roles of MKS1, ARL13B and INPP5E in Joubert syndrome. Loss of function mutations in *MKS1* cause transition zone (TZ) dysfunction and disturb ciliary localization of ARL13B and INPP5E. Our data support the hypothesis that loss of ARL13B-dependent localization of INPP5E is a central mechanism underlying JS. The downstream events are hypothetical based on data in the literature.

DISCUSSION

We report the identification of eight novel *MKS1* mutations in nine individuals with JS. Surprisingly, most of the affected individuals show a relatively mild phenotype without features typically associated with MKS. For example, postaxial polydactyly is almost always reported in fetuses with MKS due to *MKS1* mutations (41), but it was noted in only one individual with JS (Table 1). In addition, we did not observe encephalocele, which is common in *MKS1*-related MKS. However, two affected individuals developed cystic kidney disease and liver fibrosis by 4 and 25 years of age, and two developed retinal dystrophy by 2 and 13 years of age. These findings highlight the importance of monitoring for progressive retinal dystrophy, cystic renal disease, and hepatic fibrosis, so that treatment can be initiated before secondary complications occur.

Comparable to other genes that cause both JS and MKS (e.g. *CC2D2A* (40 42) or *TMEM67* (43)), individuals with *MKS1*-related JS carry mutations that are expected to be less damaging than mutations associated with MKS. All nine individuals with *MKS1*-related JS carry at least one non-truncating mutation (Table 1 and Figure 1M), in contrast to individuals with *MKS1*-related MKS, who almost always carry two truncating mutations (Supplemental Table S1 and Figure 1M). Indeed, our data support and functionally validate a recent report describing two individuals with mild JS due to *MKS1* mutations of which at least one was non-truncating (22). Concordant with the predicted severity of the mutations, the ciliary phenotype is more severe in the fibroblast line from the fetus with MKS compared to the fibroblasts from the three individuals with JS.

Several landmark studies have implicated MKS1 as a component of the B9 protein sub-complex of the TZ at the base of the cilium, which together with other TZ components, is involved in the regulation of protein trafficking in and out of the cilium and sequestering the intraciliary compartment from the cytosol (25 26 44). Mutations affecting B9 complex proteins have been associated with JS and/or MKS, but not with other ciliopathies, suggesting that this complex has a particular function within the TZ, such as trafficking of INPP5E to the cilium (34). It is likely that mutated MKS1 is partly or entirely degraded in *MKS1*-associated MKS but, in the case of mild mutations, it may localize to the TZ but have lost part of its function, as was shown for *PDE6D* mutation (34). At the TZ it could cause

a disturbance of the lateral diffusion of membrane proteins, resulting in less ARL13B and INPP5E in the cilium. It remains to be investigated how impaired TZ functioning results in more variable ciliary lengths and/or longer cilia.

Complete loss of MKS1 function has been shown to affect cilium formation, likely through effects on basal body docking (45); however, decreased cilium number was not a consistent finding across our affected cell lines. In addition, testing of different alleles in 3D spheroid assays reveals different pathological effects on ciliation. Furthermore, we confirm that *ARL13B*- and *INPP5E*-mutant fibroblasts make normal cilia numbers (29 33), while *CSPP1*-mutant fibroblasts make fewer cilia (46). Therefore, decreased cilium number is unlikely to be the primary mechanism underlying JS.

Similarly, altered cilium length is unlikely to be the primary mechanism underlying JS, since we see more variable (and sometimes longer) cilia in *MKS1*-mutant fibroblasts, while cilia are short in *CSPP1*-mutant fibroblasts (46), and normal length in *INPP5E*-mutant fibroblasts (29). More variable cilium length has also been demonstrated in *IFT172*-mutant (21) and *ARL13B*-mutant (this study) fibroblasts. Given these differences across multiple genetic causes, current data do not support abnormal cilium length as an obligate mechanism underlying JS. Our data are consistent with the hypothesis that INPP5E dysfunction, either due to mutation or mislocalization, is an essential part of the mechanism underlying JS (Figure 5E) (34).

This work and previous studies have shown that loss of *INPP5E* function causes JS (29). INPP5E localization depends on ARL13B function (33 34), and ARL13B localization depends on TZ function (25 26). Although loss of INPP5E function is sufficient to cause JS, mislocalization of other ciliary proteins due to TZ dysfunction may contribute to the spectrum and severity of phenotypes seen in affected individuals. Aberrant hedgehog and Wnt signaling could contribute to disease development downstream of ciliary dysfunction. Future work will determine the downstream effects of INPP5E dysfunction likely involving inositol phosphate and other signaling pathways, as well as how the many cellular defects associated with loss of JS gene function relate to the human phenotypes. Because INPP5E is potentially druggable, the value of finding this enzyme at the root of Joubert syndrome will hopefully open a novel therapeutic avenue to ameliorate the progression of disease.

METHODS

Participants

Participants were enrolled under approved human subjects research protocols at the University of Washington, Seattle Children's Hospital, and the University of Utrecht, Wilhelmina Children's Hospital, the Netherlands. All participants or their legal guardians provided written informed consent. Inclusion criteria were: 1) MTS on brain imaging (or

cerebellar vermis hypoplasia on computed tomography (CT) scan when an MRI was not available) and 2) clinical findings of JS (intellectual impairment, hypotonia, ataxia).

Clinical and imaging data

Clinical information was collected using a structured intake form and review of medical records. At the time of enrollment, we reviewed brain MRI and/or CT scans to confirm the MTS and to evaluate for other structural brain abnormalities. When MRI or CT images were not available, we abstracted information from the MRI or CT report.

Mutation identification

Samples from participants at the University of Washington were sequenced using a modified molecular inversion probe capture method, followed by sequencing on an Illumina HiSeq (35). Exons and consensus splice sites (+/- 2 base pairs) were targeted, and samples were considered sequenced if >80% of the targeted base pairs had >25X coverage. Samples from Utrecht University Medical Center were sequenced for 621 ciliary genes including the known Joubert genes and *MKS1* (NM_017777.3). Deep sequencing was performed on two pooled sample cohorts of 32 and 34 cases, of which 51 cases had a diagnosis of Joubert syndrome. Sixty nucleotide long probes uniquely mapping to coding sequences of the 621 ciliary genes from the GRCh37/hg19 human reference genome with 50 bp flanks into intronic regions were designed with an average tiling density of 4 bp on average for both positive and negative strands. The size of the targeted region was 2.7 Mb, covered by 779592 probes. Fragment library preparation and genomic enrichment on a 1M custom microarray (Agilent Technologies, CA, USA) was performed as previously described (36). The pooled samples were run as a full slide on the SOLiD 5500XL. Following SOLiD sequencing, color space reads were mapped against GRCH37/hg19 reference genome using a custom pipeline based on the BWA software, and variants and small indels were annotated as described previously (36). Average sample coverage was 147X and 136X, and 92 and 89% of requested sequences were covered by more than 20 reads for run 1 and 2 respectively.

Controls

The frequency of missense variants in subjects without severe congenital disorders was examined using data available through the NHLBI Exome Sequencing Project, Seattle, WA (37). For the p.S372del variant, we evaluated 182 samples from neurologically normal European American individuals by Sanger sequencing.

Cell culture

Murine inner medullary collecting duct cells (IMCD3) were cultured in Dulbecco's Modified Eagle's Medium (DMEM):F12 (1:1) (GlutaMAX, GIBCO), supplemented with 10% Fetal Calf Serum (FCS) and penicillin and streptomycin (1% P/S). Human fibroblasts were grown

from skin biopsies in DMEM supplemented with 10% FCS and 1% P/S. Cells were incubated at 37°C in 5% CO2 to approximately 90% confluence. Fibroblasts were serum starved for 48 hours prior to fixation. Details on MKS fibroblasts (MKS-158) can be found in Table S1 (Subject: Khaddour '07:562). ARL13B-277 fibroblasts have het c.246G>A (p. W82*), and het c.598C>T (p.R200C) mutations (28). INPP5E-171 fibroblasts have hom c.956G>A (p.G286R) mutations (38). ARL13B-277 and INPP5E-171 do not have mutations in other known JS-related genes.

In vitro mutagenesis

A human cDNA expression construct for MKS1 was ordered from Origene (SC123690; not full-length) and disease-associated mutations were introduced using site-directed mutagenesis (QuikChange II, Agilent) and sequence verified using Sanger sequencing (primers available upon request).

Transfection

Cells were seeded for at least 16 hours prior to transfection with Lipofectamine 2000 (Invitrogen, 11668-019) with Opti-MEM (Invitrogen, 31985-062) diluted DNA expression constructs, according to the supplier's protocol. After replating, cells were transfected with Lipofectamine RNAimax (Invitrogen, 13778-075) with ON-TARGETplus siRNA SMARTpools (Thermo Scientific Dharmacon): Non-targeting pool (D-001810-10) or *Mks1* (L-063962-01), according to the supplier's protocol.

RT-qPCR

RNA was isolated (RNeasy Mini Kit, QIAGEN, 74106) and measured (NanoDrop spectrophotometer ND-1000, Thermo Fischer Scientific Inc.). cDNA was synthesized using the iScript cDNA Synthesis Kit (Bio-Rad, 170-8891) according to the supplier's protocol. RT-qPCR determined expression of *Mks1*, normalized against reference gene *Rpl27*. The primers (Sigma) used: mMks1 forward 5′-GGAGGTTCTTCATTGGCG-3′, mMks1 reverse 5′-TTGTCTCAGTGCGGAATCC-3′, mRpl27 forward 5′- CGCCCTCCTTTCCTTTCTGC and mRpl27 reverse 5′-GGTGCCATCGTCAATGTTCTTC. Samples were run with iQ SYBR Green Supermix (Bio-Rad, 170-8880) and CFX96 Touch Real-Time PCR Detection System (Bio-Rad); 95°C for 3 min, followed by 40 cycles of 10 s at 95°C, 30 s at 60/53°C and 30 s at 72°C, then 10 s at 95°C followed by a melt of the product from 65°C-95°C.The ΔΔCT method was used for statistical analysis to determine gene expression levels. GraphPad Prism 5.0 was used to perform two-tailed Student's t-tests.

Western blotting

Protein lysates were corrected for protein content by BCA protein assay (Pierce), and western blots were performed for MKS1, ARL13B and INPP5E. β-actin was used as loading

control in combination with Coomassie Blue staining. After dry blotting (iBlot Dry Blotting System, Invitrogen, IB3010-01), the membranes were blocked in 5% powdered skim milk (ELK) in TBS with 0.5% Tween. The primary antibodies (rabbit anti-MKS1, Proteintech 16206-1-AP, 1:3000, rabbit anti-ARL13B, Proteintech 17711-1-AP, 1:1000, rabbit anti-INPP5E, Proteintech 17797-1-AP, 1:1000) and mouse anti-β-actin AC-15, Sigma A5441, 1:15000) were incubated overnight at 4ºC. The secondary HRP-conjugated antibodies (DAKO, dilution 1:2000) were incubated for 1 hour before imaging with ECL Chemiluminescent Peroxidase Substrate kit (Sigma, CPS1120-1KT) and scanning with a BioRad ChemiDoc XRS+ device with Image Lab software 4.0.

IMCD3 spheroid growth assay

After siRNA transfection cells were mixed 1:1 with growth factor-depleted matrigel (BD Bioscience). The IMCD3 spheroids were stained as previously described (39). Primary antibody used: rat anti-ZO1, Santa Cruz sc-3725 (1:500), rabbit anti-β-catenin, BD Bioscience AHO0462 (1:500) and mouse anti-acetylated tubulin, Sigma T6793 (1:20,000) Images were taken with a Zeiss LSM700 confocal microscope and 50 spheroids per condition were scored. GraphPad Prism 5.0 was used to perform one-way ANOVA with Dunnett's post hoc testing per siRNA treated group of samples.

Immunofluorescence

IMCD3 cells grown on coverslips were fixed for 5 min with ice cold methanol followed by a 1 hour blocking step in 1%BSA/PBS. Primary antibody incubations (rabbit anti-pericentrin, Novus Biologicals NB 100-68277, at 1:500, rabbit anti-MKS1, Proteintech 16206-1-AP, at 1:300, mouse anti-acetylated tubulin, Sigma T6793, at 1:20,000) were performed overnight at 4°C. Alexa Fluor conjugated secondary antibodies (Life Technologies) were performed for 1 hr at RT. Coverslips were mounted using Fluoromount G (Cell Lab, Beckman Coulter). Confocal imaging was performed using Zeiss LSM700 Confocal laser microscope and images were processed with the LSM Zen software. Approximately 250 events per condition were scored. GraphPad Prism 5.0 was used to perform two-tailed Student's t tests or one-way ANOVA tests.

Fibroblasts were grown to 80% confluency and then serum starved for 48 hours. Cells were fixed with 4% PFA for 5 minutes at room temperature followed by ice cold methanol for 4 minutes at -20°C. Cells were blocked in PBS containing 10% NDS, 1% BSA and 0.1% triton X-100 for 60 minutes. Fixed cells were incubated in primary antibodies diluted in block (mouse anti-acetylated Tubulin, Sigma T6793, 1: 1000, rabbit anti-ARL13B, ProteinTech 17711-1-AP, 1:400, rabbit anti-INPP5E, ProteinTech 17797-1-AP, 1:2000, goat anti-gamma Tubulin, Santa Cruz sc-7396, 1:200) for 80 minutes at RT and Alexa Fluor conjugated secondary antibodies (Life Technologies) for 45 minutes at RT. Coverslips were mounted using Fluoromount G with DAPI (Southern Biotech 0100-20). All images were taken with

a 63X oil objective as 4 µm z-stacks with 0.3 µm steps. Length and intensity measurements were made in FIJI on 16-bit sum-projection images of z-stacks. Using acetylated Tubulin to identify the axoneme, a mask was painted over each cilium with a 3 pixel brush and the intensities of the mask objects were measured in each channel using the ROI manager. The masks were skeletonized and the maximum branch length measured to determine cilia length. Then, the axoneme-background intensities were calculated by subtracting the intensity of an adjacent 30 pixel diameter background region of interest (ROI) from each respective cilium intensity. Axoneme-background intensities were normalized for by dividing each intensity measurement by the average intensity of Ctrl-117 or Fetal Ctrl-26153 for that batch.

Statistical analysis

One-way ANOVA with Dunnett's post hoc testing was performed to compare ciliary frequencies of affected fibroblasts and controls. The non-parametric Kruskal-Wallis test (post hoc Dunn's multiple comparison test) was performed to compare ciliary lengths of affected fibroblast and controls. F-tests were performed to compare variance in ciliary length. Confidence interval around medians for non-normally distributed values were obtained by bootstrapping (10000 iterations).

Acknowledgements

The authors thank all of the affected individuals, their families and referring physicians for participating in this study. We are grateful to Veronica Foletto for technical assistance.

Funding

This research was supported by grants from National Institutes of Health KL2-RR025015, R01NS064077 to D.D., the University of Washington Intellectual and Developmental Disabilities Research Center Genetics Core P30HD002274, and DK068306 and RC4-DK090917 to F.H, and DK090917 to E.A.O, K23NS45832 to M.A.P. and K24HD046712 to I.A.G. D.D. also received private donations from families of children with Joubert syndrome. F.H. is an investigator of the Howard Hughes Medical Institute. G.G.S., C.A.J., and R.H.G. were supported by grants from the European Union 7th Framework Programme Consortium "SYSCILIA" (241955) and H.Y.K., N.V.K. and R.H.G. receive support from the Dutch Kidney Foundation "KOUNCIL" Consortium Grant CP11.18. H.G. was supported by the Netherlands Organization for Scientific Research (ZonMw-TAS grant 116001026), C.A.J. was also supported by funding from the Sir Jules Thorn Award for Biomedical Research (JTA/09) and a Medical 719 Research Council grant (MR/K011154/1).

REFERENCES

1. Tobin JLP, Beales PLBMDF. The nonmotile ciliopathies. Genetics in Medicine 2009;11(6):386-402.
2. Basten SG, Giles RH. Functional aspects of primary cilia in signaling, cell cycle and tumorigenesis. Cilia 2013;2(1):6.
3. Parisi MA, Doherty D, Chance PF, Glass IA. Joubert syndrome (and related disorders) (OMIM 213300). Eur J Hum Genet 2007;15(5):511-21.
4. Joubert M, Eisenring JJ, Robb JP, Andermann F. Familial agenesis of the cerebellar vermis. A syndrome of episodic hyperpnea, abnormal eye movements, ataxia, and retardation. Neurology 1969;19(9):813-25.
5. Steinlin M, Schmid M, Landau K, Boltshauser E. Follow-Up in Children with Joubert Syndrome. Neuropediatr. 1997;28:204-11.
6. Saraiva JM, Baraitser M. Joubert syndrome: a review. Am. J. Med. Genet. 1992;43(4):726-31.
7. Tamada A, Kumada T, Zhu Y, et al. Crucial roles of Robo proteins in midline crossing of cerebellofugal axons and lack of their up-regulation after midline crossing. Neural Dev 2008;3:29.
8. Braddock BA, Farmer JE, Deidrick KM, Iverson JM, Maria BL. Oromotor and communication findings in joubert syndrome: further evidence of multisystem apraxia. J Child Neurol 2006;21(2):160-3.
9. Hodgkins PR, Harris CM, Shawkat FS, et al. Joubert syndrome: long-term follow-up. Developmental medicine and child neurology 2004;46(10):694-9.
10. Fennell EB, Gitten JC, Dede DE, Maria BL. Cognition, behavior, and development in Joubert syndrome. J Child Neurol 1999;14(9):592-6.
11. Gitten J, Dede D, Fennell E, Quisling R, Maria BL. Neurobehavioral development in Joubert syndrome. J Child Neurol 1998;13(8):391-7.
12. Yacobi S, Ornoy A. Is lithium a real teratogen? What can we conclude from the prospective versus retrospective studies? A review. Isr J Psychiatry Relat Sci 2008;45(2):95-106.
13. Wataya T, Muguruma K, Sasai Y. [Human pluripotent stem cell and neural differentiation]. Brain Nerve 2008;60(10):1165-72.
14. Juric-Sekhar G, Adkins J, Doherty D, Hevner RF. Joubert syndrome: brain and spinal cord malformations in genotyped cases and implications for neurodevelopmental functions of primary cilia. Acta neuropathologica 2012.
15. Poretti A, Huisman TA, Scheer I, Boltshauser E. Joubert syndrome and related disorders: spectrum of neuroimaging findings in 75 patients. AJNR. American journal of neuroradiology 2011;32(8):1459-63.
16. Romani M, Micalizzi A, Valente EM. Joubert syndrome: congenital cerebellar ataxia with the molar tooth. Lancet neurology 2013;12(9):894-905.
17. Mecke S, Passarge E. Encephalocele, polycystic kidneys, and polydactyly as an autosomal recessive trait simulating certain other disorders: the Meckel syndrome. Annales de genetique 1971;14(2):97-103.
18. Alexiev BA, Lin X, Sun CC, Brenner DS. Meckel-Gruber syndrome: pathologic manifestations, minimal diagnostic criteria, and differential diagnosis. Archives of pathology & laboratory medicine 2006;130(8):1236-8.
19. Cincinnati P, Neri ME, Valentini A. Dandy-Walker anomaly in Meckel-Gruber syndrome. Clinical dysmorphology 2000;9(1):35-8.
20. Barkovich AJ, Millen KJ, Dobyns WB. A developmental and genetic classification for midbrain-hindbrain malformations. Brain : a journal of neurology 2009;132(Pt 12):3199-230.
21. Halbritter J, Bizet AA, Schmidts M, et al. Defects in the IFT-B component IFT172 cause Jeune and Mainzer-Saldino syndromes in humans. Am J Hum Genet 2013;93(5):915-25.
22. Romani M, Micalizzi A, Kraoua I, et al. Mutations in B9D1 and MKS1 cause mild Joubert syndrome: expanding the genetic overlap with the lethal ciliopathy Meckel syndrome. Orphanet journal of rare diseases 2014;9:72.
23. Szymanska K, Hartill VL, Johnson CA. Unraveling the genetics of Joubert and Meckel-Gruber syndromes. Journal of pediatric genetics 2014;3(2):65-78.
24. Valente EM, Logan CV, Mougou-Zerelli S, et al. Mutations in TMEM216 perturb ciliogenesis and cause Joubert, Meckel and related syndromes. Nat Genet 2010;42(7):619-25.
25. Garcia-Gonzalo FR, Corbit KC, Sirerol-Piquer MS, et al. A transition zone complex regulates mammalian ciliogenesis and ciliary membrane composition. Nat Genet 2011;43(8):776-84.
26. Chih B, Liu P, Chinn Y, et al. A ciliopathy complex at the transition zone protects the cilia as a privileged membrane domain. Nature cell biology 2012;14(1):61-72.
27. Rohatgi R, Snell WJ. The ciliary membrane. Current opinion in cell biology 2010;22(4):541-6.
28. Cantagrel V, Silhavy JL, Bielas SL, et al. Mutations in the cilia gene ARL13B lead to the classical form of Joubert syndrome. Am J Hum Genet 2008;83(2):170-9.

29. Bielas SL, Silhavy JL, Brancati F, et al. Mutations in INPP5E, encoding inositol polyphosphate-5-phosphatase E, link phosphatidyl inositol signaling to the ciliopathies. Nat Genet 2009;41(9):1032-6.
30. Patzke S, Redick S, Warsame A, et al. CSPP is a ciliary protein interacting with Nephrocystin 8 and required for cilia formation. Molecular biology of the cell 2010;21(15):2555-67.
31. Bujakowska KM, Zhang Q, Siemiatkowska AM, et al. Mutations in IFT172 cause isolated retinal degeneration and Bardet-Biedl syndrome. Human molecular genetics 2015;24(1):230-42.
32. Garcia-Gonzalo FR, Reiter JF. Scoring a backstage pass: mechanisms of ciliogenesis and ciliary access. J Cell Biol 2012;197(6):697-709.
33. Humbert MC, Weihbrecht K, Searby CC, et al. ARL13B, PDE6D, and CEP164 form a functional network for INPP5E ciliary targeting. Proceedings of the National Academy of Sciences of the United States of America 2012;109(48):19691-6.
34. Thomas S, Wright KJ, Le Corre S, et al. A homozygous PDE6D mutation in Joubert syndrome impairs targeting of farnesylated INPP5E protein to the primary cilium. Human mutation 2014;35(1):137-46.
35. O'Roak BJ, Vives L, Girirajan S, et al. Sporadic autism exomes reveal a highly interconnected protein network of de novo mutations. Nature 2012;485(7397):246-50.
36. Harakalova M, Mokry M, Hrdlickova B, et al. Multiplexed array-based and in-solution genomic enrichment for flexible and cost-effective targeted next-generation sequencing. Nature protocols 2011;6(12):1870-86.
37. NHLBI Exome Sequencing Project. Secondary NHLBI Exome Sequencing Project. http://snp.gs.washington.edu/EVS/.
38. Kroes HY, Monroe GR, van der Zwaag B, et al. Joubert syndrome: genotyping a Northern European patient cohort. Eur J Hum Genet 2015.
39. Giles RH, Ajzenberg H, Jackson PK. 3D spheroid model of mIMCD3 cells for studying ciliopathies and renal epithelial disorders. Nature protocols 2014;9(12):2725-31.
40. Bachmann-Gagescu R, Ishak GE, Dempsey JC, et al. Genotype-phenotype correlation in CC2D2A-related Joubert syndrome reveals an association with ventriculomegaly and seizures. Journal of medical genetics 2012;49(2):126-37.
41. Consugar MB, Kubly VJ, Lager DJ, et al. Molecular diagnostics of Meckel-Gruber syndrome highlights phenotypic differences between MKS1 and MKS3. Human genetics 2007;121(5):591-9.
42. Mougou-Zerelli S, Thomas S, Szenker E, et al. CC2D2A mutations in Meckel and Joubert syndromes indicate a genotype-phenotype correlation. Human mutation 2009;30(11):1574-82.
43. Iannicelli M, Brancati F, Mougou-Zerelli S, et al. Novel TMEM67 mutations and genotype-phenotype correlates in meckelin-related ciliopathies. Human mutation 2010;31(5):E1319-31.
44. Sang L, Miller JJ, Corbit KC, et al. Mapping the NPHP-JBTS-MKS protein network reveals ciliopathy disease genes and pathways. Cell 2011;145(4):513-28.
45. Dawe HR, Smith UM, Cullinane AR, et al. The Meckel-Gruber Syndrome proteins MKS1 and meckelin interact and are required for primary cilium formation. Human molecular genetics 2007;16(2):173-86.
46. Tuz K, Bachmann-Gagescu R, O'Day DR, et al. Mutations in CSPP1 cause primary cilia abnormalities and Joubert syndrome with or without Jeune asphyxiating thoracic dystrophy. Am J Hum Genet 2014;94(1):62-72.
47. Kyttala M, Tallila J, Salonen R, et al. MKS1, encoding a component of the flagellar apparatus basal body proteome, is mutated in Meckel syndrome. Nat Genet 2006;38(2):155-7.
48. Khaddour R, Smith U, Baala L, et al. Spectrum of MKS1 and MKS3 mutations in Meckel syndrome: a genotype-phenotype correlation. Mutation in brief #960. Online. Human mutation 2007;28(5):523-4.
49. Frank V, Ortiz Bruchle N, Mager S, et al. Aberrant splicing is a common mutational mechanism in MKS1, a key player in Meckel-Gruber syndrome. Human mutation 2007;28(6):638-9.
50. Auber B, Burfeind P, Herold S, et al. A disease causing deletion of 29 base pairs in intron 15 in the MKS1 gene is highly associated with the campomelic variant of the Meckel-Gruber syndrome. Clinical genetics 2007;72(5):454-9.

SUPPLEMENTAL FIGURES

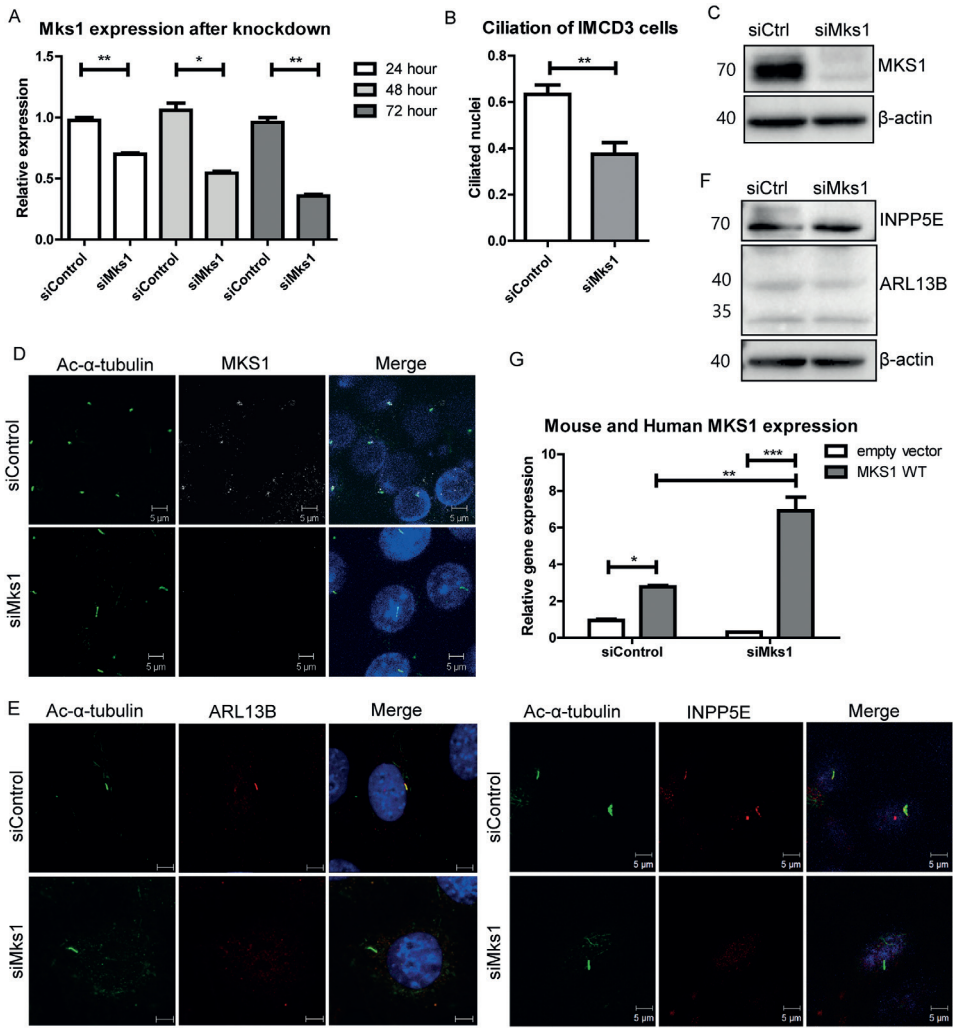

Figure S1. siRNA knockdown of *Mks1* in IMCD3 cells results in decreased MKS1 protein, fewer cilia and decreased ciliary ARL13B and INPP5E levels

(A) RT-QPCR detects lower mRNA levels of *Mks1* after siRNA depletion compared to control siRNA transfected IMCD3 cells ($p<0.02$). Error bars represent SEM ($n = 3$). **(B)** Quantification of cilia frequency in IMCD3 cells treated with control siRNA or *Mks1* siRNA for 72 hours ($p<0.004$). Error bars represent SEM ($n = 3$). **(C)** Immunoblot of MKS1 of IMCD3 lysates transfected with siControl or si*Mks1* oligonucleotides for 56 hours. Less MKS1 protein is detected in si*Mks1*-treated versus siControl-treated IMCD3 cells. β-actin is used as loading control. **(D)** Immunostaining of IMCD3 cells treated with siControl or si*Mks1* for 48 hours. Basal body (MKS1, white) and cilia (acetylated tubulin, green) staining shows less MKS1 protein at the base of primary cilia in si*Mks1*-treated versus siControl-treated IMCD3 cells. **(E)** Immunostaining of IMCD3 cells treated with siControl or si*Mks1* for 72 hours. ARL13B and INPP5E cilia staining (red) does not colocalize with cilia (acetylated tubulin, green) in si*Mks1* treated cells. **(F)** Immunoblot of ARL13B and INPP5E of IMCD3 lysates transfected with siControl or si*Mks1* oligonucleotides for 56 hours. ARL13B and INPP5E

protein levels are unchanged by MKS1 depletion. β-actin is used as loading control. **(G)** RT-QPCR with primers recognizing mouse *Mks1* and human *MKS1* detects higher levels of human *MKS1* expression in siControl and si*Mks1* oligonucleotide (56 hours) treated IMCD3 cells transfected (32 hours) with wild-type MKS1 allele (Two-way ANOVA, Bonferroni test *p<0.05, **p<0.01, ***p<0.001). Error bars represent SEM (n = 3).

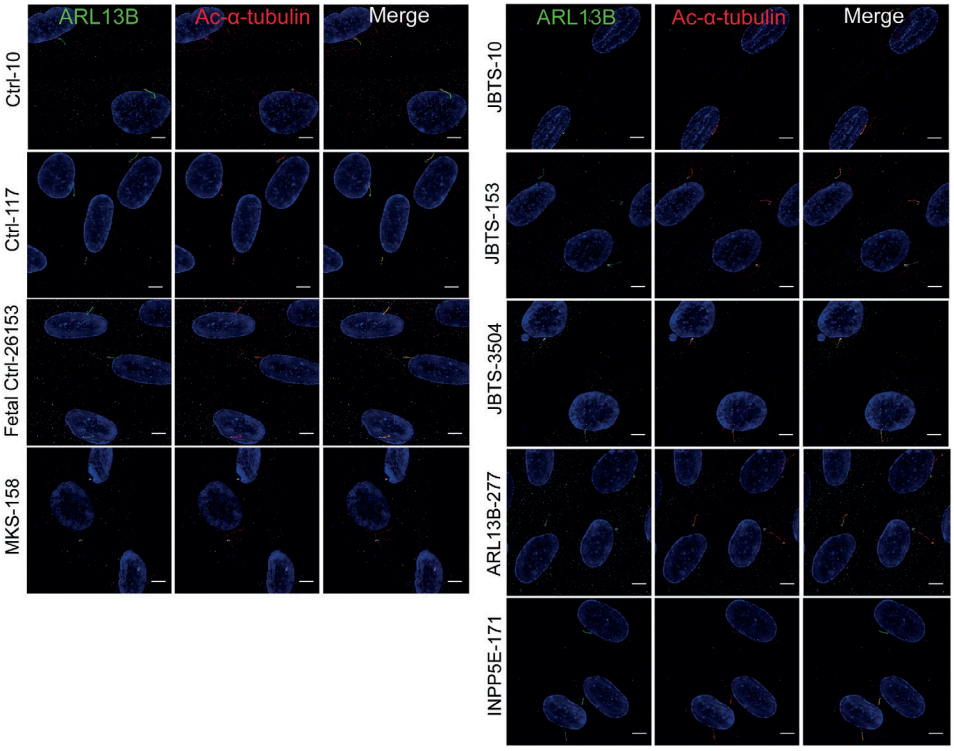

Figure S2. ARL13B cilia staining of fibroblasts
Original deconvoluted images of immunostaining of fibroblasts derived from skin biopsies of JBTS-10, JBTS-153, JBTS-3504, MKS-158, INPP5E-171, ARL13B-277 and controls. ARL13B (green), gamma tubulin (g-tub; white) and cilia (acetylated tubulin, red; scalebar 5 µm).

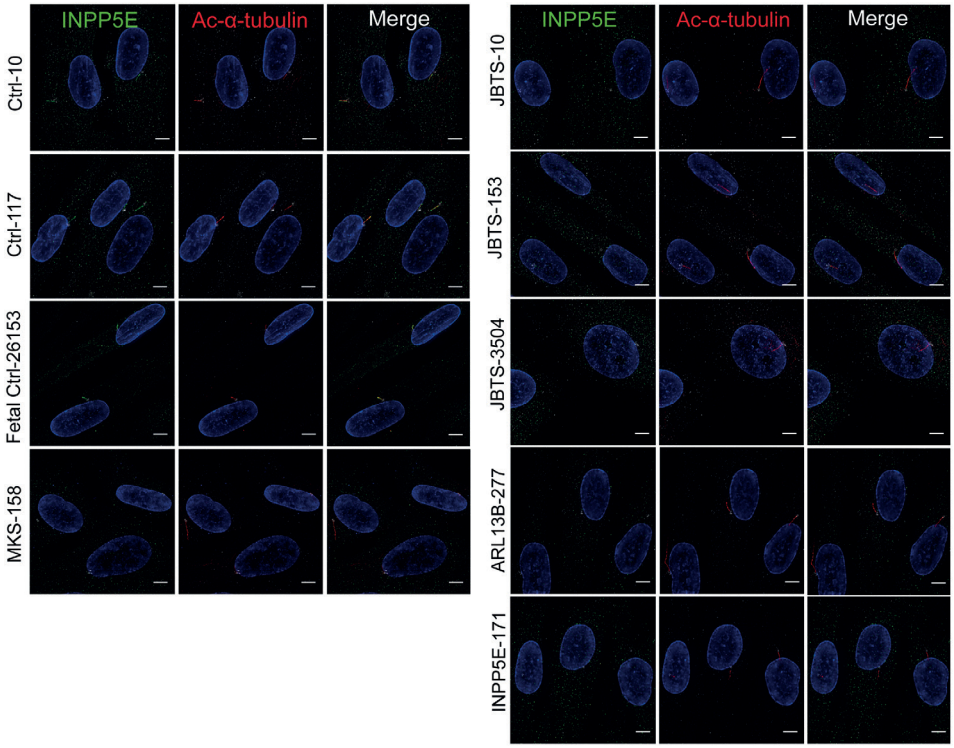

Figure S3. INPP5E cilia staining of fibroblasts
Original deconvoluted images of immunostaining of fibroblasts derived from skin biopsies of JBTS-10, JBTS-153, JBTS-3504, MKS-158, INPP5E-171, ARL13B-277 and controls. INPP5E (green), gamma tubulin (g-tub; white) and cilia (acetylated tubulin, red; scalebar 5 µm).

Table S1. MKS1 mutations in individuals with Meckel syndrome (41, 47-50)

Subject	Origin	cDNA change NM_017777.3	Protein change	EGA	MTS	OE	Ret	Col	Kid	Liver	PD	Other
Frank '07: 850	Turkish	c.262-37_179del c.262-37_179del	p.F88_E139del p.F88_E139del	ND	ND	+	ND	ND	+	+	+	DWM, hydrocephalus, cleft lip
Frank '07: 937	Turkish	c.1407+2delT c.1407+2delT	Splice Splice	ND	ND	+	ND	ND	+	+	+	
Frank '07: 951	Kuwaiti	c.515+1G>A c.515+1G>A	Splice Splice	ND	ND	+	ND	ND	+	+	+	
Frank '07: 943	German	c.1408-35del29 c.417G>A	p.G471Lfs*92 p.F88_E139del[2]	ND	ND	+	ND	ND	+	+	+	
Khaddour '07: 20	French	c.417G>A c.424C>T	p.F88_E139del[2] p.Q142*	15	ND	+	ND	ND	+	+	+	Cleft palate, situs inversus, skeletal dysplasia
Khaddour '07: 362	French	c.958G>A[3] c.1408-35del29	p.V320I(splice) p.G471Lfs*92	26	VA	+	ND	ND	+	+	+	Cleft palate, arhinencephaly, ACC, pancreatic cysts
Khaddour '07: 433	French	c.184_190del7 c.1490G>A[3]	p.T61Vfs*14 p.R497K(splice)	ND	ND	+	ND	ND	+	ND	+	
Khaddour '07: 434	French	c.184_190del7 c.1490G>A[3]	p.T61Vfs*14 p.R497K(splice)	14	ND	+	ND	ND	+	ND	+	
Khaddour '07: 522	Palestinian	c.1048C>G c.1048C>G	p.Q350* p.Q350*	Term	ND	+	ND	ND	+	ND	+	
Khaddour '07: 523	Palestinian	c.1048C>G c.1048C>G	p.Q350* p.Q350*	Term	ND	+	ND	ND	+	ND	+	Ulnar bowing
Khaddour '07: 532	Palestinian	c.1048C>G c.1048C>G	p.Q350* p.Q350*	Term	ND	+	ND	ND	+	+	+	
Khaddour '07: 533	Palestinian	c.1048C>G c.1048C>G	p.Q350* p.Q350*	Term	ND	+	ND	ND	+	ND	+	Femoral bowing
Khaddour '07: 534	Palestinian	c.1048C>G c.1048C>G	p.Q350* p.Q350*	Term	ND	+	ND	ND	+	ND	+	

Khaddour '07: 562	French	c.472C>T c.1408-35del29	p.R158* p.G471Lfs*92	13	ND	ND	ND	ND	+	+?	+	Cleft palate, IUGR, micromelia, hygroma
Khaddour '07: 106	English	c.1408-35del29 c.1408-35del29	p.G471Lfs*92 p.G471Lfs*92	19	ND	+	ND	ND	+	+	+	Epididymal cysts
Khaddour '07: 102	Pakistani	c.1448_1451dupCAGG c.1448_1451dupCAGG	p.T485Rfs*107 p.T485Rfs*107	18	ND	+	ND	ND	+	+	+	Cleft palate, situs inversus, skeletal dysplasia
Auber '07: 1	German	c.1408-35del29 c.1408-35del29	p.G471Lfs*92 p.G471Lfs*92	21	ND	+	ND	+	+	+	+	Cleft palate, campomelia
Auber '07: 2	German	c.1408-35del29 c.1408-35del29	p.G471Lfs*92 p.G471Lfs*92	31	ND	+	ND	+	+	+	+	Epididymal cysts, polysplenia, hypoplastic left heart
Auber '07: 3	German	c.1408-35del29 c.1408-35del29	p.G471Lfs*92 p.G471Lfs*92	18	ND	+	ND	+	+	+	+	Campomelia
Auber '07: 4	German	c.1408-35del29 c.1408-35del29	p.G471Lfs*92 p.G471Lfs*92	19	ND	FMC	ND	-	+	+	+	Campomelia, epididymal cysts, partial agenesis of the corpus callosum
Auber '07: 5	German	c.1408-35del29 c.1408-35del29	p.G471Lfs*92 p.G471Lfs*92	19	ND	+	ND	+	+	+	+	Cleft palate, campomelia, epididymal cysts, Robin sequence, holoprosencephaly
Auber '07: 6	German	c.1408-35del29 c.1408-35del29	p.G471Lfs*92 p.G471Lfs*92	18	ND	+	ND	+	+	+	+	Campomelia, epididymal cysts, ambiguous genitalia
Auber '07: 7	German	c.1408-35del29 c.1408-35del29	p.G471Lfs*92 p.G471Lfs*92	22	ND	+	ND	ND	+	+	+	Cleft palate, campomelia, epididymal cysts,
Auber '07: 8	German	c.1408-35del29 c.1408-35del29	p.G471Lfs*92 p.G471Lfs*92	24	ND	+	ND	ND	+	+	+	Cleft palate, epididymal cysts, horseshoe kidney

Table S1. Continued

Kyttälä '06: F1	German	c.1408-35del29 c.1408-35del29	p.G471Lfs*92 p.G471Lfs*92	ND	ND	ND	ND	ND	ND	ND	ND
Kyttälä '06: F2	Mixed European/ Portuguese	c.1408-35del29 c.1408-35del29	p.G471Lfs*92 p.G471Lfs*92	ND	ND	ND	ND	ND	ND	ND	ND
Kyttälä '06: F3	U.S.	c.1408-35del29 c.1408-35del29	p.G471Lfs*92 p.G471Lfs*92	ND	ND	ND	ND	ND	ND	ND	ND
Kyttälä '06: F4	German	c.50insCCGGG[4] c.80+2T>C[5]	p.R17Rfs*163[4] Splice	ND	ND	ND	ND	ND	ND	ND	ND
Consugar '07: M338	AA/ Caucasian	c.1099+1G>A c.1408-35del29	Splice p.G471Lfs*92	16	ND	+	ND	ND	+	ND	+
Consugar '07: M340	German	c.1408-35del29 c.417G>A	p.G471Lfs*92 p.F88_E139del	15	ND	+	ND	ND	+	ND	+
Consugar '07: M380	Mixed European/ Native American	c.1408-35del29 c.1408-35del29	p.G471Lfs*92 p.G471Lfs*92	19	ND	+	ND	ND	+	ND	+
Consugar '07: M383	Mixed European	c.1408-35del29 c.1408-35del29	p.G471Lfs*92 p.G471Lfs*92	11	ND	+	ND	ND	*	ND	+
Consugar '07: 55875	Dutch	c.417G>A c.1408-35del29	p.F88_E139del p.G471Lfs*92	16	ND	+	ND	ND	+	+	+

[1]PolyPhen-2 scores (HumDiv/HumVar)
[2]Based on RT-PCR data in Consugar et al. 2007
[3]Last base pair in exon, predicted to affect splicing
[4]designated 50insCCGGG; P17fsX163 in Kyttälä et al 2006
[5]designated IVS1+2T->C in Kyttälä et al 2006
EGA: estimated gestational age; FMC: Foramen Magnum Cephalocele; Term: baby was born and died several hours/days later; ND: not documented; ?: unknown; MTS: molar tooth sign; OE: occipital encephalocele; Ret: retinal dystrophy; Col: coloboma; Kid: kidney disease; Liver: liver fibrosis; PD: polydactyly; DWM: Dandy-Walker malformation; ACC: agenesis of the corpus callosum; VA: vermis aplasia; AA: African American; IUGR: intrauterine growth restriction; U.S.; United State

PART TWO

DNA damage response signalling in renal ciliopathies

CHAPTER 5

Renal-retinal ciliopathy gene *Sdccag8* regulates DNA damage response signaling

J Am Soc Nephrol., 25(11):2573-2583 (2014)
(Reproduced with permission of the American Society of Nephrology)

Rannar Airik, Gisela G. Slaats, Zhi Guo, Anna Carina Weiss, Khan Naheed, Amiya Ghosh, Toby W. Hurd, Simon Bekker-Jensen, Jacob M. Schrøder, Steve J. Elledge, Jens S. Andersen, Andreas Kispert, Maddalena Castelli, Alessandra Boletta, Rachel H. Giles, Friedhelm Hildebrandt

ABSTRACT

Nephronophthisis-related ciliopathies (NPHP-RC) are developmental and degenerative kidney diseases that are frequently associated with extra-renal pathologies such as retinal degeneration, obesity and intellectual disability. We recently identified mutations in a gene encoding the centrosomal protein SDCCAG8 as causing nephronophthisis type 10 (NPHP10) in humans. To study the role of *Sdccag8* in disease pathogenesis we generated an *Sdccag8* gene-trap mouse line. The homozygous *Sdccag8*$^{gt/gt}$ mice carried null alleles lacking wild type *Sdccag8* transcript and protein. They recapitulated the human phenotypes of nephronophthisis and retinal degeneration. Retinal degeneration had early onset, was associated with rhodopsin mislocalization in the photoreceptors, reduced cone cell numbers and led to progressive loss of vision in *Sdccag8*$^{gt/gt}$ mice. In contrast, renal histological changes had relatively late onset and no global ciliary defects were observed in the kidneys. Instead, renal pathology was associated with elevated levels of DNA damage response (DDR) signaling activity. Cell culture studies confirmed the aberrant activation of DDR in *Sdccag8*$^{gt/gt}$ derived cells, characterized by elevated levels of P-ATM, γH2AX and cell cycle profile abnormalities. Our analysis of *Sdccag8*$^{gt/gt}$ mice indicates that the pleiotropic phenotypes in these mice may arise through multiple different tissue specific disease mechanisms.

INTRODUCTION

Nephronophthisis-related ciliopathies (NPHP-RC) (OMIM: 256100) are heterogenetic autosomal recessive disorders that feature nephronophthisis, a degeneration disorder of the kidney.(1) To date mutations in more than 20 NPHP-RC genes have been identified,(2) that manifest nephronophthisis as part of their pathogenesis in the context of ciliopathy syndromes, such as Senior-Loken syndrome (SLSN; OMIM: 266900), Bardet-Biedl syndrome (BBS; OMIM: 209900), Joubert syndrome (JBTS; OMIM: 213300) and orofaciodigital syndrome (OFD ; OMIM: 311200).

Recently, we showed that mutations in *Serologically defined colon cancer antigen 8* (*SDCCAG8*) cause nephronophthisis type 10, characterized by retinal and renal degeneration, mild intellectual disability, obesity, hypogonadism and recurrent respiratory infections in humans.(3,4) As several of the clinical features are shared with the Bardet-Biedl syndrome, with the exception of the absence of polydactyly, individuals with *SDCCAG8* mutations are also considered as part of the BBS spectrum.(3,4) *SDCCAG8* encodes a coiled-coil domain protein with no additional conserved domains.(5) The protein localizes to the centrioles throughout the cell cycle,(3,5) to the basal body of cilia and also to the spermatocytes in rat testis. (3,6) Immunohistochemical analysis of retina has shown SDCCAG8 co-localization with Retinitis Pigmentosa Protein 1 (RP1), Retinitis pigmentosa GTPase regulator (RPGR) and Retinitis Pigmentosa GTPase Regulator Interacting Protein 1 (RPGRIP1) in the connecting cilium of the photoreceptors,(3,7) and biochemical studies have demonstrated SDCCAG8 homodimerization and direct interaction with two ciliopathy proteins - OFD1 and Family with Sequence Similarity 161, Member A (FAM161A).(3,5,8) Despite the data on SDCCAG8 protein localization and its interaction partners, the precise molecular function at centrosomes and cilia remains unknown.

Recently we demonstrated that mutations in the gene encoding the centrosomal protein CEP164 cause NPHP-RC whose pathogenesis involves defects in the DNA damage response (DDR) pathway.(9) The same study also implicated SDCCAG8 in this pathway through its co-localization with CEP164 and Tat-interactive protein 60 (TIP60) in the cell nucleus.(9) Indeed, there is a wealth of evidence in the literature that implicates centrosomal protein function in the regulation of genome stability, including the NHPH-RC proteins Jouberin,(10) NIMA-Related Kinase 8 (NEK8/NPHP9),(11) and the SDCCAG8-interacting protein OFD1.(12,13)

In order to study the role of Sdccag8 in the pathogenesis of NPHP-RC we generated a transgenic *Sdccag8*$^{gt/gt}$ mouse model. We demonstrate that *Sdccag8*$^{gt/gt}$ mice recapitulate aspects of the human disease phenotype. Furthermore, we show that Sdccag8 is involved in cell cycle S-phase progression and its loss leads to replication stress related DDR activation.

RESULTS

Generation of *Sdccag8gt/gt* Mice

To investigate the function of the *Sdccag8* gene, the embryonic stem cell line OST40418 containing the gene-trap cassette VICTR24 in the intronic region downstream of *Sdccag8* exon 1 (Supplementary Figure 1A) was microinjected and founders were bred. Allele specific primers were used to genotype the mice (Supplementary Figure 1A and B). Mice carrying the gene-trap allele are referred to as *Sdccag8*^{gt}. The absence of *Sdccag8* mRNA was verified by qRT-PCR analysis using RNA isolated from E13.5 *Sdccag8*$^{gt/gt}$ mouse embryonic fibroblasts (Supplementary Figure 1C). Immunoblotting (Supplementary Figure 1D) confirmed the absence of Sdccag8 protein from lung and kidney lysates of *Sdccag8*$^{gt/gt}$ mice. Two isoforms of the Sdccag8 protein (78kDa and 83kDa) were detected in *Sdccag8*$^{wt/gt}$ kidneys (Supplementary Figure 1D).(3) *Sdccag8*$^{gt/gt}$ mice were present at Mendelian ratios at weaning age, indicating that the *Sdccag8* gene-trap allele does not cause embryonic or early post-natal lethality.

Sdccag8 is Expressed in Kidney and Lung Epithelia

Previously, mutations in *SDCCAG8* were reported to affect two parenchymal organs in humans - the kidneys and the lungs, causing nephronophthisis and, infrequently, bronchiectasis.(3,4) To understand the underlying pathogenetic mechanisms we first examined the expression pattern of *Sdccag8* in these organs by taking advantage of the *lacZ*-cassette in the *Sdccag8* gene-trap allele. β-galactosidase activity staining of wild type and *Sdccag8*$^{wt/gt}$ whole urogenital systems at E16.5 showed strong *Sdccag8* expression in the corticomedullary region of the *Sdccag8*$^{wt/gt}$ kidneys (Figure 1A) and no staining in the wild type control (Supplementary Figure 2A). Examination of the X-gal stained kidney sections at higher resolution showed staining in the renal tubule epithelia in a pattern compatible with the distal convoluted tubule and cortical collecting ducts (Figure 1B). *Sdccag8* expression in the collecting ducts was also observed in postnatal P14 and P100 kidneys by *in situ* hybridization (Figure 1C - D), while sense probe showed no staining (Supplementary Figure 2B and C). In the lung, X-gal staining in *Sdccag8*$^{wt/gt}$ mice at E16.5 showed *Sdccag8* expression in the epithelium of the developing bronchi and bronchioles (Figure 1E). Examination of lung sections at higher resolution confirmed this observation and further showed that the blue *lacZ*$^{+}$ cells were interspersed with *lacZ*$^{-}$ cells in the bronchioles (Figure 1F). No β-galactosidase staining was detected in the epithelial cells of alveoli - the terminal ends of the airways, which do not have cilia (Figure 1F, delineated with dashed line). To determine whether the *lacZ*$^{+}$ cells in the lung epithelium represent the multiciliated cells we performed immunofluorescence analysis on E16.5 CETN2-GFP mouse lung sections using the cilia marker anti poly-glutamylated tubulin antibody and anti-SDCCAG8 antibody. CETN2-GFP fusion protein localizes to centrioles,(14) which are

presented in hundreds of copies in the multiciliated cells of the respiratory epithelium.(15) Since centriologenesis precedes multiciliogenesis, almost no cilia were detected in E16.5 distal bronchioles (Supplementary Figure 2D - F), as described before.(16) However, we found that the CETN2-GFP positive structures (Figure 1G) in the progenitors of the multiciliated cells fully overlapped with SDCCAG8 antibody staining in E16.5 bronchioles (Figure 1H and I). Together, this analysis demonstrates that *Sdccag8* is expressed in the embryonic and postnatal kidney in a pattern that partially overlaps with the localization of ciliated cells in these tissues. In lung *Sdccag8* is expressed in the prospective multiciliated cells, while Sdccag8-negative cells most likely represent the non-ciliated intercalating goblet cells.

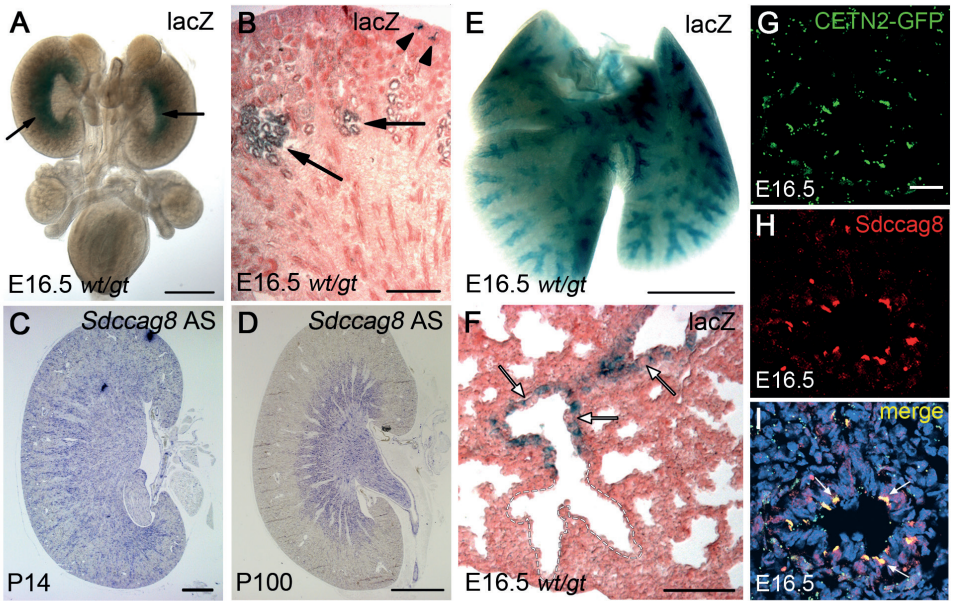

Figure 1. *Sdccag8* is expressed in kidney and lung epithelia
β-galactosidase activity staining in the urogenital system at E16.5 demonstrates *Sdccag8* expression in the corticomedullary region (arrows) in *Sdccag8*$^{wt/gt}$ kidneys (A) but not in wild type control (B). (C) X-gal staining in kidney sections shows strong *Sdccag8* expression in tubules of the corticomedullary region (arrows) and in the cortical collecting ducts (arrow heads). (D) *Sdccag8* expression in postnatal kidneys (P14) is localized to the corticomedullary region. (E) β-galactosidase activity staining on E16.5 whole lung demonstrates *Sdccag8* expression in the bronchi and bronchioles. (F) Analysis of a cross-section through the X-gal stained lung at higher resolution confirms *Sdccag8* expression localization to the epithelial layer of the bronchioles and its absence from alveoli (delineated with dashed line) and surrounding stromal mesenchyme. Notice the presence of *lacZ*-negative cells (white arrows) in the bronchioles. (G - I) CETN2-GFP expression in the bronchiole epithelium (G) overlaps (I) with SDCCAG8 antibody staining (H) in E16.5 mouse lung section, indicating that Sdccag8-positive cells correspond to the progenitors of the multiciliated cells in the lung. Scale bar: (A - B) 1mm; C, 400 μm; D, 2 mm; E, 2 mm; F, 200 μm; (G - I) 25 μm.

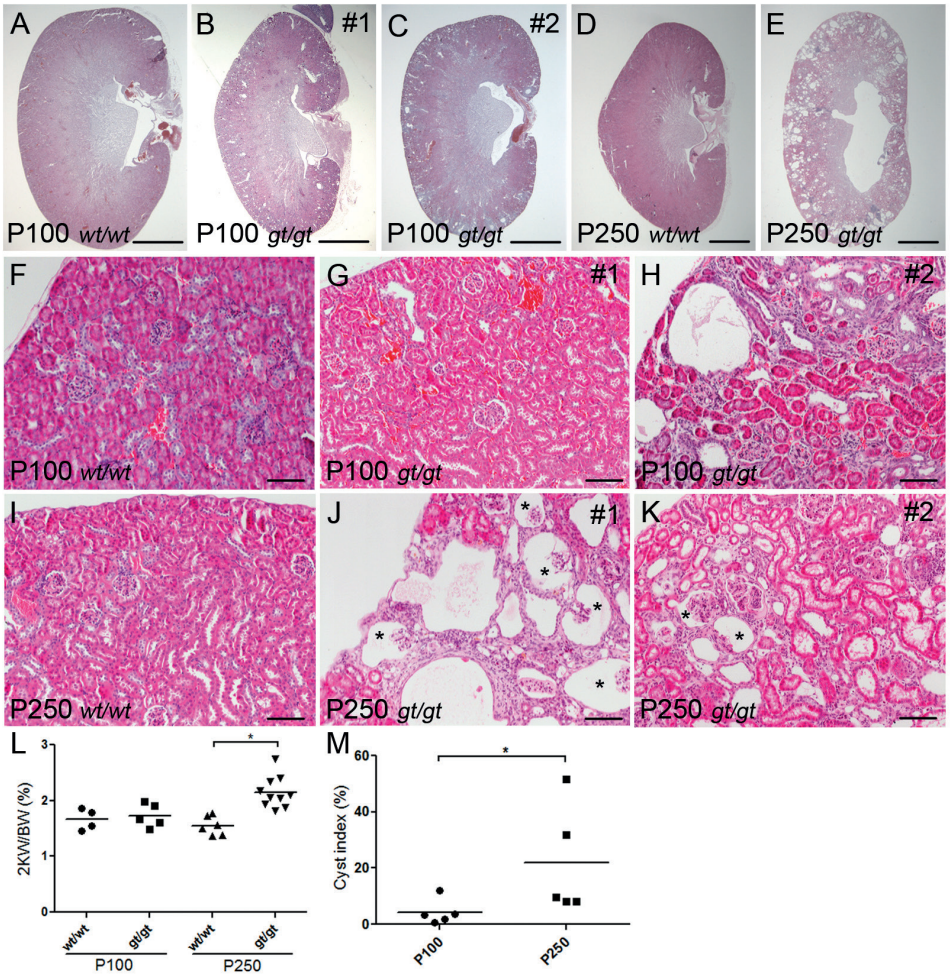

Figure 2. *Sdccag8*$^{gt/gt}$ mice develop nephronophthisis
(A - C) HE staining of sagittal sections of P100 kidneys shows the formation of cortical cysts in *Sdccag8*$^{gt/gt}$ kidneys (B and C). (D - E) Analysis of HE staining on sagittal sections of P250 kidneys shows loss of corticomedullary differentiation and progressive cyst formation in *Sdccag8*$^{gt/gt}$ kidneys (E). (F - H) HE stained *Sdccag8*$^{wt/wt}$ (F) and *Sdccag8*$^{gt/gt}$ (G and H) kidney sections demonstrate the variation in tubular cyst size and amount of interstitial infiltrate in *Sdccag8*$^{gt/gt}$ kidneys at P100 (G and H). (I - J) By P250 kidney cysts and interstitial infiltrate have replaced most of the renal parenchyma in *Sdccag8*$^{gt/gt}$ kidneys (J and K). Glomerular cysts marked with asterisks. (L) The kidney weight to body weight ratio is not changed in *Sdccag8*$^{gt/gt}$ mice at P100 (mean *wt/wt* 1.667 ± 0.09516, *gt/gt* 1.732 ± 0.09247), however the ratio is significantly increased in P250 *Sdccag8*$^{gt/gt}$ mice (mean *wt/wt* 1.554 ± 0.07007, *gt/gt* 2.151 ± 0.08878, *P<0.05). (M) Kidney cyst index is low in P100 *Sdccag8*$^{gt/gt}$ mice (mean 4.270 ± 2.024), but is greatly increased and with noticeable variation in P250 mice (mean 21.91 ± 8.662, *P<0.05). Scale bar: (A - E) 2 mm, (F – J) 100 µm. *wt*, *Sdccag8* wild type allele; *gt*, *Sdccag8* gene-trap allele.

Sdccag8$^{gt/gt}$ Mice Develop Late Onset Nephronophthisis

Given the *Sdccag8* expression pattern in the kidney, we next examined whether loss of *Sdccag8* causes nephronophthisis. The first histological signs of cyst formation and interstitial infiltration, features that are characteristic of nephronophthisis were detected at P100 in *Sdccag8*$^{gt/gt}$ kidneys (Figure 2A – C). The initial cyst formation occurred primarily in the cortical region of the kidneys (Figure 2B and C), with no (Figure 2G) or small (Figure 2H) amount of interstitial infiltrate surrounding the dilated tubules. At P250 the renal histology appeared progressively deteriorated with enlarged cortical cysts, cyst formation in the corticomedullary region, dedifferentiation of the corticomedullary junction and replacement of the renal parenchyma by interstitial infiltrate (Figure 2D and E). Besides tubular cysts also glomerular cysts were observed in *Sdccag8*$^{gt/gt}$ kidneys at P250 (Figure 2I - K). At P100 there was no difference in kidney weight to body weight ratio in *Sdccag8*$^{gt/gt}$ mice, however by P250 the mutant kidneys were significantly enlarged (Figure 2L). Similarly, the mean value of the cystic index was significantly increased between P100 and P250 (Figure 2M). We next examined the extent of renal fibrosis in *Sdccag8*$^{gt/gt}$ kidneys using Masson trichrome staining (Figure 3A - D). In a majority of P100 *Sdccag8*$^{gt/gt}$ kidneys no collagen deposits were detected (Figure 3B and E), which is in agreement with the limited amount of interstitial infiltrate seen by histological staining (Figure 2G). In contrast, the P250 *Sdccag8*$^{gt/gt}$ kidneys displayed extensive fibrosis (Figure 3D), that was significantly increased between P100 and P250 kidneys (Figure 3E).

To identify the tubular origin of the cysts, we stained P100 kidney sections using nephron segment-specific antibodies. Staining with a proximal tubule marker *Lotus tetragonolobus* lectin LTL (Figure 3F - I), a distal convoluted tubule (DCT) marker thiazide sensitive Na-Cl co-transporter (TSC) (Figure 3J - K), a distal tubule/collecting duct marker *Dolichos biflorus* agglutinin (DBA) (Figure 3F and G), revealed that the cysts in *Sdccag8*$^{gt/gt}$ kidneys originated from two sites - the cortical collecting duct (CCD) (Figure 3G) and the DCT (Figure 3K). Co-staining with an antibody against αSMA that labels the fibrogenic myofibroblasts in *Sdccag8*$^{gt/gt}$ kidneys demonstrates that both CCD and DCT cysts were surrounded by interstitial fibrosis (Figure 3G and K). We examined whether *Sdccag8*$^{gt/gt}$ mice have defective cilia in the cystic CCDs, by staining kidney sections with antibodies against the cilia marker acetylated-tubulin and CCD marker Aquaporin 2 (Aqp2). No global ciliary abnormalities in the *Sdccag8*$^{gt/gt}$ CCDs were observed (Supplementary Figure 3A and B). Deregulation of cytoskeletal rearrangements has been implicated in the pathomechanisms of the polycystic kidney disease.(17) We tested this hypothesis on *Sdccag8*$^{gt/gt}$ mouse embryonic fibroblasts using a wound healing assay, but found no changes in their ability to regulate cytoskeletal rearrangements when grown in 2D culture (Supplementary Figure 3F and G).

Taken together, our data show that *Sdccag8*$^{gt/gt}$ mice present late onset nephronophthisis characterized by cyst formation in the DCT, CCD and glomeruli. Cyst formation was not associated with global ciliary defects in the kidney. There was a marked fibrosis around the renal cysts.

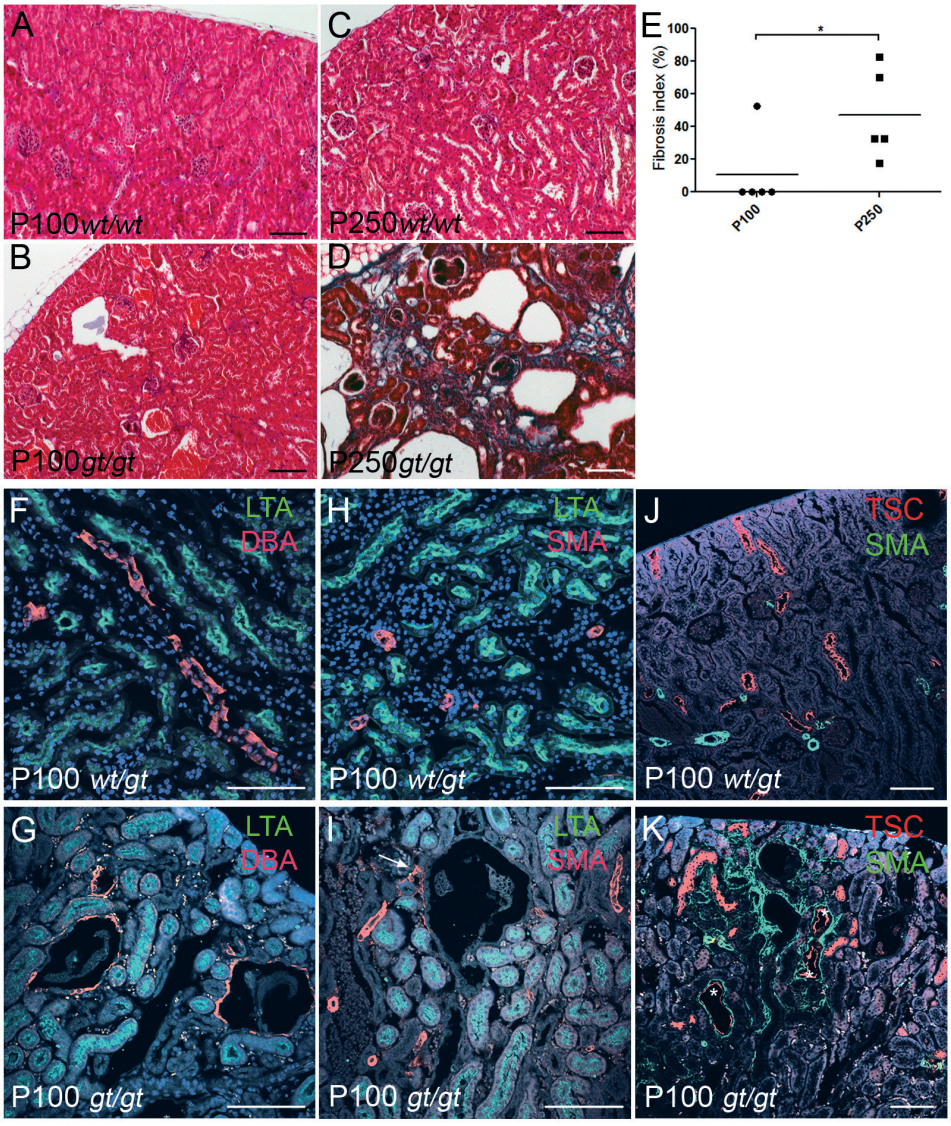

Figure 3. *Sdccag8*$^{gt/gt}$ mice develop fibrosis
(A - D) Masson trichrome staining reveals no collagen deposits in *Sdccag8*$^{gt/gt}$ kidneys at P100 (B), however, extensive fibrosis is visible in P250 *Sdccag8*$^{gt/gt}$ kidneys (D). (E) The fibrosis index is significantly increased in Sdccag8gt/gt mice between P100 (mean 10.50 ± 10.50) and P250 (mean 47.00 ± 12.41, *P<0.05). (F and G) LTA-FITC and DBA-Rhodamine staining on kidney sections demonstrates the formation of cysts in the cortical collecting ducts (DBA) and not in the proximal tubules (LTA) of *Sdccag8*$^{gt/gt}$ kidneys at P100. (H - I) Immunofluorescence staining with αSMA-Rhodamine and LTA-FITC, demonstrate the presence of myofibroblasts in the proximity of a nascent cyst (I, white arrow). (J - K) Immunofluorescence staining with αSMA-FITC and distal convoluted tubule marker – TSC show, that besides cortical collecting ducts, cysts also originate from distal convoluted tubules (marked with white asterisks) in P100 *Sdccag8*$^{gt/gt}$ kidneys (K). αSMA-FITC staining shows the myofibroblasts surrounding the affected tubules. Scale bar: (A - D) 100 μm, (F - K) 100 μm. *wt*, *Sdccag8* wild type allele; *gt*, *Sdccag8* gene-trap allele.

Loss of *Sdccag8* Causes Photoreceptor Degeneration in *Sdccag8*$^{gt/gt}$ mice

Mutations in *SDCCAG8* cause retinal degeneration in humans.(3) To study the disease progression in *Sdccag8*$^{gt/gt}$ mice we performed retinal histological analysis in P30, P100 and P250 days old mice (Figure 4A - C). Although, the retina appeared to have formed normally, we observed a slight reduction of the photoreceptor layer at P30 (Figure 4A). No other retinal abnormalities were detected at this stage. The retinal phenotype became more severe at P100 (Figure 4B) and complete loss of photoreceptor cell layer occurred by P250 (Figure 4C). We performed electroretinography (ERG) measurements to study the physiological consequences of the observed histological changes in the retina. *Sdccag8*$^{gt/gt}$ mice displayed progressive decline in ERG wave amplitudes from P100 to P250, which were in tight correlation with the degree of histological defects at the respective ages (Supplementary Figure 4A and B). SDCCAG8 localization to the photoreceptor connecting cilium is regulated by RPGRIP1.(7) Since *Rpgrip1*$^{-/-}$ mice show a defect in photoreceptor protein trafficking,(18,19) we hypothesized that loss of SDCCAG8 may also lead to impaired protein trafficking in the photoreceptors. To test this hypothesis we stained *Sdccag8*$^{gt/gt}$ retinas with an antibody against rhodopsin, that localizes to the photoreceptor outer segment and against CEP164 that labels the photoreceptor basal body. Consistent with a defect in protein trafficking, rhodopsin accumulated to the plasma membrane of the photoreceptor inner segment and cell bodies in *Sdccag8*$^{gt/gt}$ retina at P30 (Figure 4D and E) and P100 (Supplementary Figure 4D and E). Peanut agglutinin lectin (PNA) staining of photoreceptor cone sheath at P30 revealed reduced number of cones in *Sdccag8*$^{gt/gt}$ mice (Figure 4F and G, Supplementary Figure 4C). Thus, our data indicate that Sdccag8 is not essential for retina development and photoreceptor formation, but is required for the maintenance of both rod and cone photoreceptor cells. Loss of *Sdccag8* leads to progressive retinal degeneration and blindness.

Loss of *Sdccag8* Leads to Impaired S-phase Progression

We and others have shown that the pathogenesis of renal ciliopathies and renal fibrosis may involve mutations in genes that modulate cellular response to DNA damage, such as *ZNF423*, *CEP164*, *FAN1 and NEK8*.(9,11,20) Recently we demonstrated that SDCCAG8 co-localizes with CEP164 and TIP60, an activator of the DDR regulator ATM.(9,21) However, it remained unaddressed whether SDCCAG8 functions in the context of DNA damage response signaling. To test this hypothesis we first examined whether loss of *Sdccag8* causes cell cycle abnormalities due to checkpoint activation by performing FACS analysis on conditionally immortalized adult kidney cells from *Immorto;Sdccag8*$^{wt/wt}$ and *Immorto;Sdccag8*$^{gt/gt}$ mice. To perform the experiments, cells were grown at 37°C without γ-interferon to exclude any interference from the large T-antigen (Supplementary Figure 5A). Cell cycle analysis showed that *Sdccag8*$^{gt/gt}$ cells accumulated in S-phase. The number of BrdU positive S-phase cells was increased from 18% in wild type cells to 24.5% in

Sdccag8$^{gt/gt}$ cells (Figure 5A and B), and this figure was further increased from 23.4% in wild type cells to 33.6% in *Sdccag8*$^{gt/gt}$ cells after treatment with 30J UV-light, indicating that loss of *Sdccag8* affects primarily S-phase progression and makes the cells more sensitive to UV-light induced DNA damage. To study the cell cycle defect in more detail we synchronized the cells with a double thymidine block and treated with 4.5U/ml bleomycin or 30J UV-light. After release from the block *Sdccag8*$^{gt/gt}$ cells progressed the S-phase more slowly and remained in the S-phase longer than wild type cells (Figure 5C). Treatment with 30J UV-light further extended the S-phase duration, bleomycin had slightly milder effect (Figure 5C). Interestingly, G2/M checkpoint activation was not impaired in *Sdccag8*$^{gt/gt}$ cells as treatment with bleomycin or UV-light arrested both wild type and *Sdccag8*$^{gt/gt}$ cells in G2/M checkpoint (Figure 5D). There was also no difference in the levels of apoptosis between wild type and mutant cell lines after treatment with bleomycin or UV-light, although treatment with 30J UV increased the apoptotic index compared to non-treated cells (Supplementary Figure 5B and C).

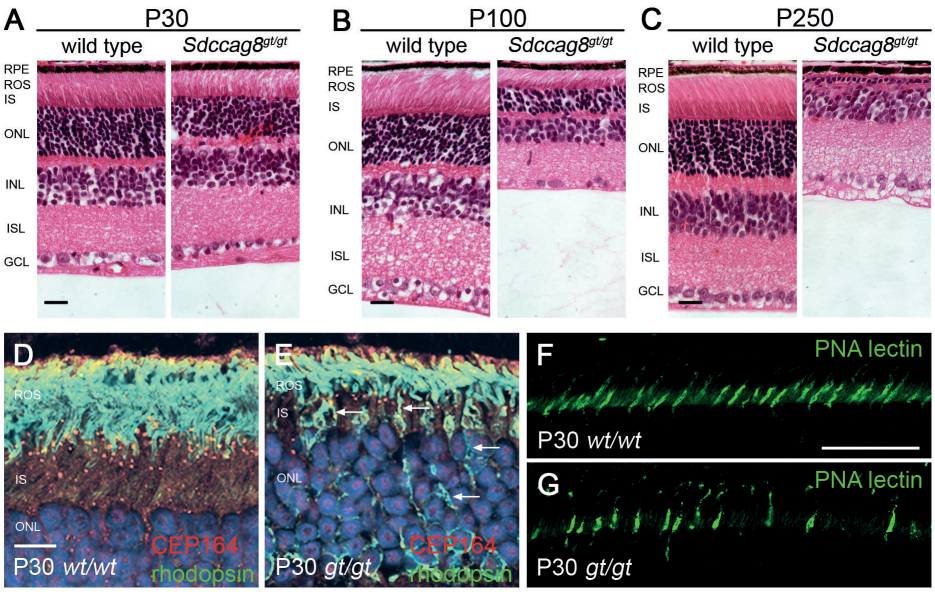

Figure 4. Sdccag8 is required for photoreceptor maintenance
(A - C) Histological analysis of HE stained wild type and *Sdccag8*$^{gt/gt}$ retinas at P30 (A), P100 (B) and P250 (C) show progressive degeneration of photoreceptor inner segments (IS) and outer segments (ROS), as well as severe reduction of the outer nuclear layer in *Sdccag8*$^{gt/gt}$ mice. (D, E) Immunolocalization of CEP164 and rhodopsin in the P30 retina shows rhodopsin accumulation (white arrows) at the photoreceptor inner segment plasma membrane and cell bodies in *Sdccag8*$^{gt/gt}$ retina (E). (F, G) PNA-FITC lectin staining of cone sheaths at P30 demonstrates reduction in cone cell number in *Sdccag8*$^{gt/gt}$ retina (G). Scale bars: (A - C) 100 µm; (D, E) 10 µm; (F, G) 50 µm. RPE, retinal pigment epithelium; ROS, retinal outer segment; IS, inner segment; ONL, outer nuclear layer; INL, inner nuclear layer; ISL, inner plexiform layer; GCL, ganglion cell layer; *wt*, *Sdccag8* wild type allele; *gt*, *Sdccag8* gene-trap allele.

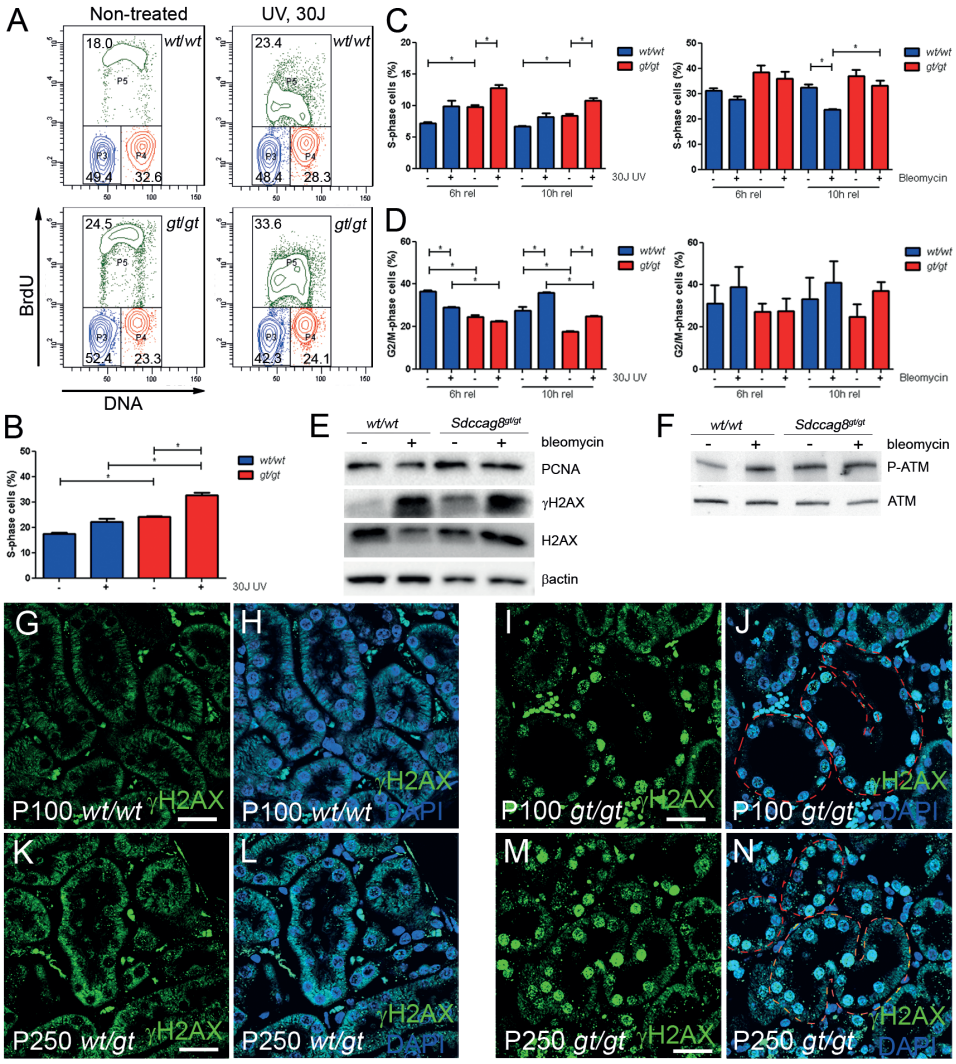

Figure 5. *Sdccag8* inactivation causes S-phase delay and replication stress
(A - B) Cell cycle profile of *Immorto;Sdccag8*$^{wt/wt}$ and *Immorto;Sdccag8*$^{gt/gt}$ non-synchronized cells, demonstrates significant accumulation of *Sdccag8*$^{gt/gt}$ cells in S-phase ($P<0.05$, n=3) compared to wild type control ($P<0.05$, n=3). The number of cells in S-phase is further increased after treatment with 30J UV-light. (C) *Sdccag8*$^{gt/gt}$ cells synchronized with double thymidine block show a delay in S-phase progression, which is further increased after treatment with UV-light. (D) *Sdccag8*$^{gt/gt}$ cells are competent in G2/M check point activation, both in response to UV-light and bleomycin treatment. (E) *Sdccag8*$^{gt/gt}$ cells have increased PCNA levels, reflecting their extended duration in S-phase. PCNA levels do not change in response to bleomycin treatment, which is in agreement with the cell cycle analysis data. Increased γH2AX levels in cultured *Sdccag8*$^{gt/gt}$ cells are a sign of replication stress. H2AX and β-actin were used as loading controls. (F) Phosphorylated ATM levels are low in cultured wild type cells, which become elevated upon bleomycin treatment. In contrast, *Sdccag8*$^{gt/gt}$ cells display high phosphorylated ATM levels even without treatment. ATM was used as a loading control. (G - J) Immunofluorescence staining with anti-γH2AX antibody on P100 *Sdccag8*$^{wt/wt}$ and *Sdccag8*$^{gt/gt}$ kidneys showed no γH2AX staining in control kidneys (G and H), while the

dilated tubules (red dashed lines) in *Sdccag8*$^{gt/gt}$ kidneys were positive for γH2AX (I and J). (K - L) γH2AX staining in P250 kidneys shows positive staining in dilated and non-dilated nephron epithelium (red dashed lines) and fibrotic mesenchyme (M and N). Scale bar: (G – J) 25 μm; (K - L) 20 μm. *wt*, *Sdccag8* wild type allele; *gt*, *Sdccag8* gene-trap allele.

We next examined whether replication stress in *Sdccag8*$^{gt/gt}$ cells leads to the activation of DDR signaling. There was a significant increase in the levels of phosphorylated H2AX (γH2AX) and ATM (S1987) proteins in *Sdccag8*$^{gt/gt}$ cells, indicating activation of DDR signaling pathway in these cells (Figure 5E and F). Treatment with bleomycin drastically increased the phosphorylation of either protein, both in wild type and *Sdccag8*$^{gt/gt}$ cells. In addition, *Sdccag8*$^{gt/gt}$ cells demonstrated increased PCNA protein levels, consistent with their prolonged stay in S-phase (Figure 5E).

We next asked whether the *in vitro* findings of abnormal DDR signaling activation in *Sdccag8*$^{gt/gt}$ cells can also be detected under *in vivo* conditions. We stained *Sdccag8*$^{gt/gt}$ and control kidneys with γH2AX antibody at P100 (Figure 5G - J) and P250 (Figure 5K - N) and indeed found increased nuclear γH2AX staining in the tubular and interstitial compartments of *Sdccag8*$^{gt/gt}$ kidneys. At P100 the γH2AX positive nuclei were observed in the dilated tubules (Figure 5I and J), while at P250 also non-dilated tubules were positive for γH2AX staining (Figure 5M - N), likely indicating a more general tubular stress in more fibrotic kidneys.(20) Together, these data suggest that Sdccag8 has an important role in DNA damage signaling and its loss leads to replication stress and slower S-phase progression during normal cell cycle. Further, *Sdccag8*$^{gt/gt}$ kidneys display elevated levels of γH2AX implicating impaired DDR in their pathogenesis.

DISCUSSION

We have generated *Sdccag8*$^{gt/gt}$ mice to study the role of *Sdccag8* in nephronophthisis type 10. *Sdccag8*$^{gt/gt}$ mice faithfully recapitulate the human *SDCCAG8*$^{-/-}$ phenotypes of retinal degeneration and nephronophthisis. Through morphological analysis of *Sdccag8*$^{gt/gt}$ mice and functional studies using cell culture assays we show that SDCCAG8 is important for photoreceptor maintenance and cell cycle regulation, impairment of which leads to blindness and aberrant DNA damage response signaling activation through replication stress.

Sdccag8 and Degenerative Phenotypes

Previously *Sdccag8* expression has been localized to the retina and testis.(3) (6-8) Our studies using the *Sdccag8 lacZ* gene-trap allele and SDCCAG8 antibody staining show *Sdccag8* expression in the multiciliated cells of the respiratory epithelium and in the distal

convoluted tubules and collecting ducts of the kidney. These expression domains are consistent with the recorded tissue pathologies in *SDCCAG8*$^{-/-}$ individuals.(3) Our ability to detect *LacZ* expression only in the ciliated cells most likely reflects higher *Sdccag8* promoter activity in ciliated cells. It does not, however, exclude that *Sdccag8* is not expressed in non-ciliated cells, whose levels may be below the detection limit of our β-galactosidase staining activity.(3)

Our histological analysis of the kidneys showed that *Sdccag8*$^{gt/gt}$ mice displayed a classical nephronophthisis phenotype at P100, with the cystic dilations originating from the distal convoluted tubules and cortical collecting ducts. Compared to other mouse models of NPHP,(22-25) the onset of the renal phenotype in *Sdccag8*$^{gt/gt}$ mice occurred relatively late. The process of cyst formation appeared to coincide with interstitial fibrosis that surrounded the glomeruli and nephrons. In progressively later stages tubular dilations were also observed in the Bowman's capsule of glomeruli. Curiously, no global cilia defects were observed in the cystic renal tubule cells. Similar results were obtained in *in vitro* studies using the spheroid assay, where loss of *Sdccag8* did not affect cilia numbers.(3,26) However, it remains to be studied whether the cilia in *Sdccag8*$^{gt/gt}$ collecting ducts have deficiencies in some aspects of cilia function, such as mechanosensation as shown for PKD or in loss of transition zone integrity.(27)

Retinal degeneration in *Sdccag8*$^{gt/gt}$ mice progresses slower than in the mouse model of its protein interactor RPGRIP1,(19) but similarly to that of its other interaction partners - RP1 and RPGR.(28,29) This suggests that RPGRIP1 functions upstream of Sdccag8 in photoreceptor cilia, which is in agreement with a recent report of RPGRIP1 dependent ciliary localization of SDCCAG8.(7) Although photoreceptor formation in *Sdccag8*$^{gt/gt}$ mice appeared intact, absence of Sdccag8 led to accumulation of rhodopsin in the photoreceptor inner segments and cell bodies at P30. Our current study did not address whether rhodopsin mislocalization was caused by structural defects in the connecting cilium or whether SDCCAG8 is directly involved in rhodopsin trafficking. Rhodopsin mislocalization to photoreceptor inner segments is known to be toxic for the photoreceptors due to membrane crowding resulting in retinal degeneration.(30,31) Our data is consistent with this mode of retinal pathogenesis and indicates a role for Sdccag8 in intraciliary trafficking. Immunohistochemical and functional analysis showed that both rod and cone photoreceptors were affected in *Sdccag8*$^{gt/gt}$ mice, demonstrating that Sdccag8 is essential for the survival and maintenance of both rods and cones, similar to RPGR function.(29)

Sdccag8 and DNA Damage Response Signaling

Examination of the molecular defects underlying the pathogenesis in *Sdccga8*$^{gt/gt}$ mice using cell culture revealed abnormalities in cell cycle progression due to activation of DNA damage response signaling, characterized by hyper-activation of ATM and elevation of γH2AX levels. DDR defects were observed both in *in vivo* and *in vitro* experiments, indicating that it is

part of the pathogenesis of *Sdccag8* loss of function. DDR deficiency is associated with degenerative diseases, such as Seckel syndrome, which is caused by mutations in genes encoding for other centrosomal and DDR proteins, such as ATR,(32) pericentrin,(33) CEP152(34) or CEP63.(35) Pathologically, Seckel syndrome shares with NPHP-RC the phenotype of premature degeneration and fibrosis of parenchymal organs, including the kidney.(36) As kidneys are constantly exposed to genotoxins they are especially prone to lesions caused by defective DDR signaling. Increased susceptibility to genotoxins has been previously reported for the *Ahi1*$^{-/-}$ mouse model of NPHP-RC,(10) and genome instability due to loss of survivin has been reported in *Pkd1*$^{-/-}$, *Pkd2*$^{-/-}$ and *Tg737*$^{Orpk/Orpk}$ isolated primary cells.(37) Recently mutations in a related ciliopathy *NEK8/NPHP9* were shown to lead to replication stress related DNA damage response signaling activation.(11) Our data is consistent with a model in which Sdccag8 has an important role in S-phase progression during normal cell cycle, where it could facilitate DNA replication from the stalled replication forks; however the molecular analysis required to answer this question is extensive and will be the focus of future work. It remains to be tested whether treatment of *Sdccag8*$^{gt/gt}$ mice with cyclin-dependent kinase (CDK) inhibitors, such as R-roscovitine or S-CR8 reverses or attenuates the renal cyst progression in *Sdccag8*$^{gt/gt}$ mice as has been shown for *jck/Nphp9*$^{-/-}$ and *Pkd1*$^{-/-}$ mice.(38,39)

CONCISE METHODS

Mouse Breeding and Maintenance

The experimental protocol was reviewed and approved by the Animal Care Committee of the University of Michigan. Embryonic stem cell line OST40418 containing gene-trap vector VICTR24 in intron 1 of *Sdccag8* was obtained from Texas Institute for Genomic Medicine (Huston, TX) and cultured as described with the use of ESGRO (Millipore).(40) ES cell-mouse chimeras were prepared by blastocyst microinjection as described and bred with C57BL/6J mice obtain germline transmission.(41) Genotyping primers and PCR conditions are available upon request.

CETN2-GFP mice were bought from Jackson Laboratories (Stock number 008234). *ImmortoMouse*® mice were bought from Charles River (Strain code 238). *Sdccag8* wild type or heterozygous littermates were used as controls for mutant mice. For timed matings; noon on the day a plug was found was designated as embryonic day 0.5 (E0.5).

Histological Analysis

Tissues were fixed in 4% (w/v) paraformaldehyde (PFA) in PBS at 4°C. All tissues were then dehydrated through an ethanol series, and embedded in paraffin. Sections were taken at 5 μm. Hematoxylin and eosin (HE) staining followed standard protocols. β-galactosidase

activity staining was carried out on whole tissues as described previously.(42) β-galactosidase stained tissues were cleared in glycerol for imaging or paraffin embedded and sectioned at 10 µm.

Cystic Index and Fibrosis Index Calculation

Representative images of HE or Masson trichrome stained kidneys were acquired. A grid was placed over the images, and the cystic index or fibrosis index was calculated as the percentage of grid intersection points that bisect cystic and noncystic or fibrotic and no-fibrotic areas.

Electroretinography

To assess rod- and cone-mediated function, electroretinograms (ERG) were performed using the Espion e^2 recording system (Diagnosys, Lowell, MA) as described previously. (43) After overnight dark-adaptation, mice were anesthetized with an intra-peritoneal injection of Ketamine (93 mg/kg) and Xylazine (8 mg/kg). Body temperature was maintained at 37°C with a heating pad. Following pupil dilation with topical phenylephrine (2.5%) and tropicamide (1.0%), corneal ERGs were recorded from both eyes using gold wire loops and a drop of 2% methylcellulose for corneal hydration. A gold wire loop placed in the mouth was used as reference, and the ground electrode was placed on the tail. The dark-adapted ERG was recorded from -5.8 to +1.09 log cd.s.m^{-2}/flash in steps of 0.5 log units. After 10 minutes of light adaptation to a white 32 cd.m^{-2} rod-suppressing background, light adapted ERGs were recorded from -0.91 to +2.0 log cd.s.m^{-2}. Ten to 25 responses were recorded at 3 to 60 s depending upon the stimulus intensity intervals.

Antibodies

For immunostaining, tissues were deparaffinized and hydrated through a graded ethanol series. Antigen retrieval was carried out in heated antigen retrieval buffer pH8 (SIG-31910-50, Covance). Primary antibodies used were as follows: rabbit polyclonal anti-CEP164 was a gift from Erich Nigg (University of Basel, Switzerland), rabbit polyclonal anti-SDCCAG8 (13471-1-AP, Proteintech), rabbit polyclonal anti-SDCCAG8 (ab101969, Abcam), mouse monoclonal anti-g-tubulin (GTU-88, Sigma), anti-acetylated tubulin (6-11B-1, Sigma), rabbit anti-AQP2 (ab15081, Abcam), rabbit polyclonal anti-TSC (AB3553, Millipore), PNA-FITC (VectorLabs), Lotus tetragonolobus lectin LTA (VectorLabs), anti-αSMA-FITC (1A4, Sigma), anti-gH2AX (9718, Cell Signaling), rabbit anti-ATM (S1981) (5883, Cell Signaling), mouse monoclonal anti-Rhodopsin (R5403, Sigma-Aldrich), rat anti-PCNA (Antibodies Online ABIN334654), mouse anti-β-actin (AC-15, Sigma A5441), rabbit anti-Histone H2A.X (Millipore 070627), mouse monoclonal anti-polyglutamylated tubulin (T9822, Sigma-Aldrich). Secondary antibodies were: goat anti-mouse Alexa Fluor 488 (Molecular Probes) and goat anti-rabbit Alexa Fluor 594 (Molecular Probes). Samples were mounted in

ProlongGold (Molecular Probes) and images captured on a Leica TSC 5SP X confocal microscope (Leica Microsystems).

Generation of Mouse Embryonic Fibroblast and Immortalized Adult Kidney Cells

Mouse embryonic fibroblasts (MEF) were established from wild type and *Sdccag8*$^{gt/gt}$ E13.5 embryos and cultured in DMEM with 10% FBS and penicillin/streptomycin. Isolation of immortalized adult kidney cells from P50 *Immorto;Sdccag8*$^{wt/wt}$ and *Immorto;Sdccag8*$^{gt/gt}$ mouse kidneys was performed as described previously.(44)

RNA Extraction and qRT–PCR

RNA was isolated from wild type, *Sdccag8*$^{wt/gt}$ and *Sdccag8*$^{gt/gt}$ MEF cells and adult kidney cells using RNeasy Mini Kit (Qiagen), and reverse transcription was performed using Superscript III (Invitrogen). Quantitative real-time PCR was carried out using Sybr Green (Qiagen) and run on a MyiQ Single-Color Real-Time PCR Detection System (Bio-Rad Laboratories, Inc). Data were normalized to *Gapdh*. Primer sequences are available upon request.

Western Blotting

Lung and kidney tissues were lysed in RIPA lysis buffer (Pierce) and homogenized with a douncer. Cleared tissue lysates were produced by centrifugation of the resulting samples at 16,000 × g for 30 min at 4°C. Gel electrophoresis of tissue lysates and immunoprecipitation eluents were performed using the NuPAGE system (Invitrogen). Samples were resolved on 4-12% Bis-Tris gels in MOPS buffer, transferred to a nitrocellulose membrane which was then probed for the protein of interest using antibodies diluted in TBS containing 5% milk and 0.1% Tween-20 (Sigma).

Apoptosis FACS

To quantify apoptosis, wild type or *Sdccag8*$^{gt/gt}$ cells were plated and incubated with or without thymidine. After two overnight thymidine blocks, cells were released and damage was induced by 1 hour 4.5U/ml Bleomycin or 30J UV exposure. After 24 hours cells were harvested and washed once with 1% BSA-PBS. Cells were collected in FACS tubes in 200 µl 1% BSA-PBS containing Vybrant DyeCycle Violet Stain (Invitrogen, V35003, 1:1000) to stain living and apoptotic cells (7 minutes at 37ºC) and 7-AAD viability stain (eBioscience, 00-6993, 1:60) to stain dead cells (10 minutes on ice). Cells were measured (20000 events) with a BD FACSCanto II flowcytometer and analyzed using BD FACSDiva Software.

BrdU FACS

To quantify cell cycle phase distribution, wild type or *Sdccag8*$^{gt/gt}$ cells were plated and incubated with or without thymidine. After double overnight thymidine block, cells were

released and damage was induced by 30J UV exposure. After 6 or 10 hour release of thymidine block, cells were incubated with 10μM BrdU for 30 minutes and fixed in 70% EtOH. Samples were stained for FACS analysis with BrdU Mouse Monoclonal Antibody (clone MoBU-1), Alexa Fluor® 647 Conjugate (Invitrogen, 1:200) in 0.1% BSA-PBS-T for 1 hour on ice and DAPI (1:2000) in PBS and measured (10000 events) with a BD FACSCanto II flow cytometer and analyzed using BD FACSDiva Software.

Statistical Methods

T-test was used to compare data between two groups. Significance was determined at $P < 0.05$ and represented by * to denote $P < 0.05$. Where appropriate, data are presented as mean +/- SEM.

Acknowledgements

We thank Erich Nigg for providing CEP164 antibody. We also thank Thomas L. Saunders, Elizabeth Hughes, Keith Childs, Galina Gavrilina and Debra Vanheyningen for preparation of ES cell-mouse chimeras from gene trapped ES clone OST40418 and the Transgenic Animal Model Core of the University of Michigan's Biomedical Core Facilities. Core support was provided by Diabetes Research and Training Center, NIH grant number DK20572 and O'Brien Renal Core Center, NIH grant number P30DK08194. This research was supported by grants from the National Institutes of Health to R.A. (1K99DK099434-01), F.H. (DK068306, RC4-DK090917) and the European Commission's 7th Framework Programme (grant agreement HEALTH-F4-2008-201648/PROSPECTS) to J.S.A. F.H. is an Investigator of the Howard Hughes Medical Institute. G.G.S. and R.H.G. were supported by grants from the EU FP7/2009 Consortium "SYSCILIA" (241955) and the Dutch Kidney Foundation Kouncil Consortium Grant CP11.

REFERENCES

1. Hildebrandt F, Benzing T, Katsanis N. Ciliopathies. *N Engl J Med.* 2011;364(16):1533-1543.
2. Hurd TW, Hildebrandt F. Mechanisms of nephronophthisis and related ciliopathies. *Nephron Exp Nephrol.* 2011;118(1):e9-14.
3. Otto EA, Hurd TW, Airik R, et al. Candidate exome capture identifies mutation of SDCCAG8 as the cause of a retinal-renal ciliopathy. *Nat Genet.* 2010;42:840-850.
4. Schaefer E, Zaloszyc A, Lauer J, et al. Mutations in SDCCAG8/NPHP10 Cause Bardet-Biedl Syndrome and Are Associated with Penetrant Renal Disease and Absent Polydactyly. *Molecular Syndromology.* 2010;1(6):273-281.
5. Kenedy AA, Cohen KJ, Loveys DA, Kato GJ, Dang CV. Identification and characterization of the novel centrosome-associated protein CCCAP. *Gene.* 2003;303(0):35-46.
6. Kamio T, Asano A, Hosaka YZ, et al. Expression of the Centrosomal Colon Cancer Autoantigen Gene during Spermatogenesis in the Maturing Rat Testis. *Bioscience, Biotechnology, and Biochemistry.* 2010;74(7):1466-1469.
7. Patil H, Tserentsoodol N, Saha A, Hao Y, Webb M, Ferreira PA. Selective loss of RPGRIP1-dependent ciliary targeting of NPHP4, RPGR and SDCCAG8 underlies the degeneration of photoreceptor neurons. *Cell Death Dis.* 2012;3:e355.
8. Di Gioia SA, Letteboer SJF, Kostic C, et al. FAM161A, associated with retinitis pigmentosa, is a component of the cilia-basal body complex and interacts with proteins involved in ciliopathies. *Human Molecular Genetics.* 2012;21(23):5174-5184.
9. Chaki M, Airik R, Ghosh AK, et al. Exome Capture Reveals ZNF423 and CEP164 Mutations, Linking Renal Ciliopathies to DNA Damage Response Signaling. *Cell.* 2012;150(3):533-548.
10. Lancaster MA, Louie CM, Silhavy JL, et al. Impaired Wnt-[beta]-catenin signaling disrupts adult renal homeostasis and leads to cystic kidney ciliopathy. *Nat Med.* 2009;15(9):1046-1054.
11. Choi Hyo Jei C, Lin J-R, Vannier J-B, et al. NEK8 Links the ATR-Regulated Replication Stress Response and S Phase CDK Activity to Renal Ciliopathies. *Molecular Cell.* 2013;51(4):423-439.
12. Ferrante MI, Zullo A, Barra A, et al. Oral-facial-digital type I protein is required for primary cilia formation and left-right axis specification. *Nat Genet.* 2006;38(1):112-117.
13. Giorgio G, Alfieri M, Prattichizzo C, Zullo A, Cairo S, Franco B. Functional characterization of the OFD1 protein reveals a nuclear localization and physical interaction with subunits of a chromatin remodeling complex. *Mol Biol Cell.* 2007;18(11):4397-4404.
14. Higginbotham H, Bielas S, Tanaka T, Gleeson JG. Transgenic mouse line with green-fluorescent protein-labeled Centrin 2 allows visualization of the centrosome in living cells. *Transgenic Res.* 2004;13(2):155-164.
15. Vladar EK, Stearns T. Molecular characterization of centriole assembly in ciliated epithelial cells. *The Journal of Cell Biology.* 2007;178(1):31-42.
16. Jain R, Pan J, Driscoll JA, et al. Temporal Relationship between Primary and Motile Ciliogenesis in Airway Epithelial Cells. *American Journal of Respiratory Cell and Molecular Biology.* 2010;43(6):731-739.
17. Boca M, D'Amato L, Distefano G, Polishchuk RS, Germino GG, Boletta A. Polycystin-1 Induces Cell Migration by Regulating Phosphatidylinositol 3-kinase-dependent Cytoskeletal Rearrangements and GSK3β-dependent Cell–Cell Mechanical Adhesion. *Molecular Biology of the Cell.* 2007;18(10):4050-4061.
18. Zhao Y, Hong D-H, Pawlyk B, et al. The retinitis pigmentosa GTPase regulator (RPGR)- interacting protein: Subserving RPGR function and participating in disk morphogenesis. *Proceedings of the National Academy of Sciences.* 2003;100(7):3965-3970.
19. Won J, Gifford E, Smith RS, et al. RPGRIP1 is essential for normal rod photoreceptor outer segment elaboration and morphogenesis. *Human Molecular Genetics.* 2009;18(22):4329-4339.
20. Zhou W, Otto EA, Cluckey A, et al. FAN1 mutations cause karyomegalic interstitial nephritis, linking chronic kidney failure to defective DNA damage repair. *Nat Genet.* 2012;44(8):910-915.
21. Ciccia A, Elledge SJ. The DNA damage response: making it safe to play with knives. *Mol Cell.* 2010;40(2):179-204.
22. Attanasio M, Uhlenhaut NH, Sousa VH, et al. Loss of GLIS2 causes nephronophthisis in humans and mice by increased apoptosis and fibrosis. *Nat Genet.* 2007;39(8):1018-1024.
23. Atala A, Freeman MR, Mandell J, Beier DR. Juvenile cystic kidneys (jck): a new mouse mutation which causes polycystic kidneys. *Kidney Int.* 1993;43(5):1081-1085.
24. Bergmann C, Fliegauf M, Brüchle NO, et al. Loss of Nephrocystin-3 Function Can Cause Embryonic Lethality, Meckel-Gruber-like Syndrome, Situs Inversus, and Renal-Hepatic-Pancreatic Dysplasia. *The American Journal of Human Genetics.* 2008;82(4):959-970.

25. Sugiyama N, Yokoyama T. Sustained cell proliferation of renal epithelial cells in mice with inv mutation. *Genes to Cells.* 2006;11(10):1213-1224.
26. Sang L, Miller JJ, Corbit KC, et al. Mapping the NPHP-JBTS-MKS protein network reveals ciliopathy disease genes and pathways. *Cell.* 2011;145(4):513-528.
27. Cantiello HF. A tale of two tails: ciliary mechanotransduction in ADPKD. *Trends in Molecular Medicine.* 2003;9(6):234-236.
28. Gao J, Cheon K, Nusinowitz S, et al. Progressive photoreceptor degeneration, outer segment dysplasia, and rhodopsin mislocalization in mice with targeted disruption of the retinitis pigmentosa-1 (Rp1) gene. *Proceedings of the National Academy of Sciences.* 2002;99(8):5698-5703.
29. Huang WC, Wright AF, Roman AJ, et al. RPGR-Associated Retinal Degeneration in Human X-Linked RP and a Murine Model. *Investigative Ophthalmology & Visual Science.* 2012;53(9):5594-5608.
30. Humphries MM, Rancourt D, Farrar GJ, et al. Retinopathy induced in mice by targeted disruption of the rhodopsin gene. *Nat Genet.* 1997;15(2):216-219.
31. Deretic D. A role for rhodopsin in a signal transduction cascade that regulates membrane trafficking and photoreceptor polarity. *Vision Research.* 2006;46(27):4427-4433.
32. Murga M, Bunting S, Montana MF, et al. A mouse model of ATR-Seckel shows embryonic replicative stress and accelerated aging. *Nat Genet.* 2009;41(8):891-898.
33. Griffith E, Walker S, Martin C-A, et al. Mutations in pericentrin cause Seckel syndrome with defective ATR-dependent DNA damage signaling. *Nat Genet.* 2008;40(2):232-236.
34. Kalay E, Yigit G, Aslan Y, et al. CEP152 is a genome maintenance protein disrupted in Seckel syndrome. *Nat Genet.* 2011;43(1):23-26.
35. Sir J-H, Barr AR, Nicholas AK, et al. A primary microcephaly protein complex forms a ring around parental centrioles. *Nat Genet.* 2011;43(11):1147-1153.
36. Ruzankina Y, Pinzon-Guzman C, Asare A, et al. Deletion of the Developmentally Essential Gene ATR in Adult Mice Leads to Age-Related Phenotypes and Stem Cell Loss. *Cell Stem Cell.* 2007;1(1):113-126.
37. AbouAlaiwi WA, Ratnam S, Booth RL, Shah JV, Nauli SM. Endothelial cells from humans and mice with polycystic kidney disease are characterized by polyploidy and chromosome segregation defects through survivin down-regulation. *Human Molecular Genetics.* 2011;20(2):354-367.
38. Bukanov NO, Smith LA, Klinger KW, Ledbetter SR, Ibraghimov-Beskrovnaya O. Long-lasting arrest of murine polycystic kidney disease with CDK inhibitor roscovitine. *Nature.* 2006;444(7121):949-952.
39. Bukanov NO, Moreno SE, Natoli TA, et al. CDK inhibitors R-roscovitine and S-CR8 effectively block renal and hepatic cystogenesis in an orthologous model of ADPKD. *Cell Cycle.* 2012;11(21):4040-4046.
40. Hansen GM, Markesich DC, Burnett MB, et al. Large-scale gene trapping in C57BL/6N mouse embryonic stem cells. *Genome Research.* 2008;18(10):1670-1679.
41. Seong E, Saunders TL, Stewart CL, Burmeister M. To knockout in 129 or in C57BL/6: that is the question. *Trends in Genetics.* 2004;20(2):59-62.
42. Airik R, Bussen M, Singh MK, Petry M, Kispert A. Tbx18 regulates the development of the ureteral mesenchyme. *The Journal of Clinical Investigation.* 2006;116(3):663-674.
43. Thompson DA, Khan NW, Othman MI, et al. Rd9 Is a Naturally Occurring Mouse Model of a Common Form of Retinitis Pigmentosa Caused by Mutations in RPGR-ORF15. *PLoS ONE.* 2012;7(5):e35865.
44. Grupp C, Begher M, Cohen D, Raghunath M, Franz H-E, Müller GA. Isolation and characterization of the lower portion of the thin limb of Henle in primary culture. *American Journal of Physiology - Renal Physiology.* 1998;274(4):F775-F782.

SUPPLEMENTAL INFORMATION

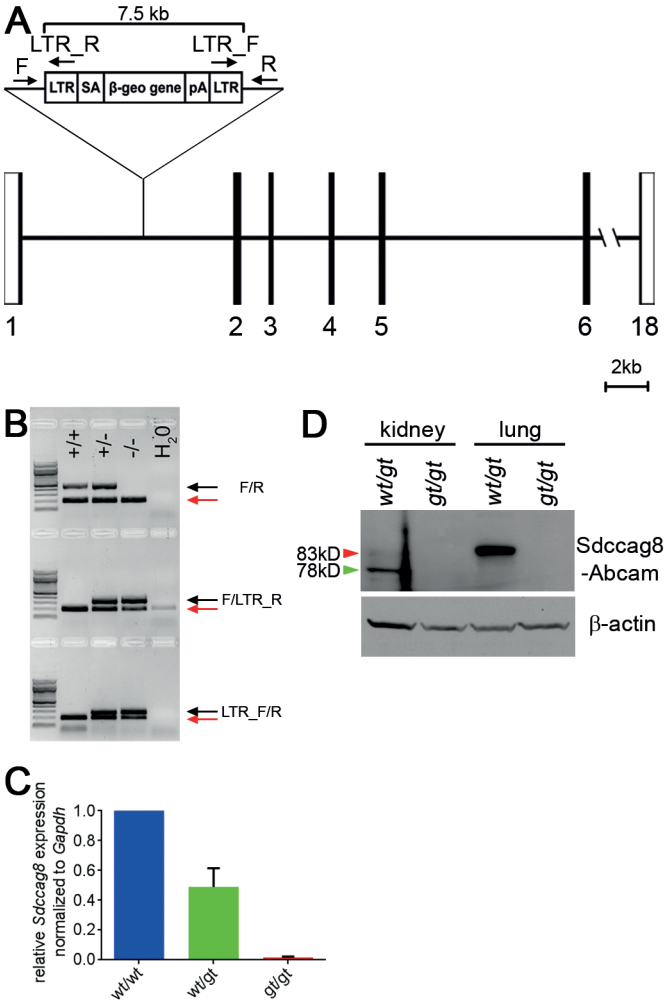

Supplementary Figure 1. Generation of *Sdccag8*$^{gt/gt}$ mice. (A) Diagram of the insertion point of the gene-trap cassette VICTR24 between exons 1 and 2 into the wild type Sdccag8 locus. Genotyping primer location indicated as F - Sdccag8-F, LTR-R - Sdccga8-LTR-R, LTR-F - Sdccag8-LTR-F and R - Sdccga8-R. Exons indicated with numbers. (B) Genotyping PCR products from tail tips. Black arrows indicate *Sdccag8* PCR bands. Primers F and R generate a 490 bp product from wild type allele, primers F and LTR_R generate 349 bp product and primers LTR_F and R generate a 290 bp product from a gene-trapped allele. Red arrows indicate internal PCR control bands (210 bp) confirming that DNA was present in each reaction mixture, except the water control. (C) qRT-PCR analysis on MEFs (n=4) demonstrates absence of any *Sdccag8* transcript in the homozygous gene-trapped animals. (D) Western blot analysis on *Sdccag8*$^{wt/gt}$ and *Sdccag8*$^{gt/gt}$ kidney and lung lysates confirms the absence of both - 78 kDa and 83 kDa *Sdccag8* protein isoforms from Sdccag8$^{gt/gt}$ tissues. β-actin was used as a loading control. *wt*, Sdccag8 wild type allele; *gt*, Sdccag8 gene-trap allele.

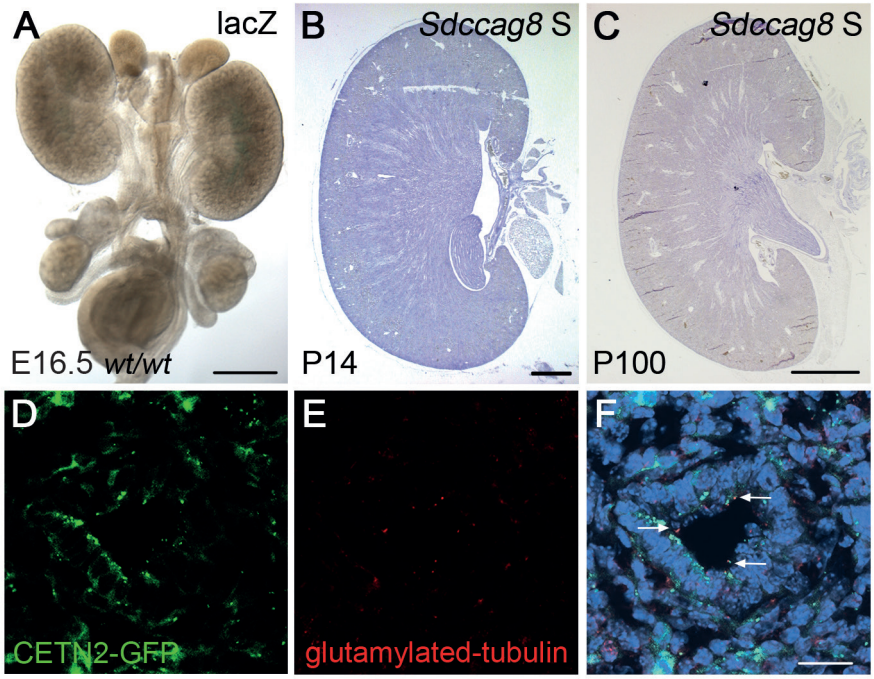

Supplementary Figure 2. *Sdccag8* expression in kidney and lung. (A) No X-gal staining is observed in E16.5 wild type urogenital system. (B and C) No signal is visible in P14 (B) and P100 (C) kidneys hybridized with *Sdccag8* sense probe. (D - F) CETN2-GFP expressing bronchiole epithelium cells (D) are negative for the cilia marker poly-glutamylated tubulin (E, white arrows) in E16.5 mouse lung section (F). Nuclei are stained with DAPI. Scale bar: (A) 400 µm; (B) 800 µm; (C) 2 mm; (D - F) 20 µm. *wt*, Sdccag8 wild type allele.

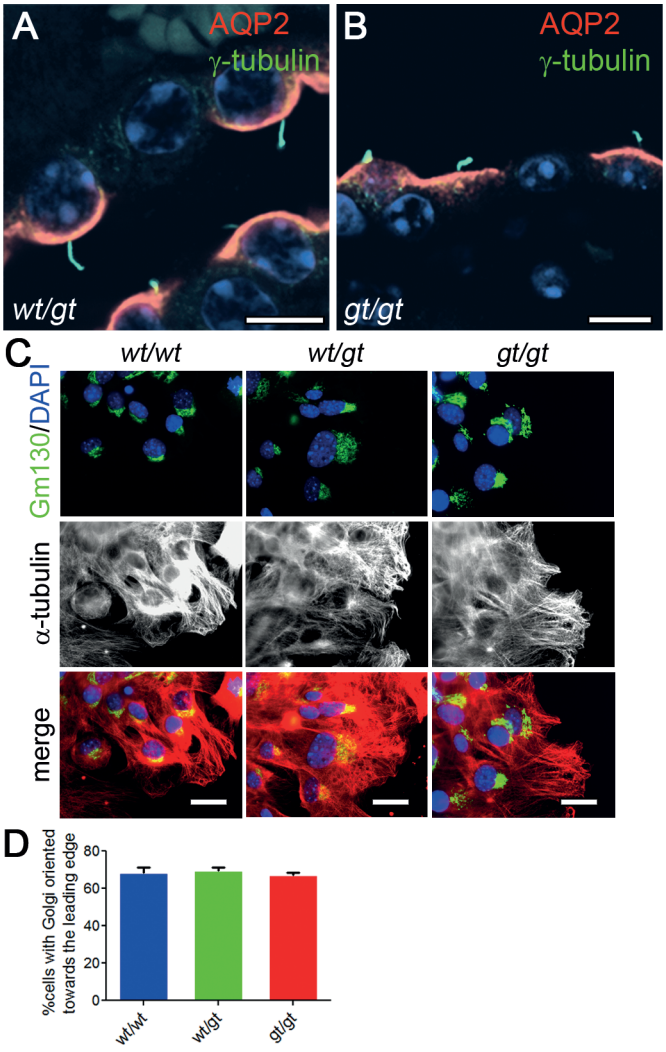

Supplementary Figure 3. *Sdccag8*$^{gt/gt}$ kidneys do not show global ciliary malformations, and Sdccag8$^{gt/gt}$ MEFs display normal cytoskeletal rearrangements in the wound healing assay. (A and B) Cortical collecting ducts (stained with AQP2 - red) bear normal looking cilia (stained with acetylated antibody - green) in *Sdccag8*$^{gt/gt}$ kidneys (B). (C) Immunofluorescence staining of wild type, *Sdccag8*$^{wt/gt}$ and *Sdccag8*$^{gt/gt}$ MEFs show similar Golgi (green) orientation towards the leading edge of the cell in the wound healing assay. DAPI labels nuclei, and α-tubulin stains microtubules. (D) Graphical representation of the percentage of cells showing Golgi orientation towards the leading edge of the cell 24 hours after wound scratch (each genotype n=3). Scale bar: (A) 7.5 µm, (B) 10 µm; (C) 40 µm. *wt*, Sdccag8 wild type allele; *gt*, *Sdccag8* gene trap allele.

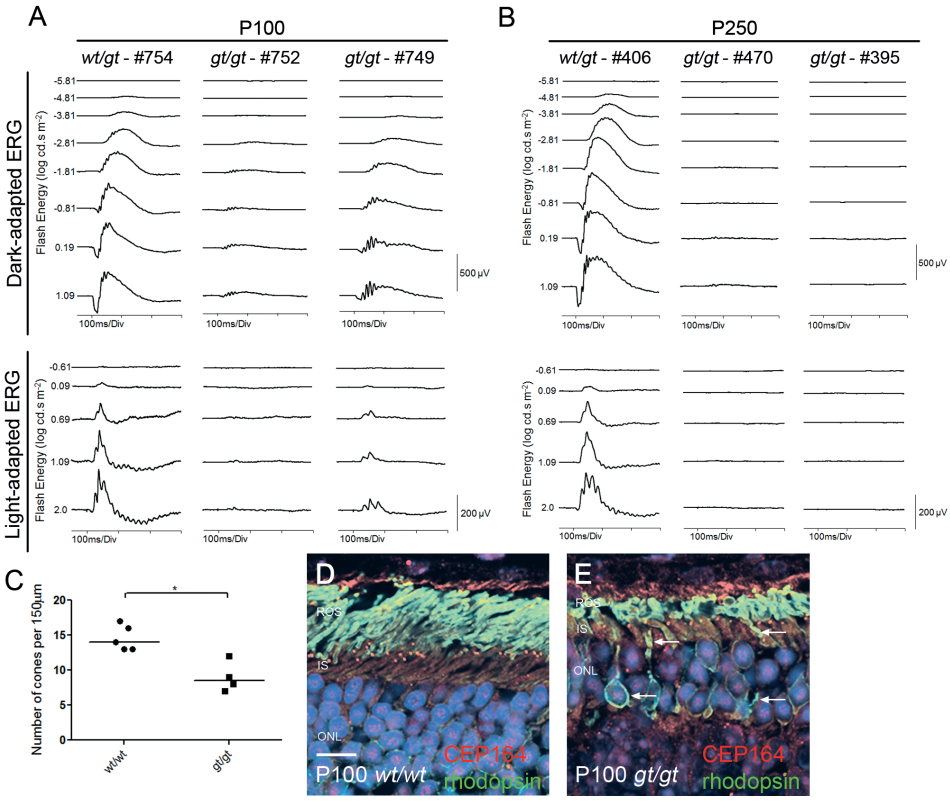

Supplementary Figure 4. *Sdccag8*$^{gt/gt}$ mice develop a progressive loss of vision and have reduced cone numbers. (A–B) Representative dark-adapted and light-adapted ERG waveforms are shown for increasing stimulus intensities for the *Sdccag8*$^{wt/gt}$ and *Sdccag8*$^{gt/gt}$ mice at P100 (A) and P250 (B). The *Sdccag8*$^{wt/gt}$ mice had normal dark- and light-adapted ERGs while the ERG responses of *Sdccag8*$^{gt/gt}$ were highly reduced in amplitude with varying degrees of loss of rod and cone function. (C) Number of PNA-FITC labeled cone cells within a 150mm area of retina. Values are mean numbers from 5 wild type and 4 *Sdccag8*$^{gt/gt}$ P30 mouse retinas. *P<0.05. (D, E) Immunolocalization of CEP164 and rhodopsin in the P100 retina shows rhodopsin accumulation (white arrows) at the photoreceptor inner segment plasma membrane and cell bodies in *Sdccag8*$^{gt/gt}$ retina (E). Scale bars: (D, E) 10 µm. ROS, retinal outer segment; IS, inner segment; ONL, outer nuclear layer; *wt*, Sdccag8 wild type allele; *gt*, *Sdccag8* gene trap allele.

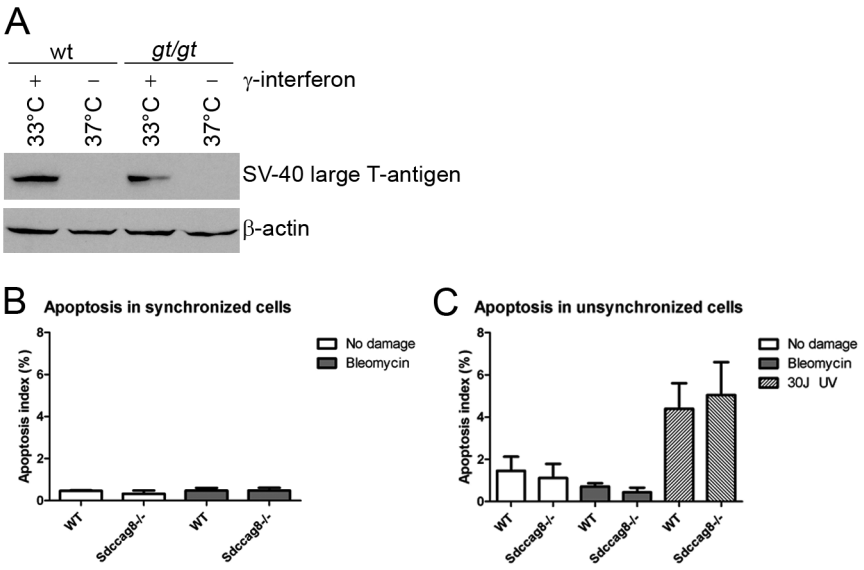

Supplementary Figure 5. Western blot analysis of SV-40 large T-antigen expression and quantitation of apoptotic index in *Sdccag8*$^{gt/gt}$ cells. (A) SV-40 large T-antigen protein is expressed in wild type and *Sdccag8*$^{gt/gt}$ isolated adult kidney cells when grown at 33°C in the presence of γ-interferon, and is absent from cells grown at 37°C without γ-interferon. β-actin was used as a loading control. *Sdccag8*$^{gt/gt}$ cells' apoptosis indices are comparable to those of wild type cells both in synchronized (B) and unsynchronized (C) cultures after treatment with a low dose of bleomycin (4.5U/ml) or 30J UV-light. *wt,* Sdccag8 wild type allele; *gt, Sdccag8* gene-trap allele.

CHAPTER 6

DNA replication stress underlies renal phenotypes in *CEP290*-associated Joubert syndrome

J Clin Invest., in press (2015)

Gisela G. Slaats, Joshua C. Saldivar, Julien Bacal, Michelle K. Zeman, Andrew C. Kile, Ann Marie Hynes, Shalabh Srivastava, Jekaterina Nazmutdinova, Krista den Ouden, Miriam S. Zagers, Veronica Foletto, Marianne C. Verhaar, Colin Miles, John A. Sayer, Karlene A. Cimprich, Rachel H. Giles

ABSTRACT

Juvenile ciliopathy syndromes that are associated with renal cysts and premature renal failure are commonly the result of mutations in the gene encoding centrosomal protein CEP290. In addition to centrosomes and the transition zone at the base of the primary cilium, CEP290 also localizes to the nucleus; however, the nuclear function of CEP290 is unknown. Here we demonstrated that reduction of cellular CEP290 in primary human and mouse kidney cells as well as in zebrafish embryos leads to enhanced DNA damage signaling and accumulation of DNA breaks *ex vivo* and *in vivo*. Compared to those from WT mice, primary kidney cells from *Cep290*-deficient mice exhibited supernumerary centrioles, decreased replication fork velocity, fork asymmetry, and increased levels of cyclin-dependent kinases (CDKs). Treatment of *Cep290*-deficient cells with CDK inhibitors rescued DNA damage and centriole number. Moreover, the loss of primary cilia that results from CEP290 dysfunction was rescued in 3D cell culture spheroids of primary murine kidney cells after exposure to CDK inhibitors. Together, our results provide a link between CEP290 and DNA replication stress and suggest CDK inhibition as a potential treatment strategy for a wide range of ciliopathy syndromes.

INTRODUCTION

Mutations in *CEP290* are known to cause the entire spectrum of ciliopathies, including childhood renal failure due to nephronophthisis (NPHP) (1), Joubert syndrome (JS; MIM 610188), the lethal Meckel Grüber syndrome (MKS; MIM 611134), Bardet-Biedl Syndrome (BBS) (MIM 209900), Senior-Løken Syndrome (SLS) (MIM 610189) and up to 25% of Leber Congenital Amaurosis cases (LCA; MIM 611755), although no precise genotype-phenotype correlations have been found (2). Around 50% of patients with JS where there is a cerebello-oculo-renal phenotype have mutations in *CEP290* (3). Progressive kidney damage, secondary to NPHP, leads to end-stage renal disease (ESRD) in affected patients and occurs at a mean age of 14 years of age (4). NPHP is the most frequent monogenic cause of ESRD in the first 3 decades of life (5) and accounts for 5-10% of all children with ESRD. Disease mechanisms underlying NPHP, which is characterized by a tubulointerstitial fibrosis, tubular atrophy and corticomedullary cyst formation, implicate abnormal ciliary and centrosomal proteins (5).

CEP290 is a large multi-domain centrosomal protein (6); identified binding partners of CEP290 include centrosomal proteins CEP131 and CCDC13, scaffold proteins pericentrin and PCM1, transcription factors including ATF4, and proteins that are implicated in the DNA damage response (DDR), for example ataxia telangiectasia and Rad3-related (ATR). (1,7-9). The localization of CEP290 to the centrosome is dynamic, depending on the stage of cell cycle and expression of the primary cilium (1). The primary cilium is expressed in G_0 after exit from the cell cycle, when the mother centriole is docked to the plasma membrane. Cells disassemble their cilium at the end of G_1 in order to duplicate their centrosome for mitotic spindle formation (10). CEP290 localizes to the transition zone at the base of the primary cilium as well as at the centrosomes, in a complex with other centrosomal proteins: NPHP1, INVS/NPHP2, NPHP4, IQCB1/NPHP5, RPGRIP1L/NPHP8 and NEK8/NPHP9 (11-13); mutations in any of these proteins can cause one or more ciliopathy syndromes as well. CEP290 also localizes to the nucleus, although its function there is entirely unknown (1). One possibility is that CEP290 acts similarly to the other ciliary proteins mutated in renal ciliopathies (CEP164, ZNF423, SDCCAG8, NEK8) which have been associated with enhanced DDR signalling (14-16). A single study examining the events leading to DNA damage in this setting recently established a role for NEK8/NPHP9 in the ATR-regulated replication stress response and in the regulation of S-phase CDK activity (16). However, only three families with mutations in *NEK8* have been described (17), making these data less clinically relevant.

We set out to extend this correlation to a broader clinical base and investigate the role of *CEP290* loss in DNA damage response signalling and replication stress. To confirm that defects in DDR signaling underlie progressive renal disease seen in NPHP would allow a novel rationale for therapeutic interventions in these patients. Our findings support the

overall hypothesis that NPHP-related ciliopathies (NPHP-RC) are initially caused by DNA damage and replication stress during early stages of development (18). Here we use primary cells isolated from kidneys of *Cep290*$^{LacZ/LacZ}$ mice with JS symptoms and their wild type littermates (19) to investigate DNA damage signalling and the replication stress response. We find enhanced DNA damage signalling and concomitant DNA breaks in *Cep290*$^{LacZ/LacZ}$ cells, in addition to supernumery centrioles. Decreased replication fork velocity and fork asymmetry underlie the DNA damage. Additionally, application of CDK inhibitors rescues the DNA damage phenotypes, and restores the ability of *Cep290*$^{LacZ/LacZ}$ cells to ciliate. These findings provide new insight into the disease mechanism of NPHP-RC and will help to refine treatment strategies.

RESULTS

CEP290 depletion causes DNA damage *ex vivo*, *in vitro*, and *in vivo*

Recent studies have implicated DDR and sensitivity to replication stress in the development of ciliopathies. To explore the breadth of molecular effects in different human ciliopathies, we tested siRNA targeting of *Ofd1* and *Mks1,* which are characteristic of Orofaciodigital syndrome (OFD; MIM 311200) and MKS respectively. Increased levels of DDR signalling are observed for all siRNAs tested (Figure S1A). To test the effect of *CEP290* mutations in patient material, we isolated urine-derived renal epithelial cells (URECs) from a Joubert syndrome patient with compound heterozygous mutations in *CEP290*, p.Q950Pfs*6 and p.K939N and observed increased γH2AX levels and decreased CEP290 levels compared to a healthy donor on Western blot (Figure 1A and S1C). We next lowered endogenous levels of CEP290 in URECs of two healthy donors, and determined siRNA efficiency to be about 70% in the single donor tested (due to limited material n=1; **p<0.01; Figure S1A). Western blots from both donors revealed increased DNA damage signalling levels (γH2AX) after 48 hours of siCEP290 transfection (Figure 1B and S1B). Similar results were observed upon siRNA knockdown of *Cep290/CEP290* in mIMCD3 and hTERT-RPE cell lines, which suggest this is not restricted to renal cells alone (n=3; Figure 1C and S1A-B). Immunofluorescence shows increased γH2AX foci in URECs from the Joubert patient, as well as in RPE and mIMCD3 cells after siRNA knockdown of *CEP290/Cep290*, compared to control (n=3; **p<0.01 and ***p<0.001 Figure 1D). Next, we examined whether DDR signalling would be induced after a *cep290* ATG-targeting morpholino (mo) was injected in zebrafish (1). Western blot of 3.5 ng or 4 ng mo-injected fish targeting *cep290* shows increased γH2AX 48 hours post fertilization (hpf), compared to control (n=3; Figure 1E and S1B, D). Furthermore, γH2AX levels increased with age of mouse *Cep290*$^{LacZ/LacZ}$ kidneys as compared to wild type littermates, suggesting a role for DNA damage or DNA damage signalling in the pathophysiology of NPHP-RC (Figure 1F-G; n=13, *p<0.05).

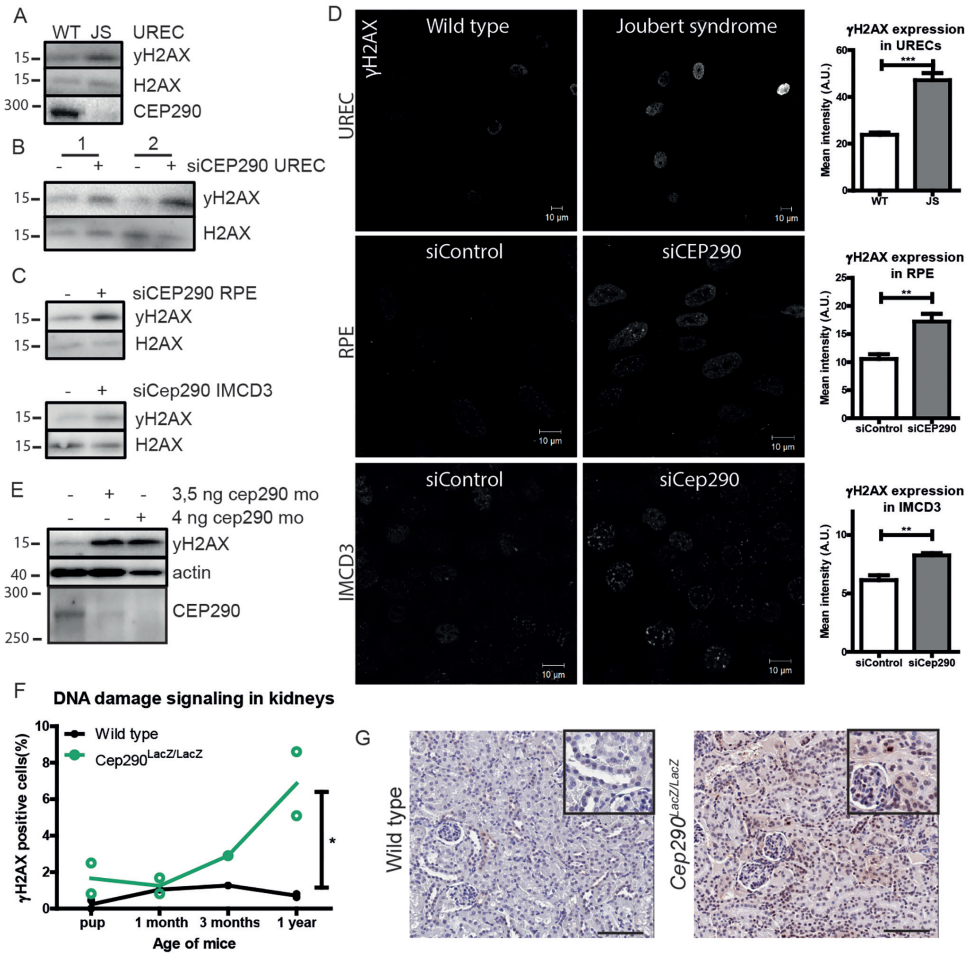

Figure 1. DDR signalling is enhanced *ex vivo, in vitro,* and *in vivo*

(A) Western blot of urine-derived epithelial cell (UREC) lysates of a healthy donor (WT) and Joubert syndrome (JS) patient with compound heterozygous mutations in *CEP290*; p.Q950Pfs*6 and p.K939N. CEP290 protein expression loss and increased γH2AX levels are detected in the JS protein lysate. H2AX is loading control. **(B)** Increased γH2AX levels are detected in siCEP290 transfected WT-URECs, 48 hours after siCEP290 transfection. H2AX is loading control. **(C)** RPE and mIMCD3 cells depleted for CEP290/Cep290 by siRNA show increased γH2AX levels compared to control siRNA transfection (56 hours). H2AX is loading control (n=3). **(D)** Immunofluorescent staining of γH2AX in WT and JS URECs, and RPE and mIMCD3 cells depleted for CEP290/Cep290 by siRNA, and quantification of intensities/nucleus (10 µm scale bar; n=3; 100 cells scored/condition; T-test **p<0.01, ***p<0.001). **(E)** Western blot of zebrafish injected with 3.5 or 4 ng cep290 ATG-targeting mo. Loss of CEP290 protein expression and increased γH2AX levels are detected in cep290 mo-injected zebrafish lysates 48 hpf. Actin is loading control (n=3). **(F)** More γH2AX (brown) staining in kidneys of homozygote *Cep290*$^{LacZ/LacZ}$ gene trap mice compared to wild type, increasing with age (n=13, between 5,000–7,000 cells scored per animal) (Linear model, goodness of fit R^2=0.86; *p<0.05). **(G)** Example of wild type mouse kidney and *Cep290*$^{LacZ/LacZ}$ gene trap mouse kidney at age 3 months stained for γH2AX (brown). Inserts show magnification. Scale bar represents 100 µm. Quantification of western blots is in Supplemental Figure 1.

Western blots support the presence of enhanced DNA damage signalling (γH2AX) in primary mouse collecting duct cells isolated from *Cep290*$^{LacZ/LacZ}$ kidneys (19) as opposed to their wild type littermates (Figure 2A). Immunofluorescence confirmed higher intensities of γH2AX expression per nucleus in the *Cep290*$^{LacZ/LacZ}$ cells, which was further enhanced by incubation with the replication stress-inducing agent aphidicolin (APH) (20) (400 nM, 18 hours; Figure 2B-C; n=3; *p<0.05).

To differentiate between actual DNA fragmentation or simply increased DDR signalling, we assessed whether DNA double-strand breaks were formed using neutral comet assays. Increased comet tail moments were observed in *Cep290*$^{LacZ/LacZ}$ cells, and exacerbated by APH incubation (400 nM, 18 hour; n=5; *p<0.05; Figure 2D-E). We conclude that loss of *CEP290* generates double-stranded breaks in DNA. Because CEP290 is a centrosomal protein, we examined centriole numbers. Supernumerary centrioles were observed in the *Cep290*$^{LacZ/LacZ}$ cells (Figure 2F-G), which might contribute to genome instability. We therefore performed DNA content analysis by FACS (DAPI and BrdU); *Cep290*$^{LacZ/LacZ}$ cells demonstrate changes in DNA content as compared to the wild type control cells. Wild type cells show a normal G1 (2N DNA) and G2 (4N DNA) cell cycle profile, whereas *Cep290*$^{LacZ/LacZ}$ cells have an aberrant DNA content profile that does not match 2N or 4N DNA (Figure 2H). To ensure this result was not confounded by contamination or clonal drift we grew *Cep290*$^{LacZ/LacZ}$ cells clonally and observed similar data in all seven clones tested (Figure S2B-C). Our data support a role for CEP290 in genome stability.

CEP290 protects cells from replication stress

The formation of DNA breaks is frequently a consequence of perturbed DNA replication, a phenomenon referred to as replication stress (21). Clonogenic survival assays using the wild type and *Cep290*$^{LacZ/LacZ}$ mouse primary kidney cells incubated with different doses of APH for 18 hours suggest that Cep290$^{LacZ/LacZ}$ cells are more sensitive to replication stress (Figure 3A; n=3; ***p<0.001). To investigate the underlying molecular mechanism we next performed single-molecule DNA fiber analysis of replication fork progression in the wild type and *Cep290*$^{LacZ/LacZ}$ mouse primary kidney cells. To label newly synthesized DNA, cells were pulsed first with iododeoxyuridine (IdU) and then with chlorodeoxyuridine (CldU), each for 15 minutes. The double-labeling with IdU and CldU allows the assessment of fork symmetry and velocity as well as origin firing (Figure 3B and 3E) (22). We first asked whether Cep290 modulated the fork velocity, also referred to as the rate of DNA synthesis, by measuring the lengths of the CldU-tracts. We found that the replication fork velocity is decreased (n=4; ***p<0.001; Figure 3B-D) in the *Cep290*$^{LacZ/LacZ}$ cells. After origin firing, forks move bidirectionally in a relatively synchronous manner, unless there is a problem with fork progression or restart. Thus, we also analyzed the symmetry of sister forks emanating from a common origin, as fork asymmetry is an indicator of fork stalling. To do so, we measured the lengths of the CldU tracts for each pair of sister forks and plotted

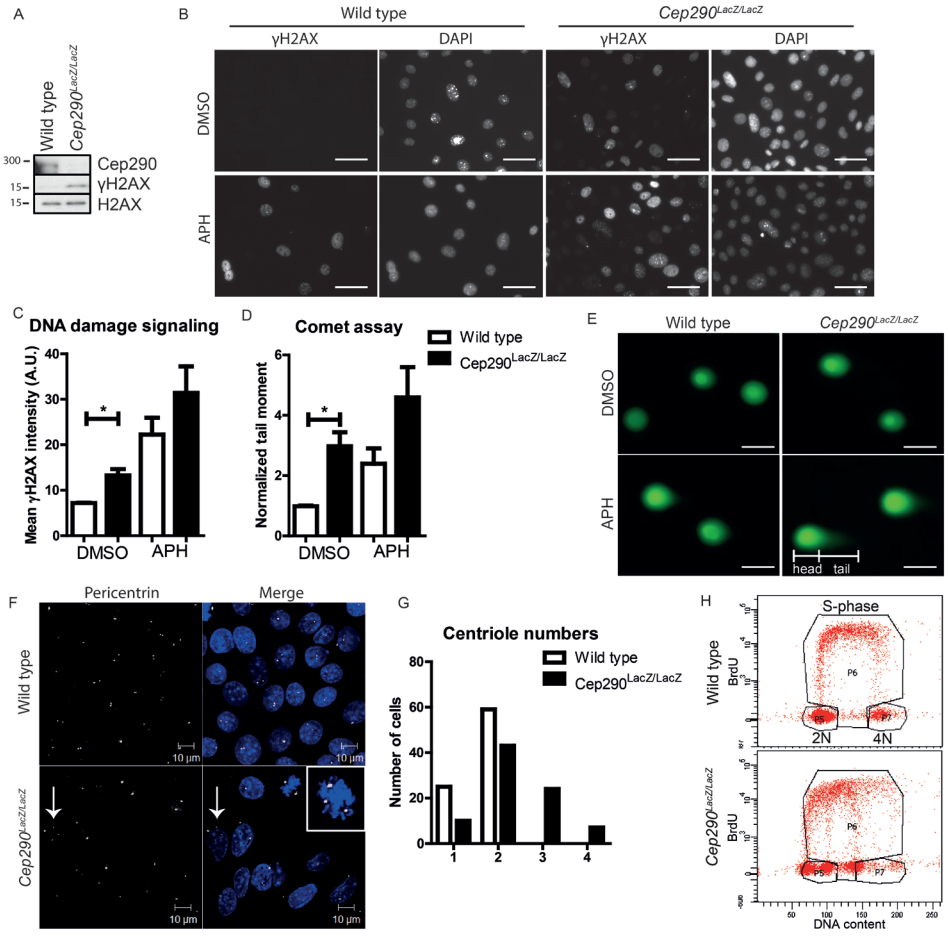

Figure 2. DNA damage is enhanced in Cep290 depleted cells
(**A**) Western blot of Cep290$^{LacZ/LacZ}$ and wild type primary mouse kidney cell lysates. Increased H2AX phosphorylation is detected in the Cep290 depleted cells, with H2AX as loading control. (**B**) Immunofluorescent staining of γH2AX in control DMSO and 400 nM APH (18 hours) treated cells, scale bar represents 10 µm. (**C**) Quantification of γH2AX intensities per nucleus of control DMSO and 400 nM APH (18 hours) treated cells (n=3; 100 cells scored/condition; Two-way ANOVA, *p<0.05). (**D**) Quantification of comet tail moments of 400 nM APH (18 hours) treated cells normalized to control DMSO treated wild type cells (n=3; 50 cells scored/condition; Two-way ANOVA, *p<0.05). (**E**) Images of SYBR-gold stained DNA in comet tail assays, scale bar represents 10 µm. (**F**) Immunofluorescent staining of wild type and *Cep290*$^{LacZ/LacZ}$ cells for pericentrin (white) reveals supernumerary centrioles (arrow) in *Cep290*$^{LacZ/LacZ}$ cells. Insert is multipolar (>2) spindle, scale bar represents 10 µm. (**G**) Quantification of centriole number in wild type and *Cep290*$^{LacZ/LacZ}$ cells (84 cells scored per cell line; n=3). (**H**) BrdU FACS of wild type and *Cep290*$^{LacZ/LacZ}$ cells shows normal DNA content and cell cycle for wild type cells, however, *Cep290*$^{LacZ/LacZ}$ cells have irregular DNA content (10,000 events measured; n=3).

each pair as the right length versus the left length. From this analysis, we found that *Cep290*$^{LacZ/LacZ}$ cells have an increase in asymmetric forks, indicative of an inherent loss of fork stability in the absence of Cep290 (n=2; ***p<0.001; Figure 3E-G). Importantly, sister fork asymmetry and reduced fork velocity are both indicators of replication stress and suggest that DNA break formation in Cep290$^{LacZ/LacZ}$ cells occurs as a result of increased replication stress. To examine cell cycle S-phase progression defects, which are potentially induced by replication stress, we quantified cells in early S-phase 18 hours after BrdU pulse labeling of cells in S-phase. IMCD3 cells revealed a higher proportion of cells in early S-phase after Cep290 siRNA treatment compared to control (Figure S3A; n=3; **p<0.01), suggesting that S-phase progression is slower due to replication fork defects. As these results mirror those seen in *Nek8*$^{-/-}$ cells (*NPHP9*), it seems likely that defective DNA replication dynamics are a common feature of NPHP-RC.

CEP290 is stabilized upon DNA damage induction

Wild type primary kidney cells were synchronized with thymidine or nocodazole and released for 5 hours to examine Cep290 expression throughout the cell cycle. We found that CEP290 levels varied, and the highest levels of CEP290 were observed in S-phase (Figure 4A-B and S2A; n=4). Since loss of Cep290 causes replication stress we examined whether CEP290 precipitates with chromatin. Standard chromatin fractionation assays convincingly show endogenous Cep290 to be enriched in the chromatin cell fraction (n=2; Figure 4C). Immunofluorescence revealed expression at the base of the primary cilium (Figure S2D) and nuclear expression as well (n=3; Figure 4D). Endogenous Cep290 protein levels did not increase or relocalize after treatment with APH (400 nM, 24 hours). However, the DNA damaging agent Adriamycin (ADR) (1 μM, 24 hours) upregulated Cep290 expression (n=4; **p<0.01; Figure 4A-B,D), indicating a response of Cep290 to DNA damage independent of DNA replication progression.

Cyclin-dependent kinase (CDK) inhibitors rescue DNA damage and cilia

The DNA fiber results suggest that CEP290 has an important function during DNA replication to ensure efficient fork progression and stability. It is known that elevated cyclin A-associated CDK1/2 activity can cause similar defects on replication fork dynamics. Furthermore, we have previously shown that partial inhibition of CDK1/2 activity can largely suppress the DNA damage resulting from NEK8 loss (16). We therefore hypothesized that enhanced CDK1/2 activity in *Cep290*$^{LacZ/LacZ}$ primary kidney cells could be responsible for the increased DNA damage signalling and DNA breaks during disturbed DNA replication (23,24). Indeed, total protein levels of CDK1 and CDK2 are higher, as well as cyclin-A and cyclin-B levels in *Cep290*$^{LacZ/LacZ}$ cells (Figure 5A). In vitro CDK1 and CDK2 kinase assays reveal a trend towards enhanced cyclin-A associated CDK activity (+26%), and cyclin-B associated CDK activity (+7%) in *Cep290*$^{LacZ/LacZ}$ cells (Figure 5B and S4A; n=4), although the intra-

experimental variation was high. In addition, the single kinase assay of WT and JS patient URECs reveals modestly increased cyclin A- (+7%) and cyclin-B associated CDK activity (+14%) as well (Figure 5C and S4B; n=1). We followed up by testing whether the increase in DNA damage signalling (using markers phosphorylated Kap1, γH2AX, phosphorylated CHK1; n=3) and the increase in DNA breaks measured by neutral comet assays (n=2) could be rescued in *Cep290*$^{LacZ/LacZ}$ cells by treatment with a CDK1/2 inhibitor (200nM, 18 hours; Figure 5D-E). Both phenotypes could be rescued by CDK1/2 inhibition. To investigate whether reduced cilia frequency could be similarly rescued by CDK1/2 inhibition, we used a 3D spheroid culture assay and compared *Cep290*$^{LacZ/LacZ}$ mouse primary kidney cells to wild type littermate cells. We observed a rescue of ciliation by CDK1/2 inhibition (n=2; *p<0.05 and **p<0.01; Figure 5F-G). Because the effects of CDK1/2 inhibition on the cell cycle might bias our ciliary frequency data, we measured cell cycle distribution; after CDK1/2 inhibition the G1 cell population decreased from 60% to 31%, whereas the G2 cell population increased from 12% to 45% (200 nM, 18 hours, n=3; Figure 5H).

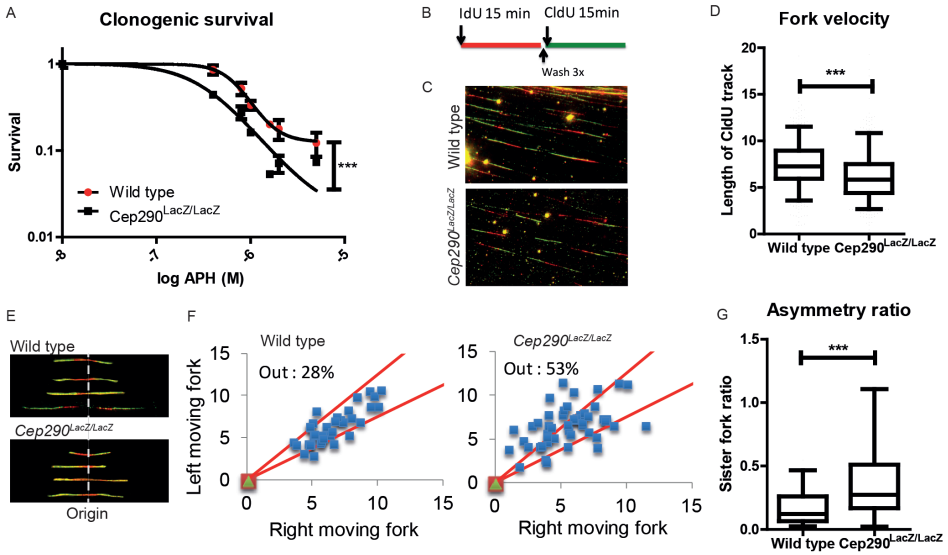

Figure 3. Loss of Cep290 leads to replication stress
(**A**) Clonogenic survival (on log scale, -6 means $1{\cdot}10^{-6}$ M) of control DMSO and 500 to 5000 nM APH (18 hours) treated cells showing sensitivity to replication stress of Cep290$^{LacZ/LacZ}$ cells. Log IC50 curves are compared (n=3; ***p<0.001) (**B**) Schematic overview of pulse labeling of cells with IdU and CldU for 15 minutes. (**C**) Immunofluorescent staining of DNA fibers after pulse labeling with IdU (red) and CldU (green) respectively. (**D**) Quantification of replication fork velocity by measuring length of the CldU track. Cep290$^{LacZ/LacZ}$ cells demonstrate decreased fork velocity (700 tracks scored/condition; n=4; T-test ***p<0.001). (**E**) Immunofluorescent staining of DNA fibers after pulse labeling with IdU (red) and CldU (green) respectively. Asymmetric replication at origins in Cep290$^{LacZ/LacZ}$ cells is present. (**F**) Quantification of fork asymmetry at origins in Cep290$^{LacZ/LacZ}$ cells. When replication track differs more than 25% between the right and left moving fork, the measurement falls out the cutoff (50 tracks scored/condition). (**G**) Fork asymmetry ratio as calculated by the ratio of the right and left moving forks (50 tracks scored/condition; n=2; 5-95 percentile; T-test ***p<0.001).

This control experiment indicates that the gain of cilia is not caused by accumulation of cells in G1. Likewise, we wanted to exclude that rescue of the DNA damage and cilia phenotypes by CDK1/2 inhibition are caused by apoptosis. FACS revealed no enhanced apoptosis after CDK1/2 inhibition (18 h 200 nM; n=3; Figure S3C). Furthermore, centriole numbers in *Cep290*$^{LacZ/LacZ}$ mouse primary kidney cells were normalized after treatment with CDK1/2 inhibitor (18 h 200 nM; Figure S3B).

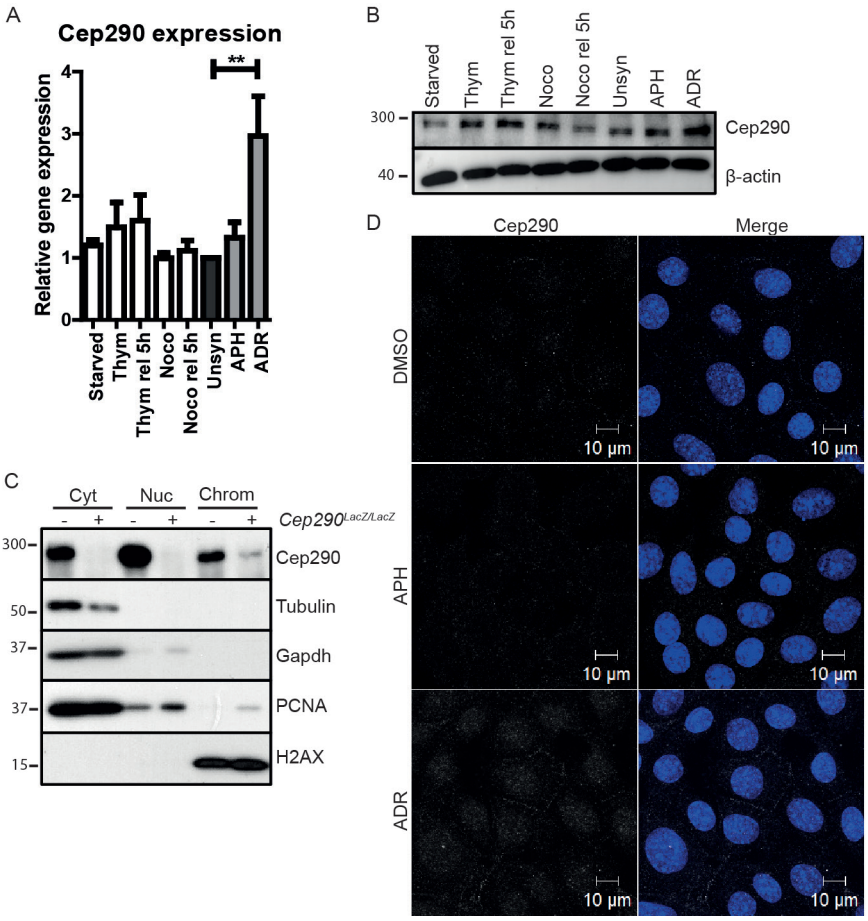

Figure 4. Expression and localization of Cep290
(**A**) Normalized *Cep290* gene expression levels were measured by RT-qPCR of wild type cells synchronized by serum starvation (G1), thymidine (S), nocodazole (G2) and release for 5 hours of these synchronizations, and unsynchronized, APH (400 nM) and ADR (1 µM) (24 hours) treated cells (n=4; One-way ANOVA **p<0.01). Concomitantly, protein expression was detected by Western blot, using β-actin as loading control (**B**). (**C**) Western blot of chromatin fractionation of wild type (-) and Cep290$^{LacZ/LacZ}$ (+) cells. Cep290 is expressed in the cytosol (GAPDH, tubulin), nucleus (PCNA) and chromatin enriched fraction (H2AX). (**D**) IF staining of Cep290 expression (white) of DMSO, APH (400 nM) and ADR (1µM) (18 hours) treated wild type cells. ADR exposure caused increased Cep290 levels. Scale bar represents 10 µm.

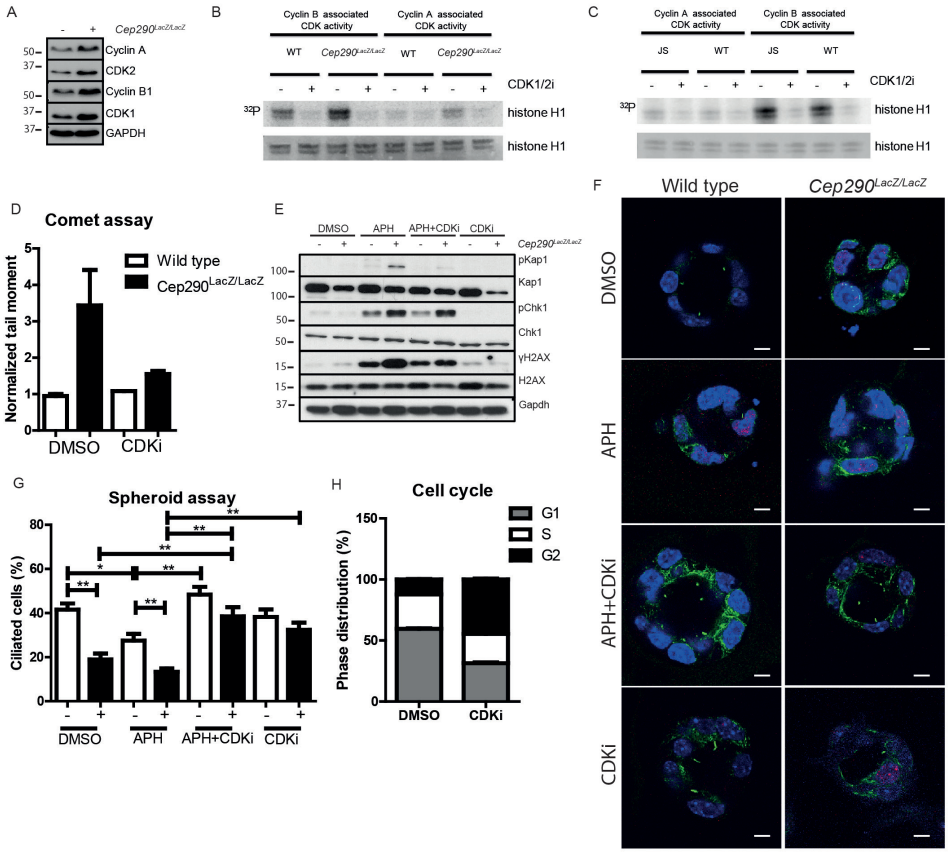

Figure 5. CDK1/2 inhibitor rescues DNA damage and primary cilia
(**A**) Western blot of *Cep290*$^{LacZ/LacZ}$ (+) and wild type (-) cell lysates show increased levels of CDK1, CKD2, Cyclin A, Cyclin B1 in Cep290-depleted cells. GAPDH is loading control. (**B**) In vitro CDK kinase assay of *Cep290*$^{LacZ/LacZ}$ and wild type (WT) cell lysates after precipitation of Cyclin A-CDK and Cyclin B1-CDK complexes (n=4). **(C)** CDK kinase assay of WT and JS patient URECs (n=1). Histone1 represents substrate level control. **(D)** DNA breaks are rescued by CDKi in comet tail moments of 200 nM CDK1/2 inhibitor (18 hours) treated cells normalized to control DMSO treated wild type cells (n=3; 50 cells scored/condition). (**E**) Western blot of Cep290$^{LacZ/LacZ}$ (+) and wild type (-) cells treated with 400 nM APH and/or 200 nM CDKi (18 hours). Higher phosphorylation levels of Kap1, H2AX, CHK1 in Cep290$^{LacZ/LacZ}$ cells with/without APH treatment, rescued by CDK1/2i. Unphosphorylated protein and GAPDH are loading controls. (**F**) 3D spheroids of wild type and Cep290$^{LacZ/LacZ}$ cells, stained for γH2AX (red) and ciliation (acetylated tubulin; green), treated with 400 nM APH and/or 200 nM CDKi (18 hours). Scale bars are 5 µm. (**G**) CDKi rescues ciliation in Cep290$^{LacZ/LacZ}$ and APH treated spheroids. (35 spheroids scored/condition) (n=3; data shown for single experiment; Three-way ANOVA *p<0.05, **p<0.01). (**H**) Cell cycle distribution of wild type cells treated with DMSO or 200 nM CDKi (18 hours) reveals increased cell number in G2 (black), decreased cell number in G1 (grey) after CDKi treatment (10,000 events measured; n=3).

DISCUSSION

CEP290 loss causes enhanced DNA damage signalling, DNA breaks, replication stress and supernumerary centrioles. These data describe the first function for CEP290 in the nucleus where the protein co-fractionates with chromatin. We show that CEP290 levels increase after DNA damage. Our data indicate a causal relationship of enhanced DNA damage response to a broad clinical range of *CEP290*-related ciliopathies. Accumulation of DNA damage can be attributed to disturbed replication forks. These insights into the pathogenesis of *CEP290*-loss are reminiscent with the molecular functions of another ciliopathy protein NEK8 (NPHP9) (16). Furthermore, increased DNA damage signalling was seen in CEP164, ZNF423, and SDCCAG8 associated NPHP (14,15), and hint at a general disease mechanism. Outside the nucleus it is interesting to note that Cep290 loss affects centriole duplication. The centriolar satellite complex including CEP290 has been previously reported to function in maintaining genome stability (7,8). A systematic analysis of all ciliopathy genes is required to confirm the breadth and depth of replication stress and centriole duplication defects. Furthermore, we demonstrate the use of disease modelling by siRNA-mediated gene depletion in URECs. Potential interventions as well as modelling molecular/cellular temporal-spatial events leading to the pathophysiology of renal ciliopathies from URECs will help tailor personalized treatments.

It is interesting to note that both Nek8 and Cep290-depleted cells demonstrate strikingly similar sensitivity to replication stress, decreased fork velocity, and fork asymmetry (16). In *Nek8*$^{-/-}$ cells enhanced cyclin-A associated CDK activity was observed and cyclin-B associated CDK activity was unchanged (16). Both *Nek8*$^{-/-}$ and *Cep290*$^{LacZ/LacZ}$ phenotypes are equally rescued by the pan CDK1/2 inhibitor, suggesting that the pathophysiology is conserved.

The functional consequences of *CEP290* depletion beyond cilia and ciliary signalling are novel. The hallmarks of the ciliopathy-associated nephronophthisis are corticomedullary cyst formation and interstitial fibrosis. The renal ciliopathy field has been dominated by studies of ciliary dysfunction and renal cysts; however, the more clinically relevant aspect of renal fibrosis has been largely ignored. We have obtained functional insight into the NPHP-RC pathogenesis and investigated the effect of CDK1/2 inhibitors on loss of function of *CEP290*. Use of CDK inhibitors as a potential treatment strategy has already shown some success in vivo (25,26), and our data confirms that changes in CDK protein levels may be widespread in NPHP patients justifying this approach. We would like to extend this knowledge to other forms of chronic kidney disease (27) and renal fibrosis, which are associated with DNA damage signalling.

METHODS

Cell culture

mIMCD3 and hTERT-RPE cells (ATCC) were grown in DMEM:F12 (1:1) medium with 10% FCS, 2 mM L-glutamine, and penicillin/streptomycin in 5% CO_2, at 37°C. *Cep290*$^{LacZ/LacZ}$*::H-2Kb-tsA58*$^{+/-}$ and *Cep290*$^{+/+}$*::H-2Kb-tsA58*$^{+/-}$ collecting duct cells were isolated from kidneys of 1-mo-old transgenic mice (19). Cells were incubated at 33 °C in 5% CO_2. CCD media was used for cell culture as previously described (28). URECs were obtained from a Joubert Syndrome patient and healthy gender- and age-matched control, and of additional healthy individuals. URECs were derived as previously described (19,29). All cells are tested for mycoplasma every two weeks and were negative.

Antibodies and Reagents

Antibodies to phospho S139-H2AX and phospho S345-CHK1 (Cell signalling 9718S, 2348L respectively); phospho S824-KAP1 (Bethyl Laboratory A300-767A); CHK1 (G-4), Cyclin A (C-19), Cyclin B1 (H433), CDK1 (Cdc2 p34 (17)), CDK2 (D-12), and PCNA (Santa Cruz Biotechnologies 8408, 596, 752, 54, 6248, 56 respectively); KAP1 (TransductionLab K57620); Pericentrin, H2AX, and GAPDH (Abcam Ab4448, Ab11175, Ab8245 respectively); α-Tubulin, Acetylated α-Tubulin and β-actin (Sigma T6199, T6793, A5441 respectively); actin (C4, ImmunO 691001); CEP290 (Novus Biologicals NB100-86991) are all commercially available. The ON-TARGETplus siRNA SMARTpools (Thermo Scientific Dharmacon) for Non-targeting pool UGGUUUACAUGUCGACUAA/UGGUUUACAUGUUGUGUGA/UGGUUUACAUGUUUUCUGA/UGGUUUACAUGUUUUCCUA (D-001810-10), and the siRNAs targeting human CEP290 GGAUUCGGAUGAAAUGAAA/GGAAUUGACUUACCUGAUG/AAAGUUAAUGAGCAAUUG/GAAGUAGAGUCCCUCAGAA (L-014590-00) and mouse Cep290 GCCAAUAAUCAGAUGGAUA/AGACUUACCCGAUGGGAUA/CGUCCAAACUCCAGAAGAU/ACUUAGAGCUGGUGAACGA (L-052034-00) were purchased from ThermoFisher. All cell transfections were performed using 20 nM siRNA with Lipofectamine RNAimax (Invitrogen, 13778-150) following the manufacturer's protocols. The CDK1/2 inhibitor (217714) was purchased from Millipore and Aphidicolin (APH) from Serva (13696).

Immunofluorescence

For immunostaining, cells were grown on coverslips and fixed for 15 minutes in 4 % paraformaldehyde or 5 minutes in ice cold methanol, followed by a 15 minutes permeabilization step in 0.1%Triton-X100/1%BSA/PBS. Primary antibody incubations were performed overnight at 4ºC in 1% BSA/PBS blocking buffer. Alexa Fluor 488/568/647 secondary antibodies (Invitrogen, dilution 1:500) and DAPI incubations were performed for 1 hour at RT. Coverslips were mounted in Fluormount G (Cell Lab, Beckman Coulter).

Confocal imaging was performed using Zeiss Confocal laser microscope and images were processed with the ZEN 2011 software. Mean γH2AX fluorescence intensity per nucleus was quantified using ImageJ Approximately 150 events per condition were scored.

Spheroids

Ten thousand collecting duct cells from *Cep290*$^{LacZ/LacZ}$ or *Cep290*$^{+/+}$ mice were mixed 1:1 with growth factor-depleted matrigel (BD Bioscience) in Labtech chamber slides. After polymerization for 30 min at 33 °C, warm medium was dripped over the matrix until just covered and cells were cultured at 33 °C/5% CO_2. The cells formed spheroids with cleared lumens 3–4 days later (19). During the last 18 hour spheroids were cultured with medium without serum containing 400 nM aphidicolin, respectively, with or without 200 nM CDK1/2i for 18 h. Medium was removed by pipetting and the gels were washed three times for 10 min with warm PBS supplemented with calcium and magnesium. General fixation and staining protocols were used (30). Images and z-stacks were taken with a Zeiss LSM700 confocal microscope and approximately 35 spheroids per condition were scored. Three-way ANOVA with Bonferroni post-hoc test was used for statistical analysis.

Western blot

Protein lysates were prepared using RIPA lysis buffer and sonicated. To correct for protein content BCA protein assay (Pierce) was performed. After blotting, the PVDF membranes were blocked in 5% BSA or 5% dried skim milk in TBS with 0.5% Tween. The primary antibodies were incubated overnight at 4ºC. Coomassie Blue staining of the gel was performed as additional loading control. The secondary HRP conjugated swine anti rabbit and rabbit anti mouse antibodies (DAKO, dilution 1:2000) were incubated for 1 hour at RT. The ECL Chemiluminescent Peroxidase Substrate kit (Sigma, CPS1120-1KT) was used for development. Scans of the blots were made with the BioRad ChemiDoc XRS+ device and Image Lab software 4.0 was used for quantification.

Comet tail assay

Comet assays were performed with the electrophoresis kit (Trevigen) according to the manufacturer's protocols. DNA was stained with SYBR-gold (Invitrogen S11494, 1:30000) and comet tail moments were calculated by counting 50 cells for each sample and analyzed with CometScore software (TriTek Corp).

In vitro kinase assay

Cells were lysed in high-salt buffer (300 mM NaCl, 50 mM Hepes, pH 7.5, 0.8 % Triton X-100, 8 % Glycerol, 1 mM EDTA, 1 mM DTT, protease inhibitors and phosphatase inhibitors). Cell lysates were clarified by centrifugation and were immunoprecipitated with Cyclin A (Santa Cruz) or Cyclin B1 (Santa Cruz) antibody-bound protein A sepharose beads

(GE Healthcare) for 2 h at 4 °C. Precipitates were washed three times with high-salt buffer and once with kinase buffer (20 mM Hepes pH 7.5, 5 mM MnCl2, 5 mM MgCl2, 5 mM beta-glycerophosphate, 1 mM NaF, 1 mM DTT, 1 mM Na3VO4). Kinase reactions were carried out by incubating immunoprecipitated Cyclin A/B1 with 50 µl of kinase buffer with 10 µM ATP, 5 µM γ32P-ATP and 5 µg of substrate histone H1 for 30 min at 30 °C with and without 2 µM CDKi, and stopped by adding SDS sample buffer. Samples were boiled in Leammli buffer and analyzed by SDS-PAGE. Ponceau S or Coomassie blue staining were used to validate equal substrate loading.

Chromatin fractionation

Chromatin fractionations were processed as previously described (16,31). Approximately 10^7 cells were used and fractions were resuspended in laemmli sample buffer and analyzed by western blotting. The chromatin fraction was sheared by sonication. Equal loading of fractions was verified by Ponceau S staining and immunoblotting against α-Tubulin and GAPDH (cytosolic fraction), PCNA (nuclear and chromatin fractions) and H2AX (nuclear fraction).

Clonogenic survival

Cep290$^{LacZ/LacZ}$ or *Cep290*$^{+/+}$ cells were treated with aphidicolin at the concentrations indicated for 18 hours. Subsequently, cells were seeded onto 6 cm plates at a density of 1000 cells. After 11 days, cells were fixed in 1% formaldehyde in PBS, stained with 0.5% crystal violet (Sigma) for 10 min, and rinsed with tap water. Resulting colonies were manually counted. Each point was performed as three experimental replicates.

DNA fiber analysis

Fiber analysis was performed and processed as previously described (22). Briefly, *Cep290*$^{LacZ/LacZ}$ or wild type cells were pulsed-labeled with IdU (Sigma) for 30 min, quickly washed with PBS and pulse-labeled with CldU (Sigma) for 30 min. DNA fibers were visualized using primary antibodies specific for IdU and CldU (BD Bioscience 347580 (1:50) and Abcam Ab6326 (1:100), respectively) and stained with AlexaFluor 488 or 594 (1:500) conjugated secondary antibodies (Molecular Probes). The DNA fibers were captured with fluorescence microscopy and ImageJ was used for pulse labeling analysis.

RT-qPCR

Cells were lysed and total RNA was isolated (RNeasy Mini Kit, Qiagen, 74106) and measured (NanoDrop spectrophotometer ND-1000, Thermo Fischer Scientific Inc.). cDNA was synthesized from 1000 ng RNA template using the iScript cDNA Synthesis Kit (Bio-Rad, 170-8891) according to the supplier's protocol. Dilutions were made for RT-qPCR analysis to determine mRNA expression levels which were normalized against a reference gene.

The iQ SYBR Green Supermix (Bio-Rad, 170-8880) was used to multiply and measure the cDNA with a CFX96 Touch Real-Time PCR Detection System (Bio-Rad). All samples were run in triplicate in 20 µl reactions. The following PCR program was used: 95°C for 3 min, followed by 40 cycles of 10s at 95°C, 30s at the indicated annealing temperature and 30s at 72°C, then 10s at 95°C followed by a melt of the product from 65°C-95°C. The primer sequences (Sigma) used and concomitant annealing temperatures are: hRPLP0 forward 5′-TGCACAATGGCAGCATCTAC, hRPLP0 reverse 5′-ATCCGTCTCCACAGACAAGG, 58°C, hCEP290 forward 5´-TGACTGCTAAGTACAGGGACATCTTG, hCEP290 reverse 5´-AGGAGATGTTTTCACACTCCAGGT, 65°C, mRpl27 forward 5′-CGCCCTCCTTTCCTTTCTGC, mRpl27 reverse 5′-GGTGCCATCGTCAATGTTCTTC, 53°C, mCep290 forward 5´-GACAGTGACTACCGATCACAGT, mCep290 reverse 5´-CGCTTTCATCCTGTTGTACTCA, 64°C, The ΔΔCT method was used for statistical analysis to determine gene expression levels.

Histology

Immunocytochemistry was performed as previously described (27). Mouse kidney tissue sections (n=13) embedded in paraffin were deparaffinized, treated with peroxidase block for 15 min and incubated at 100 °C in citrate-HCl buffer (pH 6) for 20 min. The sections were stained with rabbit antibody to γH2AX (1:200) overnight at 4 °C. Samples were incubated with BrightVision anti-rabbit poly horseradish peroxidase (HRP) for 1 h at room temperature. The Nova RED substrate kit for Peroxidase (Vector, SK-4800) was used, and samples were counterstained with hematoxylin. Analysis was performed using Aperio ImageScope software. Five random tubular fields (approximately 1000 cells per field) were analyzed for positively stained nuclei using an in-house ImageJ macro. Linear model analysis was used for statistical analysis.

FACS

To quantify cell cycle phase distribution, wild-type or *Cep290*$^{LacZ/LacZ}$ cells were incubated with 10 µM BrdU for 30 minutes and fixed in ice cold 70% EtOH. To quantify S-phase progression, IMCD3 cells (48 hour after siRNA) were incubated with 10 µM BrdU for 30 minutes, cultured for 18 hours and fixed in ice-cold 70% EtOH. Samples were stained for FACS analysis with BrdU mouse mAb Alexa Fluor 647 conjugate (1:200; Invitrogen) in 0.1% BSA-PBS-T for 1 hour on ice, and DAPI in PBS. To quantify apoptosis, unfixed cells were stained with 7-AAD and Hoechst as described previously (32). 10,000 events were measured with a BD FACSCanto II flow cytometer and analyzed using BD FACSDiva Software.

Zebrafish

Wild-type embryos at the 1–2 cell stage were injected with 3.5 ng or 4 ng of a morpholino oligonucleotide targeting *cep290* ATG codon sequence (Gene-Tools) (1) in pure water with 0.1% Phenol Red using a nanoject2000 microinjector (World Precision Instruments). The sequence of the standard control morpholino was: 5′-CCTCTTACCTCAGTTACAATTTATA-3′. For western blot 18 embryos were pooled in 36 µL Triton X-100 lysis buffer and were sonicated.

Statistics

P-values (*p<0.05, **p<0.01, ***p<0.001) were calculated of normally distributed data sets using a two-tailed Student's t test, or One-way ANOVA with Dunnett's post-hoc test, or Two-way ANOVA and Three-way ANOVA with Bonferroni post-hoc tests or otherwise indicated. Statistical analyses represent the mean of at least three independent experiments or otherwise indicated. Error bars represent SEM.

Study approval

URECs were obtained from a Joubert syndrome patient, with compound heterozygous mutations in *CEP290*, p.Q950Pfs*6 het and p.K939N het in a 3 year old male child with clinical Joubert syndrome with a retinal, renal and cerebellar phenotype. Ethical approval was obtained from the NRES Committee North East (14/NE/1076). URECs were obtained from healthy controls that have been included in the AGORA (Aetiologic research into Genetic and Occupational/environmental Risk factors for Anomalies in children) biobank project. The regional Committee on Research involving Human Subjects (CMO Arnhem/Nijmegen) approved the study protocol. Written informed consent was obtained from the parents.

All mouse work was performed under licenses granted from the Home Office (United Kingdom) in accordance with the guidelines and regulations for the care and use of laboratory animals outlined by the Animals (Scientific Procedures) Act 1986 and with the approval of the Newcastle University Ethical Review Committee. Mice with a *Cep290*$^{LacZ/LacZ}$ hypomorphic mutation bred on a pure 129/Ola genetic background (F1 heterozygotes were backcrossed with C57/b6 for 6 generations) were used as previously described (19). Male and female mice were sacrificed at various ages and genotyped.
All zebrafish experiments were conducted in accordance with the Dutch guidelines for the care and use of laboratory animals, with the approval of the Animal Experimentation Committee (DEC) of the Royal Netherlands Academy of Arts and Sciences (KNAW), and were approved by the Animal Care Committee of the University Medical Center Utrecht in the Netherlands.

Acknowledgements

We thank the patients and the controls for their participation in this study. We thank the Flow cytometry core facility and the Cell Microscopy Center at the UMC Utrecht for providing expert services. We thank Ive Logister and Henry Ajzenberg for culturing urine cells, and Hendrik Gremmels for help with statistics and all Cimprich and Giles lab members for scientific input. We thank Sophie Saunier for help with the molecular genetic diagnosis of JS patients. We acknowledge generous support from Kids Kidney Research (ref 07/05/13; to AMH), Kidney Research UK (RP40/2009 and TF1/2013; JAS, CM, AMH, SS), the MRC (MR/M012212/1 to JAS and CM) and Northern Counties Kidney Research Fund (ref 07.2013; JAS), an NIH grant (ES016486; to K.A.C.), American Cancer Society Postdoctoral Fellowship (123391-PF-12-156-01-DMC; to ACK), Postdoctoral Enrichment Program Award from the Burroughs Wellcome Fund and NIH training grant (T32CA09151; to JCS), the European Community's Seventh Framework Programme FP7/2009 under grant agreement no: 241955, SYSCILIA, the Dutch Kidney Foundation Consortium CP11.18 "KOUNCIL" and 13A3D103 (RHG). GGS further acknowledges support from Foundation 'De Drie Lichten' in the Netherlands (14/13), the Dutch Kidney Foundation (14OKK01), Simons Foundation Fund (1059) and the EMBO fellowship program (554-2013). The funders had no role in study design, data collection and analysis, decision to publish, or preparation of the manuscript.

REFERENCES

1. Sayer JA, Otto EA, O'Toole JF, et al. The centrosomal protein nephrocystin-6 is mutated in Joubert syndrome and activates transcription factor ATF4. *Nat. Genet.* 2006;38(6):674-681.
2. Coppieters F, Lefever S, Leroy BP, De Baere E. CEP290, a gene with many faces: mutation overview and presentation of CEP290base. *Hum. Mutat.* 2010;31(10):1097-1108.
3. Valente EM, Brancati F, Boltshauser E, Dallapiccola B. Clinical utility gene card for: Joubert syndrome--update 2013. *Eur. J. Hum. Genet.* 2013;21(10).
4. Halbritter J, Diaz K, Chaki M, et al. High-throughput mutation analysis in patients with a nephronophthisis-associated ciliopathy applying multiplexed barcoded array-based PCR amplification and next-generation sequencing. *J. Med. Genet.* 2012;49(12):756-767.
5. Hildebrandt F, Attanasio M, Otto E. Nephronophthisis: disease mechanisms of a ciliopathy. *J. Am. Soc. Nephrol.* 2009;20(1):23-35.
6. Moradi P, Davies WL, Mackay DS, Cheetham ME, Moore AT. Focus on molecules: centrosomal protein 290 (CEP290). *Exp. Eye Res.* 2011;92(5):316-317.
7. Staples CJ, Myers KN, Beveridge RD, et al. The centriolar satellite protein Cep131 is important for genome stability. *J. Cell Sci.* 2012;125(Pt 20):4770-4779.
8. Staples CJ, Myers KN, Beveridge RD, et al. Ccdc13 is a novel human centriolar satellite protein required for ciliogenesis and genome stability. *J. Cell Sci.* 2014;127(Pt 13):2910-2919.
9. Valdes-Sanchez L, De la Cerda B, Diaz-Corrales FJ, et al. ATR localizes to the photoreceptor connecting cilium and deficiency leads to severe photoreceptor degeneration in mice. *Hum. Mol. Genet.* 2013;22(8):1507-1515.
10. Basten SG, Giles RH. Functional aspects of primary cilia in signaling, cell cycle and tumorigenesis. *Cilia.* 2013;2(1):6.
11. Sang L, Miller JJ, Corbit KC, et al. Mapping the NPHP-JBTS-MKS protein network reveals ciliopathy disease genes and pathways. *Cell.* 2011;145(4):513-528.
12. Wolf MT, Hildebrandt F. Nephronophthisis. *Pediatr. Nephrol.* 2011;26(2):181-194.
13. Omran H. NPHP proteins: gatekeepers of the ciliary compartment. *J. Cell Biol.* 2010;190(5):715-717.
14. Chaki M, Airik R, Ghosh AK, et al. Exome capture reveals ZNF423 and CEP164 mutations, linking renal ciliopathies to DNA damage response signaling. *Cell.* 2012;150(3):533-548.
15. Airik R, Slaats GG, Guo Z, et al. Renal-retinal ciliopathy gene Sdccag8 regulates DNA damage response signaling. *J. Am. Soc. Nephrol.* 2014;25(11):2573-2583.
16. Choi HJ, Lin JR, Vannier JB, et al. NEK8 links the ATR-regulated replication stress response and S phase CDK activity to renal ciliopathies. *Mol. Cell.* 2013;51(4):423-439.
17. Otto EA, Trapp ML, Schultheiss UT, Helou J, Quarmby LM, Hildebrandt F. NEK8 mutations affect ciliary and centrosomal localization and may cause nephronophthisis. *J. Am. Soc. Nephrol.* 2008;19(3):587-592.
18. Slaats GG, Giles RH. Are renal ciliopathies (replication) stressed out? *Trends Cell Biol.* 2015.
19. Hynes AM, Giles RH, Srivastava S, et al. Murine Joubert syndrome reveals Hedgehog signaling defects as a potential therapeutic target for nephronophthisis. *Proc. Natl. Acad. Sci. U. S. A.* 2014;111(27):9893-9898.
20. Baranovskiy AG, Babayeva ND, Suwa Y, Gu J, Pavlov YI, Tahirov TH. Structural basis for inhibition of DNA replication by aphidicolin. *Nucleic Acids Res.* 2014;42(22):14013-14021.
21. Zeman MK, Cimprich KA. Causes and consequences of replication stress. *Nat. Cell Biol.* 2014;16(1):2-9.
22. Jackson DA, Pombo A. Replicon clusters are stable units of chromosome structure: evidence that nuclear organization contributes to the efficient activation and propagation of S phase in human cells. *J. Cell Biol.* 1998;140(6):1285-1295.
23. Sanchez Y, Wong C, Thoma RS, et al. Conservation of the Chk1 checkpoint pathway in mammals: linkage of DNA damage to Cdk regulation through Cdc25. *Science.* 1997;277(5331):1497-1501.
24. Beck H, Nahse V, Larsen MS, et al. Regulators of cyclin-dependent kinases are crucial for maintaining genome integrity in S phase. *J. Cell Biol.* 2010;188(5):629-638.
25. Bukanov NO, Moreno SE, Natoli TA, et al. CDK inhibitors R-roscovitine and S-CR8 effectively block renal and hepatic cystogenesis in an orthologous model of ADPKD. *Cell Cycle.* 2012;11(21):4040-4046.
26. Bukanov NO, Smith LA, Klinger KW, Ledbetter SR, Ibraghimov-Beskrovnaya O. Long-lasting arrest of murine polycystic kidney disease with CDK inhibitor roscovitine. *Nature.* 2006;444(7121):949-952.
27. Zhou W, Otto EA, Cluckey A, et al. FAN1 mutations cause karyomegalic interstitial nephritis, linking chronic kidney failure to defective DNA damage repair. *Nat. Genet.* 2012;44(8):910-915.
28. Bens M, Vallet V, Cluzeaud F, et al. Corticosteroid-dependent sodium transport in a novel immortalized mouse collecting duct principal cell line. *J. Am. Soc. Nephrol.* 1999;10(5):923-934.

29. Zhou T, Benda C, Dunzinger S, et al. Generation of human induced pluripotent stem cells from urine samples. *Nat. Protoc.* 2012;7(12):2080-2089.
30. Giles RH, Ajzenberg H, Jackson PK. 3D spheroid model of mIMCD3 cells for studying ciliopathies and renal epithelial disorders. *Nat. Protoc.* 2014;9(12):2725-2731.
31. Smits VA, Reaper PM, Jackson SP. Rapid PIKK-dependent release of Chk1 from chromatin promotes the DNA-damage checkpoint response. *Curr. Biol.* 2006;16(2):150-159.
32. Schmid I, Uittenbogaart C, Jamieson BD. Live-cell assay for detection of apoptosis by dual-laser flow cytometry using Hoechst 33342 and 7-amino-actinomycin D. *Nat. Protoc.* 2007;2(1):187-190.

SUPPLEMENTAL FIGURES

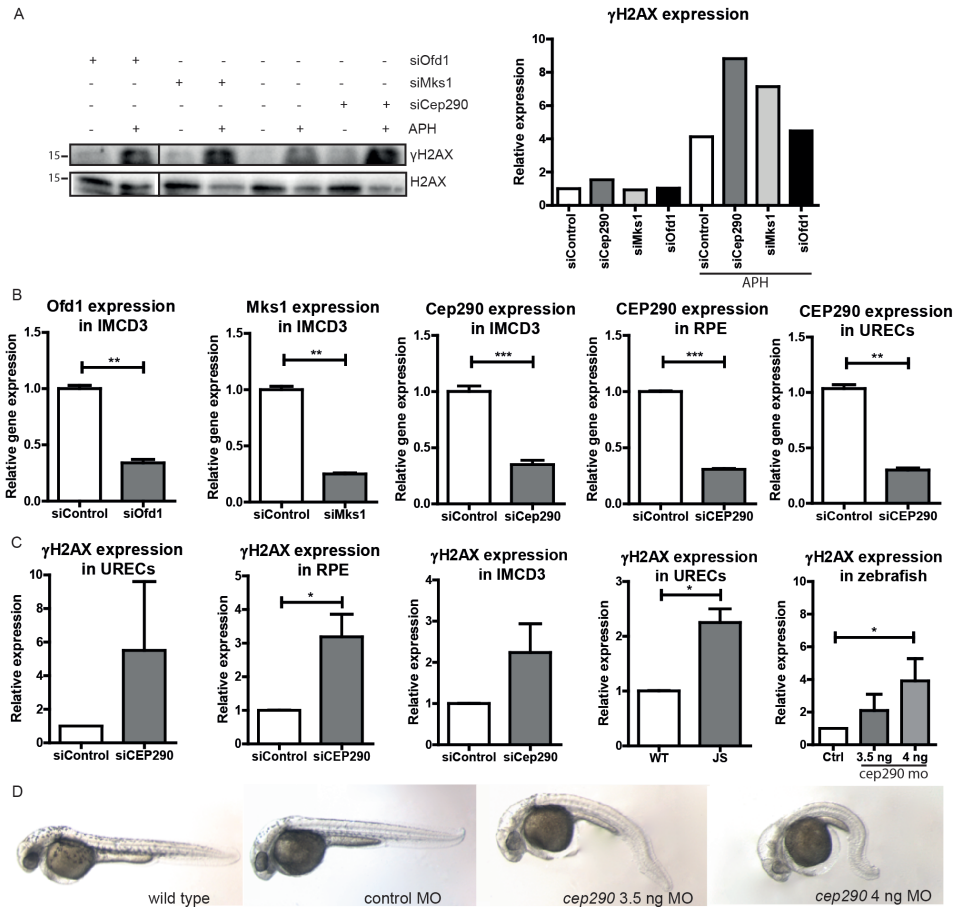

Supplemental Figure 1. Quantification of siRNA efficiency and γH2AX protein levels on western blot (**A**) mIMCD3 cells depleted for Ofd1, Mks1 and Cep290 by siRNA show increased γH2AX levels compared to control siRNA transfection (56 hours) after aphidicolin (APH) incubation (400 nM, 18 hours). Quantification is normalized to H2AX (loading control). Lanes were run on the same gel, but were noncontiguous. (**B**) Normalized *CEP290* gene expression levels were measured by RT-qPCR of 20 nM control or CEP290 siRNA treated (48 hours) URECs and (72 hours) RPE cells (*RPLP0* reference gene), and normalized *Cep290, Mks1* and *Ofd1* gene expression levels were measured of 20 nM control or Cep290, Mks1 and Ofd1 siRNA treated (48 hours) IMCD3 cells (*RPL27* reference gene; n=3; T-test ***p<0.01, ***p<0.001). (**C**) Quantification of γH2AX protein expression of Western blots (see Figure 1A-C,E) of URECs, RPE and IMCD3 cells after *Cep290*-targeting siRNA transfection, URECs from a wild type and Joubert patient, and zebrafish injected with *cep290* mo vs control clutchmates (48 hpf). Expression was normalized to H2AX or actin (n=3; T-test *p<0.05). (**D**) Representative phenotype of zebrafish embryos 36 hours post fertilization (hpf) of wild type zebrafish embryo and control morpholino (MO) injected embryo. Embryos injected with a morpholino against *cep290* exhibit a range with phenotypes, in a dose-dependent manner: majority of 3.5 ng MO-injected embryos have milder phenotype with ventral body curvature, hydrocephalus, lack of pigmentation, underdeveloped eyes and pericardial edema, while 4 ng MO-injected embryos are more severely affected with poor survival rate beyond 48 hpf.

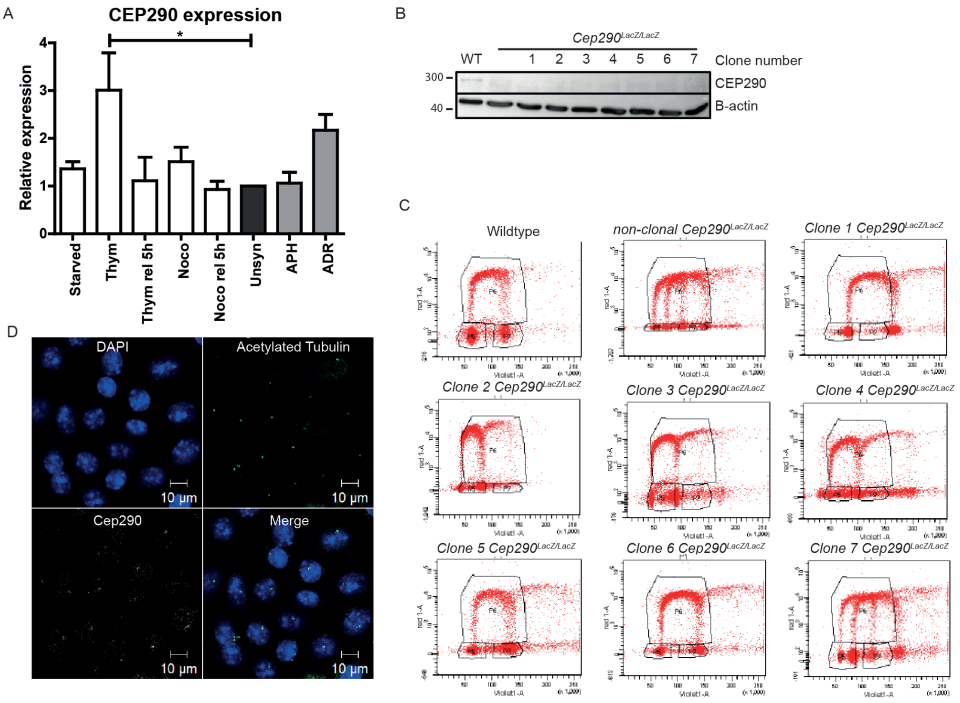

Supplemental 2. CEP290 expression and clonal Cep290$^{LacZ/LacZ}$ cell lines
(**A**) Quantification of CEP290 protein expression of Western blots (see Figure 4B). Expression was normalized to β-actin (n=3; One-way ANOVA; *p<0.05). (**B**) Western blot of wild type, Cep290$^{LacZ/LacZ}$ and seven clonal Cep290$^{LacZ/LacZ}$ cell lines. Only wild type cells show CEP290 expression. β-actin is loading control. (**C**) BrdU FACS of wild type and clonal *Cep290$^{LacZ/LacZ}$* cell lines showing normal DNA content and cell cycle for wild type cells, however, *Cep290$^{LacZ/LacZ}$* cell lines have irregular DNA content (BrdU on y-axes, DAPI on x-axes; 10,000 events measured; n=3). (**D**) Immunofluorescent (IF) staining of Cep290 of wild type cells indicating centrosomal Cep290 expression (white), which is at the base of primary cilia (acetylated tubulin, green). Scale bar represents 10 µm.

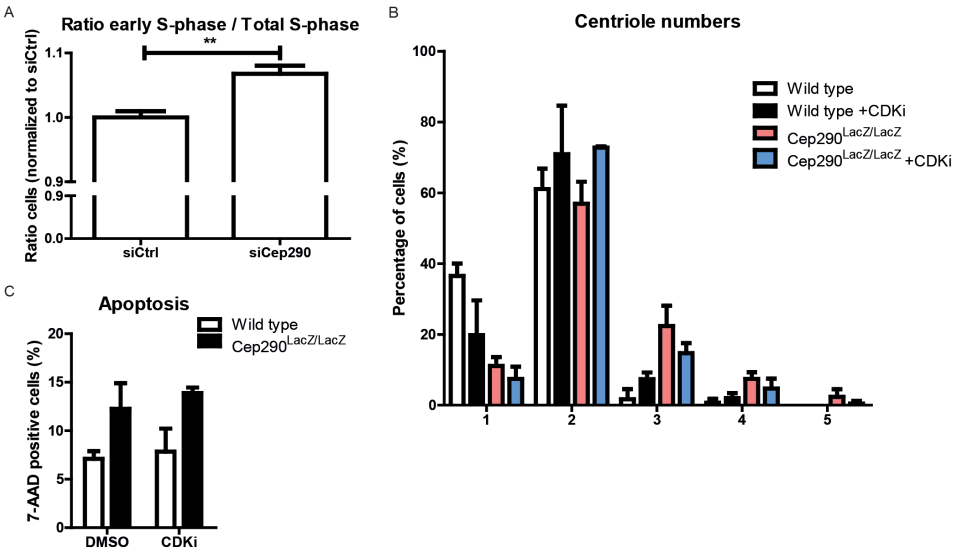

Supplemental 3. Cell cycle S-phase progression and effects of CDK inhibition
(**A**) IMCD3 cells transfected with control or Cep290 siRNA were examined after BrdU pulse labeling by FACS after 18 hours of 30 min BrdU pulse labeling. Cep290 depleted IMCD3 cells lag in early S-phase, whereas control transfected IMCD3 cells progress normally. Early S-phase cells are relative to total number of cells in S-phase and normalized to siCtrl set to 1 (n=3 in duplicate, 10,000 events were measured. T-test **p<0.01). (**B**) Wild type and Cep290$^{LacZ/LacZ}$ cells were incubated with 200 nM CDKi for 18 hours. Quantification of centrioles (immunofluorescence staining of pericentrin) revealed decreased supernumerary centriole number in the Cep290$^{LacZ/LacZ}$ cells after CDKi treatment. Mean centriole numbers were 1.7 for Wild type, 2.3 for Cep290$^{LacZ/LacZ}$ cells, and 2.1 for Cep290$^{LacZ/LacZ}$ cells after CDKi treatment (n=3; >100 cells quantified; T-test *p<0.05). (**C**) FACS 7-AAD staining of wild type and Cep290$^{LacZ/LacZ}$ cells revealed no enhanced apoptosis after CDKi (18 h 200 nM, n=3, 10,000 events measured in triplicate, no differences after 2-way ANOVA).

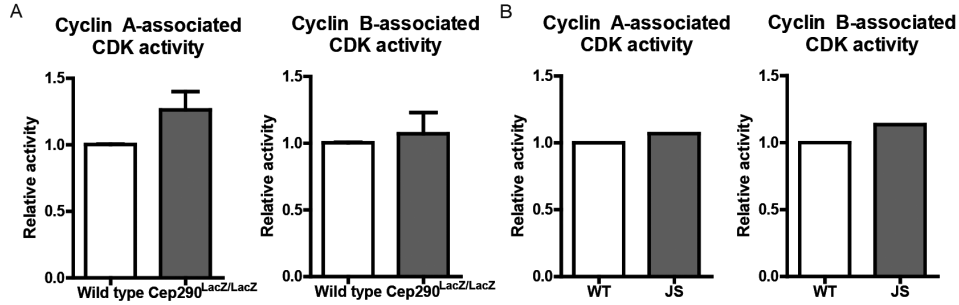

Supplemental Figure 4. Quantification of kinase activity
(**A**) Quantification of Cyclin A- and Cyclin B-associated CDK activity in wild type and Cep290$^{LacZ/LacZ}$ primary mouse kidney cells (see Figure 5B). Expression was normalized to activity in wild type cells (n=4). (**B**) Quantification of Cyclin A- and Cyclin B-associated CDK activity in wild type and Joubert patient URECs with *CEP290* mutations (see Figure 5C). Expression was normalized to activity in wild type cells (n=1 due to lack of patient material).

CHAPTER 7

Nephronophthisis-associated *CEP164* regulates cell cycle progression, apoptosis and epithelial-to-mesenchymal transition

PLoS Genet., 10(10):e1004594 (2014)

Gisela G. Slaats, Amiya K. Ghosh*, Lucas L. Falke*, Stéphanie Le Corre, Indra A. Shaltiel, Glenn van de Hoek, Timothy D. Klasson, Marijn F. Stokman, Ive Logister, Marianne C. Verhaar, Roel Goldschmeding, Tri Q. Nguyen, Iain A. Drummond, Friedhelm Hildebrandt, Rachel H. Giles

* These authors contributed equally

ABSTRACT

We recently reported that centrosomal protein 164 (CEP164) regulates both cilia and the DNA damage response in the autosomal recessive polycystic kidney disease nephronophthisis. Here we examine the functional role of *CEP164* in nephronophthisis-related ciliopathies and concomitant fibrosis. Live cell imaging of RPE-FUCCI (fluorescent, ubiquitination-based cell cycle indicator) cells after siRNA knockdown of *CEP164* revealed an overall quicker cell cycle than control cells although early S-phase was significantly longer. Follow-up FACS experiments with renal IMCD3 cells confirm that *Cep164* siRNA knockdown promotes cells to accumulate in S-phase. We demonstrate that this effect can be rescued by human wild-type *CEP164* but not disease-associated mutants. siRNA of *CEP164* revealed a proliferation defect over time, as measured by CyQuant assays. The discrepancy between accelerated cell cycle and inhibited overall proliferation could be explained by induction of apoptosis and epithelial-to-mesenchymal transition. Reduction of *CEP164* levels induces apoptosis in immunofluorescence, FACS and RT-QPCR experiments. Furthermore, knockdown of *Cep164* or overexpression of dominant negative mutant allele *CEP164 Q525X* induces epithelial-to-mesenchymal transition, and concomitant upregulation of genes associated with fibrosis. Zebrafish injected with *cep164* morpholinos likewise manifest developmental abnormalities, impaired DNA damage signaling, apoptosis and a pro-fibrotic response *in vivo*. This study reveals a novel role for *CEP164* in the pathogenesis of nephronophthisis, in which mutations cause ciliary defects coupled with DNA damage induced replicative stress, cell death, and epithelial-to-mesenchymal transition, and suggests that these events drive the characteristic fibrosis observed in nephronophthisis kidneys.

INTRODUCTION

Nephronophthisis (NPHP) is an autosomal recessive polycystic kidney disease (PKD) attributed to dysfunction of the primary cilia,(1) antennae-like structures projecting from the cell surface which have sensory or mechanical functions.(2) To date, mutations in seventeen genes have been identified as causing NPHP, yet fewer than half of all NPHP cases segregate with these disease loci.(3) Although ciliary dysfunction with consequent defective planar cell polarity among the epithelial cells in the kidney is believed to be the fundamental etiology of cystogenesis in both NPHP and other types of PKD,(4) the overall size of kidneys in NPHP is considerably smaller than in autosomal dominant PKD.(5) This discrepancy is partly due to tubulointerstitial renal fibrosis in NPHP, which is far more evident than in autosomal dominant PKD-affected kidneys. Epithelial-to-mesenchymal transition (EMT) is a hallmark of tubulointerstitial renal fibrosis.(6) Recent studies associating NPHP proteins with defective DNA damage response (DDR) signaling (7,8) support the notion that accumulation of DNA damage and cilia loss result in cell cycle arrest or cell death with associated renal function loss and fibrosis,(9) but exactly how these processes are linked remains unknown.

One of the proteins linking these cellular processes in NPHP is centrosomal protein 164 (*CEP164*) (NM_014956, NP_055771). CEP164 regulates primary cilium formation(10) by promoting vesicular trafficking to the mother centriole during initiation of ciliogenesis.(11) Germline mutations in *CEP164* have been reported in families with *NPHP15* (MIM:614845).(7) Furthermore, *CEP164* has a role in DDR signaling.(7,12,13) Cep164 interacts with checkpoint kinases ATR and ATRIP *in vivo*(12) and localizes with DNA damage proteins TIP60, SC-35 and phosphorylated Chk1.(7) *CEP164* expression is cell cycle stage-dependent; most protein is present at the end of S phase and the beginning of the G_2/M phase when cilia are not typically present. Reduction of endogenous levels of *CEP164* by siRNA knockdown in HeLa cells abrogates the G_2/M checkpoint,(12) suggesting a critical role in cell cycle regulation. Because disturbance of the cell cycle contributes to the cystic and fibrotic renal phenotype of NPHP,(14) we interrogated whether these non-ciliary functions of *CEP164* might contribute to the particular phenotype observed in NPHP kidneys.

Here we investigate the role of *CEP164* in the cell cycle, particularly in S-phase progression and proliferation. We test wild-type and mutant alleles of *CEP164* and verify that disease alleles of *CEP164* affect cilia as well as cell cycle progression. Live cell imaging studies suggest that CEP164 protects cells from apoptosis. Furthermore we observe upregulation of EMT and fibrosis markers as a result of reduced cellular levels of *CEP164 in vitro* and *in vivo* that could partially explain the cystic and fibrotic renal phenotype of *CEP164* mutant patients.

RESULTS

CEP164 knockdown accelerates cell cycle, but delays S phase progression

To establish the cell cycle progression of cells after knockdown of endogenous *CEP164*, we generated RPE-FUCCI cells (15) stably expressing mKO2-hCdt1(30/120) (red) and mAG-hGem(1/110) (green) (16) and confirmed that knockdown due to either a pool of four siRNAs (siCEP164-p) or an individual siRNA (siCEP164-i) causes down-regulation of *CEP164* mRNA levels (Figure S1A), resulting in a 5-fold reduction of cilia in these cells capable of forming cilia after serum starvation (Figure S1B-D). Live cell imaging of unsynchronized RPE-FUCCI cells for 72 hours (Figure S1E and Movies S1-2) reveals a significantly shorter cell cycle in si*CEP164* transfected cells than control non-targeting siRNA (siControl) transfected RPE-FUCCI cells (~35 hours versus ~48 hours) (Figure 1A). However, these same videos show that si*CEP164* transfected cells remain significantly longer in early S-phase (8.6 hours) compared to siControl transfected cells (5.7 hours). Accordingly, G1, G2 and M phases in siCEP164 transfected RPE-FUCCI cells are shorter (Figure 1B, S1E and Movies S1-2). RPE-FUCCI cells expressing both mKO2-hCdt1(30/120) and mAG-hGem(1/110), always demonstrated EdU incorporation, supporting the accuracy of the early S-phase values scored (Figure 1C). To determine how defective ciliogenesis in the siCEP164 cells is affecting cell cycle progression, we performed a time series experiment with RPE-FUCCI cells synchronized at G_0/G_1. The reduced ciliation frequency observed in cells with reduced levels of CEP164 (Figure S1B-C) is consistent with the increased tendency to enter the cell cycle and with the speed with which they proceed through the cell cycle. Both decreased ciliary frequency and increased cell cycle entry were observed. It takes siControl transfected cells about 10 hours to enter S-phase, whereas siCEP164 treated cells require only 6 hours (Figure 1D).

Despite accelerated cell cycle, proliferation is decreased after *CEP164* knockdown in IMCD3 as well as RPE cells

We next wanted to validate whether the accelerated cell cycling of si*CEP164* knockdown cells conferred a growth disadvantage as had been suggested by Chaki *et al.* (7). We performed CyQUANT NF Cell proliferation assays and then measured fluorescence 72 hours after siRNA knockdown of *CEP164* or siControl in RPE and IMCD3 cells. Mouse Cep164 siRNA reduces endogenous mouse *Cep164* expression significantly (Figure S2A-B). DNA staining by the CyQuant assay revealed a decreased cell number after knockdown in both cell lines (**p<0.01; Figure 1E). Standard growth curves in IMCD3 cells reveal a significant growth advantage for cells treated with siCtrl over cells treated with siCep164. Previously, these results were seen to be rescued by WT-CEP164 in IMCD3 cells.(7) These results are supporting the conclusion that increased cell cycle progression does not result in decreased population doubling time in the context of CEP164 loss.

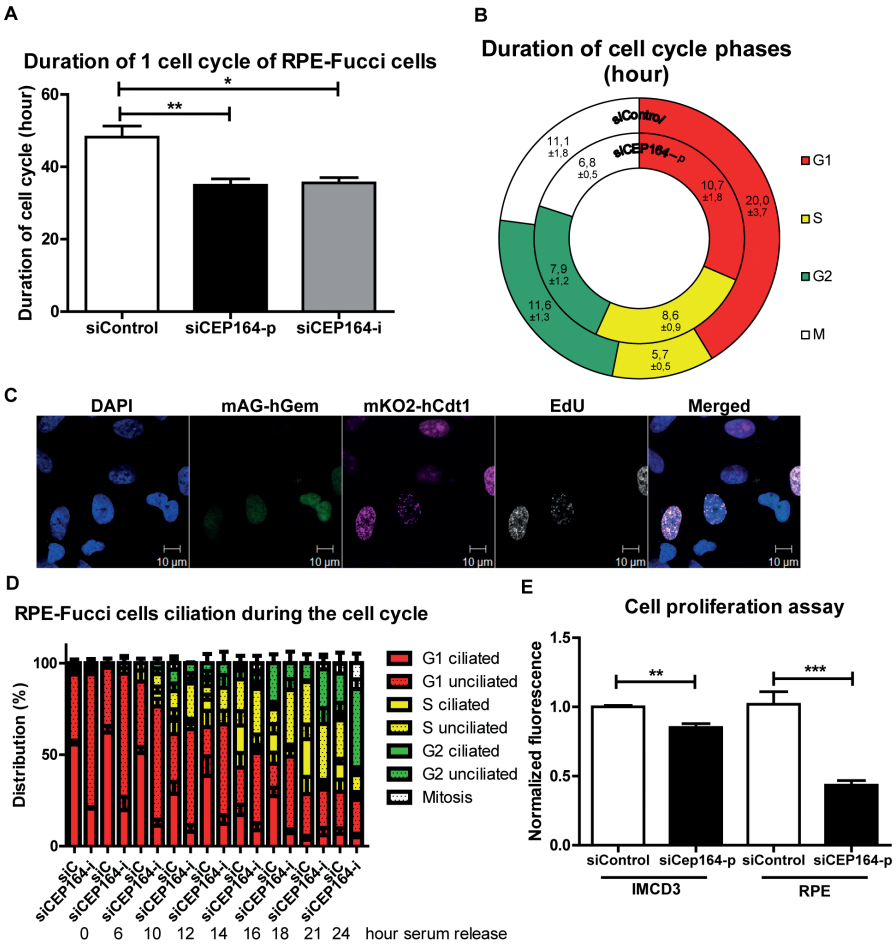

Figure 1. CEP164 regulates cell cycle progression and proliferation

(A) RPE-FUCCI cells and their daughter cells were tracked by live cell imaging for 72 hours (hr) after transfection. *CEP164* depleted cells have a quicker cell cycle (~35 hr) compared to control cells (~48 hr) (>25 cells and their daughter cells per position (n=3) per experimental condition per experiment (n=3), One-way ANOVA (Dunnett's post hoc) (*p<0.05). Error bars represent SEM. (B) Each cell cycle stage in siControl and si*CEP164* transfected cells was measured. S-phase took significantly longer in si*CEP164* transfected cells and their daughter cells (8.6 hour) compared to control (5.7 hour) (**p<0.01). G_1-phase is significantly shorter in si*CEP164* transfected cells (10.7 hour) compared to control (20 hr) (*p<0.05). G_2- and M-phase were almost significantly shorter in si*CEP164* transfected cells (7.9 and 6.8 hr respectively) compared to control (11.6 and 11.1 hour respectively; both p=0.06) (>25 cells and their daughter cells per position (n=3) per experimental condition per experiment (n=3), ± represent SEM, see Figure S1E for details. (C) Fluorescence images of RPE-FUCCI cells expressing mKO2-hCdt1 (30/120) (magenta) and mAG-hGem (1/110) (green) constructs were pulsed for 30 minutes with EdU (10 µM) and stained with Alexa anti-EdU-647 to visualize cells in early S-phase (white) and DAPI to visualize the nuclei (blue). Cells expressing both constructs also show EdU incorporation (white). Scale bar represents 10 µm. (D) Quantification of a time series of serum released RPE-FUCCI cells after 24 hour serum starvation. Cell cycle stage and ciliation were quantified and correlated. Both decreased ciliary frequency and increased cell cycle entry were observed in *CEP164* depleted cells. Error bars represent SEM. (E) Quantification of RPE and IMCD3 cell proliferation using the CyQUANT NF Cell Proliferation Assay Kit. Fluorescence intensities of quadruplicate samples after 72 hours after transfection were measured. A significant reduction in cell number is visible after respectively *CEP164* and *Cep164* knockdown (n=3, **p=0.007, ***p=0.001). Error bars represent SEM.

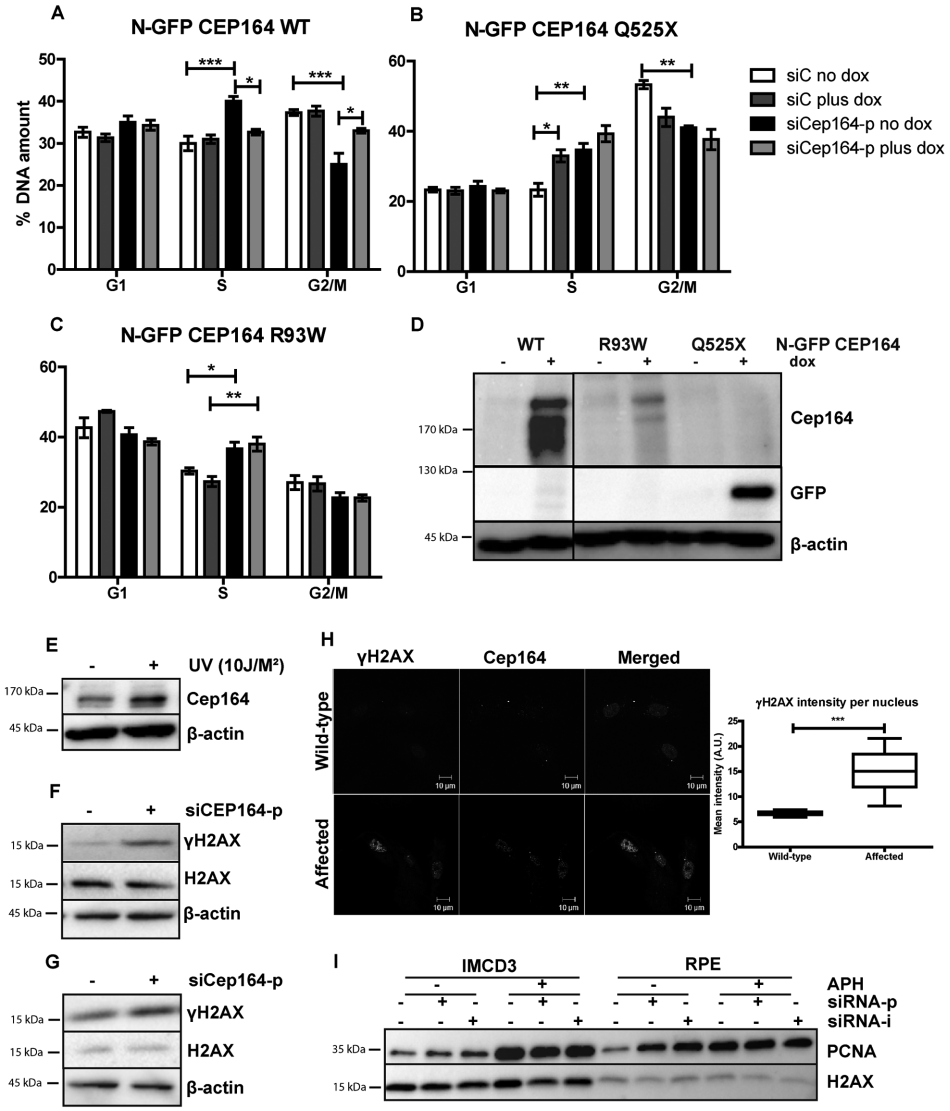

Figure 2. Knockdown of *Cep164* causes S-phase delay

(A-D) Endogenous *Cep164* knockdown leads to block in S-phase and is rescued by inducible human wild type *CEP164* but not by human mutant *CEP164*. Under thymidine synchronization, *Cep164* knockdown cells (black) were lagging in the transition from S to G_2/M phase in comparison to the control siRNA treated cells (white) in all IMCD3 *N-GFP-CEP164-WT* (A) IMCD3 *N-GFP-CEP164-Q525X* (B) and IMCD3 *N-GFP-CEP164-R93W* (C) cell lines. Upon doxycycline induction of wild type human CEP164 construct IMCD3 *N-GFP-CEP164-WT* (light grey) cells were rescued from arrest in S-phase (A). In contrast, overexpression of the cDNA clone that represents the human truncating mutant *N-GFP-CEP164-Q525X* cells did not rescue the S-phase lag. In addition, overexpression of *N-GFP-CEP164-Q525X* (dark grey) caused an increase of cells in S-phase, indicating a dominant negative effect of the human truncating mutant (B). Cells were not rescued by *N-GFP-CEP164-R93W* (C) from the S-phase lag upon doxycycline induction. P values were calculated using two-way ANOVA and Bonferroni multiple comparison test. (n=3, *p< 0.05). (D) Western blot showing

expression of N-GFP CEP164 WT and R93W by CEP164 antibody and N-GFP CEP164 Q525X by GFP antibody upon doxycycline induction. b-actin is used as loading control. (E) Lysates of IMCD3 cells were made 1 hour after 10J UV exposure. Western blot was performed for Cep164 and loading control β-actin. Stabilization of Cep164 is visible after DNA damage induction (n=3). (F) Lysates of RPE cells were made 56 hours after knockdown of *CEP164* with 20 nM siRNA. Upregulation of DNA damage marker γH2AX is shown on western blot with loading controls H2AX and β-actin (n=3). (G) Lysates of thymidine synchronized IMCD3 cells were made 56 hours after knockdown of *Cep164* with 20 nM siRNA. Upregulation of DNA damage marker γH2AX is shown on western blot with loading control H2AX and β-actin 6 hours after release of the thymidine block (n=3). (H) Urine derived renal cells stained for γH2AX (green) and CEP164 (magenta) of NPHP patient and unaffected control. γH2AX intensities were quantified by ZEN2011 software. T-test reveals statistical difference (***p<0.001) (n=15). (I) S-phase marker PCNA expression is increased in RPE and IMCD3 cells transfected with siCep164/CEP164p and –i compared to control transfected cells. b-actin was used as loading control. APH exposure (18 hour, 400 nM) enhanced the PCNA expression levels in both cell lines.

Wild-type CEP164 overexpression rescues S phase accumulation

We stably transfected murine renal inner medullary collecting duct (IMCD3) cells and RPE cells with doxycycline (Dox) -inducible constructs expressing GFP-tagged CEP164 wild-type (Figure 2D, S2D, S5A) or human disease-associated cDNA N-GFP-CEP164-R93W and -Q525X. Upon induction with doxycycline, all constructs showed GFP expression at the base of the cilium, in the cytoplasm and occasionally in the nucleus (Figure S2D, S5A). These cells were then transfected with either siControl or siCep164-p/-i or siCEP164-p/-i to reduce endogenous expression (Figure S2A,B). We observed a reduction in the percent of ciliated cells in all cell lines after knockdown of endogenous *Cep164/CEP164* (Figure S2E, S5B). Rescue of cilia numbers in cells was observed upon induction of wild-type allele CEP164-WT (Figure S2E, S5B) by the addition of doxycyline, a finding which is consistent with our previously published results and extends upon them, although not quantified in a 3D experimental setting in this study.(7) To induce cell cycle arrest and attain synchronization, we used a double thymidine block prior to release (Figure S2C) and then followed the IMCD3 inducible stable cell lines using FACS. Upon siRNA knockdown of *Cep164*, cell cycle histograms of IMCD3-N-GFP-CEP164-WT cells revealed increased accumulation of DNA in S-phase at the expense of G_2/M phase (40%±2) when compared to the control siRNA treated cells (30%±3) (Figure 2A) indicating cell cycle delay or arrest in transition from S to G_2/M phase. Upon doxycycline induction of wild-type human CEP164 construct N-GFP-CEP164-WT cells were rescued from S-phase arrest (32.7%±1.2) (Figure 2A). The observed S-phase block cannot be rescued by overexpression of the human nonsense mutant CEP164-Q525X, a mutation from NPHP family F59 (7) (Figure 2B); however, it should be noted that simply expressing the CEP164-Q525X allele alone had a nearly identical statistically significant effect as siCep164 treatment, suggesting a dominant negative interference of N-GFP-CEP164-Q525X with murine endogenous Cep164 function (Figure 2B). To rule out the possibility of clonal drift, we repeated these experiments in IMCD3 polyclonal lines expressing N-GFP-CEP164-WT and N-GFP-CEP164-Q525X (Figures S2F) and again observed a rescue with the wild-type allele and a dominant negative effect upon expression of the Q525X allele.

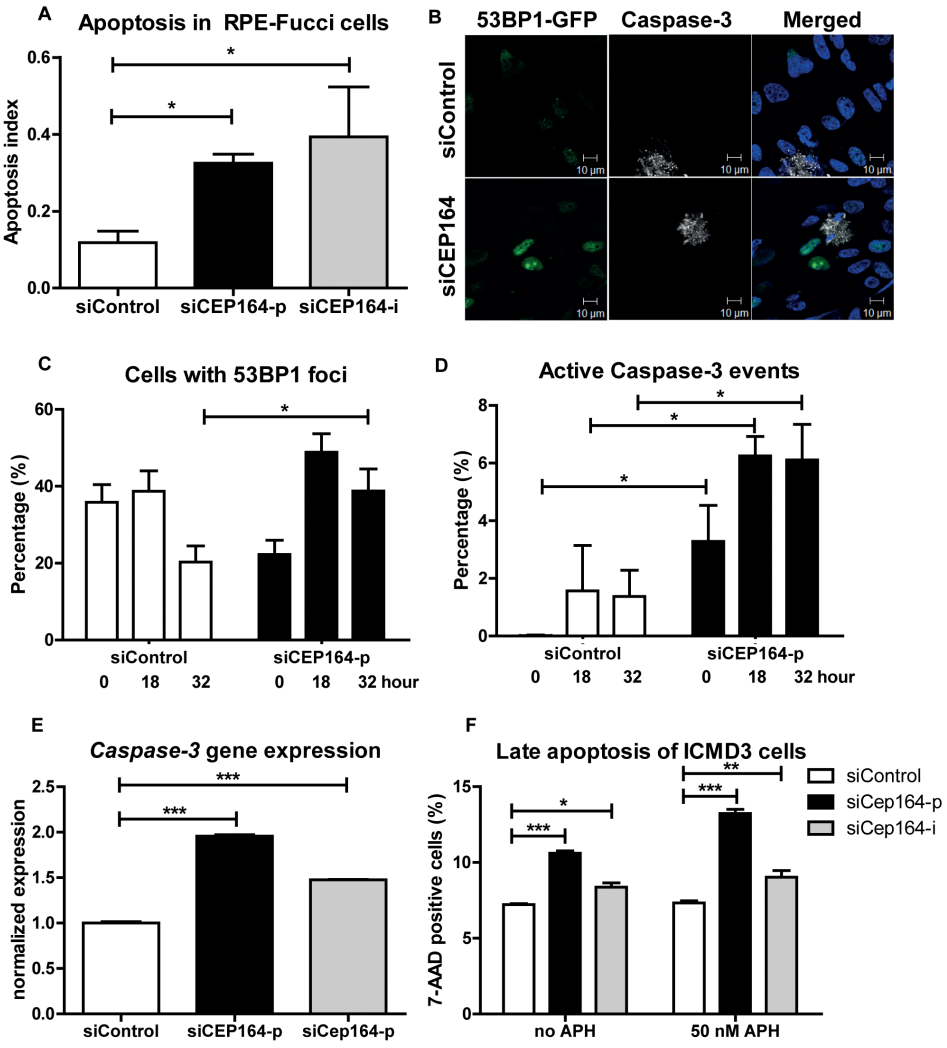

Figure 3. Induced apoptosis and DNA damage accumulation after loss of *CEP164*

(A) RPE-FUCCI cells and, after mitosis, their daughter cells are followed during 72 hours after transfection. The number of apoptotic events was scored and normalized to the total number of RPE-FUCCI cells (150 cells). *CEP164* depleted cells show more apoptosis in their population compared to control cells (n=3, One-way ANOVA (Dunnett's post hoc) *p<0.05). Error bars represent SEM. (B-D) RPE 53BP1-GFP cells were transfected with siControl or si*CEP164* oligos and serum starved for 24 hours. Samples were fixed after 0, 18, and 32 hours and prepared for confocal imaging (B). (C) Cells with 53BP1-GFP foci were quantified and normalized against the total number of cells. At t=0, and 18 hours cells displayed no significant differences in the number of scored 53BP1 foci after knockdown of *CEP164*, but at t=32 (*p<0.05) more 53BP1 foci are observed. (D) More apoptosis events (*p<0.05) are seen at all time points after knockdown of *CEP164*. (n=3, >150 events scored per condition, error bars represent SEM.). (E) Relative gene expression levels of pro-apoptotic marker Caspase-3 as measured by RT-QPCR in RPE-FUCCI and IMCD3 cells, normalized to *RPLP0* and *Rpl27* respectively. Total RNA was isolated 24 hours after transfection with siControl or si*CEP164* oligos. After 24 hours of transient transfection Caspase-3 mRNA levels are increased (***p<0.0001; n=3). Error bars represent SEM. (F) IMCD3 cells were transfected with control or *Cep164–p/i* siRNA. Cells were

incubated with 0 or 50 nM aphidicolin (APH) to induce replicative stress for 16 hours. Cells were harvested and stained for 7-AAD to measure late apoptosis (n=3, 10,000 events, error bars represent SEM). P-values were calculated using two-way ANOVA and Bonferroni multiple comparison tests.

Cells expressing NPHP missense mutation N-GFP-CEP164-R93W (7) exhibited S-phase accumulation upon siRNA knockdown of endogenous mouse *Cep164* (increase from 30% to 36.7% ± 3.2) indicating that this disease-causing variant affects this function of CEP164 (Figure 2C). We conclude that CEP164 plays a role in early S-phase progression and that mutations in *CEP164* associated with NPHP are defective in this function. Because S-phase arrest may reflect increased DNA damage response signaling, we examined Cep164 levels in the presence or absence of DNA damage and observed increased levels of Cep164 protein (Figure 2E). Importantly, IMCD3 and RPE cells depleted of *Cep164* accumulate the DNA damage marker phosphorylated H2AX (γH2AX) (Figure 2F-G), which is accompanied by stabilization of PCNA, after transfection with a species-specific pooled (siCEP164-p/siCep164-p) or individual siRNA (siCEP164-i/siCep164-i) or exposure to replication stress agent aphidicolin (APH) (Figure 2I). To examine the pathophysiological relevance of these data, we obtained a urine sample from a newly diagnosed and untransplanted NPHP patient and isolated urine-derived renal epithelial cells. Compared to a healthy age- and gender-matched control, localization of CEP164 was observed to be more nuclear and γH2AX was quantitatively more evident (***p<0.001) (Figure 2H). Although this is an isolated patient, these data would indicate that DDR processes are relevant to advent of NPHP.

Apoptosis and DNA damage are enhanced in *CEP164* depleted cell populations

Despite the fact that reduction of cellular levels of *CEP164* by si*CEP164* knockdown results in a quicker cell cycle than controls (Figure 1A), we consistently observed a decreased cell number during CyQUANT assays using different cell lines (Figure 1E). This paradox led us to investigate whether apoptosis might explain the discrepancy between the accelerated cell cycle in RPE-FUCCI cells after knockdown of *CEP164* and decreased net proliferation which was determined by several assays. The time-lapse data from RPE-FUCCI cells transfected with si*CEP164* or control were analyzed for the number of cells characteristically appearing apoptotic (passive or Brownian movement, blebbing, detaching, and/or lacking fluorescence) within 72 hours of filming. These events were significantly higher after *CEP164* knockdown, normalizing for the total number of cells per field (*p<0.05) (Figure 3A). For molecular analysis of apoptotic markers, RNA from RPE-FUCCI cells and IMCD3 cells was isolated after transfection with control or si*CEP164-p or siCep164-p* oligos respectively and we performed RT-QPCR to measure *Caspase-3* mRNA expression (Figure 3E). Twenty-four to 48 hours after transfection there was increased expression of *Caspase-3* mRNA (***p<0.0001) which we visualized by live cell imaging of dual immunofluorescent staining of Annexin V and Caspase-3 substrate (Figure S5C-D). As further validation, we transfected *CEP164* siRNA into RPE cells stably expressing 53BP1-GFP, a protein which

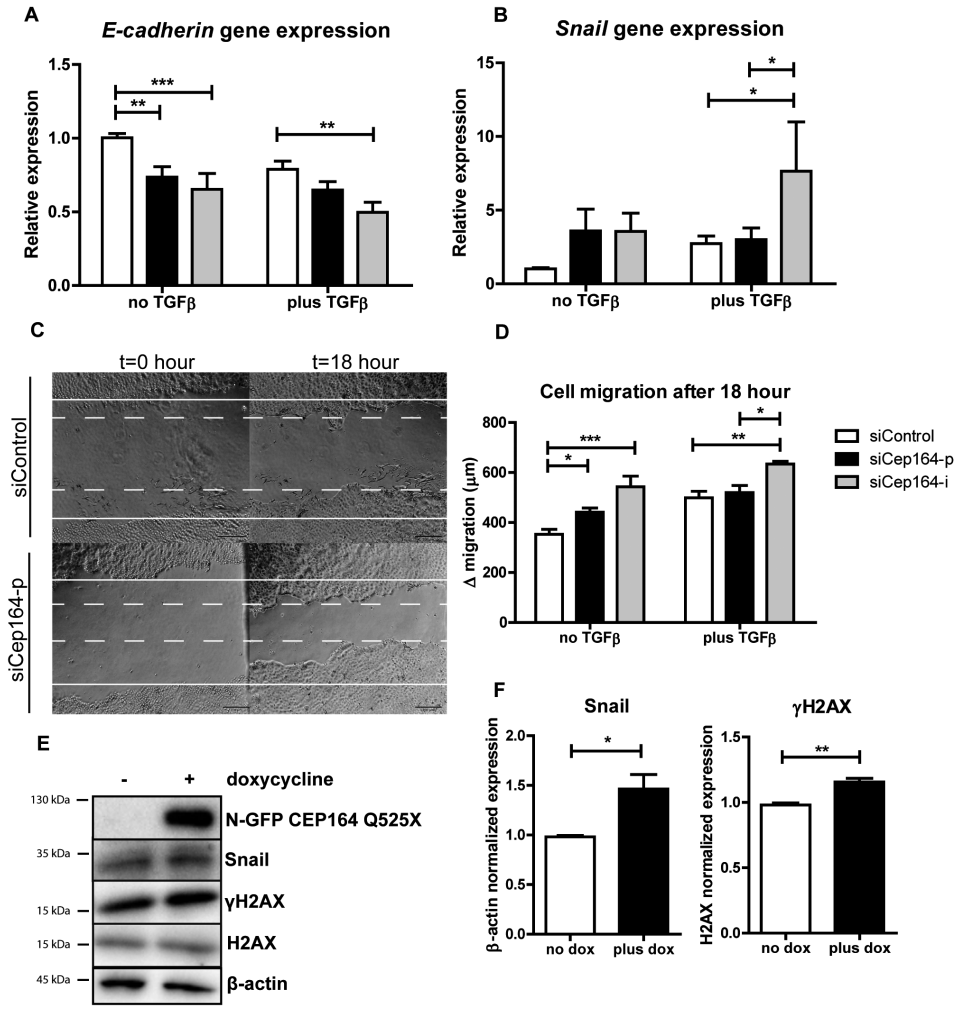

Figure 4. Loss of Cep164 induces EMT

(A) Relative gene expression levels of epithelial marker E-cadherin as measured by RT-QPCR in IMCD3 cells, normalized to RPL27. Total RNA was isolated 6 days after transfection with siControl or siCep164 oligos with or without TGFβ incubation (5 ng/mL) in serum-free medium. After 6 days of transient transfection (siRNA transfection occurred at day 0 and day 3) E-cadherin mRNA levels are significantly decreased. (**p<0.01; n=4, error bars represent SEM). (B) Relative gene expression levels of mesenchymal marker Snail as measured by RT-QPCR in IMCD3 cells, normalized to RPL27. Total RNA was isolated 6 days after transfection (siRNA transfection occurred at day 0 and day 3) with siControl or siCep164 oligos with or without TGFβ incubation (5 ng/mL) in serum-free medium. After 6 days of transient transfection Snail mRNA levels (*p<0.05) are increased. (n=4, error bars represent SEM). (C) Representative scratch healing images of IMCD3 cells taken by light microscope before and 18 h after a scratch was made in a confluent monolayer of cells. The white solid lines represent the wound edges at t=0 h and the white dashed lines indicate the edges at t=18 h. Scale bar represents 200 μm. (D) Quantification of absolute distance (μm) of cell migration after 18 hours after a scratch. IMCD3 *Cep164* depleted cells migrate (*p<0.05) more than siControl cells 48 hour after transfection. TGFβ incubation (5 ng/mL) in serum-free medium enhances this effect (n=4, error bars represent SEM). P-values were calculated using two-way ANOVA and Bonferroni multiple comparison test. (E-F) Lysates of IMCD3 *N-GFP-CEP164-Q525X* cells treated with doxycycline

were made 24 hours after addition to the culture medium. Western blot was performed for Snail and γH2AX and loading controls β-actin and H2AX respectively. Upregulation of both Snail and γH2AX are visible after induction of dominant negative allele *N-GFP-CEP164-Q525X* (n=3). Quantification of the protein expression of Snail (Student´s t-test *p<0.05) and γH2AX (**p<0.01) in lysates of IMCD3 *N-GFP-CEP164-Q525X* cells normalized to loading control β-actin and H2AX respectively was performed using Image Lab software (n=3, error bars represent SEM).

accumulates at double strand breaks,(17) and stained those cells for Caspase-3 after fixation. RPE nuclei showing 53BP1-GFP foci were counted as well as Caspase-3 positive nuclei and were normalized against the total number of nuclei analyzed. After 32 hours more 53BP1-GFP positive cells were counted in si*CEP164* cells compared to controls (*p<0.05) (Figure 3B-C). During all time points significantly (*p<0.05) more apoptosis events were scored (Figure 3B,D). We performed a FACS assay for measuring apoptosis of *Cep164* siRNA transfected IMCD3 cells incubated with 50 nM aphidicolin (APH) for 16 hours, a treatment which causes replicative stress and synchronizes cells in S-phase (8). *Cep164* knockdown caused apoptosis of IMCD3 cells which was further enhanced by APH treatment (Figure 3F), suggesting that S-phase prolongation and/or replicative stress may predispose renal cells to apoptosis (Figure 2).

CEP164 regulates epithelial-to-mesenchymal transition

Epithelial-to-mesenchymal transition (EMT) slows down cell proliferation and provides cells an alternative to apoptosis.(18) A pro-fibrotic mesenchymal transition is characterized by expression of Snail.(19) E-cadherin expression decreases as cells lose their epithelial characteristics and become more mesenchymal.(20) We investigated the role of siCep164 (Figure S3F) in the induction of EMT using TGFβ1 incubation (5 ng/mL) as a positive control for EMT in IMCD3 cells.(21,22) Six days after knockdown of *Cep164* in IMCD3 cells we measured decreased gene expression levels of *E-cadherin* (Figure 4A) and increased levels of *Snail* (Figure 4B). *Tieg1*, *TGF-β1, αSMA, Fibronectin1* and *CTGF* (Figure S3A-E) are concomitantly upregulated after Cep164 depletion as measured by RT-QPCR (*p<0.05).
Because mesenchymal cells migrate faster than epithelial cell populations,(21) we performed a scratch wound migration assay (23) to investigate the cell migration capacity of IMCD3 cells after knockdown of *Cep164*. Cells with reduced levels of *Cep164* migrated significantly faster than siControl cells (*p<0.05). TGFβ1 incubation had a comparable effect on migration in this experimental set-up (Figure 4C-D). Accordingly, expressing the dominant negative allele *N-GFP-CEP164-Q525X* resulted in increased Snail and γH2AX protein levels (*p<0.05) (Figure 4E-F).
Finally, we investigated the role of siCep164 in the induction of fibrosis in mouse embryonic fibroblasts (MEFs). Six days after knockdown of *Cep164* in MEFs (Figure S4F) we measured increased levels of *TGF-β1, Fibronectin1* and *CTGF*, but not of *Tieg1* and *αSMA* (Figure S4A-E), by RT-QPCR. We conclude that *Cep164* has a role in inducing EMT and fibrosis in renal epithelial and mesenchymal cells. Furthermore, our data suggest this effect to be

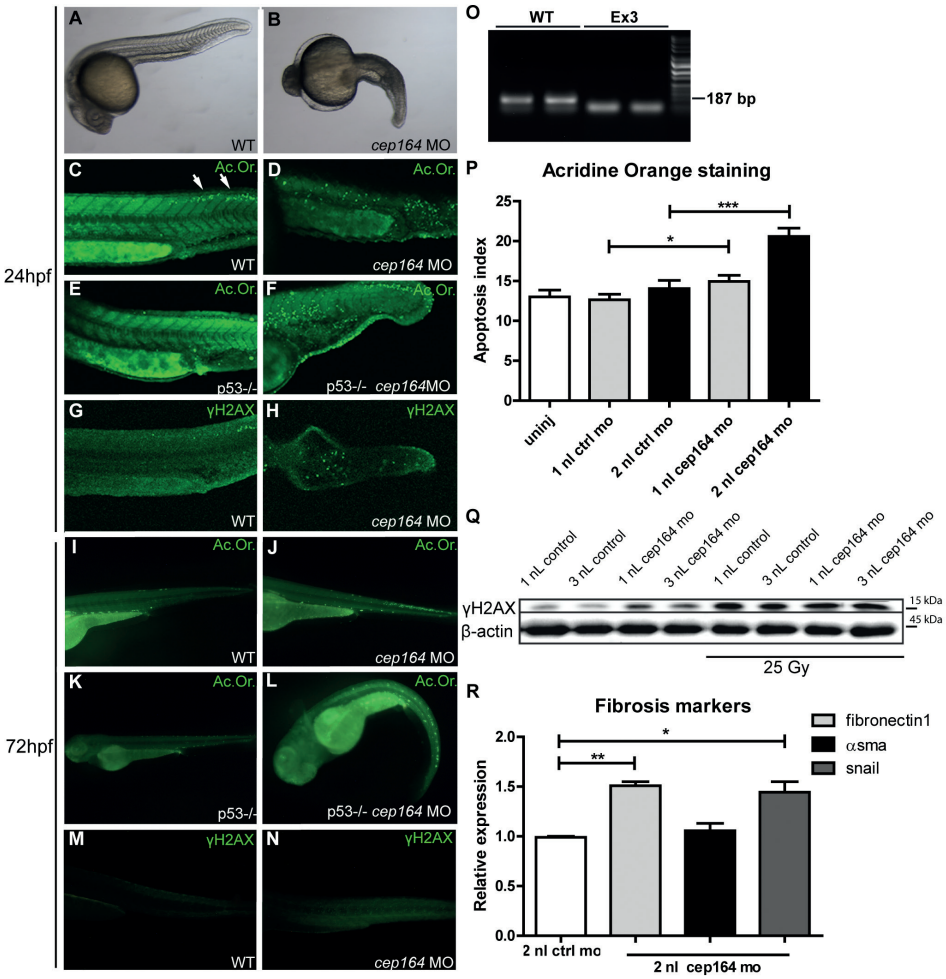

Figure 5. Apoptosis, DNA damage signaling and fibrosis in zebrafish
Zebrafish *cep164* knockdown leads to developmental abnormalities associated with apoptosis and DNA damage. A *cep164* morpholino targeting the exon 3 splice donor reduces wildtype mRNA (lanes WT) and results in a smaller cep164 RT-PCR product indicating an internal deletion (lanes Ex3) (O) was injected into 1-2 cell embryos. Compared to wild-type embryos at 24hpf (A), morphant embryos (B) were stunted and displayed shorten body axis, body axis curvature, and edema. No cysts or other specific phenotypes were observed in the pronephros of morphant fish. Acridine orange staining revealed a low level of apoptosis in control injected WT (C) and *p53 -/-* embryos (E) restricted primarily to the posterior neural tube (arrows in C). *cep164* knockdown induced widespread apoptosis (D) in the trunk and tail which was not affected by p53-deficiency as indicated by the *cep164* knockdown-induced apoptosis in *p53-/-* mutants (n=30) (F). Staining with γH2AX antibody revealed enhanced DNA damage signaling in *cep164*-deficient embryos (n=10) (H) but not controls (G). Acridine orange staining (Ac. Or.) also revealed a low level of apoptosis in 72 hours post fertilization (hpf) control injected WT (I) and *p53-/-* embryos (K). *cep164* knockdown induced widespread apoptosis (J) which was not affected by p53-deficiency as indicated by the *cep164* knockdown-induced apoptosis in *p53-/-* mutants (n=45) (L). Quantified acridine orange staining (Ac. Or.) reveals significantly increased apoptosis in WT zebrafish after *cep164* knockdown (P). Student's t-test were used to calculate p-values (*<0.05, ***<0.001) (n=70 in 4 experiments, error bars represent SEM). Staining with γH2AX antibody revealed enhanced DNA damage signaling in *cep164*-deficient embryos (N) but not control injected

WT embryos (n=10) (M). Western blot of γH2AX protein levels from lysates of 15 pooled embryos, two hours after irradiation with 25 Gy, show increased DNA damage signaling (Q). RT-QPCR reveals significant induction of *snail* and *fibronectin1* in cep164 MO injected embryos at 32hpf (R). mRNA expression from 12 pooled embryos is normalized to 2 nL control MO injected zebrafish. Student's t-test was used to calculate p-values (*<0.05, **<0.01).

possibly specific to the kidney; RPE cells in similar experimental settings do not undergo EMT and do not migrate (Figure S5E-G).

Apoptosis, DNA damage and fibrosis are enhanced in *cep164* depleted zebrafish

To evaluate *cep164* loss of function *in vivo* we performed morpholino oligonuclotide (MO) knockdown in zebrafish using a different MO targeting the splice donor site of exon 3 (Figure 5O) than previously published (7). This more effective morpholino induced consistent and robust developmental abnormalities. *cep164* knockdown caused microcephaly, shortened body axis, axis curvature and edema (Figure 5B, L) compared to wildtype zebrafish after control injection (Figure 5A) and in general recapitulates the results of the other published MO (7). This phenotype was associated with massive cell death as demonstrated by widespread acridine orange (Ac.Or. green) staining in morphant embryos (Figure 5D) compared to control injected siblings (Figure 5C). Homozygous *p53* mutant zebrafish embryos injected with *cep164* morpholino displayed cell death as well compared to control injections (Figure 5E-F). DDR signaling was also activated in morphant embryos as indicated by an increased signal of γH2AX immunofluorescence compared to control (Figure 5G-H). 72 (hours post fertilization, hpf) morphant embryos displayed increased apoptosis (Figure 5I-L, 5P) and increased γH2AX levels as well (Figure 5M-N-Q). No specific pronephros DNA damage or apoptosis accumulation was observed; however, the pronephros at this embryonic stage is exquisitely regenerative. Similarly, we examined *cep164* morphant zebrafish for induction of EMT and a profibrotic response after depletion of cep164. Indeed, RT-QPCR revealed significant induction of *snail* and *fibronectin1* in cep164 MO injected embryos at 32 (Figure 5R), 72 and 96 (Figure S6) hpf.

DISCUSSION

NPHP is a common cause of renal end-stage disease in children and young adults. Although NPHP-associated ciliary defects and impaired DNA damage response have been associated with *CEP164* dysfunction (NPHP15),(7,10,12,13) the exact mechanism linking these processes to NPHP is unclear. Here we identify novel functions for CEP164 relevant to NPHP pathogenesis, namely in cell cycle progression, apoptosis, EMT and fibrosis regulation. We show that despite accelerated cell cycle progression, total cell number is decreased after *CEP164* knockdown. Our data further indicate a role for CEP164 in S-phase

progression. Accumulation of cells in S-phase could be rescued by wild-type *CEP164*, but not by its disease-associated variant alleles. We observed that *Cep164*-loss promotes apoptosis *in vitro* characterized by increased levels of 53BP1 and γH2AX. Zebrafish with reduced levels of cep164 show developmental abnormalities, increased apoptosis, enhanced DDR signaling and a profibrotic response, demonstrating the *in vivo* relevance of our findings. These novel functions are highly relevant to the etiology of NPHP which features increased apoptosis and fibrosis. Our data suggests functional similarity between CEP164 and at least one other NPHP protein, *GLIS2* (*NPHP7*), which also protects renal cells from apoptosis and fibrosis.(5) With two of the seventeen known nephronophthisis-associated proteins clearly associated with these processes, as well as the ongoing large-scale proteomics efforts to understand the nephronphthisis interactome (www.syscilia.org) (24), we anticipate that additional NPHP-genes will be implicated in these processes. In short, we propose that these non-ciliary functions of NPHP genes help to explain differences in disease progression between NPHP and other types of PKD (Figure 6).

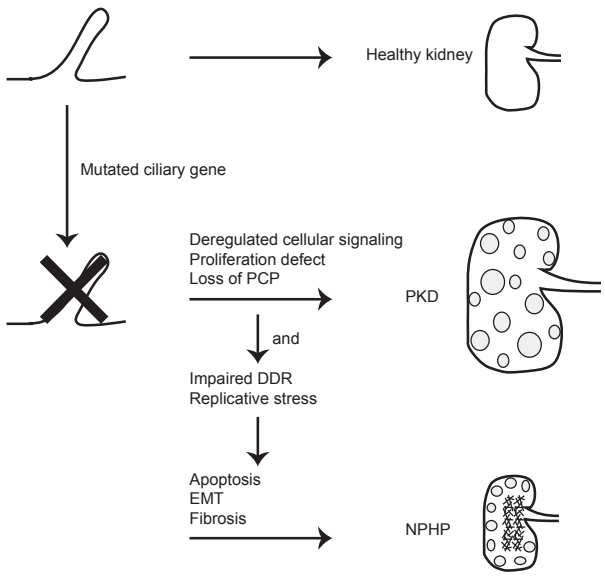

Figure 6. Schematic overview of signaling cascade involved in development of PKD and NPHP
Mutations in ciliary genes cause ciliary defects. Ciliary defects result in proliferation defects, loss of planar cell polarity (PCP) and deregulated cellular signaling. This causes cystic kidney disease. When the gene mutated is also involved in the DNA damage response (DDR) or DNA replication, impairments of these processes cause apoptosis, epithelial-to-mesenchymal transition (EMT) and consequently fibrosis in the NPHP patients.

Studies from Graser *et. al.* show that *CEP164* expression is cell cycle stage-dependent. (10) Most protein is present at the end of the S-phase and the beginning of G_2/M in HeLa cells. Knockdown of *CEP164* in HeLa cells showed abrogation of the G2/M checkpoint,(12) suggesting a role of *CEP164* in the G_2/M checkpoint. In line with these published findings, we find that *CEP164* knockdown in RPE-FUCCI cells accelerates G_1, G_2 and M cell cycle phase durations but delays S-phase progression. Human wild-type *CEP164,* but not its disease-associated mutants, rescue IMCD3 cells from accumulation in S-phase. Activation of the intra-S checkpoint occurs when replication forks cannot stall at damaged DNA,(25) ensuring that the cell cycle progression only reinitiates after damage repair. Because *CEP164* mutant alleles were not able to rescue S-phase accumulation, we suggest that replicative stress might contribute to NPHP development in general. In a similar manner, *Nek8(NPHP9)*-mediated replication stress contributes to the NPHP etiology.(8)

EMT is a hallmark of tubulointerstitial renal fibrosis.(6) Upon *CEP164* mutation, induction of apoptosis might compete with EMT as has previously been described.(18,26,27) The reduced total cell number after si*Cep164* can partially be explained by induced apoptosis but probably by transdifferentiation of the epithelial kidney cells as well. Accordingly, mesenchymal marker Snail is increased upon reduction of cellular levels of Cep164 in conjunction with a decrease of epithelial marker E-cadherin, indicating that cells lose their epithelial characteristics. The pathological significance of the tubular EMT in renal fibrosis is becoming increasingly accepted.(28) *Snail* activation associates with patients' renal fibrosis, and disrupts renal homeostasis.(29) The principal effector cells of renal fibrosis are myofibroblasts; evidence suggests that both cells of epithelial origin and cells of mesenchymal origin as progeny for myofibroblasts.(6) We observe that epithelial cells *in vitro* and *in vivo* undergo the process of EMT upon *Cep164* knockdown, a proposed mechanism contributing to the rise of myofibroblasts during fibrosis. Furthermore, we saw that *Cep164* depletion was capable of inducing fibrotic genes in MEF cells, presumably because MEFs are already mesenchymal and thus no longer require EMT. These results obtained from cell types of both epithelial and mesenchymal origin indicate that *Cep164* loss can induce fibrosis regardless of the origin of the myofibroblast. In NPHP patients, excessive deposition of extracellular matrix (fibrosis) by mesenchymal cells replaces functional tissue.(30)

Briefly, this manuscript shows *in vitro* S-phase arrest, quicker cell cycle progression and EMT and fibrosis induction upon loss of *Cep164*. Accumulation of DNA damage signaling during replicative stress could be the cause of the observed apoptosis. Apoptosis is known to contribute to initiation of renal cyst formation.(31,32) Our data support the hypothesis proposed by Choi *et al*. which states that, in addition to cilia loss-of-function, replicative stress contributes to the disease mechanism of NPHP as well(8). We show that loss of *Cep164* results in EMT and fibrosis in different cell types as well as in zebrafish. The induced overall pro-apoptotic and pro-fibrotic response of different cell types may explain

the non-cystic features of nephronophthisis such as reduced kidney size (Figure 6). Since the fibrotic nature of NPHP kidneys is progressive with a time window of several years for therapeutic intervention, understanding and curing this aspect of juvenile kidney disease will potentially delay the need for renal replacement therapy. Our data support the hypothesis that the NPHP-interactome encoded by the 17 NPHP genes coordinates cilia loss-of-function with concomitant DNA damage response, apoptosis, and the creation of a pro-fibrotic environment, all of which directly contribute to the renal phenotype in these patients.

MATERIALS AND METHODS

Ethics Statement

Renal epithelial cells were obtained from a nephronophthisis patient that had been included in the AGORA (Aetiologic research into Genetic and Occupational/environmental Risk factors for Anomalies in children) biobank project. The regional Committee on Research involving Human Subjects (CMO Arnhem/Nijmegen) approved the study protocol. Written informed consent was obtained from the patient and the parents. All zebrafish experiments were approved by the Animal Care Committee of the University Medical Center Utrecht in the Netherlands.

Urine-derived renal epithelial cells

Renal epithelial cells were obtained from a nephronophthisis patient and a healthy gender- and age-matched control. The patient was determined to have isolated clinical diagnosis of NPHP. Urine-derived renal epithelial cells were derived as we have previously described. (33)

IMCD3 cell culture

Mouse Inner Medullar Collecting Duct (IMCD3) cells were cultured in Dulbecco's Modified Eagle's Medium (DMEM):F12 (1:1) (GlutaMAX, Gibco), supplemented with 10% Fetal Calf Serum (FCS) and penicillin and streptomycin (1% P/S). Cells were incubated at 37 °C in 5% carbon dioxide (CO_2) to approximately 90% confluence. IMCD3 cells were stably transfected with CEP164 constructs in a retroviral vector (pRetroX-Tight-Pur) for doxycyclin-inducible expression. Inducible overexpression was obtained of N terminally GFP-tagged human full-length *CEP164* isoform 1 (NGFP-CEP164-WT), or truncated *CEP164*, corresponding with the p.Q525X mutation, or non-functional *CEP164*, corresponding with the p.R93W mutation by addition of 2 ng/ml doxycycline.(7)

RPE cell culture

Human retinal pigment epithelial (RPE) cells were cultured in DMEM:F12 (1:1) (GlutaMAX, Gibco), supplemented with 10% FCS and 1% P/S. Cells were incubated at 37 °C in 5% CO_2 to approximately 90% confluence. RPE cells were transfected with lentiviral vectors containing mKO2-hCdt1(30/120) and mAG-hGem(1/110). Fluorescent, ubiquitination-based cell cycle indicator (FUCCI)(16) expressing stable transformants were generated (15). RPE 53BP1-GFP cells are described in Janssen *et. al.*(17) RPE cells were stably transfected with CEP164 constructs in a retroviral vector (pRetroX-Tight-Pur) for doxycyclin-inducible expression. Inducible overexpression was obtained of N terminally GFP-tagged human full-length *CEP164* isoform 1 (NGFP-CEP164-WT). RPE cells were serum starved >24 hour in experiments for cilia quantification.

MEF cell culture

Mouse embryonic fibroblasts (MEFs) were cultured in DMEM (Gibco), supplemented with 10% FCS and 1% P/S. Cells were incubated at 37 °C in 5% CO_2 to approximately 90% confluence.

Transfections

At least 6 hours after plating, cells were transfected with Lipofectamine RNAimax (Invitrogen, 13778-075), according to the supplier's protocol. Opti-MEM (Invitrogen, 31985-062) was used to dilute the ON-TARGETplus siRNA SMARTpools (Thermo Scientific Dharmacon) for Non-targeting pool UGGUUUACAUGUCGACUAA / UGGUUUACAUGUUGUGUGA / UGGUUUACAUGUUUUCUGA / UGGUUUACAUGUUUUCCUA (D-001810-10), human *CEP164* GAGUGAAGGUGUAUCGCUU / GAGAAGUGGCGCAAGUAUU / GGACCAUCCAUGUGACGAA / GAAGAGUGAACCUAAGAUU (L-020351-02), human *CEP164* GAGUGAAGGUGUAUCGCUU (J-020351-17), or mouse *Cep164* GGAGAGUGCAGGAGGGAGA / ACCCAGUGCAGGCAGGAAA / AGUCAGAGAUCCACGGACA / CCACAGAAAGAAAACGAGA (L-057068-01), mouse *Cep164* CCACAGAAAGAAAACGAGA (J-057068-09) to 20 nM.

Real time imaging

RPE-FUCCI cells were seeded in 8 well Lab-Tek Chamber Slides (Thermo Scientific) without addition of serum. After 16 hours, the cells were transfected with Lipofectamine RNAimax. Seven hours after transfection, medium in the Lab-Tek Chamber Slides was replaced with Leibovitz's medium without phenol red (Gibco), supplemented with 6% FCS, 1% P/S and 1% Ultraglutamine. Real time imaging was performed using a Zeiss microscope using a 10x lens. Every 15 minutes images were made of the RPE-FUCCI cells in LED, GFP and dsRED channels for 72 hours. Three positions were imaged per experimental condition.

Images were processed with the MetaMorph software. GraphPad Prism 5.0 was used to perform one-way ANOVA with Dunnett's post test.

Immunofluorescence and confocal imaging

For immunostaining, IMCD3, RPE-FUCCI, urine derived renal epithelial cells or RPE 53BP1-GFP cells were grown on coverslips and fixed for 30 minutes in 4%PFA at the indicated time points, followed by a 15 minutes permeabilization step in 0.5%Triton-X100/1%BSA/PBS. Primary antibody incubations (mouse anti-acetylated tubulin (Sigma, T7451, dilution 1:20000), rabbit anti-CEP164, Novus 45330002, 1:500, mouse anti-phospho-Histone H2A.X (Ser139), clone JBW301, Millipore 05-636, 1:500 or rabbit anti-active Caspase-3 (BD Pharmingen, 559565, dilution 1:250) were performed overnight in 1% BSA/PBS. Goat anti-mouse/rabbit Alexa 647 secondary antibody (Invitrogen, dilution 1:500) incubations were performed for 2.5 hours at RT. DAPI incubations were performed for 10 minutes at RT. Coverslips were mounted in Fluormount G (Cell Lab, Beckman Coulter). Confocal imaging was performed using Zeiss Confocal laser microscope and images were processed with the ZEN 2011 software. Approximately 250 events per condition were scored. GraphPad Prism 5.0 was used to perform statistical analysis. To observe centrosomal localization of N-GFP-CEP164-WT, clonally inducible IMCD3 cell lines doxycylcin (Dox)-inducibly expressing human *N-GFP-CEP164-WT* were treated by double thymidine block (2 mM). Cells were also induced with doxycycline (10 ng/mL) during the thymidine block to express *N-GFP-CEP164-WT*. Cells were stained with CEP164-SR antibody followed by anti-rabbit-alexa fluor 594 antibody for confocal imaging to observe colocalization with the induced *N-GFP-CEP164-WT*-expressing cells. For live cell imaging, RPE cells were seeded in Lab-Tek Chamber Slides with cells at 30% confluency. RPE cells were transfected and after 16 hours, wells were washed once with PBS and once with 1x Binding Buffer (NucView Dual Apoptosis Kit for Live Cells, Biotium, 30067). Cells were incubated 40 minutes at RT with NucView 488 Caspase-3 substrate (5μM) and CF 594-Annexin V (1:40) in 1x Binding Buffer. Cells were washed once with 1x Binding buffer and confocal imaging was performed using a Zeiss Confocal laser microscope and images were processed with the LSM500 software. GraphPad Prism 5.0 was used to perform two-tailed student t-tests.

EdU staining

To examine cells in S phase, RPE-FUCCI cells were seeded on coverslips. After 48 hour EdU (Invitrogen, A10044) incorporation took place for 30 minutes using 10 μM in culture medium. The cells were fixed in 3% PFA and washed with PBS. Cells were shortly incubated with EdU staining buffer (100 mM Tris pH 8,5; 1 mM $CuSO_4$). Then the cells were incubated with EdU staining buffer containing Alexa Fluor 647 azide (1:1000) (Invitrogen, A10277) and ascorbic acid (0.1 M) (Merck) for 30 minutes at RT in the dark. The coverslips were washed twice with PBS and incubated with DAPI for 30 minutes at

RT in the dark. The coverslips were mounted with Fluormount G (Cell Lab, Beckman Coulter) after washing them once with PBS. Confocal imaging was performed using Zeiss Confocal laser microscope and images were processed with the ZEN 2011 software.

CyQUANT NF Cell Proliferation assay

RPE and IMCD3 cells were transfected in 96 well plates seeded with cells at 30% confluency. CyQUANT NF reagent (Invitrogen, C35006) was prepared according to the manufacturer's protocol. After 72 hour of incubation, 50 µl of CyQUANT NF Cell Proliferation Assay reagent was added to each well after aspiration of medium. After incubation for 30 minutes at 37°C, fluorescence was measured (excitation 485 nm, emission 538 nm) on a Fluoroskan Ascent FL apparatus (Thermo Scientific, 374-90441C) using Ascent Software version 2.6. Blanc measurement subtraction was performed and GraphPad Prism 5.0 was used to perform two-tailed student t-tests.

Real-Time-Quantitative PCR (RT-QPCR)

Cells were lysed and total RNA was isolated (RNeasy Mini Kit, Qiagen, 74106) and measured (NanoDrop spectrophotometer ND-1000, Thermo Fischer Scientific Inc.). cDNA was synthesized from 500 ng RNA template using the iScript cDNA Synthesis Kit (Bio-Rad, 170-8891) according to the supplier's protocol. Dilutions were made for RT-QPCR analysis to determine mRNA expression levels which were normalized against a reference gene. The iQ SYBR Green Supermix (Bio-Rad, 170-8880) was used to multiply and measure the cDNA with a CFX96 Touch Real-Time PCR Detection System (Bio-Rad). All samples were run in triplicate in 20 µl reactions. The following PCR program was used: 95°C for 3 min, followed by 40 cycles of 10 s at 95°C, 30s at the indicated annealing temperature and 30 s at 72°C, then 10 s at 95°C followed by a melt of the product from 65°C-95°C. The primer sequences (Sigma) used and concomitant annealing temperatures are: hCEP164 forward 5'-GGCAAAGCTGTCAACTTCTGG, hCEP164 reverse 5'-GAACTGGGGCTAATGAGGAAC, 61°C, mCep164 forward 5'-AGAGTGACAACCAGAGTGTCC, mCep164 reverse 5'-GGAGACTCCTCGTACTCAAAGTT, 61°C, hRPLP0 forward 5'-TGCACAATGGCAGCATCTAC, hRPLP0 reverse 5'-ATCCGTCTCCACAGACAAGG, 58°C, hCaspase-3 forward 5'-ACATGGCGTGTCATAAAATACC, hCaspase-3 reverse 5'-CACAAAGCGACTGGATGAAC, 60°C, mE-cadherin forward 5'-CAGTTCCGAGGTCTACACCTT, mE-cadherin reverse 5'-TGAATCGGGAGTCTTCCGAAAA, 66°C, mCaspase-3 forward 5'-GGCTTGCCAGAAGATACCGGT, mCaspase-3 reverse 5'-GCATAAATTCTAGCTTGTGCGCGT, 67°C, mSnail forward 5'-CACACGCTGCCTTGTGTCT, mSnail reverse 5'- GGTCAGCAAAAGCACGGTT, 66°C, hSnail forward 5'-TCGGAAGCCTAACTACAGCGA, hSnail reverse 5'-AGATGAGCATTGGCAGCGAG, 64°C , mRPL27 forward 5'-CGCCCTCCTTTCCTTTCTGC, mRPL27 reverse 5'-GGTGCCATCGTCAATGTTCTTC,

53°C, hVimentin forward 5′-GACAATGCGTCTCTGGCACGTCTT, hVimentin reverse 5′-TCCTCCGCCTCCTGCAGGTTCTT, 67°C, ZfαSMA forward 5′-CATGTACCCGGGCATTGCAGA, , ZfαSMA reverse 5′- GGAAGGTGGAGAGAGAGGCCA, zfSnail forward 5′-CTCCTGCCCACACTGTAACCG, zfSnail reverse 5′-CATGCGACTGAAGGTGCGAGA, zfFibronectin1 forward 5′-TCCCAGACATCACGGGCTACA, zfFibronectin1 reverse 5′-GCATGAGTTCTGTCCGGCCTT, zfβ-actin forward 5′-TCTGGATCTGGCTGGTCGTGA, zfβ-actin reverse 5′- CTCCTGCTCAAAGTCCAGGGC 63°C. Taqman assays were performed to measure mouse CTGF (Applied Biosystems, probe number Mm01546133_m1), Tieg1 (Mm00449812_m1), TGFβ1 (Mm01178820_m1), ACTA2 (αSMA, Mm00725412_s1), and Fn1 (Mm01256744_m1) gene expression levels. The following PCR program was used: 40 cycles of 15 s at 95°C, 60s at 60°C. The ΔΔCT method was used for statistical analysis to determine gene expression levels.

Immunoblotting

Protein lysates were prepared using RIPA lysis buffer. To correct for protein content BCA protein assay (Pierce) was performed. Western blots were performed for *Cep164*. β-actin was used as loading control in combination with Coomassie Blue staining. After blotting, the PVDF membranes were blocked in 5% dried skim milk in TBS with 0.5% Tween. And western blots were performed for γH2AX, PCNA and Snail. H2AX and β-actin were used as loading control in combination with Coomassie Blue staining. After dry blotting (iBlot Dry Blotting System, Invitrogen, IB3010-01), the nitrocellulose membranes were blocked in 5% BSA in TBS with 0.5% Tween. The primary antibodies (rabbit anti-Cep164, Novus 45330002, 1:2000, rabbit anti-H2AX (pSer^{139}), Calbiochem DR1017, 1:1000, mouse anti-phospho-Histone H2A.X (Ser139), clone JBW301, Millipore 05-636, 1:1000 (Specificity of the gamma H2AX antibodies was determined by pre-treatment with phosphatases), rabbit anti-Histone H2A.X, Millipore 070627, 1:1000, rat anti-PCNA, Antibodies Online ABIN334654, 1:1000, rabbit anti-Snai1, Santa Cruz sc-28199, 1:400, and mouse anti-β-actin AC-15, Sigma A5441, 1:15000, rabbit anti-GFP Abcam, 1:1000) were incubated overnight at 4ºC. The secondary swine anti rabbit, goat anti rat and rabbit anti mouse antibodies which are HRP conjugated (DAKO, dilution 1:2000) were incubated for 1 hour at RT. The ECL Chemiluminescent Peroxidase Substrate kit (Sigma, CPS1120-1KT) was used for development. Scans of the blots were made with the BioRad ChemiDoc XRS+ device with Image Lab software 4.0. GraphPad Prism 5.0 was used to perform two-tailed student t-tests.

Fluorescence-activated cell sorting (FACS)

To investigate S-phase progression, dox-inducible non-clonally and clonally selected mouse IMCD3 cells expressing wild type human *CEP164* cDNA construct *N-GFP-CEP164-WT* or

mutant human *CEP164* construct *N-GFP-CEP164-Q525X* or *N-GFP-CEP164-R93W* were transfected with either negative control siRNA (50 nM) or anti-mouse *Cep164* siRNA (50 nM) using Polyplus transfection reagents. Cells were treated for double thymidine block (2 mM) from time point 24-42 to 50-68 hrs post transfection. Cells were then also induced with doxycycline (10 ng/ml) at 24 hrs post siRNA transfection for expression of human wild type construct *N-GFP-CEP164-WT* or human mutant constructs. Cells were released from second thymidine block for 6 hrs and fixed with 2% PFA and stained with PI/RNAse staining solution. Events were acquired in a FACSCalibur flow cytometer (BD Biosciences) for the cell cycle histogram Mean and SD of percent of DNA amount for different phases (triplicate samples) were calculated and plotted as histograms.

Apoptosis FACS

To quantify apoptosis, IMCD3 cells were plated and transfected with siControl or siCep164. After 24 hours cells were exposed to 0 and 50 nM aphidicolin for 16 hours. Cells were harvested and washed once with 1% BSA-PBS. Cells were collected in FACS tubes in 200 µl 1% BSA-PBS containing Vybrant DyeCycle Violet Stain (Invitrogen, V35003, 1:1000) to stain living and early apoptotic cells (7 minutes at 37ºC) and 7-AAD viability stain (eBioscience, 00-6993, 1:60) to stain late apoptotic cells (10 minutes on ice). Cells were measured (10.000 events) with a BD FACSCanto II flowcytometer and analyzed using BD FACSDiva Software.(34) GraphPad Prism 5.0 was used to perform two-way ANOVA with Bonferroni post hoc test.

Migration assay

IMCD3 cells were transfected overnight with non-targeting siControl or siCep164 oligonucleotides in 24 well plates seeded with cells at 40% confluency. 48 hour later, when the cells were >85% confluent, a plastic disposable pipette tip was used to create a scratch wound in the cell monolayer. After washing the wells once with PBS, the cells were incubated with serum-free medium for 18 hours containing no or 5 ng/mL TGFβ (Peprotech, 100-21). Images of the same positions of the scratch were made with a light microscope (4x objective) after 0 and 18 hours. Migration of cells was measured with Image-Pro. GraphPad Prism 5.0 was used to perform two-way ANOVA with Bonferroni post hoc test.

Zebrafish morpholino injections

Wild-type and p53-/- embryos (*tp53 M214K*) (35) at the 1-2 cell stage were injected with 1 or 2 nL of a 0.1 mM antisense morpholino oligonucleotide targeting *Cep164* exon 3 in pure water with 0.1% Phenol Red using a nanoject2000 microinjector (World Precision Instruments). The sequence of the exon 3 morpholino was: TGTGTTGTGGAGTGTGTGTTACCAT. The sequence of the standard control morpholino was:
5′-CCTCTTACCTCAGTTACAATTTATA-3′. Primers amplifying exon 3 (Cep164 ex 2-4

product length = 187) forward primer GGTGCTGGAGGAGGATTATG and reverse primer GTAGTAGACCTCGCCCGTCA were used. For western blot 15 embryos were pooled in 60 µL Triton X-100 lysis buffer. For RT-QPCR 5 embryos were pooled in 100 µL TRIzol reagent (Invitrogen, 15596-026) and RNA was isolated following standard procedures.

Zebrafish acridine orange staining

24 and 72 (PTU treated) hpf live dechorionated embryos are incubated in a 2 mg/mL solution of acridine orange (Sigma) in PBS for 30 min at room temperature. Embryos are washed quickly in E3, then 5 X 5 minutes in E3 and visualized on a Zeiss LSM5 Pascal confocal microscope. No autofluorescence was detected in the regions analyzed. GraphPad Prism 5.0 was used to perform two-tailed student t-tests.

Zebrafish γH2AX staining

Anti-phospho H2AX antibody was a kind gift from James Amatruda (University of Texas Southwestern Medical Center, Dallas, Texas 75390). Embryos were fixed in 4% PFA overnight at 4°C and stained with Anti-phospho H2AX (1:1500), Alexa 488 goat-anti-rabbit (Invitrogen A11008) secondary antibody and visualized on a Zeiss LSM5 confocal microscope.

Acknowledgements

We thank the patient and the control human subject for their participation in this study. We thank Jeroen van Reeuwijk for performing a systems biology analysis and Livio Kleij and the Cell Microscopy Center at the UMC Utrecht for providing expert microscopy services. We thank Henry Ajzenberg for culturing urine cells, and Olivier de Jong for zebrafish primers, and Hendrik Gremmels for help with statistics.

REFERENCES

1. Otto EA, Schermer B, Obara T, O'Toole JF, Hiller KS, et al. (2003) Mutations in INVS encoding inversin cause nephronophthisis type 2, linking renal cystic disease to the function of primary cilia and left-right axis determination. Nat Genet 34: 413-420.
2. Basten SG, Giles RH (2013) Functional aspects of primary cilia in signaling, cell cycle and tumorigenesis. Cilia 2: 6.
3. Otto EA, Ramaswami G, Janssen S, Chaki M, Allen SJ, et al. (2011) Mutation analysis of 18 nephronophthisis associated ciliopathy disease genes using a DNA pooling and next generation sequencing strategy. J Med Genet 48: 105-116.
4. Fischer E, Legue E, Doyen A, Nato F, Nicolas JF, et al. (2006) Defective planar cell polarity in polycystic kidney disease. Nat Genet 38: 21-23.
5. Attanasio M, Uhlenhaut NH, Sousa VH, O'Toole JF, Otto E, et al. (2007) Loss of GLIS2 causes nephronophthisis in humans and mice by increased apoptosis and fibrosis. Nat Genet 39: 1018-1024.
6. Lebleu VS, Taduri G, O'Connell J, Teng Y, Cooke VG, et al. (2013) Origin and function of myofibroblasts in kidney fibrosis. Nat Med.
7. Chaki M, Airik R, Ghosh AK, Giles RH, Chen R, et al. (2012) Exome capture reveals ZNF423 and CEP164 mutations, linking renal ciliopathies to DNA damage response signaling. Cell 150: 533-548.
8. Choi HJ, Lin JR, Vannier JB, Slaats GG, Kile AC, et al. (2013) NEK8 links the ATR-regulated replication stress response and S phase CDK activity to renal ciliopathies. Mol Cell 51: 423-439.
9. Lans H, Hoeijmakers JH (2012) Genome stability, progressive kidney failure and aging. Nat Genet 44: 836-838.
10. Graser S, Stierhof YD, Lavoie SB, Gassner OS, Lamla S, et al. (2007) Cep164, a novel centriole appendage protein required for primary cilium formation. J Cell Biol 179: 321-330.
11. Schmidt KN, Kuhns S, Neuner A, Hub B, Zentgraf H, et al. (2012) Cep164 mediates vesicular docking to the mother centriole during early steps of ciliogenesis. J Cell Biol 199: 1083-1101.
12. Sivasubramaniam S, Sun X, Pan YR, Wang S, Lee EY (2008) Cep164 is a mediator protein required for the maintenance of genomic stability through modulation of MDC1, RPA, and CHK1. Genes Dev 22: 587-600.
13. Pan YR, Lee EY (2009) UV-dependent interaction between Cep164 and XPA mediates localization of Cep164 at sites of DNA damage and UV sensitivity. Cell Cycle 8: 655-664.
14. Pan J, Seeger-Nukpezah T, Golemis EA (2013) The role of the cilium in normal and abnormal cell cycles: emphasis on renal cystic pathologies. Cell Mol Life Sci 70: 1849-1874.
15. Shaltiel IA, Aprelia M, Saurin AT, Chowdhury D, Kops GJ, et al. (2014) Distinct phosphatases antagonize the p53 response in different phases of the cell cycle. Proc Natl Acad Sci U S A 111: 7313-7318.
16. Sakaue-Sawano A, Kurokawa H, Morimura T, Hanyu A, Hama H, et al. (2008) Visualizing spatiotemporal dynamics of multicellular cell-cycle progression. Cell 132: 487-498.
17. Janssen A, van der Burg M, Szuhai K, Kops GJ, Medema RH (2011) Chromosome segregation errors as a cause of DNA damage and structural chromosome aberrations. Science 333: 1895-1898.
18. Vega S, Morales AV, Ocana OH, Valdes F, Fabregat I, et al. (2004) Snail blocks the cell cycle and confers resistance to cell death. Genes Dev 18: 1131-1143.
19. Yoshino J, Monkawa T, Tsuji M, Inukai M, Itoh H, et al. (2007) Snail1 is involved in the renal epithelial-mesenchymal transition. Biochem Biophys Res Commun 362: 63-68.
20. Cano A, Perez-Moreno MA, Rodrigo I, Locascio A, Blanco MJ, et al. (2000) The transcription factor snail controls epithelial-mesenchymal transitions by repressing E-cadherin expression. Nat Cell Biol 2: 76-83.
21. Naber HP, Drabsch Y, Snaar-Jagalska BE, ten Dijke P, van Laar T (2013) Snail and Slug, key regulators of TGF-beta-induced EMT, are sufficient for the induction of single-cell invasion. Biochem Biophys Res Commun 435: 58-63.
22. Ivanova L, Butt MJ, Matsell DG (2008) Mesenchymal transition in kidney collecting duct epithelial cells. Am J Physiol Renal Physiol 294: F1238-1248.
23. Liang CC, Park AY, Guan JL (2007) In vitro scratch assay: a convenient and inexpensive method for analysis of cell migration in vitro. Nat Protoc 2: 329-333.
24. Sang L, Miller JJ, Corbit KC, Giles RH, Brauer MJ, et al. (2011) Mapping the NPHP-JBTS-MKS protein network reveals ciliopathy disease genes and pathways. Cell 145: 513-528.
25. Hu J, Sun L, Shen F, Chen Y, Hua Y, et al. (2012) The intra-S phase checkpoint targets Dna2 to prevent stalled replication forks from reversing. Cell 149: 1221-1232.
26. Lin F, Moran A, Igarashi P (2005) Intrarenal cells, not bone marrow-derived cells, are the major source for regeneration in postischemic kidney. J Clin Invest 115: 1756-1764.

27. Strutz F, Muller GA (2006) Renal fibrosis and the origin of the renal fibroblast. Nephrol Dial Transplant 21: 3368-3370.
28. Liu Y (2004) Epithelial to mesenchymal transition in renal fibrogenesis: pathologic significance, molecular mechanism, and therapeutic intervention. J Am Soc Nephrol 15: 1-12.
29. Boutet A, De Frutos CA, Maxwell PH, Mayol MJ, Romero J, et al. (2006) Snail activation disrupts tissue homeostasis and induces fibrosis in the adult kidney. EMBO J 25: 5603-5613.
30. Simonson MS (2007) Phenotypic transitions and fibrosis in diabetic nephropathy. Kidney Int 71: 846-854.
31. Lin HH, Yang TP, Jiang ST, Yang HY, Tang MJ (1999) Bcl-2 overexpression prevents apoptosis-induced Madin-Darby canine kidney simple epithelial cyst formation. Kidney Int 55: 168-178.
32. Woo D (1995) Apoptosis and loss of renal tissue in polycystic kidney diseases. N Engl J Med 333: 18-25.
33. Hynes A GR, Srivastava S, Eley L, Whitehead J, Danilenko M, Raman S, Slaats GG, Colville JG, Ajzenberg H, Kroes HY, Thelwall PE, Simmons NL, Miles CG, Sayer JA (2014) Novel Joubert syndrome model reveals Hedgehog defects underlying nephronophthisis. Proc Natl Acad Sci U S A in press.
34. Schmid I, Uittenbogaart C, Jamieson BD (2007) Live-cell assay for detection of apoptosis by dual-laser flow cytometry using Hoechst 33342 and 7-amino-actinomycin D. Nat Protoc 2: 187-190.
35. Berghmans S, Murphey RD, Wienholds E, Neuberg D, Kutok JL, et al. (2005) tp53 mutant zebrafish develop malignant peripheral nerve sheath tumors. Proc Natl Acad Sci U S A 102: 407-412.

SUPPLEMENTAL FIGURES

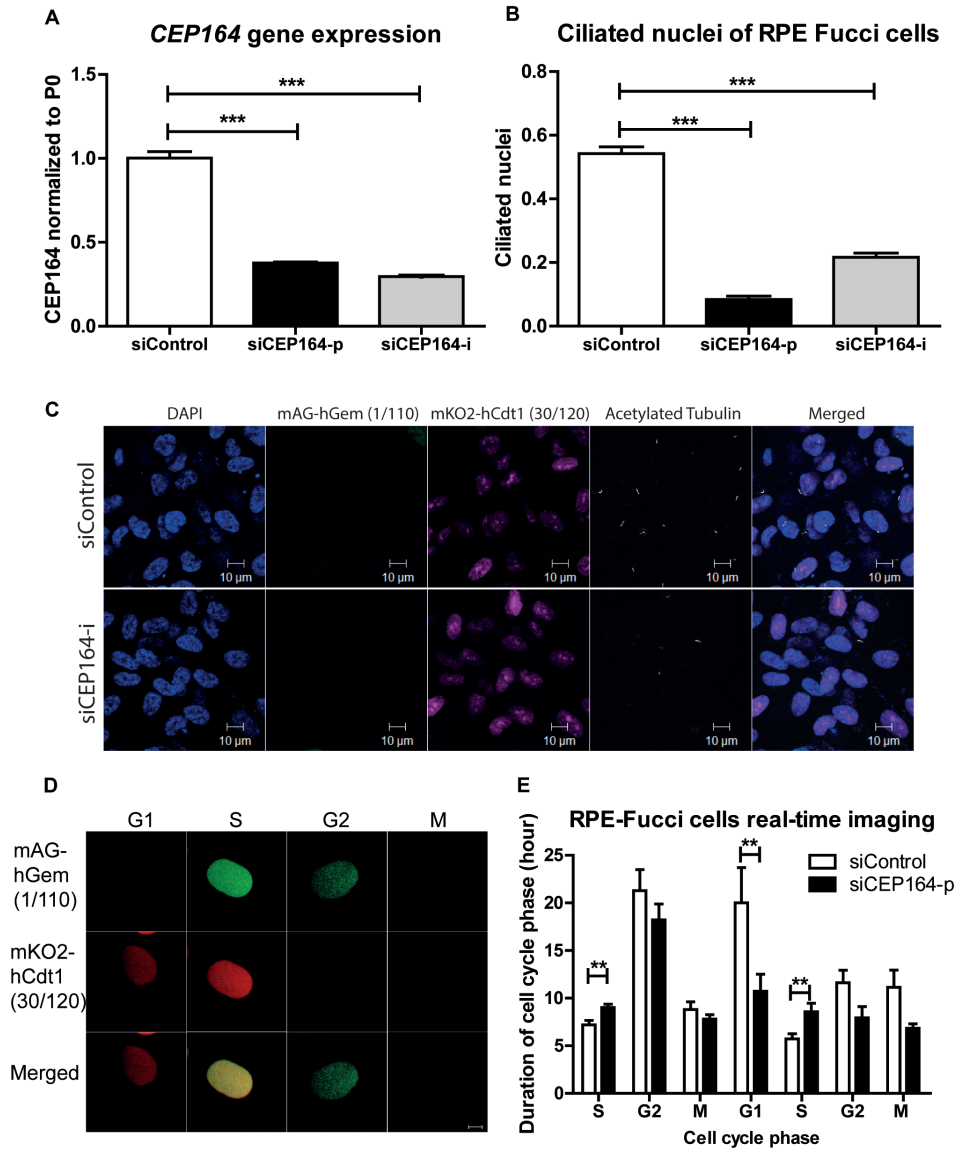

Figure S1. Validation of RPE-FUCCI cells and knockdown of human *CEP164*
(A) Relative *CEP164* gene expression levels as measured by RT-QPCR in RPE-FUCCI cells, normalized to *RPLP0*. Total RNA was isolated 48 hours after transfection with siControl or siCEP164-p or -i oligos. After 48 hour of transient transfection *CEP164* levels are significantly reduced (***p<0.001) (one-way ANOVA (Dunnett's post hoc)) (n=3, error bars represent SEM). (B) Depletion of CEP164 by siRNA causes a ciliary defect in RPE-FUCCI cells 55 hours after transfection, of which the last 30 hours are serum-starved (***p<0.0001). Nuclei and cilia were scored to generate ciliary frequencies. siCEP164 transfected cells manifest lower cilia frequencies (8-20%) compared to control transfected RPE FUCCI cells (50%). 300 cells

per condition were analyzed. Error bars represent SEM. (one-way ANOVA (Dunnett's post hoc)). (C) RPE-FUCCI cells have a primary cilium in G_1- and S-phase of the cell cycle, but not during G_2- or M-phase (see also Figure 1D). Cells were immunostained for acetylated tubulin (white) and DAPI stains nuclei (blue). Scale bar represents 10 µm. (D) Fluorescence images of RPE-FUCCI cells expressing mKO2-hCdt1(30/120) during G_1/early S-phase and mAG-hGem(1/110) constructs during the complete S-phase/G_2 phase of the cell cycle, as previously characterized [15]. Cells expressing both construct simultaneously appear yellow/orange, which we classify as early S-phase. Mitotic cells express neither of these constructs and are not fluorescent. Scale bar represents 5 µm. (E) RPE-FUCCI cells and their daughter cells after mitosis are followed during 72 hours after transfection. Duration of each cell cycle stage in siControl and si*CEP164* transfected cells was measured. S-phase took significantly longer in si*CEP164* transfected cells and their daughter cells compared to control (**$p<0.01$). G_1 phase was significantly shorter in si*CEP164* transfected cells compared to control (*$p<0.05$). G_2- ($p=0.06$) and M- ($p=0.06$) phase were almost significantly shorter in si*CEP164* transfected cells compared to control (>25 cells and their daughter cells per position (n=3) per experimental condition per experiment (n=3), error bars represent SEM).

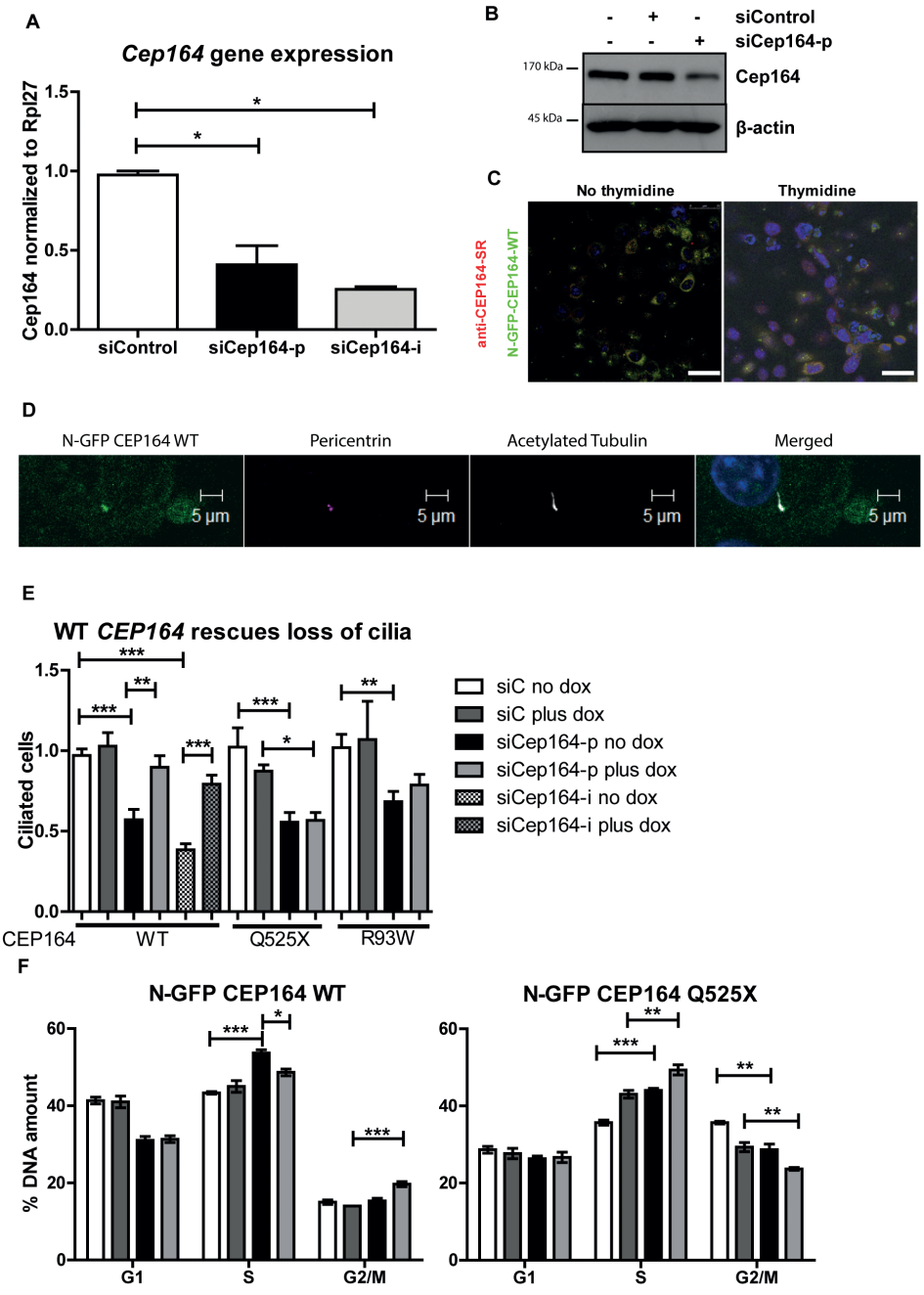

Figure S2. Validation of IMCD3 cells expressing *N-GFP- CEP164* alleles and knockdown of mouse *Cep164*

(A) *Cep164* mRNA expression 48 hour after siRNA transfection normalized to *RPL27*. (*p<0.05) One-way ANOVA, Dunnett's multiple comparisons test (n=3, error bars represent SEM). (B) Western blot of IMCD3 cells transfected with siCep164-p with β-actin as loading control to quantify protein levels after

knockdown. (C) Clonally doxycycline (Dox)-inducible IMCD3 cell line expressing human *N-GFP-CEP164-WT* was treated with doxycycline (10 ng/mL) during the double thymidine block (2 mM). Cells were fixed and stained with CEP164-SR antibody to observe colocalization. Distinct centrosomal localization of N-GFP-CEP164-WT (green), in the presence or absence of thymidine was observed when costained with CEP164-SR antibody (red). Scale bars represent 25 µm. (D) Induction of *N-GFP-CEP164* wild-type allele in IMCD3 cells with doxycycline results in expression of GFP-tagged CEP164 at the base ot he cilium as shown by immunofluorescence. Centrosomes were stained with Pericentrin (magenta) and cilia with Acetylated Tubulin (white). (E) Functional testing of *CEP164* alleles shows rescue of ciliation after knockdown of mouse *Cep164* after induction of wild-type human *CEP164* (**p<0.01) but not mutants (Q525X and R93W). Ciliary frequency was quantified from IMCD3 cells with stable *CEP164* constructs transfected with siCtrl (white) or si*Cep164* (black) and normalized to siCtrl. Transient knockdown results in significant loss of ciliation (***p<0.001). (>250 cells scored per condition, error bars represent SEM.). P-values were calculated using two-way ANOVA and Bonferroni multiple comparison test. (F) Endogenous *Cep164* knockdown in a non-clonally selected IMCD3 cell line leads to a block in S-phase under thymidine-induced synchronization and is rescued by inducible human wild-type *CEP164* (*p<0.05) but not by human mutant Q525X. After transfection with either control or *Cep164* siRNA cells were released from second thymidine block for 6 hrs. In addition, overexpression of the human truncating mutant *N-GFP-CEP164-Q525X* (dark grey) leads to block in S-phase, indicating a dominant negative effect of the human truncating mutant . P-values were calculated using two-way ANOVA and Bonferroni multiple comparison test.

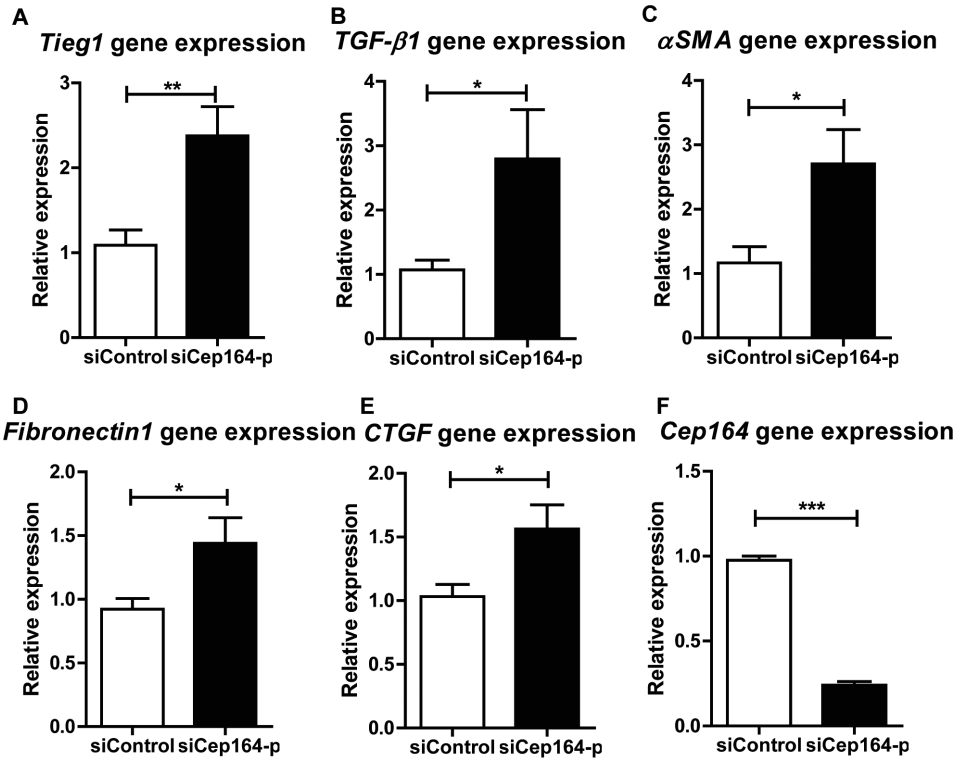

Figure S3. Expression levels of fibrosis markers in IMCD3 cells
(A-F) Relative gene expression levels of *Tieg1* (A), *TGFβ1* (B), α*Sma* (C), *Fibronectin1* (D), *CTGF* (E) and *Cep164 (F)* as measured by RT-QPCR in IMCD3 cells, normalized to *RPL27*. Total RNA was isolated 6 days after transfection with siControl or siCep164-p oligos (A) After 6 days of transient transfection (two rounds) *Tieg1* mRNA levels are significantly (**p<0.01) increased. (B) After 6 days and two rounds of siRNA transfection,

TGFβ1 mRNA levels are significantly (*p<0.05) increased, (C) After 6 days of transient transfection α*Sma* mRNA levels are significantly (*p<0.05) increased. (D) After 6 days of transient transfection *Fibronectin1* mRNA levels are significantly (*p<0.05) increased. (E) After 6 days of transient transfection *CTGF* mRNA levels are significantly (*p<0.05) increased. (F) After 6 days of transient transfection *Cep164* mRNA levels are significantly (***p<0.001) decreased (n=4, error bars represent SEM).

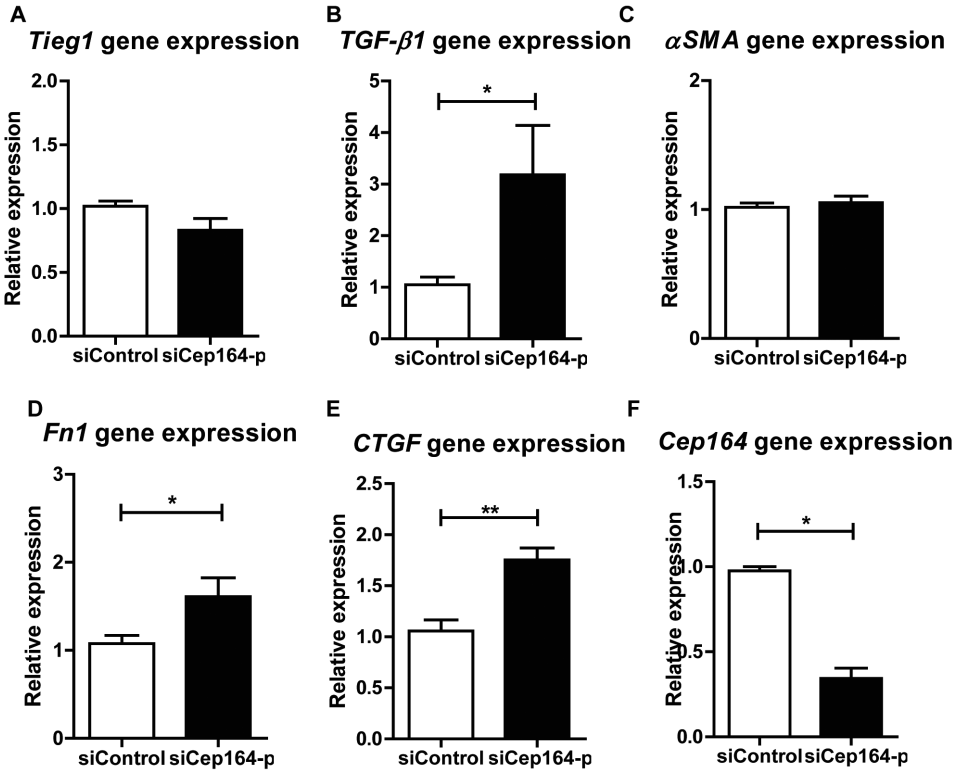

Figure S4. Expression levels of fibrosis markers in MEFs
(A-F) Relative gene expression levels of *Tieg1* (A), *TGFβ1* (B), α*Sma* (C), *Fibronectin1* (D), *CTGF* (E) and *Cep164 (F)* as measured by RT-QPCR in MEFs, normalized to *RPL27*. Total RNA was 6 days and after two rounds of siRNA transfection with siControl or siCep164-p oligos (A) After 6 days *Tieg1* mRNA levels are not changed (B) After 6 days of transient transfection *TGFβ1* mRNA levels are significantly (*p<0.05) increased. (C) After 6 days α*Sma* mRNA levels are not changed (D) After 6 days of transient transfection *Fibronectin1* mRNA levels are significantly (*p<0.05) increased. (E) After 6 days of transient transfection *CTGF* mRNA levels are significantly (**p<0.01) increased. (F) After 6 days of transient transfection *Cep164* mRNA levels are significantly (*p<0.05) decreased. (n=3, error bars represent SEM).

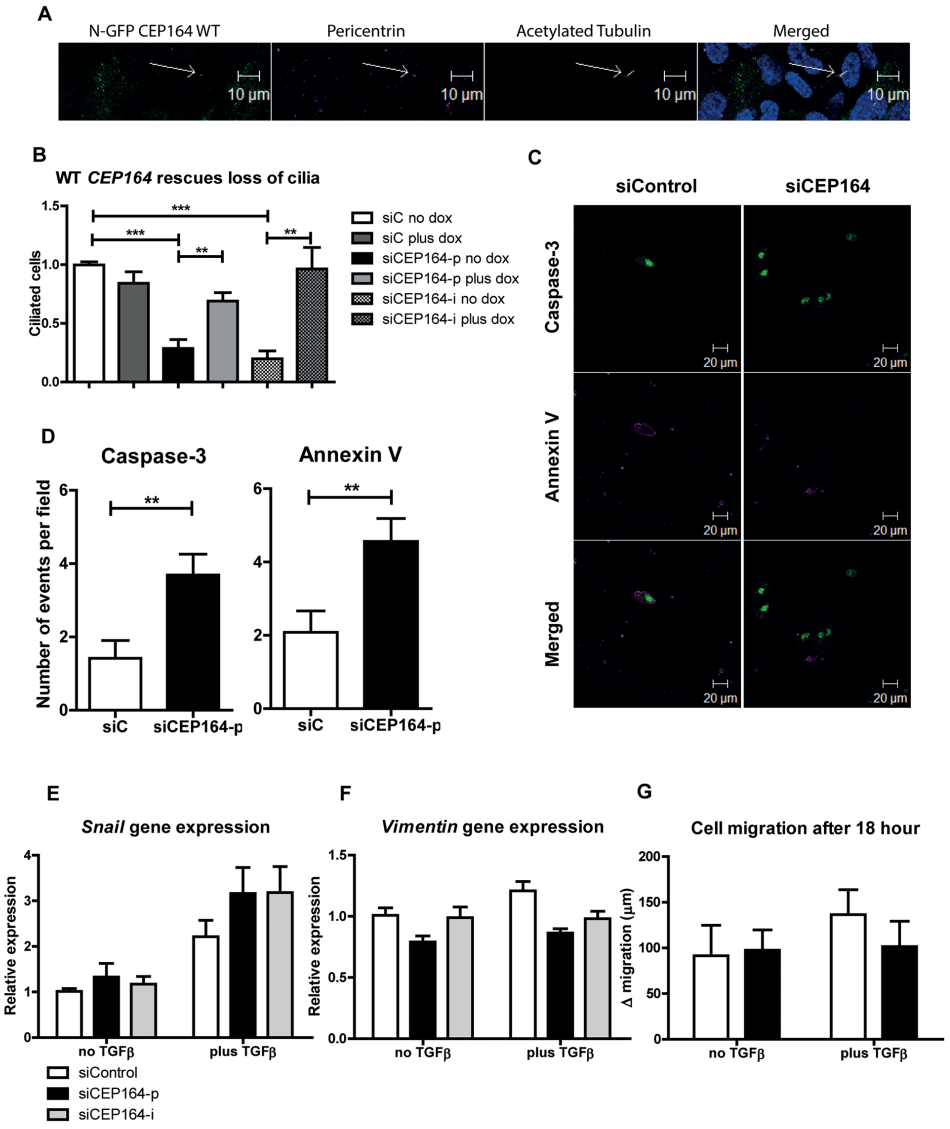

Figure S5. Validation of RPE cells expressing *N-GFP- CEP164* alleles and quantification of apoptosis and EMT

(A) Induction of *N-GFP-CEP164* wild-type allele in RPE cells with doxycycline results in expression of GFP-tagged CEP164 at the base of the cilium as shown by immunofluorescence. Centrosomes were stained with pericentrin (magenta) and cilia with acetylated tubulin (white). (B) Functional testing of *CEP164* alleles shows rescue of ciliation after knockdown of endogenous *CEP164* after induction of wild-type human *CEP164* (**p<0.01). Ciliary frequency was quantified from RPE cells with stable *CEP164* constructs transfected with siCtrl (white) or si*CEP164-p* (black) *or siCEP164-i* (patterned) and normalized to siCtrl. Transient knockdown results in significant loss of ciliation (***p<0.001). (>250 cells scored per condition, error bars represent SEM.). P-values were calculated using two-way ANOVA and Bonferroni multiple comparison test. (C) Immunofluorescence imaging of Annexin V (magenta) and Caspase-3 substrate (green) using NucView dual apoptosis assay for live cells. RPE cells were stained 16 hours after knockdown. More

apoptosis is observed after knockdown of *CEP164* compared to control. Scale bar represents 50 µm. (D) Five fields per condition were quantified for Caspase-3 and Annexin V, student's t-test was used to calculate difference between siControl of siCEP164-p transfected samples (**p<0.01; n=3, SEM). (E) Relative gene expression levels of *Snail* as measured by RT-QPCR in RPE cells, normalized to *RPLP0*. Total RNA was isolated 6 days after transfection with siControl, siCEP164-i or siCEP164-p oligos (p=NS, n=3, SEM), (F) Relative gene expression levels of *Vimentin* as measured by RT-QPCR in RPE cells, normalized to *RPLP0*. Total RNA was isolated 6 days after transfection with siControl, siCEP164-i or siCEP164-p oligos (p=NS, n=3, SEM), (G) Quantification of absolute distance (µm) of cell migration after 18 hours after a scratch. RPE *CEP164* depleted cells do not migrate more than siControl cells 48 hour after transfection. TGFβ incubation (5 ng/mL) in serum-free medium did not enhance this effect (n=3, error bars represent SEM). P-values were calculated using two-way ANOVA and Bonferroni multiple comparison test.

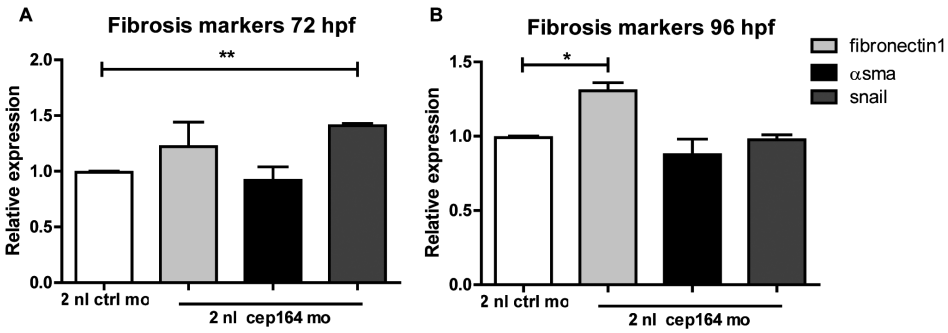

Figure S6. Induction of profibrotic gene expression in zebrafish
mRNA expression from 12 pooled embryos is normalized to 2 nL control MO injected zebrafish. (A) RT-QPCR reveals significant induction of *snail* in cep164 MO injected embryos at 72hpf. (B) RT-QPCR reveals significant induction of *fibronectin1* in cep164 MO injected embryos at 96hpf. Student's t-test was used to calculate p-values (*<0.05, **<0.01).

SUPPLEMENTAL MOVIES

Movie S1. Real time imaging of cell cycle progression in control transfected RPE-FUCCI cells
Representative movie of RPE-FUCCI cells transiently transfected with siControl oligos which are imaged for 3 days to examine cell cycle progression. http://syscilia.org/Giles/Supplemental_movie_1_RPE_FUCCI_siControl.mp4

Movie S2. Real time imaging of cell cycle progression in siCEP164 transfected RPE-FUCCI cells
Representative movie of RPE-FUCCI cells transiently transfected with siCEP164-p oligos which are imaged for 3 days to examine cell cycle progression. http://syscilia.org/Giles/Supplemental_movie_2_RPE_FUCCI_siCEP164.mp4

PART THREE

Future perspectives

CHAPTER 8

Nephronophthisis: should we target cysts or fibrosis?

Pediatr Nephrol., in press (2015)
(With permission of Springer Science+Business Media, doi: 10.1007/s00467-015-3162-y)

Gisela G. Slaats, Marc R. Lilien, Rachel H. Giles

ABSTRACT

Ciliopathy nephronophthisis (NPHP) is a common cause of end-stage renal disease (ESRD) in children and young adults, characterized by tubular basement membrane disintegration with irregular thickening and attenuation, interstitial fibrosis and tubular atrophy, and occasionally cortico-medullary cyst formation. Pharmacological approaches that delay the development of ESRD could potentially extend the window of therapeutic opportunity for this group of patients, generating time to find an appropriate donor or even new treatments to mature. This review provides an overview of compounds that have been tested to ameliorate kidney cysts and/or fibrosis. Furthermore, paclitaxel is revisited as a potential strategy to target fibrosis in NPHP. At low dosage it shows promising results in rodent models of renal fibrosis. Possible adverse events and safety of paclitaxel treatment in pediatric patients would need to be investigated, as well as efficacy, optimum dose and administration schedule for treatment of renal fibrosis in NPHP patients. Paclitaxel is an approved drug for human use with known pharmacokinetics, which could potentially be used in other ciliopathies, through targeting the microtubule skeleton.

Nephronophthisis

Familial juvenile nephronophthisis (NPHP; MIM 256100) was first described in 1951 (1) and is a leading genetic cause of kidney disease in children and young adults (2). During the last fifteen years, mutations in nineteen genes have been identified as causing NPHP, yet less than fifty percent of all NPHP cases can be diagnosed by these disease loci (3). The most common identified molecular cause of isolated NPHP is deletion or mutation of the *NPHP1* gene, accounting for approximately twenty percent of NPHP cases (3). NPHP gene products do not share sequence similarities, but they do all localize to the primary cilium-centrosome complex, linking renal cystic disease to primary cilia function (4). NPHP can also be a feature in other congenital syndromes, the "ciliopathies", such as Joubert syndrome (MIM 213300), Senior-Løken syndrome (MIM 266900), Bardet-Biedl syndrome (MIM 615993), Oro-facial-digital syndrome (MIM 311200) and Meckel-Gruber syndrome (MIM 249000), and presents variably with abnormalities of the retina, kidney, brain, bone and liver (5). The occurrence of NPHP is estimated to be from one in 50,000 - 900,000 (6), and the median age of NPHP diagnosis is ten years. The NPHP phenotype presents in three forms, depending on the time of onset of end-stage renal disease (ESRD): infantile, juvenile and adolescent. Patients develop ESRD approximately four years from the initial symptoms (7). The timespan between the first symptoms, diagnosis and ESRD is relatively short. Therefore it would be of great interest to extend the window of therapeutic opportunity. Currently, treatment options for NPHP patients are limited to symptomatic treatment of renal failure and include blood pressure control to delay disease progression and renal replacement therapy (RRT) for ESRD. Pediatric NPHP transplant recipients have excellent outcomes which have been shown to be better compared to the general pediatric transplant population (8). Donor kidneys usually function for around twenty years, and NPHP patients will likely require additional transplants (9). There are no drug-based therapies available to ameliorate disease progression in NPHP kidneys currently being used in the clinic. Pharmacological approaches that delay the development of ESRD could potentially extend the window of therapeutic opportunity for this group of patients, generating time to find an appropriate donor or even new treatments to mature.

Treating renal cysts?

During the last decade the focus of pharmacological intervention for NPHP has targeted renal cysts. This is partly because the field is driven by the knowledge we have from the proliferative phenotype of autosomal dominant polycystic kidney disease (ADPKD; MIM 173900). Like NPHP, ADPKD is classified as a ciliopathy as well; loss of cilia and cyst development are causally related (10). Ciliary dysfunction with consequent defective planar cell polarity affecting renal epithelial cells in the kidney is believed to be the fundamental etiology of cystogenesis in ADPKD (11). Research groups have investigated the use of several drugs to reduce renal cysts mostly in murine models of ADPKD. One group

of drugs tested consists of cyclin-dependent kinase inhibitors, which have been shown to ameliorate cyst formation in *cpk* (human orthologue is *PKHD1*, a mouse model for polycystic kidney and hepatic disease, MIM 263200)*, jck* (*NEK8/NPHP9*, a NPHP mouse model) and *pkd1* (*PKD1,* an ADPKD mouse model) mice *in vivo* (12,13). The response in the different mouse models may be possibly attributable to the rescue of cilia by cyclin-dependent kinase inhibitors as observed *in vitro* (14). Similarly, mammalian target of rapamycin (mTOR) inhibitors reverse renal cystogenesis in a rodent model of ADPKD, by decreasing proliferation (15). Inducing cellular calcium release by triptolide treatment in kidney-specific *Pkd1* depletion in mice also retarded cystic kidney disease (16). The proto-oncogene *c-myc* is overexpressed in PKD cystic tissue, and antisense oligonucleotide treatment targeting c-myc was shown to inhibit the cyst progression in *cpk* mice (17). Curcumin is shown to inhibit cystogenesis in a murine *Pkd1*-deletion model, possibly by inhibiting pathways upregulated in ADPKD, e.g. the transcription factors activator protein-1, nuclear factor-κβ (NF-κB), Wnt/β-catenin signaling, TNF-α, MAPKs, early growth response gene-1, hypoxia inducible factor-1, notch-1, and also the mTOR-regulated signaling (18). Furthermore, ginkgolide B inhibits cyst formation and enlargement in a PKD mouse model by inducing cyst cell differentiation and altering the Ras/MAPK signaling pathway to inhibit abnormal proliferation in cyst cells (19). Trichostatin A, a pan-histone deacetylase (HDAC) inhibitor, and valproic acid, a class I HDAC inhibitor, were identified as compounds that inhibited cyst formation in zebrafish injected with morpholinos reducing levels of *pkd2* (20). Finally, short-term effects in a clinical trial of ADPKD patients suggest that patients with low GFRs might benefit from treatment with the vasopressin V_2 receptor antagonist tolvaptan (21,22). A follow-up of 36 months of tolvaptan treatment of ADPKD patients revealed reduced total kidney volume growth and reduced rate of kidney tissue decline, providing a potential effective therapy (23).

Or targeting renal fibrosis?

ADPKD is a relatively common disease always characterized by cysts. However, NPHP patients are rare and the disease usually leads to ESRD in childhood. Moreover, many, if not most NPHP patients do not have renal cysts, and this observation is confirmed in NPHP mouse models as well (24) (Figure 1). A prominent feature of NPHP is renal fibrosis, characterized by thickening of tubular basement membranes, tubular atrophy and interstitial inflammation. The rapid development of ESRD after detection of the disease suggests it is the result of an active process, rather than just due to an uninhibited attempt to repair damage (25). Furthermore, there are questions about the etiology of ADPKD versus NPHP that would explain the balance between cysts versus fibrosis in each disease. Recent data suggest that DNA damage signalling upstream of or concomitant with ciliary dysfunction underlies NPHP (26). One could argue whether targeting renal cysts is actually the right approach in the clinic for NPHP. We propose that ameliorating fibrosis would be at least

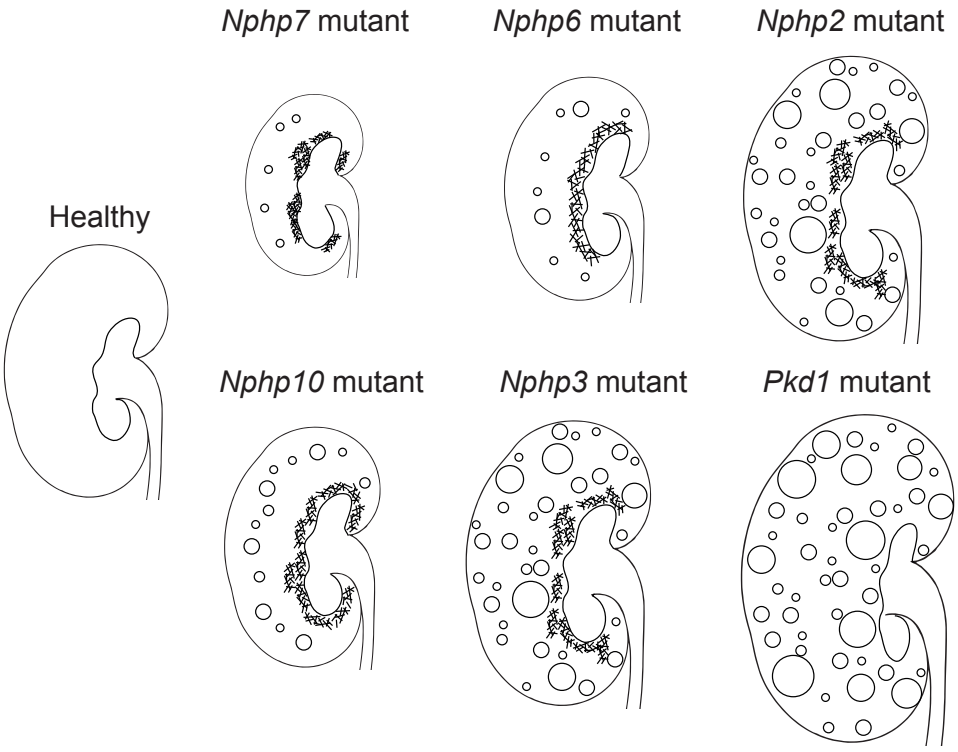

Figure 1. Different mouse kidney models for renal cysts and fibrosis
Schematic overview of renal degeneration of *Nphp7* (*Glis2*), *Nphp6* (*Cep290*), *Nphp3* (*pcy*), *Nphp2* (*Inv*), *Nphp10* (*Sdccag8*) and *Pkd1* mutant mice, which are characterized by varying levels of interstitial fibrosis and renal cysts when compared to healthy kidneys. *Nphp7*, *Nphp6* and *Nphp10* mutant mice kidneys are smaller, which display more fibrosis and do not display excessive cyst development. The more cystic models, e.g. *Nphp2* and *Nphp3*, show enlarged kidneys, like *Pkd1* mutant kidneys.

an equally relevant approach when designing therapeutic intervention of renal failure in NPHP. Fibrosis ultimately leads to irreversible renal damage; however, the underlying molecular mechanisms are targetable and potentially reversible. While targeting the cystic disease in ADPKD is easily justifiable, we argue that in NPHP targeting fibrosis is more relevant.

Fibrosis development is multi-facetted and the underlying mechanism is a complex cross-talk of signalling pathways, including inflammatory responses. The principal effector cells of fibrosis are myofibroblasts, which excessively deposit extracellular matrix (27). Myofibroblasts can be derived from different cell sources, including epithelial or endothelial cells (28). Tubulointerstitial fibrosis is characterized by increased epithelial-to-mesenchymal transition (EMT) (29), which can be induced by transforming growth factor beta (TGF-β) (30). It has been shown that children with NPHP have increased urinary secretion of TGF-β, and their TGF-β excretion was among the highest in groups with different etiolo-

gies for pediatric ESRD (31). Targeting the key fibrosis-promoting molecule TGF-β (32) is one possible strategy to treat fibrosis. By using antisense TGF-β oligodeoxynucleotides, researchers were able to block interstitial fibrosis in unilateral ureteral obstruction (UUO) animal model (33). Amongst other signals, angiotensin II upregulates TGF-β expression. Angiotensin converting enzyme inhibitors (ACEi) and angiotensin II receptor blockers (ARB) are used extensively in various renal diseases to prevent progression of fibrosis by inhibiting proteinuria (34,35) and have been proven to be safe in children (36). Blocking angiotensin production by ACEi or ARB leads to increased expression of renin. Increased levels of renin may partly offset the downregulation of TGF-β production by ACEi and ARB, given that TGF-β expression is upregulated by angiotensin-independent signaling of renin to the (pro)renin receptor. Therefore, combined interventions aimed at key regulators of TGF-β expression might be more effective approaches (37).

Fibrosis signalling involves connective tissue growth factor (CTGF), epidermal growth factor (EGF) and platelet-derived growth factor (PGDF) and their receptors as well, making them likewise targets for intervention of fibrosis. Targeting CTGF, EGF and PDGF pathways in renal disease progression has been extensively reviewed recently (38,39). CTGF reduction by antisense treatment in 7-day UUO mouse model ameliorates fibrosis (40) and antibody FG-3019 targeting CTGF in 14-day UUO mice reduces matrix deposition (41). Molecular inhibition of EGF by Gefitinib (42) and Erlotinib (43) similarly reduces fibrosis. A knockout mouse model of the EGF receptor reduces interstitial fibrosis after kidney injury (43). Inhibition of PDGF by Imatinib (44) and Trapidil (45), as well as PDGF targeting by antibody and *Pdgf* gene knockout reduce renal interstitial fibrosis (46). In addition, a selective p38 mitogen-activated protein kinase (MAPK) inhibitor FR167653 and extracellular signal-regulated protein kinase kinase (MEK) inhibitor decreased the degree of renal fibrosis in a *Nphp2* mouse model, although it did not extend the overall life span (47). Collectively these studies support possible medical intervention of fibrotic pathways in the treatment of injury-related as well as nephronophthisis-related renal fibrosis.

To date, researchers have no idea what the role of mutations affecting primary cilia function (e.g. NPHP) might be in fibrosis initiation or progression. Downstream ciliary signalling, or signalling of cilia proteins with extra-ciliary functions could play a role in fibrosis. Recent reports describe a link with replication stress and enhanced DNA damage response (DDR) signaling and NPHP. This suggests that replication stress and DDR could be a underlying mechanism of NPHP development (14,26,48-50). Increased cyclin-dependent kinase (CDK) activity causing replication stress and DDR can be rescued by a CDK1/2 inhibitor (14), however, whether CDK inhibition can rescue fibrosis remains to be investigated. One study showed that the cilium is lost during EMT, nevertheless, it is required for the initiation of the transition (51). In the pro-fibrotic tissue environment EMT and cilium loss are thought to require two triggers: (1) disassembly of cellular contacts and (2) TGF-β exposure (51). Molecular mechanisms of EMT are reviewed by Lamouille and collegues,

and cilia-signalling ligands such as canonical Wnt, Hh and Notch signalling are also listed as potential regulators of EMT. Furthermore, crosstalk between pathways (enhanced in cilia) regulating EMT will accelerate the transition (52). Interestingly, HDAC inhibitors ameliorate fibrosis via TGF-β suppression in models of diabetic nephropathy (DN), focal segmental glomerulosclerosis (FSGS) and tubulointerstitial injury (53-55). These same HDAC inhibitors rescue primary cilia by inhibiting ciliary resorption (56); however, no direct link of cilia to DN, FSGS or tubulointerstitial injury has been described. Applications of HDAC inhibitors in kidney disease are reviewed by Brilli et al. (57). In conclusion, while HDAC inhibitors may stabilize renal cilia as well as suppress fibrosis, this promising approach has not been intensively tested in humans, let alone children, and may be a long way off from testing in NPHP patients.

The key fibrosis molecule TGF-β activates fibrotic signalling when TGF-β/Smad signaling is upregulated in the nucleus after destabilization of microtubules (58). Smad proteins cannot enter the nucleus while bound to microtubules; therefore it follows that pro-fibrotic gene transcription will be blocked by stabilizing microtubules (Figure 2) (58). The ciliary axoneme requires stabilized microtubules to avoid resorption as well, and taxol/paclitaxel treatment facilitates α-tubulin acetylation and consequent stabilization (59). Microtubule-stabilizing agents could be the common denominator in treating both cysts and fibrosis. Interestingly, paclitaxel has been examined in several cystic and fibrotic rodent models (Tables 1-2).

Reviving paclitaxel?

One possibly interesting approach to revisit with regard to NPHP patients is paclitaxel (taxol), which is derived from the bark of the Pacific yew tree. Originally, paclitaxel was discovered in the U.S. in 1971 and is used in cancer chemotherapy (60). Paclitaxel and comparable tubulin-active taxane analogues stabilize GDP-bound tubulin in microtubules, inhibit depolymerization, alter the normal equilibrium between tubulin dimers and microtubules, and promote cells to accumulate in G_0 or mitosis and consequently undergo apoptosis if used at higher dosages (Figure 2) (61,62). There is limited clinical experience with short-term use of taxanes in pediatric oncology (63). Three phase I clinical trials using taxanes to treat refractory solid tumors are reported (64,65), and one phase II trial studied recurrent solid tumors (66). The phase I trials determined the maximum tolerable dose as being 350 mg/m^2/day; the (dose-limiting) toxicities included neutropenia (64), acute neurotoxicities (transient coma, somnolence, agitation), as well as delayed neurotoxicities (paraesthesia, dysaesthesia, excitation, headache, and ileus) (65). Additional pulmonary, dermatologic, and infectious side effects as well as edema were significant.

Paclitaxel and related taxanes have the ability to promote microtubule assembly (61), which is shown to inhibit progression of polycystic kidney disease (67). From different studies (Table 1) we can conclude that paclitaxel has limited effectiveness as a therapeutic

agent in the treatment of slowly progressing cystic kidneys, but rapidly progressive forms of PKD in rodent models benefit from paclitaxel (68). Treating NPHP with high-dose of paclitaxel would cause cell death, and potentially worsen interstitial fibrosis and overall renal function. However, low-dose taxol ameliorates renal fibrosis *in vivo* (Table 2) (69,70). Low-dose paclitaxel was found to be more renal-protective than taurine in unilateral ureteral obstruction (UUO) rats (70). In addition, paclitaxel blocks Toll-like receptor 4 (TLR-4), and thereby inhibits inflammation (Figure 2) (71), which significantly contributes to fibrotic signaling (25). TLR-4 is present on renal epithelial cells, including cells of the proximal tubule and collecting ducts. CD14 is expressed at high levels in macrophages and monocytes, and low levels in nonmyeloid cells, including cells of the kidney and liver, where it is membrane bound through glycosyl phosphatidylinositol linkage. Normally, CD14 facilitates the binding of lipopolysaccharides (LPSs) to TLR-4 to stimulate the innate immune response.

Table 1. Paclitaxel studies in rodent models of cystic kidney disease

Rodent model	Human ortholog	Dose paclitaxel	Observed effect	Ref.
C57BL/6J-c*pk/cpk* mice	*PKHD1*	150 µg/wk (max 28 wks)	Prolonged survival with 170 days, minimal loss of renal function, limited collecting-duct cyst enlargement, attain adult size	(95)
C57BL/6J-c*pk/cpk* mice	*PKHD1*	50 µg/every other wk (max 17 wks)	Increased survival, fewer/smaller cysts, more (hypertrophied) nephrons and fibrosis	(67)
C57BL/6J-c*pk/cpk* mice	*PKHD1*	150 µg/wk (max 8 wks)	Prolonged survival >40 days, decreased relative kidney weight, increased interstitial fibrosis	(68)
Orpk mice	*IFT88*	10 µg/g body weight/wk (~200 µg/wk) (7 wks)	No effect on PKD progression	(96)
DBA/2FG-*pcy/pcy* mice	*NPHP3*	100 to 150 µg/wk (9-11 wks)	No effect on increased kidney weight or serum urea nitrogen level, premature death	(68)
Han:SPRD-*Cy/Cy* 7-10d old rats	*PKDR1*	0.15 to 15 mg/kg/wk (~1.5-150 µg/wk for max 1.5 wks)	Severe side effects, premature death	(68)
Han:SPRD-*Cy/+* male rats	*PKDR1*	7, 15, or 27 mg/kg/wk (~438, 3750, 6750 µg/wk for 6 wks)	Inconsistent effect on relative kidney weight, no effect on serum urea nitrogen concentration, increased mortality at higher dosages	(68)

Table 2. Paclitaxel studies in rodent models of renal fibrosis

Rodent model	Dose paclitaxel	Observed effect	Ref.
UUO[1] Wistar rats	2xwk 0.3 mg/kg (~90 µg 2xwk for 1 or 2 wks)	Ameliorate renal tubulointerstitial fibrosis	(69)
UUO[1] rats	2x wk 0.3 mg/kg (~48 µg 2xwk for 4 wks)	Preservation of nephrons, 53% less necrosis and fibrosis, longer renal tubules	(70)
5/6 nephrectomy of male Wistar rats	2xwk 0.3 mg/kg (~90 µg 2xwk for 8 wks)	Reduced progression of glomerular injury and interstitial fibrosis, improved kidney function	(97)

[1]Unilateral ureteral obstruction (UUO)

However, TLR-4 signaling can also be activated by interaction with extracellular matrix (ECM) degradation products. In PKD, there is an upregulation of CD14 expression and increased levels of the proteolytically shed CD14 variant, indicative of immunological activation or cell injury. Consequently, the renal tubule-derived CD14 could activate TLR-4 signaling either locally or in more distal segments of the nephron, long before the infiltration of inflammatory cells. Additionally, proteolytically shed CD14 is found in the urine of both recessive PKD and autosomal dominant PKD (ADPKD) patients, where, in the case of male ADPKD patients, the levels correlate with kidney volume. Thus, CD14 could be a potential biomarker for the early progression of PKD (72).

Ciliary architecture and function closely rely on the microtubule (MT) cytoskeleton. Loss of NPHP protein function causes disturbance of microtubule organizing centers (MTOCs) at the centrosomes, so subsequently this might lead to defective cilia, mitotic spindles and transport. Taxol treatment leads to suppressed tubule dynamics, which blocks ciliary absorption before entering the cell cycle, and blocking of TGF-β expression (Figure 2) (58,73). Intracellular transport of ECM proteins like matrix metalloproteinase-9 along stabilized microtubules is decreased by paclitaxel (74). There are many factors which could play a role in inhibiting fibrosis by blocking MT dynamics. MTs are involved in many cellular processes including cilium formation, maintenance of cell polarity, intracellular transport, mitosis, differentiation and migration (75-77). By inhibiting MT dynamics one could possibly evade pathological processes such as hyperproliferation, TGF-β expression, epithelial-to-mesenchymal transition (Figure 2) and senescence, all of which contribute to renal fibrosis. There is only limited clinical experience with taxanes in pediatric oncology, and as administration of these drugs for the prevention of fibrosis in patients with NPHP would require an extensive timeframe, possible damaging effects of long-term use of these antimitotic agents on growth and development should be considered.

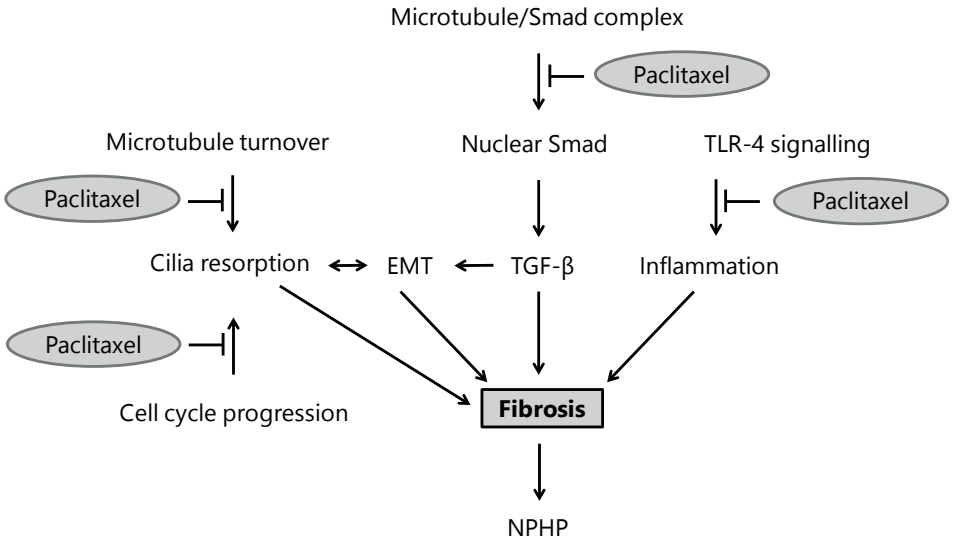

Figure 2. Paclitaxel inhibits renal fibrosis by interfering with several pathophysiological routes in NPHP
Paclitaxel blocks Toll-like receptor 4 (TLR-4) and thereby inhibits inflammation. Furthermore, paclitaxel stabilizes microtubules, and prevents Smad signalling in the nucleus, which in turn, upregulates transforming growth factor beta (TGF-β) transcription. TGF-β subsequently induces epithelial-to-mesenchymal transition (EMT), contributing to tubulointerstitial fibrosis. In addition, inhibiting microtubule turnover by paclitaxel will prevent cilia resorption. Finally, paclitaxel arrests the cell cycle which prevents cilia resorption as well. Loss of cilia is linked to EMT, moreover, loss of cilia and its downstream signalling are involved in regulating nephronophthisis (NPHP). All four pathways which are targeted by paclitaxel contribute to fibrosis development which leads to the clinical phenotype NPHP

Two birds with one stone: targeting both cysts and fibrosis

NPHP as well as ADPKD patients would benefit most from interventions reducing both renal cysts and fibrosis. Calcimimetic R-568 and octreotide normalize intracellular calcium and cyclic adenosine monophosphate (cAMP) levels and inhibited the progression of renal cysts. Treatment inhibits the development of renal fibrosis equally well in *pcy* mice and pck rats (orthologous to *NPHP3* and *PKHD1*/fibrocystin respectively) (78,79). In a randomized clinical trial, the long-acting somatostatin analog octreotide has been reported to slow down disease progression in patients with polycystic kidney and liver disease (80). Secondly, rapamycin (mTOR inhibitor) reduced cyst enlargement and fibrosis in *pcy* mice during late-stage treatment and ameliorated renal function (81). In addition, a 10 nM rapamycin treatment of zebrafish injected with *nphp2* (*INVS*) and *nphp6* (*CEP290*) morpholinos reduced an increase of kidney size significantly (82). Furthermore, rapamycin-loaded microspheres inhibited local fibrotic response in UUO mice by inhibiting mTOR activity (83). mTOR inhibitors were also tested in several large-scale clinical trials. Disappointingly, in humans with ADPKD, different rapamycin and everolimus dosages have not revealed a clear-cut benefit regarding the total kidney volume or GFR (84-88). The potential effects

of mTOR inhibitors in ADPKD patients remain to be determined. However, in a retrospective study of patients with ADPKD who had been transplanted with rapamycin as an immunosuppressant, their native kidneys showed reduced size of the cysts (89). Folate conjugation of rapamycin inhibited mTOR activity exclusively in the kidneys of PKD mice, suggesting renal efficacy and decreased side effects when applied to ADPKD patients (90). Everolimus, an orally available single agent mTOR inhibitor, is already in use for treatment of subependymal giant astrocytomas in children with tuberous sclerosis complex (91). Finally, vasopressin receptor antagonist OPC-31260 and tolvaptan ameliorate fibrosis and cystogenesis in pck rats and *pcy* mice (92,93). The vasopressin receptor antagonist clinical trials for humans with ADPKD have reported beneficial effects on renal cysts, but did not include analysis of renal fibrosis.

Concluding remarks

Unfortunately, treatment options for NPHP patients are limited; however there may be possibilities to extend the window of therapeutic opportunity for these juvenile patients. Understanding how fibrosis is initiated and propagated upon functional loss of NPHP (and to a lesser extent ADPKD) gene products needs to be further elucidated. It is also entirely unclear whether pro-fibrotic cellular changes are a consequence of ciliary function or whether they are a response to extraciliary functions of these gene products. We propose paclitaxel as a potential therapeutic for NPHP, nevertheless the appropriate timing and dosage of paclitaxel are currently unknown. It would be very interesting to investigate low-dose paclitaxel administration in an early stage of a NPHP animal model such as *Cep290* gene trap mice (94) to establish efficacy in delaying renal failure.

Assuming NPHP symptoms are not fully reversible, the extensive cystic and fibrotic kidney animal model data showing benefits of low-dose paclitaxel treatment, coupled with the fact that paclitaxel is an approved drug for human use with known pharmacokinetics, may warrant an exploratory phase II trial in NPHP patients with low-dose paclitaxel treatment soon after first symptoms or diagnosis with a primary endpoint of time to progression of renal end-stage disease. Possible adverse events upon paclitaxel treatment in pediatric patients would need to be investigated. Research will determine efficacy, optimum dose and administration schedule for renal fibrosis treatment in children and young adults with NPHP.

Complimentarily, treating other ciliopathies with low-dose microtubule stabilizing agents as paclitaxel and HDAC inhibitors should be explored, since these drugs also stabilize microtubules in the cilium. Several lines of evidence suggest stabilizing MTs and the cilium show promising results *in vivo,* as discussed in this work. However, the window of opportunity to prevent rapid loss of renal function in ciliopathies will generally present in childhood. Therefore, the safety of these anti-proliferative drugs for the growing and developing child is a major issue that should be resolved before we can start offering this alternative to our NPHP patients.

Funding

This study was funded by the European Community's Seventh Framework Programme FP7/2009 under grant agreement no: 241955, SYSCILIA, and the Dutch Kidney Foundation Consortium CP11.18 "KOUNCIL".

REFERENCES

1. Fanconi G, Hanhart E, von AA, Uhlinger E, Dolivo G, Prader A. [Familial, juvenile nephronophthisis (idiopathic parenchymal contracted kidney)]. *Helvetica paediatrica acta.* 1951;6(1):1-49.
2. Hildebrandt F, Zhou W. Nephronophthisis-associated ciliopathies. *Journal of the American Society of Nephrology : JASN.* 2007;18(6):1855-1871.
3. Otto EA, Ramaswami G, Janssen S, et al. Mutation analysis of 18 nephronophthisis associated ciliopathy disease genes using a DNA pooling and next generation sequencing strategy. *J. Med. Genet.* 2011;48(2):105-116.
4. Sang L, Miller JJ, Corbit KC, et al. Mapping the NPHP-JBTS-MKS protein network reveals ciliopathy disease genes and pathways. *Cell.* 2011;145(4):513-528.
5. Hildebrandt F, Benzing T, Katsanis N. Ciliopathies. *The New England journal of medicine.* 2011;364(16):1533-1543.
6. Ala-Mello S, Koskimies O, Rapola J, Kaariainen H. Nephronophthisis in Finland: epidemiology and comparison of genetically classified subgroups. *European journal of human genetics : EJHG.* 1999;7(2):205-211.
7. Hildebrandt F, Waldherr R, Kutt R, Brandis M. The nephronophthisis complex: clinical and genetic aspects. *The Clinical investigator.* 1992;70(9):802-808.
8. Hamiwka LA, Midgley JP, Wade AW, Martz KL, Grisaru S. Outcomes of kidney transplantation in children with nephronophthisis: an analysis of the North American Pediatric Renal Trials and Collaborative Studies (NAPRTCS) Registry. *Pediatric transplantation.* 2008;12(8):878-882.
9. Groothoff JW, Cransberg K, Offringa M, et al. Long-term follow-up of renal transplantation in children: a Dutch cohort study. *Transplantation.* 2004;78(3):453-460.
10. Pan J, Seeger-Nukpezah T, Golemis EA. The role of the cilium in normal and abnormal cell cycles: emphasis on renal cystic pathologies. *Cellular and molecular life sciences : CMLS.* 2013;70(11):1849-1874.
11. Fischer E, Legue E, Doyen A, et al. Defective planar cell polarity in polycystic kidney disease. *Nature genetics.* 2006;38(1):21-23.
12. Bukanov NO, Smith LA, Klinger KW, Ledbetter SR, Ibraghimov-Beskrovnaya O. Long-lasting arrest of murine polycystic kidney disease with CDK inhibitor roscovitine. *Nature.* 2006;444(7121):949-952.
13. Bukanov NO, Moreno SE, Natoli TA, et al. CDK inhibitors R-roscovitine and S-CR8 effectively block renal and hepatic cystogenesis in an orthologous model of ADPKD. *Cell cycle.* 2012;11(21):4040-4046.
14. Choi HJ, Lin JR, Vannier JB, et al. NEK8 links the ATR-regulated replication stress response and S phase CDK activity to renal ciliopathies. *Mol. Cell.* 2013;51(4):423-439.
15. Ravichandran K, Zafar I, Ozkok A, Edelstein CL. An mTOR kinase inhibitor slows disease progression in a rat model of polycystic kidney disease. *Nephrology, dialysis, transplantation : official publication of the European Dialysis and Transplant Association - European Renal Association.* 2015;30(1):45-53.
16. Leuenroth SJ, Bencivenga N, Igarashi P, Somlo S, Crews CM. Triptolide reduces cystogenesis in a model of ADPKD. *Journal of the American Society of Nephrology : JASN.* 2008;19(9):1659-1662.
17. Ricker JL, Mata JE, Iversen PL, Gattone VH. c-myc antisense oligonucleotide treatment ameliorates murine ARPKD. *Kidney international.* 2002;61(1 Suppl):S125-131.
18. Leonhard WN, van der Wal A, Novalic Z, et al. Curcumin inhibits cystogenesis by simultaneous interference of multiple signaling pathways: in vivo evidence from a Pkd1-deletion model. *American journal of physiology. Renal physiology.* 2011;300(5):F1193-1202.
19. Zhou H, Gao J, Zhou L, et al. Ginkgolide B inhibits renal cyst development in in vitro and in vivo cyst models. *American journal of physiology. Renal physiology.* 2012;302(10):F1234-1242.
20. Cao Y, Semanchik N, Lee SH, et al. Chemical modifier screen identifies HDAC inhibitors as suppressors of PKD models. *Proceedings of the National Academy of Sciences of the United States of America.* 2009;106(51):21819-21824.
21. Boertien WE, Meijer E, de Jong PE, et al. Short-term Effects of Tolvaptan in Individuals With Autosomal Dominant Polycystic Kidney Disease at Various Levels of Kidney Function. *American journal of kidney diseases : the official journal of the National Kidney Foundation.* 2015;65(6):833-841.
22. Boertien WE, Meijer E, de Jong PE, et al. Short-term renal hemodynamic effects of tolvaptan in subjects with autosomal dominant polycystic kidney disease at various stages of chronic kidney disease. *Kidney international.* 2013;84(6):1278-1286.
23. Muto S, Kawano H, Higashihara E, et al. The effect of tolvaptan on autosomal dominant polycystic kidney disease patients: a subgroup analysis of the Japanese patient subset from TEMPO 3:4 trial. *Clinical and experimental nephrology.* 2015.

24. Attanasio M, Uhlenhaut NH, Sousa VH, et al. Loss of GLIS2 causes nephronophthisis in humans and mice by increased apoptosis and fibrosis. *Nature genetics.* 2007;39(8):1018-1024.
25. Wynn TA, Ramalingam TR. Mechanisms of fibrosis: therapeutic translation for fibrotic disease. *Nature medicine.* 2012;18(7):1028-1040.
26. Slaats GG, Giles RH. Are renal ciliopathies (replication) stressed out? *Trends in cell biology.* 2015;25(6):317-319.
27. Simonson MS. Phenotypic transitions and fibrosis in diabetic nephropathy. *Kidney international.* 2007;71(9):846-854.
28. Falke LL, Gholizadeh S, Goldschmeding R, Kok RJ, Nguyen TQ. Diverse origins of the myofibroblast-implications for kidney fibrosis. *Nature reviews. Nephrology.* 2015;11(4):233-244.
29. Liu Y. Epithelial to mesenchymal transition in renal fibrogenesis: pathologic significance, molecular mechanism, and therapeutic intervention. *Journal of the American Society of Nephrology : JASN.* 2004;15(1):1-12.
30. Naber HP, Drabsch Y, Snaar-Jagalska BE, ten Dijke P, van Laar T. Snail and Slug, key regulators of TGF-beta-induced EMT, are sufficient for the induction of single-cell invasion. *Biochemical and biophysical research communications.* 2013;435(1):58-63.
31. Grenda R, Wuhl E, Litwin M, et al. Urinary excretion of endothelin-1 (ET-1), transforming growth factor-beta1 (TGF- beta1) and vascular endothelial growth factor (VEGF165) in paediatric chronic kidney diseases: results of the ESCAPE trial. *Nephrology, dialysis, transplantation : official publication of the European Dialysis and Transplant Association - European Renal Association.* 2007;22(12):3487-3494.
32. Schnaper HW, Hayashida T, Poncelet AC. It's a Smad world: regulation of TGF-beta signaling in the kidney. *Journal of the American Society of Nephrology : JASN.* 2002;13(4):1126-1128.
33. Isaka Y, Tsujie M, Ando Y, et al. Transforming growth factor-beta 1 antisense oligodeoxynucleotides block interstitial fibrosis in unilateral ureteral obstruction. *Kidney international.* 2000;58(5):1885-1892.
34. Tylicki L, Biedunkiewicz B, Chamienia A, et al. Renal allograft protection with angiotensin II type 1 receptor antagonists. *American journal of transplantation : official journal of the American Society of Transplantation and the American Society of Transplant Surgeons.* 2007;7(1):243-248.
35. Lizakowski S, Tylicki L, Renke M, et al. Aliskiren and perindopril reduce the levels of transforming growth factor-beta in patients with non-diabetic kidney disease. *American journal of hypertension.* 2012;25(6):636-639.
36. Group ET, Wuhl E, Trivelli A, et al. Strict blood-pressure control and progression of renal failure in children. *The New England journal of medicine.* 2009;361(17):1639-1650.
37. Zhang J, Gu C, Noble NA, Border WA, Huang Y. Combining angiotensin II blockade and renin receptor inhibition results in enhanced antifibrotic effect in experimental nephritis. *American journal of physiology. Renal physiology.* 2011;301(4):F723-732.
38. Kok HM, Falke LL, Goldschmeding R, Nguyen TQ. Targeting CTGF, EGF and PDGF pathways to prevent progression of kidney disease. *Nature reviews. Nephrology.* 2014;10(12):700-711.
39. Falke LL, Goldschmeding R, Nguyen TQ. A perspective on anti-CCN2 therapy for chronic kidney disease. *Nephrology, dialysis, transplantation : official publication of the European Dialysis and Transplant Association - European Renal Association.* 2014;29 Suppl 1:i30-i37.
40. Yokoi H, Mukoyama M, Nagae T, et al. Reduction in connective tissue growth factor by antisense treatment ameliorates renal tubulointerstitial fibrosis. *Journal of the American Society of Nephrology : JASN.* 2004;15(6):1430-1440.
41. Wang Q, Usinger W, Nichols B, et al. Cooperative interaction of CTGF and TGF-beta in animal models of fibrotic disease. *Fibrogenesis & tissue repair.* 2011;4(1):4.
42. Liu N, Guo JK, Pang M, et al. Genetic or pharmacologic blockade of EGFR inhibits renal fibrosis. *Journal of the American Society of Nephrology : JASN.* 2012;23(5):854-867.
43. Chen J, Chen JK, Harris RC. Deletion of the epidermal growth factor receptor in renal proximal tubule epithelial cells delays recovery from acute kidney injury. *Kidney international.* 2012;82(1):45-52.
44. Lassila M, Jandeleit-Dahm K, Seah KK, et al. Imatinib attenuates diabetic nephropathy in apolipoprotein E-knockout mice. *Journal of the American Society of Nephrology : JASN.* 2005;16(2):363-373.
45. Avlan D, Tamer L, Ayaz L, et al. Effects of trapidil on renal ischemia-reperfusion injury. *Journal of pediatric surgery.* 2006;41(10):1686-1693.
46. Eitner F, Bucher E, van Roeyen C, et al. PDGF-C is a proinflammatory cytokine that mediates renal interstitial fibrosis. *Journal of the American Society of Nephrology : JASN.* 2008;19(2):281-289.
47. Sugiyama N, Kohno M, Yokoyama T. Inhibition of the p38 MAPK pathway ameliorates renal fibrosis in an NPHP2 mouse model. *Nephrology, dialysis, transplantation : official publication of the European Dialysis and Transplant Association - European Renal Association.* 2012;27(4):1351-1358.
48. Chaki M, Airik R, Ghosh AK, et al. Exome capture reveals ZNF423 and CEP164 mutations, linking renal ciliopathies to DNA damage response signaling. *Cell.* 2012;150(3):533-548.

49. Airik R, Slaats GG, Guo Z, et al. Renal-retinal ciliopathy gene Sdccag8 regulates DNA damage response signaling. *Journal of the American Society of Nephrology : JASN.* 2014;25(11):2573-2583.
50. Slaats GG, Ghosh AK, Falke LL, et al. Nephronophthisis-associated CEP164 regulates cell cycle progression, apoptosis and epithelial-to-mesenchymal transition. *PLoS genetics.* 2014;10(10):e1004594.
51. Rozycki M, Lodyga M, Lam J, et al. The fate of the primary cilium during myofibroblast transition. *Molecular biology of the cell.* 2014;25(5):643-657.
52. Lamouille S, Xu J, Derynck R. Molecular mechanisms of epithelial-mesenchymal transition. *Nature reviews. Molecular cell biology.* 2014;15(3):178-196.
53. Noh H, Oh EY, Seo JY, et al. Histone deacetylase-2 is a key regulator of diabetes- and transforming growth factor-beta1-induced renal injury. *American journal of physiology. Renal physiology.* 2009;297(3):F729-739.
54. Van Beneden K, Geers C, Pauwels M, et al. Valproic acid attenuates proteinuria and kidney injury. *Journal of the American Society of Nephrology : JASN.* 2011;22(10):1863-1875.
55. Pang M, Zhuang S. Histone deacetylase: a potential therapeutic target for fibrotic disorders. *The Journal of pharmacology and experimental therapeutics.* 2010;335(2):266-272.
56. Prodromou NV, Thompson CL, Osborn DP, et al. Heat shock induces rapid resorption of primary cilia. *Journal of cell science.* 2012;125(Pt 18):4297-4305.
57. Brilli LL, Swanhart LM, de Caestecker MP, Hukriede NA. HDAC inhibitors in kidney development and disease. *Pediatric nephrology.* 2013;28(10):1909-1921.
58. Dong C, Li Z, Alvarez R, Jr., Feng XH, Goldschmidt-Clermont PJ. Microtubule binding to Smads may regulate TGF beta activity. *Molecular cell.* 2000;5(1):27-34.
59. Piperno G, LeDizet M, Chang XJ. Microtubules containing acetylated alpha-tubulin in mammalian cells in culture. *The Journal of cell biology.* 1987;104(2):289-302.
60. Wani MC, Taylor HL, Wall ME, Coggon P, McPhail AT. Plant antitumor agents. VI. The isolation and structure of taxol, a novel antileukemic and antitumor agent from Taxus brevifolia. *Journal of the American Chemical Society.* 1971;93(9):2325-2327.
61. Schiff PB, Fant J, Horwitz SB. Promotion of microtubule assembly in vitro by taxol. *Nature.* 1979;277(5698):665-667.
62. Donaldson KL, Goolsby GL, Wahl AF. Cytotoxicity of the anticancer agents cisplatin and taxol during cell proliferation and the cell cycle. *International journal of cancer. Journal international du cancer.* 1994;57(6):847-855.
63. Vaz P, Macassa E, Jani I, et al. Treatment of Kaposi sarcoma in human immunodeficiency virus-1-infected Mozambican children with antiretroviral drugs and chemotherapy. *The Pediatric infectious disease journal.* 2011;30(10):891-893.
64. Blaney SM, Seibel NL, O'Brien M, et al. Phase I trial of docetaxel administered as a 1-hour infusion in children with refractory solid tumors: a collaborative pediatric branch, National Cancer Institute and Children's Cancer Group trial. *Journal of clinical oncology : official journal of the American Society of Clinical Oncology.* 1997;15(4):1538-1543.
65. Doz F, Gentet JC, Pein F, et al. Phase I trial and pharmacological study of a 3-hour paclitaxel infusion in children with refractory solid tumours: a SFOP study. *British journal of cancer.* 2001;84(5):604-610.
66. Zwerdling T, Krailo M, Monteleone P, et al. Phase II investigation of docetaxel in pediatric patients with recurrent solid tumors: a report from the Children's Oncology Group. *Cancer.* 2006;106(8):1821-1828.
67. Woo DD, Tabancay AP, Jr., Wang CJ. Microtubule active taxanes inhibit polycystic kidney disease progression in cpk mice. *Kidney international.* 1997;51(5):1613-1618.
68. Martinez JR, Cowley BD, Gattone VH, 2nd, et al. The effect of paclitaxel on the progression of polycystic kidney disease in rodents. *American journal of kidney diseases : the official journal of the National Kidney Foundation.* 1997;29(3):435-444.
69. Zhang D, Sun L, Xian W, et al. Low-dose paclitaxel ameliorates renal fibrosis in rat UUO model by inhibition of TGF-beta/Smad activity. *Laboratory investigation; a journal of technical methods and pathology.* 2010;90(3):436-447.
70. Karbalay-Doust S, Noorafshan A, Pourshahid SM. Taxol and taurine protect the renal tissue of rats after unilateral ureteral obstruction: a stereological survey. *Korean journal of urology.* 2012;53(5):360-367.
71. Zhang D, Li Y, Liu Y, Xiang X, Dong Z. Paclitaxel ameliorates lipopolysaccharide-induced kidney injury by binding myeloid differentiation protein-2 to block Toll-like receptor 4-mediated nuclear factor-kappaB activation and cytokine production. *The Journal of pharmacology and experimental therapeutics.* 2013;345(1):69-75.
72. Zhou J, Ouyang X, Cui X, et al. Renal CD14 expression correlates with the progression of cystic kidney disease. *Kidney international.* 2010;78(6):550-560.
73. Zhang D, Yang R, Wang S, Dong Z. Paclitaxel: new uses for an old drug. *Drug design, development and therapy.* 2014;8:279-284.

74. Hanania R, Sun HS, Xu K, Pustylnik S, Jeganathan S, Harrison RE. Classically activated macrophages use stable microtubules for matrix metalloproteinase-9 (MMP-9) secretion. *The Journal of biological chemistry.* 2012;287(11):8468-8483.
75. Basten SG, Giles RH. Functional aspects of primary cilia in signaling, cell cycle and tumorigenesis. *Cilia.* 2013;2(1):6.
76. Zhang J, Guo WH, Wang YL. Microtubules stabilize cell polarity by localizing rear signals. *Proceedings of the National Academy of Sciences of the United States of America.* 2014;111(46):16383-16388.
77. Song Y, Brady ST. Post-translational modifications of tubulin: pathways to functional diversity of microtubules. *Trends in cell biology.* 2015;25(3):125-136.
78. Chen NX, Moe SM, Eggleston-Gulyas T, et al. Calcimimetics inhibit renal pathology in rodent nephronophthisis. *Kidney international.* 2011;80(6):612-619.
79. Masyuk TV, Masyuk AI, Torres VE, Harris PC, Larusso NF. Octreotide inhibits hepatic cystogenesis in a rodent model of polycystic liver disease by reducing cholangiocyte adenosine 3',5'-cyclic monophosphate. *Gastroenterology.* 2007;132(3):1104-1116.
80. Hogan MC, Masyuk TV, Page LJ, et al. Randomized clinical trial of long-acting somatostatin for autosomal dominant polycystic kidney and liver disease. *Journal of the American Society of Nephrology : JASN.* 2010;21(6):1052-1061.
81. Gattone VH, 2nd, Sinders RM, Hornberger TA, Robling AG. Late progression of renal pathology and cyst enlargement is reduced by rapamycin in a mouse model of nephronophthisis. *Kidney international.* 2009;76(2):178-182.
82. Tobin JL, Beales PL. Restoration of renal function in zebrafish models of ciliopathies. *Pediatric nephrology.* 2008;23(11):2095-2099.
83. Falke LL, van Vuuren SH, Kazazi-Hyseni F, et al. Local therapeutic efficacy with reduced systemic side effects by rapamycin-loaded subcapsular microspheres. *Biomaterials.* 2015;42:151-160.
84. Perico N, Antiga L, Caroli A, et al. Sirolimus therapy to halt the progression of ADPKD. *Journal of the American Society of Nephrology : JASN.* 2010;21(6):1031-1040.
85. Walz G, Budde K, Mannaa M, et al. Everolimus in patients with autosomal dominant polycystic kidney disease. *The New England journal of medicine.* 2010;363(9):830-840.
86. Serra AL, Poster D, Kistler AD, et al. Sirolimus and kidney growth in autosomal dominant polycystic kidney disease. *The New England journal of medicine.* 2010;363(9):820-829.
87. Braun WE, Schold JD, Stephany BR, Spirko RA, Herts BR. Low-dose rapamycin (sirolimus) effects in autosomal dominant polycystic kidney disease: an open-label randomized controlled pilot study. *Clinical journal of the American Society of Nephrology : CJASN.* 2014;9(5):881-888.
88. Stallone G, Infante B, Grandaliano G, et al. Rapamycin for treatment of type I autosomal dominant polycystic kidney disease (RAPYD-study): a randomized, controlled study. *Nephrology, dialysis, transplantation : official publication of the European Dialysis and Transplant Association - European Renal Association.* 2012;27(9):3560-3567.
89. Shillingford JM, Murcia NS, Larson CH, et al. The mTOR pathway is regulated by polycystin-1, and its inhibition reverses renal cystogenesis in polycystic kidney disease. *Proceedings of the National Academy of Sciences of the United States of America.* 2006;103(14):5466-5471.
90. Shillingford JM, Leamon CP, Vlahov IR, Weimbs T. Folate-conjugated rapamycin slows progression of polycystic kidney disease. *Journal of the American Society of Nephrology : JASN.* 2012;23(10):1674-1681.
91. Krueger DA, Care MM, Agricola K, Tudor C, Mays M, Franz DN. Everolimus long-term safety and efficacy in subependymal giant cell astrocytoma. *Neurology.* 2013;80(6):574-580.
92. Gattone VH, 2nd, Wang X, Harris PC, Torres VE. Inhibition of renal cystic disease development and progression by a vasopressin V2 receptor antagonist. *Nature medicine.* 2003;9(10):1323-1326.
93. Aihara M, Fujiki H, Mizuguchi H, et al. Tolvaptan delays the onset of end-stage renal disease in a polycystic kidney disease model by suppressing increases in kidney volume and renal injury. *The Journal of pharmacology and experimental therapeutics.* 2014;349(2):258-267.
94. Hynes AM, Giles RH, Srivastava S, et al. Murine Joubert syndrome reveals Hedgehog signaling defects as a potential therapeutic target for nephronophthisis. *Proceedings of the National Academy of Sciences of the United States of America.* 2014;111(27):9893-9898.
95. Woo DD, Miao SY, Pelayo JC, Woolf AS. Taxol inhibits progression of congenital polycystic kidney disease. *Nature.* 1994;368(6473):750-753.
96. Sommardahl CS, Woychik RP, Sweeney WE, Avner ED, Wilkinson JE. Efficacy of taxol in the orpk mouse model of polycystic kidney disease. *Pediatric nephrology.* 1997;11(6):728-733.
97. Sun L, Zhang D, Liu F, et al. Low-dose paclitaxel ameliorates fibrosis in the remnant kidney model by down-regulating miR-192. *The Journal of pathology.* 2011;225(3):364-377.

CHAPTER 9

Are renal ciliopathies (replication) stressed out?

Trends Cell Biol., 25(6):317-319 (2015)
(Reprinted with permission of Elsevier, doi: 10.1016/j.tcb.2015.03.005)

Gisela G. Slaats, Rachel H. Giles

ABSTRACT

Juvenile renal failure is commonly caused by the ciliopathy nephronophthisis (NPHP). Since all NPHP genes regulate cilia function, it has been assumed that NPHP onset is due to cilia loss. However, recent data suggest that DNA damage caused by replication stress, possibly concomitant with or upstream of cilia dysfunction, causes NPHP.

Renal ciliopathies: not just loss of cilia

The leading genetic causes of pediatric as well as adult kidney failure can be traced back to an organelle called the cilium. Cilia loss of function is thought to be the cellular defect responsible for two classes of renal ciliopathies: the common autosomal dominant polycystic kidney disease (ADPKD), which affects adults; and the rare, recessive pediatric/juvenile ciliopathies collectively referred to as nephronophthisis-related ciliopathies (NPHP-RC) (Box 1). For example, all 19 NPHP-associated genes reported to date encode gene products known to localize to primary cilia and regulate ciliary structure or function. In addition, many NPHP-associated proteins possess extraciliary functions that potentially contribute to the development of disease, and these functions have only recently been explored.

Box 1. Disease etiology of renal ciliopathies ADPKD and NPHP-RC

There are two classes of renal ciliopathies: the common ADPKD (MIM 173900) affecting adults and the rare, recessive pediatric/juvenile ciliopathies including NPHP (MIM 256100), Joubert syndrome (MIM 213300), Meckel-Grüber Syndrome (MIM 249000), Senior-Løken Syndrome (MIM 266900), and Bardet Biedel Syndrome (MIM 615993), collectively referred to as NPHP-RCs. In ADPKD, kidney tissue is damaged by hyperproliferative cystic tissue with some fibrotic tissue, which continues to grow over the life of the patient. In NPHP-RC, cyst development does not always occur, but when it does, it is limited to the cortico-medullary junction. Furthermore, NPHP-RC kidneys remain small throughout life and are primarily characterized by excessive interstitial fibrosis. To date, it is unknown how loss of NPHP genes leads to rapid development of fibrosis (5,8,9). While genes affecting both diseases have been shown to localize to ciliary components, presumably exercising some local function to regulate cilia and/or their signalling, the distinct phenotypes of ADPKD and NPHP suggest different mechanisms. Extraciliary functions of gene products mutated in ciliopathies remain to be investigated for a role in disease pathophysiology; four NPHP genes - NEK8, CEP164, SDCCAG8, and ZNF423 - have been implicated in DDR signalling to date (1-3).

Recent molecular evidence argues that the nuclear/DNA damage response (DDR) functions of some NPHP proteins may be critical in disease onset or progression. DDR signalling includes mechanisms to detect DNA damage (lesions), signal the presence of damage, arrest the cell cycle, and promote repair. The question is raised of whether nuclear effects of NPHP gene mutations are upstream, downstream, or independent of cilia dysfunction (1-3). Initial studies of the NPHP genes *ZNF423 (NPHP14),* and *CEP164 (NPHP15)* revealed that they colocalize with the DDR proteins SC-35 (a splicing factor), Checkpoint kinase 1 (CHK1), and Tat-interactive protein 60 (TIP60) in the nucleus (2). Additionally, morpholino injection of zebrafish embryos targeting *znf423* or *cep164* induced sensitivity to DNA damage-causing reagents (2), suggesting that a role for NPHP proteins in DDR signalling may contribute to the pathophysiology of NPHP. Moreover, CEP164 interacts with the cell

cycle checkpoint proteins Ataxia telangiectasia mutated (ATM) and ataxia telangiectasia and Rad3-related protein (ATR) during activated DDR signalling (4) and depletion of *Cep164* increases phosphorylation of H2AX in healthy, undamaged cells *in vitro* and *in vivo* (5). Supporting this hypothesis, a *Sdccag8 (Nphp10)* mouse model showed increased DNA damage signalling, as evidenced by increased phosphorylation of ATM and H2AX *in vivo* and *in vitro*, and disturbed cell cycle progression (3). These findings strengthen the link between DNA damage signalling and NPHP, but they fail to address the molecular mechanism of how enhanced DDR signalling is initiated in NPHP. Is the DDR signalling activated by phosphorylation of proteins followed by repair and cell cycle arrest, or are DNA breaks actually accumulating?

Replication stress at the root of the stalk

Recent studies with cells depleted for CEP164, SDCCAG8, and NEK8 are beginning to address the relation between the DDR and NPHP onset (1-3,5). Mutation in one of the less-frequently mutated NPHP proteins, the ciliary kinase NEK8 (NPHP9), which associates with NPHP and polycystic kidney disease, results in replication stress as evidenced by accumulating DNA damage in S-phase cells and increased replication fork defects in mouse embryonic fibroblasts derived from *Nek8* mutant *jck* mice (1). Replication stress is the slowing or stalling of the replication fork progression and/or DNA synthesis, which can lead to decreased cell survival and genome stability (1). Stalled replication forks are unstable and can collapse, leading to double-strand break formation and chromosomal rearrangements. Moreover, immunohistochemistry of kidneys from 3-week-old *jck* mice shows higher basal levels of phosphorylated H2AX compared with wild type siblings (1), suggesting that these effects are early.

What are the molecular mechanisms linking NPHP proteins to DNA damage? Depletion of NEK8 results in DDR signalling through enhanced cyclin A-associated cyclin-dependent kinase (CDK) activity, leading to replication stress, and activated ATR-CHK1 signalling upon replication stress induction in S-phase. Similarly, live-cell imaging of *CEP164*-depleted cells showed delayed S-phase progression that could be rescued with wild type, but not *CEP164* patient alleles (5), suggesting that these variants are causative for cell cycle impairment in patients. Since cells in S-phase do not have cilia, an increase of unciliated cells in S-phase would mimic a loss-of-cilia condition (Figure 1). Ciliation was rescued in Nek8-depleted cells treated with CDK inhibitors, although architectural changes of 3D renal spheroids were not rescued, possibly due to cell migration defects (1). It is important to note that, while NEK8 depletion results in enhanced CDK activity, the role of other NPHP proteins in CDK activity remains to be tested (1). Furthermore, pharmaceutical reduction of CDK activity by inhibitors of CDK requires further investigation to determine its role in ameliorating cell cycle defects associated with depletion of other NPHP-proteins. Cell cycle progression can also be indirectly regulated through ciliary signalling that is mediated by growth factor

receptors and mechanosensation (6). Therefore, NPHP-associated DDR signalling could interfere with normal cell cycle progression via both nuclear DNA damage-associated cell cycle control and by cilia-associated cell cycle control. While the details are far from complete, the present data support the notion that cell cycle disturbances consistent with replication stress are present in many ciliopathies (7).

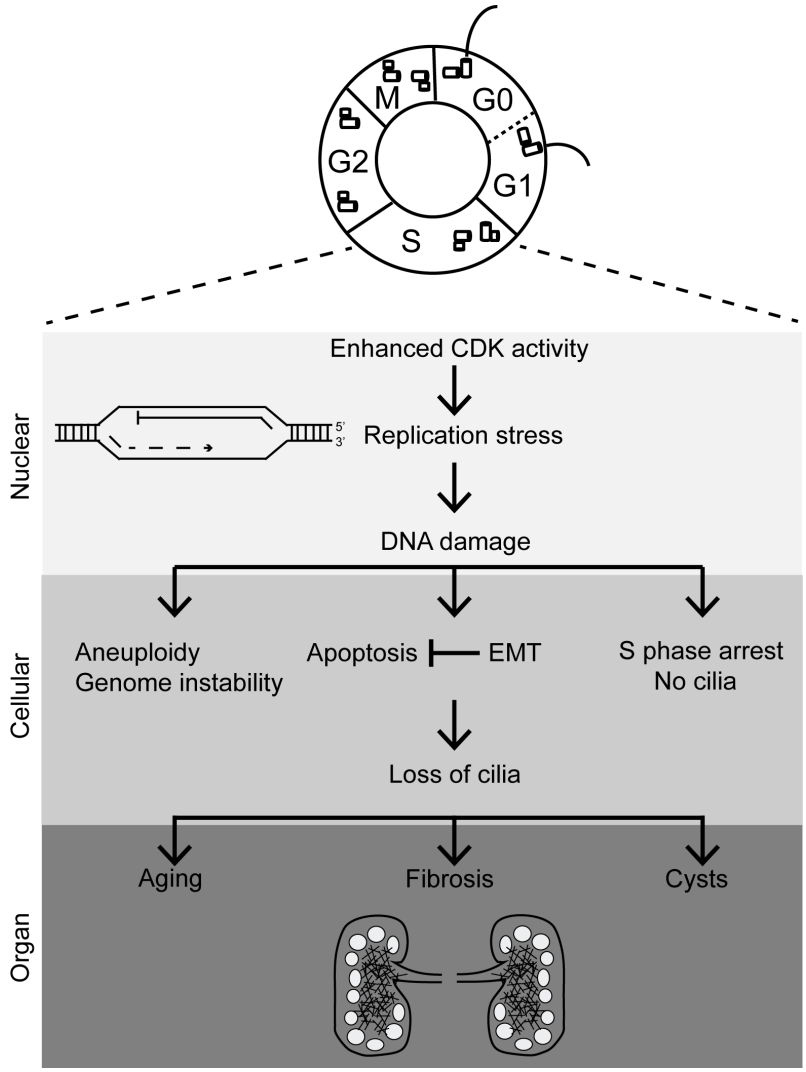

Figure 1. Overview of molecular signalling, cellular responses and organ pathology in nephronophthisis-related ciliopathies (NPHP-RCs)
The organ-, cellular-, and molecular/nuclear-understanding of the pathophysiology leading to NPHP. Besides the cilium, expressed in G_0 and G_1, replication stress in S-phase is central in NPHP-RC development. DDR, DNA damage response; CDK, cyclin-dependent kinase; EMT, epithelial-to-mesenchymal transition.

Why excessive fibrosis?

Cyst formation is attributed to loss of primary cilia, planar cell polarity defects, and hyperproliferation (8); however, molecular evidence linking cilia loss to the hallmark feature of NPHP, renal fibrosis, has been largely lacking. In addition to cell cycle progression defects, mutations in the NPHP gene *CEP164* appear to increase apoptosis and epithelial-to-mesenchymal transition (EMT) of renal inner medullary collecting duct cells (typically found at the cortico-medullary border of the kidney), coupled with a pro-fibrotic response in fibroblasts (5). Similar regulatory functions are described for *GLIS2 (NPHP7)* regarding apoptosis and fibrosis (9) (Figure 1). One recent study in myofibroblasts suggests that while the cilium is required for the initiation of EMT, cilia are lost thereafter, suggesting that the pro-fibrotic tissue environment characterized by EMT and cilium loss requires two triggers: disassembly of cellular contacts and transforming growth factor beta (TGF-β) exposure (10).

The question remains: what causes NPHP-associated fibrosis? One explanation could be sought in the association of NPHP proteins with an enhanced DDR (1-3), coupled with apoptosis and fibrosis-associated EMT (5). Linking ATR-regulated replication stress response and S-phase CDK activity to renal ciliopathies supports the suggestion that replication stress is complicit in the pathophysiology of NPHP-RCs. From the clinical perspective, this new hypothesis is interesting since, in contrast to cysts, replication stress and ciliation are reversible to a certain extent. Children diagnosed with NPHP-RC often have a 5-10 year window of therapeutic opportunity before requiring renal replacement therapy. The effect of CDK inhibition on renal fibrosis will still need to be thoroughly addressed, because fibrosis is the major damage inflicted on the kidney, and it is not typically reversible. The CDK inhibitor roscovitine has been shown to rescue renal cystic phenotypes in jck (*Nek8*/*Nphp9*), cpk (*Cys1*) (11) and *Pkd1* mouse models (12). The mechanism of action investigated in these murine models suggests that roscovitine induces cell cycle arrest and transcriptional inhibition. Regulation of apoptosis by roscovitine remains disputed; nevertheless, apoptosis is decreased in jck and *Pkd1* mice (11,12). However, the effect of CDK inhibition on primary cilia and fibrosis remains to be investigated in these murine models.

Concluding remarks

We contend that replication stress is an essential element of the origin of NPHP pathophysiology, which consequently results in decreased cell survival, EMT, and genome instability, leading to the fibrosis observed in NPHP (Figure 1 and Box 1). Loss of cilia in these "ciliopathies" may therefore be partly or entirely a secondary effect of nuclear events leading to cell cycle retardation, initiated by replication stress as a result of CDK activation. Accordingly, effectors of replication stress and the DDR in the nucleus partly overlap or interact with centrosomal components. Many proteins have multiple localizations, and nuclei and cilia also share molecular, structural, and mechanistic components that regulate

import (13); it is conceivable that NPHP proteins utilize the same import mechanism for both the nucleus and the cilium.

The roles of the replication stress response and DNA damage signalling in NPHP-RCs link this disease to inappropriate fibrosis and age-related diseases associated with DDR genes. We argue that DNA damage syndromes such as Seckel (MIM 210600) may be closer in etiology to NPHP-RCs than ADPKD. Some phenotypic overlap between Seckel syndrome and Joubert syndrome (JBTS) (MIM 213300), such as the characteristic cerebellar vermis hypoplasia ("molar tooth sign"), suggests a common etiology. A new avenue for NPHP therapeutic strategies focusing on the upstream molecular signalling defects, such as CDK1/2 inhibitors, could therefore be justified (11,12,14). The rescue of the ATR-CHK1 DDR may also be a viable option when determining targets for fibrosis and age-related characteristics. One extra allele of *Chk1* prolonged the survival of ATR-Seckel mice (15). Differences in extraciliary protein functions among the NPHP proteins might be at least part of the explanation of why the different ciliopathies have different clinical manifestations. In addition, the extent of cilia and nuclear dysfunction could be related to the variability between ciliopathies. Looking beyond the cilium and focusing on alternative mechanisms of disease eitiology is opening an exciting new chapter for "ciliopathy" research.

Acknowledgements

The authors acknowledge support from the European Community's Seventh Framework Programme FP7/2009 under grant agreement no: 241955, SYSCILIA, and the Dutch Kidney Foundation Consortium CP11.18 "KOUNCIL".

REFERENCES

1. Choi HJ, Lin JR, Vannier JB, et al. NEK8 links the ATR-regulated replication stress response and S phase CDK activity to renal ciliopathies. *Mol. Cell.* 2013;51(4):423-439.
2. Chaki M, Airik R, Ghosh AK, et al. Exome capture reveals ZNF423 and CEP164 mutations, linking renal ciliopathies to DNA damage response signaling. *Cell.* 2012;150(3):533-548.
3. Airik R, Slaats GG, Guo Z, et al. Renal-retinal ciliopathy gene Sdccag8 regulates DNA damage response signaling. *J. Am. Soc. Nephrol.* 2014;25(11):2573-2583.
4. Sivasubramaniam S, Sun X, Pan YR, Wang S, Lee EY. Cep164 is a mediator protein required for the maintenance of genomic stability through modulation of MDC1, RPA, and CHK1. *Genes Dev.* 2008;22(5):587-600.
5. Slaats GG, Ghosh AK, Falke LL, et al. Nephronophthisis-associated CEP164 regulates cell cycle progression, apoptosis and epithelial-to-mesenchymal transition. *PLoS genetics.* 2014;10(10):e1004594.
6. Pan J, Seeger-Nukpezah T, Golemis EA. The role of the cilium in normal and abnormal cell cycles: emphasis on renal cystic pathologies. *Cell. Mol. Life Sci.* 2013;70(11):1849-1874.
7. Basten SG, Giles RH. Functional aspects of primary cilia in signaling, cell cycle and tumorigenesis. *Cilia.* 2013;2(1):6.
8. Patel V, Li L, Cobo-Stark P, et al. Acute kidney injury and aberrant planar cell polarity induce cyst formation in mice lacking renal cilia. *Hum. Mol. Genet.* 2008;17(11):1578-1590.
9. Attanasio M, Uhlenhaut NH, Sousa VH, et al. Loss of GLIS2 causes nephronophthisis in humans and mice by increased apoptosis and fibrosis. *Nat. Genet.* 2007;39(8):1018-1024.
10. Rozycki M, Lodyga M, Lam J, et al. The fate of the primary cilium during myofibroblast transition. *Mol. Biol. Cell.* 2014;25(5):643-657.
11. Bukanov NO, Smith LA, Klinger KW, Ledbetter SR, Ibraghimov-Beskrovnaya O. Long-lasting arrest of murine polycystic kidney disease with CDK inhibitor roscovitine. *Nature.* 2006;444(7121):949-952.
12. Bukanov NO, Moreno SE, Natoli TA, et al. CDK inhibitors R-roscovitine and S-CR8 effectively block renal and hepatic cystogenesis in an orthologous model of ADPKD. *Cell Cycle.* 2012;11(21):4040-4046.
13. Kee HL, Verhey KJ. Molecular connections between nuclear and ciliary import processes. *Cilia.* 2013;2(1):11.
14. Beck H, Nahse V, Larsen MS, et al. Regulators of cyclin-dependent kinases are crucial for maintaining genome integrity in S phase. *J. Cell Biol.* 2010;188(5):629-638.
15. Lopez-Contreras AJ, Gutierrez-Martinez P, Specks J, Rodrigo-Perez S, Fernandez-Capetillo O. An extra allele of Chk1 limits oncogene-induced replicative stress and promotes transformation. *J. Exp. Med.* 2012;209(3):455-461.

CHAPTER 10

General discussion

In this work, I have investigated the group of inherited diseases called "ciliopathies", involving defects in proteins localizing to the cilium or associated complexes and pathways. The main focus of this thesis was to unravel molecular and cell biological mechanisms playing a role in ciliopathy development. The first symptoms of ciliopathies are visible at a young age, sometimes even before birth; besides developmental anomalies, tissue degeneration takes place at early-onset, and often affects the kidneys of these young patients. Since renal degeneration including fibrosis and cyst growth rapidly leads to renal end-stage disease, usually before the age of 20, the patients require a donor kidney or dialysis until transplantation can be arranged. This thesis describes several novel aspects of the renal ciliopathy field: (1) Optimizing new sources of patient cells to model ciliopathies *ex vivo*; (2) Identification of new ion channel genes which affect renal cilia; (3) The mechanism of disease involving both ciliary and nuclear functions of ciliopathy gene products, supplying a novel layer to the disease mechanism, and (4) Potential solutions to target renal cysts and fibrosis development to slow down disease progression and postpone kidney transplantation.

One limitation during the research described here is the availability of primary patient material. After clinical and/or genetic diagnosis, the logical next step is studying the disease mechanism *ex vivo* or *in vitro*. Unfortunately, in most cases there is no or very limited patient material available, because renal biopsies are not taken and kidneys are not removed after transplantation. In ciliopathy research, blood samples are not of great value after DNA diagnosis, as blood cells are not representative for the tissue(s) affected and not all types of blood cells are ciliated. In selected cases skin biopsies are taken, which provide decent sources of ciliated cells; however, skin "punches" are painful, fibroblasts are not always tissue-relevant or applicable in all experimental set-ups (e.g. 3D spheroids) and cause inconvenience for the patients at time of biopsy. During the last decade of cilium research several model organisms have been explored, including the nematode *C. elegans*, but most often rodent models have been used since these are -for the most part- reasonably analogous to human disease (**Chapter 5**). *Danio rerio* (zebrafish) are a very powerful tool in investigating ciliopathy genetics. Unfortunately, they are not a good model for kidney fibrosis. Notwithstanding these useful animal models, studying human disease and patient-specific mutations is actually best in patient-derived material. Using non-invasive sources of ciliated cells from children and adults, we developed protocols to culture ciliated cells from urine and from spontaneously shed milk teeth (**Chapter 2**). The main disadvantage of these cell sources is the risk of contamination due to semi-sterile collection conditions and, moreover, these types of primary cells grow slow compared to immortalized cells lines. Future research could focus on induced pluripotent stem cells (iPSCs). iPSCs are differentiated cells that are genetically re-programmed to become embryonic stem cell-like, and are a useful tool for modeling disease and drug development, and for possible future use in transplantation medicine (1). One study demonstrated genetic restoration of a

genomic heterozygous *Pkd1* (polycystic kidney disease 1) mutation, which causes autosomal dominant polycystic kidney disease (ADPKD) in mice. The cyst growth in kidneys of adult chimeric mice, which were transplanted with iPSCs, was reduced (2). The effectiveness and safety of iPSCs in ameliorating renal cysts and fibrosis is unidentified, but of broad clinical relevance.

Ciliopathies cover a wide range of genotypes and phenotypes, and the list of ciliopathies is expanding. Our findings in a siRNA screen of all mouse ion channels showed that reduction of cellular levels of *Kcnq1, Kcnj10, Kcnf1* and *Clcn4* RNA causes defects in ciliogenesis (**Chapter 3**), suggesting these genes are novel candidates for ciliopathies. This may explain the ciliopathy-like phenotypes (such as kidney tubulopathy and deafness) seen in patients with mutations in these genes. However, the phenotypes can also be caused by defects in the ion channel function, independent of the ciliogenesis function as observed when we tested Epilepsy, Ataxia, Sensorineural deafness, and Tubulopathy (EAST syndrome, alternately named SESAME syndrome; MIM 612780)-associated mutations in *KCNJ10*. In contrast to congenital heart disease Long QT syndrome (MIM 192500)-associated mutations in *KCNQ1*, which showed that ion channel function can be concurrent with ciliary function. These findings not only implicate primary cilia in the pathophysiology of conditions such as Long QT syndrome, but they offer new insights into the general importance of ion channels and ion signalling in ciliopathies. Furthermore, our data suggests that mutations in *KCNF1* and *CLCN4* may be present in other human ciliopathies. With help of the hypothesis-free siRNA screen identifying these four candidates, an hypothesis about the role of ion balance in renal homeostasis, in the context of renal progression of nephronophthisis or ADPKD has been successfully generated. By elucidating the exact role of these ion channels in primary cilia and disease, we offer new insights into potential therapeutic approaches.

Are nephronophthisis-related ciliopathies one disease?

Loss of cilia and ciliary-mediated signalling causes a wide variety of phenotypes ranging from mild to severe, and involves different organs and tissues. Therefore, the different ciliopathies can be organized by severity of the clinical phenotype and by the spectrum of organs/tissues affected. From extensive genetic work in *Chlamydomonas* algae, we know that mutations in genes coding for proteins involved in cytoplasmic assembly or transport of outer- and inner-dynein arms in motile cilia, all cause virtually the same ciliopathy: Primary Ciliary Dyskinesia (MIM 244400), characterized by bronchiectasis with or without *situs inversus* (3). The concept of functional "modules" of proteins being involved in ciliopathy etiologies, in which dysfunction of individual proteins in that module would disturb the function of the module was further supported by the isolation of the BBSome; mutations in 19 different proteins, being part of the BBSome, cause Bardet-Biedl syndrome (BBS) with nearly identical phenotypes (4). The phenotypically similar renal nephronophthisis-

related ciliopathies (NPHP-RCs) diseases, such as Meckel Grüber syndrome (MKS), nephronophthisis (NPHP), Joubert syndrome (JBTS), and Senior-Løken syndrome (SLS), with overlap to BBS, share the same protein network (5). This suggests that, when the concept of functional modules holds true for the NPHP-RCs, all of these syndromes are in fact just scaled severities of the same disease, depending on the gene(s) and type of mutation, with a broad range of clinical features (6,7). To summarize the detailed overview presented in **Chapter 1**, isolated NPHP involves only a renal phenotype, however, in SLS retinal degeneration is also observed. Both ciliopathies are relatively mild compared to JBTS, in which the central nervous system primarily is affected (the characteristic radiographic "molar tooth sign") and sometimes NPHP, liver degeneration, polydactyly and *situs inversus* can occur. BBS is somewhere between SLS and JBTS, with cognitive problems, blindness, obesity, and polydactyly. At the edge of the scale we find MKS, with all of the phenotypes above in addition to craniofacial abnormalities, but this condition is invariably lethal in the fetal or neonatal period. In addition to phenotypic overlap, there is genetic overlap among the different ciliopathies, which supports the idea that some ciliopathies are one disease with a broad range of phenotypes. It has been speculated that mutations occurring in genes whose products contribute to the overall vesicle trafficking to the cilium (i.e. affecting cilia assembly) will lead to more severe symptoms, whereas those involved in the transport of specific cargo within intact cilia will result in milder phenotypes (8). Loss of *MKS1* can cause JBTS, BBS and MKS, loss of *CEP290* can cause NPHP, JBTS, MKS, BBS, SLS and Leber Congenital Amaurosis (LCA; MIM 611755), and *NPHP3* mutations cause NPHP, SLS, and MKS for example. We have contributed to the body of evidence that NPHP-RCs are variations of a single disease to a certain extent in **Chapter 4**. Nonsense mutations in *MKS1* underlie MKS, and missense mutations cause JBTS, pointing to a genotype-phenotype correlation of these neurodevelopmental disorders. Mutation of *MKS1* disturbs the ciliary structure element transition zone (TZ), and causes variable cilium length and mislocalization of JBTS-associated protein INPP5E in the cilium in both MKS and JBTS. Interestingly, this study reveals that JBTS missense mutations do not always cause loss of cilia, but MKS nonsense mutations do. This implies that loss of cilia is not essential for JBTS disease development; ciliary phosphoinositide signaling appears to be more robustly linked to both syndromes. Future work will determine the downstream effects of INPP5E dysfunction, likely involving phosphoinositide signalling and other signaling pathways, as well as how the many cellular defects associated with loss of JBTS and MKS gene function relate to the human phenotypes. Aberrant Hedgehog (Hh) signalling (9) and Wnt signaling are also found in JBTS and could be responsible for patient phenotypes as well. Because INPP5E is potentially druggable, the value of finding this enzyme at the root of JBTS and MKS will hopefully open a novel therapeutic avenue to ameliorate the progression of disease.

In genotype-phenotype studies, robust correlations have not yet been found for all ciliopathy-associated loci. In addition, it seems plausible that mutation of certain domains of a gene associates with specific cellular functions to become disturbed, as shown in *Cep290* mouse models (10), although the picture is far from complete (11). It is unknown whether patients with LCA or BBS bearing *CEP290* homozygous mutations, will demonstrate enhanced replication stress-induced DNA damage, like we have shown in JBTS renal phenotypes (**Chapter 6**), but we would predict that BBS patients would resemble JBTS patients in this respect, whereas LCA patients have isolated retinopathy and will not. Another genetic factor that could play a role is mutational load. Accumulation of mutations in ciliopathy-associated loci could contribute to differential phenotypes (12,13). Investigation of combinations of mutations in several genes will be challenging *in vivo*, but essential to examine the role of mutational load in ciliopathy development. To date, approximately 50% of all NPHP cases can be explained by 19 disease loci. Identifying new genes and mutations by matured techniques including next-generation sequencing becomes financially more attractive (14). In cases of very rare genetic causes of NPHP-RCs, physicians need those genetic tools to obtain a precise molecular diagnosis in one family or even in one individual at a time. In those cases, whole genome screening (**Chapter 3**) and bioinformatic approaches and predictions are of great value, since these can reveal ciliopathy genes as well (15).

Tissue specificity in ciliopathies

The kidney is the organ most commonly affected in ciliopathies, in varying combinations with degeneration of the retina and liver, and in addition bone and brain tissue can be affected during development (6). To date, no strong evidence exists to explain the tissue specificity of these phenotypes. How does loss of cilia/ciliary signalling proteins, or disturbed upstream events, cause degeneration in one organ and not in the other? Speculation about tissue specificity limited to the kidney sketch a scene using the data suggesting that flow in the nephron instigates ciliary second-messenger calcium release by mechanosensation to repress mitosis. This led to the hypothesis that the cilium normally functions as a brake on the cell cycle in the particular context of the nephron (16). When ciliary-calcium signaling is disturbed upon mutation of *PKD1* or *PKD2*, renal epithelial cells continue dividing, driving proliferation. One can imagine that during NPHP, loss of cilia therefore might similarly promote hyperproliferation, which results in concomitant supplementary replication stress caused by a shortage of resources like nucleotides and replication factors. Other organs lacking flow through a lumen e.g. skin, or organs which are characterized by such high proliferation rates that cells are naturally shed before they exit the cell cycle and ciliate, e.g. the intestine, will probably experience less stress, and will therefore "suffer" less upon NPHP protein inactivation. Furthermore, differential expression levels of NPHP genes among diverse organs and tissues could contribute to

dissimilar impact of loss of those NPHP genes. In addition, as kidneys are constantly exposed to genotoxins, they are especially prone to lesions caused by impaired DNA damage response (DDR) signaling. Repair defects after cisplatin exposure have been reported for the *Ahi1-/-* mouse model of NPHP-RC, whereas those mice were not more susceptible for renal injury caused by ischemic reperfusion (17), implicating a role for impaired DDR signalling in this model. Finally, differential levels of hypoxia could be involved in tissue-specific degeneration in a background with active DNA damage signalling: hypoxia makes cells more resistant to DNA damage and extends the life-span of *C. elegans* (18,19). Resistance to DNA damage protects against cancer and elicits a protective survival response that promotes healthy aging and longevity (20).

Extra-ciliary protein functions: implications for NPHP disease etiology

PKD and NPHP-RCs are diseases resulting in renal failure usually before the ages of 55 and 25, respectively. Both diseases are characterized by renal cysts, and the molecular disease mechanisms, including loss of cilia, planar cell polarity and proliferation defects, were thought to be highly similar (21,22). However, recent findings in cilia biology point to a conflict in this assumption. NPHP is categorized as a cystic kidney disease, however, cysts are not always present or occur at a later stage; rather, fibrosis seems to be a more prominent phenotype (23,24). Gene products mutated in NPHP-RCs have recently been linked to DNA damage signalling; it is not yet entirely clear whether nuclear function of NPHP gene products is a major contributor to NPHP development (25,26) (**Chapter 5 and 7**). Evidence for the hypothesis that replication stress and DDR proteins in the nucleus and at the centrosome are partly overlapping and interacting is accumulating. In addition to *Nek8*-depleted (*Nphp9*) (26), *Sdccag8*-depleted (*Nphp10*) (27) and *Cep164*-depleted (*Nphp15*) (25,28) cells, upregulation of replication stress-induced DNA damage was found in *Cep290*-depleted cells as well; *CEP290* is a gene frequently mutated in NPHP-RCs as well as in LCA (**Chapter 6**). In **Chapter 9** this hypothesis, suggesting that replication stress is the molecular mechanism underlying DNA damage response signalling and consequent cell cycle disturbance in NPHP, is further discussed (29). Researchers have assumed that ciliopathies are universally caused by loss of cilia or ciliary function, leading to disturbances in signalling and in the cell cycle, eventually causing renal cysts and fibrosis. However, recent findings argue that replication stress is upstream of cilia loss, causing a lag in an unciliated cell cycle stage (S-phase). Given that replication stress is present at the early onset of disease (26), a mechanism is proposed that loss of cilia and cyst formation are secondary to replication stress and perhaps fibrosis (**Chapter 7**). This provides new insights into the order of events during NPHP development, which is important for designing follow-up research and novel targeted therapies. Furthermore, the timing of loss of primary cilia leading to cysts and which ciliary signalling pathways are disturbed upon loss of cilia (e.g. Hh, Wnt) could influence the patient phenotypes as well. Many questions remain to be

investigated, such as whether perturbations in cilia signalling, in a background with activated DDR or independently, contribute to NPHP, and if cilia or ciliary dysfunction somehow contributes to DDR. Furthermore, it is unknown whether the NPHP proteins shuttle between the cilium and nucleus or whether the protein pools at the cilium and the nucleus are distinct. Lastly, how replication stress/DDR exactly contributes to cyst and/or fibrosis development is a field that will demand further investigation. To date there is preliminary evidence that impaired DDR is not present in ADPKD (unpublished); however, this should be examined as well.

What causes renal fibrosis in DDR models?

Renal fibrosis is a common morbidity, characterized by glomerulosclerosis and tubulointerstitial fibrosis, and is the final step of a wide variety of chronic kidney diseases (CKD) associated with the aging individual (30). In NPHP patients the development of fibrosis is accelerated when compared to healthy individuals, but how could this be regulated by DNA damage signalling? Cisplatin has been used to induce renal DNA damage in rats, by causing DNA crosslinks. The main phenotype found in the cisplatin-treated rats is interstitial fibrosis (31,32), linking DNA damage to fibrosis development as well. Besides regulating cell cycle and repair processes, DNA damage signalling activates the innate immune system (33). Immune cell infiltrations are seen in fibrotic NPHP and CKD tissue (24,34), facilitating fibrotic signalling (35). Finally, enhanced DDR, when beyond repair, leads to cellular death by apoptosis. Alternatively, cells can undergo epithelial-to-mesenchymal transition (EMT) to escape apoptosis (36,37) (**Chapter 7**). Mesenchymal cells are the major progenitors of the scar-forming cells (myofibroblasts) in the kidney (38). Because renal tissue in children and murine models with nephronophthisis have characteristics of accelerated aging (increased apoptosis, pro-fibrotic, reduced regenerative capacity), it is tempting to speculate that NPHP is a result of DNA damage and accelerated aging, rather than the calcium-signalling induced model of proliferation proposed for ADPKD (16). This idea is supported by the Seckel mouse model depleted for the ATR kinase, which has high levels of replication stress during proliferative stages of life, which results in accelerated aging later-in-life. This supports the hypothesis that replication stress *in utero* results in early onset aging in postnatal life (39), possibly by loss of stem cells (40). Additionally, models of defective DNA damage repair, like FANCD2/FANCI-associated nuclease 1 (*FAN1*), are characterized by chronic kidney failure (34). It would be of interest to examine cilia or ciliary signalling in the *Ercc1-/-* progeroid mouse model. ERCC1 acts in the same protein complex as FAN1. The phenotype of *Ercc1-/-* mice covers accelerated loss of hearing and vision (41), neuron degeneration and mild abnormalities in kidney and liver tissue (42,43), which are common phenotypes among ciliopathies (**Chapter 1, table 1**). Collectively these studies with DDR mouse models support the hypothesis that replication stress and DDR are upstream of cilia loss by causing ciliopathy phenotypes. These DDR mouse models

could be valuable in examining whether cilia, or ciliary dysfunction somehow contributes to DDR, or whether perturbations in cilia signalling, in a background with activated DDR or independently, contribute to NPHP.

Furthermore, studies of NPHP protein NEK8 (NPHP9) have shown that it has a role in Hippo signalling by promoting the nuclear delivery and activation of the oncogenic transcriptional regulator TAZ (44). Besides the role of the Hippo pathway in disturbed ciliary signalling resulting in renal cyst growth, by promoting nuclear YAP accumulation (45,46), it promotes fibrosis development as well, by functionally interacting with the transforming growth factor beta (TGF-β) pathway and regulating connective tissue growth factor (CTGF) (47). There might be a, up till now unrevealed, crosstalk between DDR signalling and Hippo signalling in NPHP-RCs, working together in renal fibrosis development. However, it is unknown if all NPHP-RC gene products are involved in both Hippo signalling and DDR signalling.

Treating fibrosis

Understanding fibrosis is complex. Insights into the involved signalling pathways can help us find therapeutics to delay the onset of end-stage renal disease in young NPHP patients, since no curative treatment is available beyond renal replacement therapy. There is call for approaches for therapeutic intervention with a focus on fibrosis treatment, the major player in renal tissue degeneration in NPHP. Enhanced cyclin-dependent kinase (CDK) activity has been shown to underlie the replication stress in *NEK8* (*NPHP9*) and *CEP290* (*NPHP6*) ciliopathy models (26) (**Chapter 6**). Future studies could catalogue cyclin-A associated CDK versus cyclin-B associated CDK activity per patient genotype across a large number of ciliopathy patients to examine the role of CDK activity in NPHP-RCs. CDK inhibitors like roscovitine/S-CR8 have been shown to ameliorate cysts formation in rodent models of PKD (48,49) and CDK1/2 inhibitors rescued primary cilia in spheroids depleted for *Nek8* and *Cep290 (26)* (**Chapter 6**). *In vitro*, CDK inhibitor roscovitine treatment of normal and scleroderma fibroblasts revealed anti-fibrotic effects (50). It is of clinical interest to test whether CDK inhibition ameliorates fibrosis in NPHP-RC, however, these inhibitors could have relevant side effects in the clinic. Dose-dependent adverse events observed are fatigue, skin rash, hyponatraemia, hypokalaemia, raised creatinine, abnormal liver function, emesis, nausea and asthenia (51-53). Roscovitine has mainly been tested in phase I and II clinical trials for cancer, with inconsistent tumor reduction or stable disease recorded (51-53). Further research is required to determine optimum dose, administration schedule and efficacy studies when it comes to renal fibrosis treatment with CDKi in children and young adults with NPHP-RC. Long-term CDK inhibition in children may be too harmful, since it may interfere with normal growth and development. Therefore, we propose that targeting downstream events of replication stress and DDR like immune response, cell cycle, EMT or DNA damage repair could be attractive. For this reason we have revisited taxanes as potential medical intervention strategy, as described in **Chapter 8**. Several

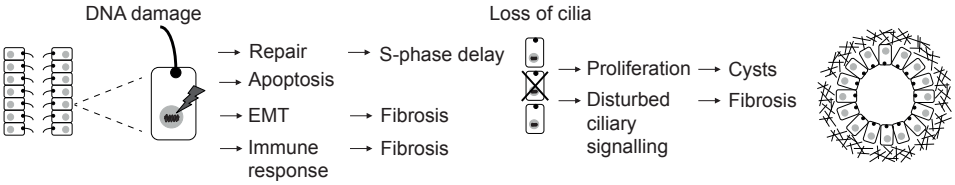

Figure 1. Simplified overview of the order of events during NPHP-RC which lead to fibrosis
Renal tubule cells of NPHP-RC patients carry autosomal recessive mutations in genes encoding proteins important for ciliary structure or function. Additionally, these proteins are genome maintenance factors as well, protecting the DNA from replication stress-induced DNA damage. Loss of the genome maintenance proteins causes enhanced DNA damage with several downstream cellular responses: S-phase cell cycle arrest to create time for DNA repair, apoptosis in case the damage is beyond repair, or epithelial-to-mesenchymal transition (EMT) to escape from apoptosis. EMT contributes to fibrosis development in the kidney. Furthermore, the immune response is activated upon DNA damage signaling, which facilitates fibrosis signalling. Cells lose their cilium in S-phase and as a result of EMT, which causes hyperproliferation that contributes to cyst development. Additionally, ciliary signalling will be disturbed (e.g. Hippo), which could contribute to fibrosis development as well in NPHP-RC patients.

strategies were tested to improve paclitaxel administration by increasing its solubility, because a mixture of paclitaxel with poly castor oil (Cremophor EL) and dehydrated ethanol caused irritation in patients (54). Conjugation with poly L-glutamic acid (55), albumin (56) and delivery systems as micelles (57) and liposomes (58) have been studied to improve water solubility and decrease side effects. Conjugation of taxol with dextran and folic acid improved the *in vitro* targeting and solubility of taxol as well (59).

Another approach for medical intervention of replication stress and age-related characteristics could be sought in targeting the ATR-CHK1-WEE1 pathway, which protects the genome (60,61). Controlled replication initiation is crucial for genome stability. Nucleotide consumption during replication could be disturbed in NPHP-RCs with enhanced CDK activity, suggesting we perhaps could treat ciliopathies by supplementing with nucleotides which are shown to reduce replication stress (62). Furthermore, protection of replication stress by an extra Chk1 allele is shown to prolong the survival in ATR-Seckel mice, but not in ATM-deficient mice (63), suggesting that targeting ATR-CHK1 is protective.

Centrosome dysfunction and genome instability

A whole-genome siRNA screen for novel regulators of DDR revealed ciliopathy loci *NEK8*, *NPHP1* and *MKS1* to protect against DNA damage (γH2AX) (64). From this screen *NEK8* was extensively validated (26). The screen successfully identified three classical ciliopathy genes (*NEK8*, *NPHP1* and *MKS1*) (64), and coupled with the three additional genes discussed in this thesis (**Chapter 5-7**), the data is mounting support for the DDR mechanism to underlie all NPHP-RC diseases. However, a systematic review of all the genes simultaneously is lacking.

How does the centrosomal function of NPHP proteins (e.g. CEP290) contribute to the effects observed? Defects in centrosome separation or overreplication drive aneuploidy and centrosome deficiency itself can result in genomic DNA damage (65) (**Chapter 6**). Loss of polycystin-1 function was shown to be sufficient to produce aberrant centrosome amplification and multipolar spindle formation in PKD, suggesting DNA damage plays a role in ADPKD too. The genetic mechanism leads to genomic instability characterized by polyploidism and mitotic catastrophe (66). Centrosome dysfunction generates G1-S cell cycle arrest with reduced Cyclin A-associated CDK activity (67). However, continuous CDK2 activity promotes aneuploidy, which could be modulated in mice by inhibiting CDK2 *in vivo* with knock-in mouse technology. The same knock-in mouse demonstrates that CDK inhibition normalizes DNA replication misregulation and centrosome duplication (68), suggesting that supernumerary centrosomes and CDK activity are linked.
Furthermore, origin recognition complex subunit 1 (ORC1) controls centriole and centrosome copy number in human cells (69). In ciliopathy Meier-Gorlin syndrome mutations disrupt an ORC1 CDK inhibitory domain and cause centrosome reduplication (70). Additionally, mutations in Polo-like kinase 4 (*PLK4)* encoding a master regulator of centriole biogenesis cause microcephaly, growth failure and retinopathy in humans, resembling a ciliopathy (71). PLK4 regulates ciliogenesis *in vitro* as well (unpublished), suggesting that centriole defects leading to chromosome instability (CIN), contribute to ciliopathy phenotypic characteristics. However, could those characteristics be rescued by CDK inhibition like fibrosis (**Chapter 6**)?

Separate ciliary and extra-ciliary protein function

Both replication stress and centriole defects appear to be caused by enhanced CDK activity in NPHP-RC (**Chapter 6**). A systematic analysis of all ciliopathy genes is required to confirm the breadth and depth of replication stress and centriole duplication defects. Replication stress is thought to be an independent function of the NPHP proteins, since no evidence has yet been found that ciliary signalling involves replication stress response. The most likely model is that there are two separate functions for the same proteins. Whether these cellular functions are regulated by the same pool of proteins or by local protein pools in the nucleus and at the centrosome remains to be elucidated. This model also allows for replication stress in only some tissues but not in others. Similar mechanisms regulate ciliary import at the transition zone and nuclear import (72), which is regulated by pore exclusion at both compartments, which does not exclude that it is the same pool of proteins. Strikingly, we observed γH2AX at the centrosome in IMCD, RPE and urine-derived epithelial cells (unpublished). Our unpublished finding that this phosphorylated histone also resides at the centrosome, where to the best of our knowledge DNA is not present, suggests it might function in signalling somehow. However, trafficking of proteins between the cilium and nuclear compartment could be a microtubule-dependent event, possibly mediated by

centriolar satellite components and/or dynein. Centriolar satellites are involved in centrosome maintenance and ciliogenesis, and contain centrosome proteins like pericentrin, centrin (73), and CEP290 (74), which regulates ciliary trafficking (75). Interestingly, two studies demonstrated that prior to the formation of supernumerary centrosomes during a prolonged S-phase, an increase in nuclear accumulation of centrin was visible (76,77). This suggests an interesting link between centrosome over-duplication, a hallmark of cancer cells, and nuclear molecular mechanisms linked to CIN (78).

No cancer predisposition in NPHP

Genomic instability contributes to many diseases, such as cancer and developmental disorders (79,80). To date, cancers have been rarely observed in renal ciliopathy patients (81), and when cancer is observed, it is usually due to immunosuppression after renal transplantation. When DNA damage lesions caused by replication stress are not repaired or removed, cells have a mechanism to bypass DNA lesions and leaving them behind, referred to as DNA damage tolerance pathways (82). Activation of DNA damage tolerance results in accumulation of genetic lesions, potentially affecting tumor suppressor genes or leading to genomic instability, which one might consider a cancer-promoting environment. In contrast, NPHP-RC patients do not seem to be predisposed to cancer, but do have aging-associated phenotypic characteristics. This thin line between the balance of cancer and aging has been examined in nucleotide excision repair disorders; two segmental progeria (aging) syndromes, Cockayne syndrome (MIM 216400) and trichothiodystrophy (MIM 601675) only display aging aspects, and are not cancer prone. Interestingly, mutations in genes in the same pathway do give rise to elevated cancer rates (83,84). Experimental modulation of cancer and aging pathways has been shown for stability (caretaker) proteins, which are responsible for DNA repair and maintenance (84). The NPHP-RC proteins do not seem to have tumor suppressor functions or act as gatekeepers for cancer predisposition, however, they could be caretaker proteins. This supports the general notion that aging by cell death and senescence protects from cancer. Tumor suppressor gene *TP53* is intact in NPHP-RCs, consequently, gene product p53's function in cellular and systemic DDR in cancer and aging results in intact cell cycle arrest, senescence, apoptosis and innate immune response activation. Both apoptosis and senescence are tumor-suppressive pathways while simultaneously contributing to tissue degeneration (85). These findings provide clues to the underlying causes of tissue decline and one day we may add the NPHP-RC genes to the mounting list of genome maintenance factors that protect against premature aging (86). Although there is phenotypic and mechanistic overlap between NPHP and classical aging syndromes like progeria, classifying NPHP as a premature aging disease is not the complete story. We cannot ignore the ciliary phenotypes (renal degeneration) in NPHP-RCs. The reality will probably be the tissue-specific balance of replication stress management and ciliogenesis and maintenance.

Concluding remarks

The model that loss of ciliary structure or function leads to ciliopathies appears to be an oversimplified model. From the work presented in this thesis we can conclude that there is another layer to the disease mechanism. We propose that upstream events could play a role in tissue degeneration, initiated by replication stress and DNA damage response signalling. Whether replication stress is underlying all renal or extra-renal manifestations of ciliopathies remains to be investigated. Differences in extra-ciliary protein functions among the NPHP proteins might be at least part of the explanation why the different ciliopathies have different clinical manifestations. In addition, the extent of ciliary and nuclear dysfunction could be related to the variability between ciliopathies. The ciliary research field is rapidly evolving, with new genes, new signalling networks and new ciliopathies being identified, implicating the importance of proper functioning of the primary cilium and highlights the need for therapeutic intervention. Collaborations between clinicians, molecular biologists and bioinformaticians are required to examine the complexity of the cilium in the future to obtain a better understanding of ciliopathies, with as ultimate goal to define treatment strategies. Looking beyond the cilium and focusing on alternative mechanisms of disease etiology is opening an exciting new chapter for 'ciliopathy' research.

REFERENCES

1. Dekkers JF, Wiegerinck CL, de Jonge HR, et al. A functional CFTR assay using primary cystic fibrosis intestinal organoids. *Nature medicine.* 2013;19(7):939-945.
2. Cheng LT, Nagata S, Hirano K, et al. Cure of ADPKD by selection for spontaneous genetic repair events in Pkd1-mutated iPS cells. *PloS one.* 2012;7(2):e32018.
3. Kurkowiak M, Zietkiewicz E, Witt M. Recent advances in primary ciliary dyskinesia genetics. *Journal of medical genetics.* 2015;52(1):1-9.
4. Nachury MV, Loktev AV, Zhang Q, et al. A core complex of BBS proteins cooperates with the GTPase Rab8 to promote ciliary membrane biogenesis. *Cell.* 2007;129(6):1201-1213.
5. Sang L, Miller JJ, Corbit KC, et al. Mapping the NPHP-JBTS-MKS protein network reveals ciliopathy disease genes and pathways. *Cell.* 2011;145(4):513-528.
6. Baker K, Beales PL. Making sense of cilia in disease: the human ciliopathies. *American journal of medical genetics. Part C, Seminars in medical genetics.* 2009;151C(4):281-295.
7. Wolf MT. Nephronophthisis and related syndromes. *Current opinion in pediatrics.* 2015;27(2):201-211.
8. Madhivanan K, Aguilar RC. Ciliopathies: the trafficking connection. *Traffic.* 2014;15(10):1031-1056.
9. Hynes AM, Giles RH, Srivastava S, et al. Murine Joubert syndrome reveals Hedgehog signaling defects as a potential therapeutic target for nephronophthisis. *Proceedings of the National Academy of Sciences of the United States of America.* 2014;111(27):9893-9898.
10. Rachel RA, Yamamoto EA, Dewanjee M, et al. CEP290 alleles in mice disrupt tissue-specific cilia biogenesis and recapitulate features of syndromic ciliopathies. *Human molecular genetics.* 2015.
11. Halbritter J, Porath JD, Diaz KA, et al. Identification of 99 novel mutations in a worldwide cohort of 1,056 patients with a nephronophthisis-related ciliopathy. *Human genetics.* 2013;132(8):865-884.
12. Hoefele J, Wolf MT, O'Toole JF, et al. Evidence of oligogenic inheritance in nephronophthisis. *Journal of the American Society of Nephrology : JASN.* 2007;18(10):2789-2795.
13. Katsanis N, Ansley SJ, Badano JL, et al. Triallelic inheritance in Bardet-Biedl syndrome, a Mendelian recessive disorder. *Science.* 2001;293(5538):2256-2259.
14. Renkema KY, Stokman MF, Giles RH, Knoers NV. Next-generation sequencing for research and diagnostics in kidney disease. *Nature reviews. Nephrology.* 2014;10(8):433-444.
15. van Dam TJ, Wheway G, Slaats GG, Group SS, Huynen MA, Giles RH. The SYSCILIA gold standard (SCGSv1) of known ciliary components and its applications within a systems biology consortium. *Cilia.* 2013;2(1):7.
16. Nauli SM, Alenghat FJ, Luo Y, et al. Polycystins 1 and 2 mediate mechanosensation in the primary cilium of kidney cells. *Nature genetics.* 2003;33(2):129-137.
17. Lancaster MA, Louie CM, Silhavy JL, et al. Impaired Wnt-beta-catenin signaling disrupts adult renal homeostasis and leads to cystic kidney ciliopathy. *Nature medicine.* 2009;15(9):1046-1054.
18. Sugrue T, Lowndes NF, Ceredig R. Hypoxia enhances the radioresistance of mouse mesenchymal stromal cells. *Stem cells.* 2014;32(8):2188-2200.
19. Leiser SF, Fletcher M, Begun A, Kaeberlein M. Life-span extension from hypoxia in Caenorhabditis elegans requires both HIF-1 and DAF-16 and is antagonized by SKN-1. *The journals of gerontology. Series A, Biological sciences and medical sciences.* 2013;68(10):1135-1144.
20. Hoeijmakers JH. DNA damage, aging, and cancer. *The New England journal of medicine.* 2009;361(15):1475-1485.
21. Fischer E, Legue E, Doyen A, et al. Defective planar cell polarity in polycystic kidney disease. *Nature genetics.* 2006;38(1):21-23.
22. Simons M, Walz G. Polycystic kidney disease: cell division without a c(l)ue? *Kidney international.* 2006;70(5):854-864.
23. Hildebrandt F, Waldherr R, Kutt R, Brandis M. The nephronophthisis complex: clinical and genetic aspects. *The Clinical investigator.* 1992;70(9):802-808.
24. Attanasio M, Uhlenhaut NH, Sousa VH, et al. Loss of GLIS2 causes nephronophthisis in humans and mice by increased apoptosis and fibrosis. *Nature genetics.* 2007;39(8):1018-1024.
25. Chaki M, Airik R, Ghosh AK, et al. Exome capture reveals ZNF423 and CEP164 mutations, linking renal ciliopathies to DNA damage response signaling. *Cell.* 2012;150(3):533-548.
26. Choi HJ, Lin JR, Vannier JB, et al. NEK8 links the ATR-regulated replication stress response and S phase CDK activity to renal ciliopathies. *Molecular cell.* 2013;51(4):423-439.
27. Airik R, Slaats GG, Guo Z, et al. Renal-retinal ciliopathy gene Sdccag8 regulates DNA damage response signaling. *Journal of the American Society of Nephrology : JASN.* 2014;25(11):2573-2583.
28. Slaats GG, Ghosh AK, Falke LL, et al. Nephronophthisis-associated CEP164 regulates cell cycle progression, apoptosis and epithelial-to-mesenchymal transition. *PLoS genetics.* 2014;10(10):e1004594.
29. Slaats GG, Giles RH. Are renal ciliopathies (replication) stressed out? *Trends in cell biology.* 2015.

30. Coresh J, Astor BC, Greene T, Eknoyan G, Levey AS. Prevalence of chronic kidney disease and decreased kidney function in the adult US population: Third National Health and Nutrition Examination Survey. *American journal of kidney diseases : the official journal of the National Kidney Foundation.* 2003;41(1):1-12.
31. Yano R, Golbar HM, Izawa T, Sawamoto O, Kuwamura M, Yamate J. Participation of bone morphogenetic protein (BMP)-6 and osteopontin in cisplatin (CDDP)-induced rat renal fibrosis. *Experimental and toxicologic pathology : official journal of the Gesellschaft fur Toxikologische Pathologie.* 2015;67(2):99-107.
32. Yuasa T, Yano R, Izawa T, Kuwamura M, Yamate J. Calponin expression in renal tubulointerstitial fibrosis induced in rats by Cisplatin. *Journal of toxicologic pathology.* 2014;27(1):97-103.
33. Ermolaeva M, Schumacher B. The innate immune system as mediator of systemic DNA damage responses. *Communicative & integrative biology.* 2013;6(6):e26926.
34. Zhou W, Otto EA, Cluckey A, et al. FAN1 mutations cause karyomegalic interstitial nephritis, linking chronic kidney failure to defective DNA damage repair. *Nature genetics.* 2012;44(8):910-915.
35. Imig JD, Ryan MJ. Immune and inflammatory role in renal disease. *Comprehensive Physiology.* 2013;3(2):957-976.
36. Vega S, Morales AV, Ocana OH, Valdes F, Fabregat I, Nieto MA. Snail blocks the cell cycle and confers resistance to cell death. *Genes & development.* 2004;18(10):1131-1143.
37. Cano A, Perez-Moreno MA, Rodrigo I, et al. The transcription factor snail controls epithelial-mesenchymal transitions by repressing E-cadherin expression. *Nature cell biology.* 2000;2(2):76-83.
38. Nakagawa N, Duffield JS. Myofibroblasts in Fibrotic Kidneys. *Current pathobiology reports.* 2013;1(3).
39. Murga M, Bunting S, Montana MF, et al. A mouse model of ATR-Seckel shows embryonic replicative stress and accelerated aging. *Nature genetics.* 2009;41(8):891-898.
40. Ruzankina Y, Pinzon-Guzman C, Asare A, et al. Deletion of the developmentally essential gene ATR in adult mice leads to age-related phenotypes and stem cell loss. *Cell stem cell.* 2007;1(1):113-126.
41. Spoor M, Nagtegaal AP, Ridwan Y, et al. Accelerated loss of hearing and vision in the DNA-repair deficient Ercc1(delta/-) mouse. *Mechanisms of ageing and development.* 2012;133(2-3):59-67.
42. McWhir J, Selfridge J, Harrison DJ, Squires S, Melton DW. Mice with DNA repair gene (ERCC-1) deficiency have elevated levels of p53, liver nuclear abnormalities and die before weaning. *Nature genetics.* 1993;5(3):217-224.
43. de Waard MC, van der Pluijm I, Zuiderveen Borgesius N, et al. Age-related motor neuron degeneration in DNA repair-deficient Ercc1 mice. *Acta neuropathologica.* 2010;120(4):461-475.
44. Habbig S, Bartram MP, Sagmuller JG, et al. The ciliopathy disease protein NPHP9 promotes nuclear delivery and activation of the oncogenic transcriptional regulator TAZ. *Human molecular genetics.* 2012;21(26):5528-5538.
45. Happe H, van der Wal AM, Leonhard WN, et al. Altered Hippo signalling in polycystic kidney disease. *The Journal of pathology.* 2011;224(1):133-142.
46. Habbig S, Bartram MP, Muller RU, et al. NPHP4, a cilia-associated protein, negatively regulates the Hippo pathway. *The Journal of cell biology.* 2011;193(4):633-642.
47. Fujii M, Toyoda T, Nakanishi H, et al. TGF-beta synergizes with defects in the Hippo pathway to stimulate human malignant mesothelioma growth. *The Journal of experimental medicine.* 2012;209(3):479-494.
48. Bukanov NO, Smith LA, Klinger KW, Ledbetter SR, Ibraghimov-Beskrovnaya O. Long-lasting arrest of murine polycystic kidney disease with CDK inhibitor roscovitine. *Nature.* 2006;444(7121):949-952.
49. Bukanov NO, Moreno SE, Natoli TA, et al. CDK inhibitors R-roscovitine and S-CR8 effectively block renal and hepatic cystogenesis in an orthologous model of ADPKD. *Cell cycle.* 2012;11(21):4040-4046.
50. Steinman RA, Robinson AR, Feghali-Bostwick CA. Antifibrotic effects of roscovitine in normal and scleroderma fibroblasts. *PloS one.* 2012;7(11):e48560.
51. Benson C, White J, De Bono J, et al. A phase I trial of the selective oral cyclin-dependent kinase inhibitor seliciclib (CYC202; R-Roscovitine), administered twice daily for 7 days every 21 days. *British journal of cancer.* 2007;96(1):29-37.
52. Hsieh WS, Soo R, Peh BK, et al. Pharmacodynamic effects of seliciclib, an orally administered cell cycle modulator, in undifferentiated nasopharyngeal cancer. *Clinical cancer research : an official journal of the American Association for Cancer Research.* 2009;15(4):1435-1442.
53. Le Tourneau C, Faivre S, Laurence V, et al. Phase I evaluation of seliciclib (R-roscovitine), a novel oral cyclin-dependent kinase inhibitor, in patients with advanced malignancies. *European journal of cancer.* 2010;46(18):3243-3250.
54. Wang J, Mongayt D, Torchilin VP. Polymeric micelles for delivery of poorly soluble drugs: preparation and anticancer activity in vitro of paclitaxel incorporated into mixed micelles based on poly(ethylene glycol)-lipid conjugate and positively charged lipids. *Journal of drug targeting.* 2005;13(1):73-80.
55. Li C, Yu DF, Newman RA, et al. Complete regression of well-established tumors using a novel water-soluble poly(L-glutamic acid)-paclitaxel conjugate. *Cancer research.* 1998;58(11):2404-2409.

56. Gradishar WJ. Albumin-bound paclitaxel: a next-generation taxane. *Expert opinion on pharmacotherapy.* 2006;7(8):1041-1053.
57. Seow WY, Xue JM, Yang YY. Targeted and intracellular delivery of paclitaxel using multi-functional polymeric micelles. *Biomaterials.* 2007;28(9):1730-1740.
58. Wu J, Liu Q, Lee RJ. A folate receptor-targeted liposomal formulation for paclitaxel. *International journal of pharmaceutics.* 2006;316(1-2):148-153.
59. Nakamura J, Nakajima N, Matsumura K, Hyon SH. Water-soluble taxol conjugates with dextran and targets tumor cells by folic acid immobilization. *Anticancer research.* 2010;30(3):903-909.
60. Beck H, Nahse V, Larsen MS, et al. Regulators of cyclin-dependent kinases are crucial for maintaining genome integrity in S phase. *The Journal of cell biology.* 2010;188(5):629-638.
61. Beck H, Nahse-Kumpf V, Larsen MS, et al. Cyclin-dependent kinase suppression by WEE1 kinase protects the genome through control of replication initiation and nucleotide consumption. *Molecular and cellular biology.* 2012;32(20):4226-4236.
62. Kotov IN, Siebring-van Olst E, Knobel PA, et al. Whole genome RNAi screens reveal a critical role of REV3 in coping with replication stress. *Molecular oncology.* 2014;8(8):1747-1759.
63. Lopez-Contreras AJ, Gutierrez-Martinez P, Specks J, Rodrigo-Perez S, Fernandez-Capetillo O. An extra allele of Chk1 limits oncogene-induced replicative stress and promotes transformation. *The Journal of experimental medicine.* 2012;209(3):455-461.
64. Paulsen RD, Soni DV, Wollman R, et al. A genome-wide siRNA screen reveals diverse cellular processes and pathways that mediate genome stability. *Molecular cell.* 2009;35(2):228-239.
65. Nigg EA, Stearns T. The centrosome cycle: Centriole biogenesis, duplication and inherent asymmetries. *Nature cell biology.* 2011;13(10):1154-1160.
66. Battini L, Macip S, Fedorova E, et al. Loss of polycystin-1 causes centrosome amplification and genomic instability. *Human molecular genetics.* 2008;17(18):2819-2833.
67. Mikule K, Delaval B, Kaldis P, Jurcyzk A, Hergert P, Doxsey S. Loss of centrosome integrity induces p38-p53-p21-dependent G1-S arrest. *Nature cell biology.* 2007;9(2):160-170.
68. Zhao H, Chen X, Gurian-West M, Roberts JM. Loss of cyclin-dependent kinase 2 (CDK2) inhibitory phosphorylation in a CDK2AF knock-in mouse causes misregulation of DNA replication and centrosome duplication. *Molecular and cellular biology.* 2012;32(8):1421-1432.
69. Hemerly AS, Prasanth SG, Siddiqui K, Stillman B. Orc1 controls centriole and centrosome copy number in human cells. *Science.* 2009;323(5915):789-793.
70. Hossain M, Stillman B. Meier-Gorlin syndrome mutations disrupt an Orc1 CDK inhibitory domain and cause centrosome reduplication. *Genes & development.* 2012;26(16):1797-1810.
71. Martin CA, Ahmad I, Klingseisen A, et al. Mutations in PLK4, encoding a master regulator of centriole biogenesis, cause microcephaly, growth failure and retinopathy. *Nature genetics.* 2014;46(12):1283-1292.
72. Dishinger JF, Kee HL, Jenkins PM, et al. Ciliary entry of the kinesin-2 motor KIF17 is regulated by importin-beta2 and RanGTP. *Nature cell biology.* 2010;12(7):703-710.
73. Tollenaere MA, Mailand N, Bekker-Jensen S. Centriolar satellites: key mediators of centrosome functions. *Cellular and molecular life sciences : CMLS.* 2015;72(1):11-23.
74. Kim J, Krishnaswami SR, Gleeson JG. CEP290 interacts with the centriolar satellite component PCM-1 and is required for Rab8 localization to the primary cilium. *Human molecular genetics.* 2008;17(23):3796-3805.
75. Barbelanne M, Hossain D, Chan DP, Peranen J, Tsang WY. Nephrocystin proteins NPHP5 and Cep290 regulate BBSome integrity, ciliary trafficking and cargo delivery. *Human molecular genetics.* 2015;24(8):2185-2200.
76. Prosser SL, Straatman KR, Fry AM. Molecular dissection of the centrosome overduplication pathway in S-phase-arrested cells. *Molecular and cellular biology.* 2009;29(7):1760-1773.
77. Loffler H, Fechter A, Liu FY, Poppelreuther S, Kramer A. DNA damage-induced centrosome amplification occurs via excessive formation of centriolar satellites. *Oncogene.* 2013;32(24):2963-2972.
78. Pihan GA, Wallace J, Zhou Y, Doxsey SJ. Centrosome abnormalities and chromosome instability occur together in pre-invasive carcinomas. *Cancer research.* 2003;63(6):1398-1404.
79. Hoeijmakers JH. Genome maintenance mechanisms for preventing cancer. *Nature.* 2001;411(6835):366-374.
80. Harper JW, Elledge SJ. The DNA damage response: ten years after. *Molecular cell.* 2007;28(5):739-745.
81. Beales PL, Reid HA, Griffiths MH, Maher ER, Flinter FA, Woolf AS. Renal cancer and malformations in relatives of patients with Bardet-Biedl syndrome. *Nephrology, dialysis, transplantation : official publication of the European Dialysis and Transplant Association - European Renal Association.* 2000;15(12):1977-1985.

82. Lopes M, Foiani M, Sogo JM. Multiple mechanisms control chromosome integrity after replication fork uncoupling and restart at irreparable UV lesions. *Molecular cell*. 2006;21(1):15-27.
83. Andressoo JO, Hoeijmakers JH, Mitchell JR. Nucleotide excision repair disorders and the balance between cancer and aging. *Cell cycle*. 2006;5(24):2886-2888.
84. Andressoo JO, Mitchell JR, de Wit J, et al. An Xpd mouse model for the combined xeroderma pigmentosum/Cockayne syndrome exhibiting both cancer predisposition and segmental progeria. *Cancer cell*. 2006;10(2):121-132.
85. Reinhardt HC, Schumacher B. The p53 network: cellular and systemic DNA damage responses in aging and cancer. *Trends in genetics : TIG*. 2012;28(3):128-136.
86. Lans H, Hoeijmakers JH. Genome stability, progressive kidney failure and aging. *Nature genetics*. 2012;44(8):836-838.

APPENDICES

Nederlandse samenvatting
Curriculum vitae
List of publications
Acknowledgements / Dankwoord

NEDERLANDSE SAMENVATTING

ook voor niet-ingewijden

We hebben er (bijna) allemaal twee: nieren. Goed functioneren van onze nieren is van levensbelang. Er zijn verschillende oorzaken die kunnen leiden tot nierschade, met als gevolg nierfalen. Dit proefschrift beschrijft het onderzoek naar vrij zeldzame genetische mutaties die moleculaire en celbiologische mechanismen verstoren, en daarmee nierfalen veroorzaken. De eerste symptomen van deze aangeboren aandoeningen worden zichtbaar bij een kind en soms al voor de geboorte: het nierweefsel is fibrotisch, en er kunnen cysten aanwezig zijn. Omdat de ontwikkeling van fibrose en cysten niet reversibel is, is er uiteindelijk een donornier nodig voor deze (jonge) patiënten. Fibrose en cysten ontstaan door een mutatie in de genen die verantwoordelijk zijn voor het goed functioneren van het cilium. Het cilium is een organel dat op bijna alle cellen van ons lichaam voorkomt en doet denken aan een trilhaar of antenne. In de nieren zijn er gespecialiseerde cilia die cruciaal zijn voor het goed functioneren van de nieren. Ze registreren vloeistofstromen en reguleren signalering in de cellen. Aandoeningen die geassocieerd zijn met verstoringen van de cilia zijn de zogenoemde ciliopathieën. Deze aandoeningen kennen verschillende verschijningsvormen, van zeer mild tot niet levensvatbaar. Naast de nieren kunnen ook hersenen, ogen, oren, lever en soms ook botten zijn aangetast. Het feit dat er vaak meerdere organen zijn verstoord bij ciliopathieën, onderstreept het belang van cilia in het menselijk lichaam. Dit proefschrift beschrijft het onderzoek naar nefronoftise en het hieraan verwante Joubert syndroom: twee ciliopathieën waarbij fibrose en cysten in de nier ontwikkelen. Indien we meer inzicht hebben in de moleculaire mechanismen van ciliopathieën, kan onderzoek gedaan worden naar mogelijke therapieën voor patiënten.
Een gedetailleerde introductie over cilia, ciliopathieën en signalering die betrokken is bij ciliumfunctie is beschreven in **Hoofdstuk 1**. Om onderzoek te kunnen verrichten naar celdefecten van ciliopathiepatiënten wordt in **Hoofdstuk 2** beschreven hoe op niet-invasieve wijze cellen met cilia kunnen worden geïsoleerd uit urine of melktanden. Deze gecilieerde cellen zijn onder andere zeer bruikbaar voor het onderzoek van patiëntspecifieke mutaties en voor het testen van medicijnen. Omdat er vaak sprake is van jonge patiënten, is het gunstig wanneer materiaal voor onderzoek zonder al te veel ongemak kan worden verkregen. Daarom bieden deze niet-invasieve methoden uitkomst. Er worden vandaag de dag steeds nieuwe genen geassocieerd met cilia en ciliopathieën. Alle 19059 genen van het muisgenoom zijn getest in gecilieerde muizen-niercellen door SYSCILIA consortium onderzoekers, waardoor nieuwe genen zijn opgespoord die essentieel zijn voor ciliumformatie op niercellen. In **Hoofdstuk 3** zijn genen die coderen voor vier ionkanalen (belangrijk voor de zoutbalans in het lichaam) en hun nieuw geïdentificeerde rol in cilia beschreven. Doordat deze kalium- of chloridekanalen niercilia reguleren, kan verstoring van de ionkanalen mogelijk leiden tot symptomen die karakteristiek zijn voor ciliopathieën.

Verder is er in **Hoofdstuk 4** van dit proefschrift onderzoek gedaan naar het *MKS1*-gen. Mutaties in dit gen zijn recentelijk geassocieerd met Joubert syndroom en veroorzaken defecten in cilia. In cellen gegroeid uit huidbiopten van Joubert-patiënten met *MKS1* mutaties is het aantal cilia niet altijd lager, maar de lengte van cilia varieert. Dit komt door verstoring van eiwitten die het cilium in- en uitgaan. Een sleuteleiwit in deze verstoring is INPP5E, dat belangrijk is voor celsignalering.

Het tweede gedeelte van dit proefschrift richt zich op recente onderzoeken die hebben aangetoond dat verschillende van de negentien nefronoftise-genen en de door hen gecodeerde eiwitten niet alleen een rol spelen bij ciliumformatie en signalering, maar ook in de celkern voorkomen, waar het DNA zich bevindt. De functie van deze eiwitten in de celkern is nader onderzocht. In de celkern zorgt verlies van deze eiwitten voor verhoogde signalering van DNA-schade, die is veroorzaakt door stress tijdens DNA-replicatie. In **Hoofdstuk 5** wordt een muismodel, dat een homozygote nefronoftise type 10 gen (*SDCCAG8*) mutatie heeft, beschreven. In de fibrotische en cysteuze nieren van deze muis wordt verhoogde DNA-schade signalering gevonden. Het onderliggende mechanisme van deze verhoogde DNA-schade respons wordt in **Hoofdstuk 6** verder onderzocht. Mutaties in het nefronoftise type 6/Joubert syndroom type 5 gen (*CEP290*), veroorzaken stress tijdens DNA-replicatie wat resulteert in DNA-schade. De stress tijdens DNA-replicatie wordt veroorzaakt door verhoogde activiteit van enzymen (CDK1 en CDK2), wat er voor zorgt dat de replicatie op (te) veel plaatsen op het DNA wordt geïnitieerd. Schade aan het DNA hoopt op doordat de replicatie-complexen instabiel worden. Dit heeft tot gevolg dat de celdeling niet plaats kan vinden, omdat DNA eerst gerepareerd moet worden. Indien reparatie niet mogelijk is, wordt dit catastrofaal voor de cel. Echter, door farmacologische interventie met CDK-remmers kunnen we de enzymactiviteit remmen en zo DNA-schade voorkomen. Een ander DNA-schade geassocieerd eiwit, nefronoftise type 15 (*CEP164*), is in **Hoofdstuk 7** nader onderzocht. Verlies van dit eiwit leidt niet alleen tot een verstoorde celcyclus (waaronder vertraagde DNA-replicatie fase), maar ook tot celdood, en transformatie van cellen van epitheel naar mesenchym. Mesenchymale cellen zijn belangrijk in het fibrotisch worden van gezond weefsel. In zebravissen zonder het *cep164* gen vonden we verhoogde DNA-schade signalering, meer celdood en activatie van fibrosegenen.

De stress tijdens DNA-replicatie verstoort de voortgang van de celdeling dusdanig, dat cellen in een fase verblijven waar tijdelijk geen cilium aanwezig is. In **Hoofdstuk 9** wordt deze afwezigheid van cilia nader verklaart: enerzijds zijn de gemuteerde genen direct betrokken bij ciliaformatie en ciliasignalering, en anderzijds worden de cellen geblokkeerd in de celcyclus fase zonder cilium door aanwezigheid van DNA-replicatie stress. Op deze manier zijn er twee aanleidingen voor de cellen om geen cilium te kunnen vormen en fibrose en cysten te ontwikkelen in het weefsel. De cysten in nefronoftise zijn minder prominent aanwezig dan in polycysteuze nierziekte. Daarentegen lijkt fibrose de hoofdoorzaak van nierfalen in nefronoftise en Joubert syndroom.

In **Hoofdstuk 8** wordt bediscussieerd hoe we behandeling van nefronoftise patiënten het best kunnen aanpakken naar aanleiding van de nieuwe inzichten verworven tijdens dit promotieonderzoek in combinatie met bestaande literatuur. De laatste jaren is de focus van behandeling op cysten geweest. Componenten van huidige chemotherapeutica komen in het vizier, aangezien deze ingrijpen op de celdeling en mogelijk de cilia op cellen fixeren. Deze farmacologische interventie heeft als doel het verlies van nierfunctie door fibrose te vertragen, zodat dialyse uitgesteld kan worden en er meer tijd is om op een donornier te wachten.
Er is een verscheidenheid aan moleculaire en celbiologische mechanismen betrokken bij de ontwikkeling van nefronoftise en het hieraan verwante Joubert syndroom. Het beperkt zich niet tot de ciliumbiologie en signalering, maar ook processen in de celkern en de celcyclus zijn verstoord. In **Hoofdstuk 10** wordt de significantie van dit werk bediscussieerd, en wordt ingegaan op potentieel toekomstig onderzoek.

CURRICULUM VITAE

Gisela Gijsbertje Gerretje Slaats was born on July 4th, 1985 in Geldrop. Gisela followed her athenaeum with the profile "Science and Health" at the Strabrecht College in Geldrop, where she graduated in 2003. She continued her study path with the Bachelor Molecular Life Sciences with a minor in Business Management and Marketing at Wageningen University and Research Center. She continued with her Masters in Molecular Life Sciences with a specialization in Biomedical Research at Wageningen University and Research Center. As part of her Masters program she had three research internships, of which the first one at the Department of Nutrition and Pharmacology at the Wageningen University and Research Center under the supervision of Dr. Jocelijn Meijerink and Prof. dr. Renger Witkamp on anti-inflammatory effects of cannabinoids. During her second internship she went to the Erasmus Medical Center in Rotterdam, where she conducted research at the Department of Genetics about the role of microRNAs in the DNA damage response under the supervision of Dr. Joris Pothof. For her final internship she moved to Stockholm for seven months, where she was an intern at the Department of Medicine at the Karolinska Institutet, under the supervision of Dr. Maaike Joerink. During this internship, she studied the intrauterine environment and the impact on developing allergies later in life. In 2011 Gisela began her PhD research under the supervision of Dr. Rachel Giles, Prof. dr. Marianne Verhaar and Prof. dr. Nine Knoers at the Department of Nephrology and Hypertension at the University Medical Center Utrecht, which resulted in this thesis. During her PhD she visited the lab of Prof. dr. Karlene Cimprich at Stanford University School of Medicine for 3 months to learn several techniques. Starting September 2015, Gisela works as a Postdoc at the CECAD Research Center in Cologne at the Department of Nephrology led by Prof. dr. Bernhard Schermer and Prof. dr. Thomas Benzing.

LIST OF PUBLICATIONS

DNA replication stress underlies renal phenotypes in *CEP290*-associated Joubert syndrome. (2015) **Slaats GG**, Saldivar JC, Bacal J, Zeman MK, Kile AC, Hynes AM, Srivastava S, Nazmutdinova J, Den Ouden K, Zagers MS, Foletto V, Verhaar MC, Miles C, Sayer JA, Cimprich KA, Giles RH. *J Clin Invest., in press*

Nephronophthisis: should we target cysts or fibrosis? (2015) **Slaats GG**, Lilien MR, Giles RH. *Pediatr Nephrol., in press*

An siRNA-based functional genomics screen for the identification of regulators of ciliogenesis and ciliopathy genes. (2015) Wheway G*, Schmidts M*, Mans DA*, Szymanska K*, Nguyen TM*, Racher H, Phelps IG, Toedt G, Kennedy J, Wunderlich KA, Sorusch N, Abdelhamed ZA, Natarajan S, Herridge W, van Reeuwijk J, Horn N, Boldt K, Parry DA, Letteboer SJF, Roosing S, Adams M, Bell SM, Bond J, Higgins J, Morrison EE, Tomlinson DC, **Slaats GG**, van Dam TJ, Huang L, Kessler K, Giessl A, Logan CV, Boyle EA, Shendure J, Anazi S, Aldahmesh M, Al Hazzaa S, Hegele RA, Ober C, Frosk P, Mhanni AA, Chodirker BN, Chudley AE, Lamont R, Bernier FP, Beaulieu CL, Gordon P, Pon RT, Donahue C, Barkovich AJ, Wolf L, Toomes C, Thiel CT, Boycott KM, McKibbin M, Inglehearn CF, UK10K Consortium, University of Washington Center for Mendelian Genomics, Stewart F, Omran H, Huynen MA, Sergouniotis PI, Alkuraya FS, Parboosingh JS, Innes AM, Willoughby CE, Giles RH, Webster AR, Ueffing M, Blacque O, Gleeson JG, Wolfrum U, Beales PL, Gibson T, Doherty D, Mitchison HM, Roepman R, Johnson CA. *Nat Cell Biol.* 17(8):1074-87.

DL-propargylglycine reduces blood pressure and renal injury but increases kidney weight in angiotensin-II infused rats. (2015) Oosterhuis NR*, Frenay AS*, Wesseling S, Snijder PM, **Slaats GG**, Yazdani S, Fernandez BO, Feelisch M, Giles RH, Verhaar MC, Joles JA*, van Goor H*. *Nitric Oxide.* 49:56-66.

Non-invasive sources of cells with primary cilia from pediatric and adult patients. (2015) Ajzenberg H*, **Slaats GG***, Stokman MF, Arts HH, Logister I, Kroes HY, Renkema KY, van Haelst MM, Terhal PA, Van Rooij IA, Keijzer-Veen MG, Knoers NV, Lilien MR, Jewett MA, and Giles RH. *Cilia.* 4:8.

Are renal ciliopathies (replication) stressed out? (2015) **Slaats GG**, Giles RH. *Trends Cell Biol.* 25(6):317-319.

Nephronophthisis-associated *CEP164* regulates cell cycle progression, apoptosis and epithelial-to-mesenchymal transition. (2014) **Slaats GG**, Ghosh AK*, Falke LL*, Le Corre S, Shaltiel IA, van de Hoek G, Klasson TD, Stokman MF, Logister I, Verhaar MC, Goldschmed-

ing R, Nguyen TQ, Drummond IA, Hildebrandt F, Giles RH. *PLoS Genet.* 10(10):e1004594.

Murine Joubert syndrome reveals Hedgehog signaling defects as a potential therapeutic target for nephronophthisis. (2014) Hynes AM, Giles RH, Srivastava S, Eley L, Whitehead J, Danilenko M, Raman S, **Slaats GG**, Colville JG, Ajzenberg H, Kroes HY, Thelwall PE, Simmons NL, Miles CG, Sayer JA. *Proc Natl Acad Sci U S A.* 111(27):9893-8.

Renal-retinal ciliopathy gene *Sdccag8* regulates DNA damage response signaling. (2014) Airik R, **Slaats GG**, Guo Z, Weiss AC, Khan N, Ghosh A, Hurd TW, Bekker-Jensen S, Schrøder JM, Elledge SJ, Andersen JS, Kispert A, Castelli M, Boletta A, Giles RH, Hildebrandt F. *J Am Soc Nephrol.* 25(11):2573-83.

NEK8 links the ATR-regulated replication stress response and S phase CDK activity to renal ciliopathies. (2013) Choi HJ, Lin JR, Vannier JB, **Slaats GG**, Kile AC, Paulsen RD, Manning DK, Beier DR, Giles RH, Boulton SJ, Cimprich KA. *Mol Cell.* 51(4):423-39.

The SYSCILIA gold standard (SCGSv1) of known ciliary components and its applications within a systems biology consortium. (2013) van Dam TJ, Wheway G, **Slaats GG**; SYSCILIA Study Group, Huynen MA, Giles RH. *Cilia.* 2(1):7.

Reduced cilia frequencies in human renal cell carcinomas versus neighboring parenchymal tissue. (2013) Basten SG, Willekers S, Vermaat JS, **Slaats GG**, Voest EE, van Diest PJ, Giles RH. *Cilia.* 2(1):2.

Exome capture reveals *ZNF423* and *CEP164* mutations, linking renal ciliopathies to DNA damage response signaling. (2012) Chaki M*, Airik R*, Ghosh AK, Giles RH, Chen R, **Slaats GG**, Wang H, Hurd TW, Zhou W, Cluckey A, Gee HY, Ramaswami G, Hong CJ, Hamilton BA, Cervenka I, Ganji RS, Bryja V, Arts HH, van Reeuwijk J, Oud MM, Letteboer SJ, Roepman R, Husson H, Ibraghimov-Beskrovnaya O, Yasunaga T, Walz G, Eley L, Sayer JA, Schermer B, Liebau MC, Benzing T, Le Corre S, Drummond I, Janssen S, Allen SJ, Natarajan S, O'Toole JF, Attanasio M, Saunier S, Antignac C, Koenekoop RK, Ren H, Lopez I, Nayir A, Stoetzel C, Dollfus H, Massoudi R, Gleeson JG, Andreoli SP, Doherty DG, Lindstrad A, Golzio C, Katsanis N, Pape L, Abboud EB, Al-Rajhi AA, Lewis RA, Omran H, Lee EY, Wang S, Sekiguchi JM, Saunders R, Johnson CA, Garner E, Vanselow K, Andersen JS, Shlomai J, Nurnberg G, Nurnberg P, Levy S, Smogorzewska A, Otto EA, Hildebrandt F. *Cell.* 150(3):533-48.

FAN1 mutations cause karyomegalic interstitial nephritis, linking chronic kidney failure to defective DNA damage repair. (2012) Zhou W*, Otto EA*, Cluckey A, Airik R, Hurd TW, Chaki M, Diaz K, Lach FP, Bennett GR, Gee HY, Ghosh AK, Natarajan S, Thongthip S,

Veturi U, Allen SJ, Janssen S, Ramaswami G, Dixon J, Burkhalter F, Spoendlin M, Moch H, Mihatsch MJ, Verine J, Reade R, Soliman H, Godin M, Kiss D, Monga G, Mazzucco G, Amann K, Artunc F, Newland RC, Wiech T, Zschiedrich S, Huber TB, Friedl A, **Slaats GG**, Joles JA, Goldschmeding R, Washburn J, Giles RH, Levy S, Smogorzewska A, Hildebrandt F. *Nat Genet.* 44(8):910-5.

DNA methylation levels within the *CD14* promoter region are lower in placentas of mothers living on a farm. (2012) **Slaats GG**, Reinius LE, Alm J, Kere J, Scheynius A, Joerink M. *Allergy.* 67(7):895-903.

TMEM107 recruits ciliopathy proteins to anchored ring-like subdomains of the ciliary transition zone membrane and is mutated in ciliary disease. Lambacher NJ*, Bruel A*, van Dam TJP*, **Slaats GG**, Szymańska K, McManus GJ, Kennedy JE, Gaff K, van der Lee R, Burglen L, Doummar D, Rivière J, Faivre L, Attié-Bitach T, Saunier S, Johnson CA, Giles RH, Huynen MA, Thauvin-Robinet C, Blacque OE. *submitted*

De Novo 14q24.2q24.3 Microdeletion Including *IFT43* is Associated with Intellectual Disability, Skeletal Anomalies, Cardiac Anomalies and Myopia. Stokman MF, Oud MM, van Binsbergen E, Nicolaou N, **Slaats GG**, Renkema KY, Nijman IJ, Roepman R, Giles RH, Arts HH, Knoers NVAM, van Haelst MM. *submitted*

Environmental influences on endothelial to mesenchymal transition in developing implanted cardiovascular tissue-engineered grafts. Muylaert DEP, de Jong OG, **Slaats GG**, Nieuweboer FE, Fledderus JO, Goumans M, Hierck BP, Verhaar MC. *submitted*

MKS1 Regulates Ciliary INPP5E Levels in Joubert Syndrome. **Slaats GG***, Isabella CR*, Kroes HY*, Dempsey JC, Gremmels H, Monroe GR, Duran KJ, Adkins J, Kumar SA, Knutzen DM, Knoers NV, Mendelsohn NJ, Neubauer D, Mastroyianni SD, Vogt J, Worgan L, Karp N, Bowdin S, Glass IA, Parisi MA, Otto EA, Johnson CA, Hildebrandt F, van Haaften G, Giles RH*, Doherty D*. *submitted*

Screen-based identification and validation of four novel ion channels as regulators of renal ciliogenesis. **Slaats GG***, Wheway G*, Foletto V, Szymanska K, van Balkom BW, Logister I, den Ouden K, Keijzer-Veen MG, Lilien MR, Johnson CA, Giles RH. *submitted*

* These authors contributed equally

ACKNOWLEDGEMENTS / DANKWOORD

Thank you all!!! Ik ben alle mensen om me heen tijdens mijn PhD traject enorm dankbaar! Het tot stand laten komen van een proefschrift, dat bereik je niet alleen.

Vanaf ons eerste contact voelde het al goed met jou, **Rachel**. Ik ben ontzettend blij met jou als copromotor. Je bent een lief mens, en een fantastische wetenschapper. Bedankt voor de vele kopjes thee, inspiratie, de duwtjes in de rug, en de eindeloze support. Je hebt me geholpen om er zoveel mogelijk uit te halen. Ik heb veel van je geleerd en ik heb heel veel waardering voor hoe we samen hebben gewerkt. Je zult altijd een voorbeeld voor me zijn.

Prof. dr. M.C. Verhaar, beste **Marianne**, we spraken elkaar eigenlijk maar enkele keren per jaar, maar dat heb ik altijd als zeer waardevol en als fijne coaching ervaren. Kort en krachtig! Bedankt dat je me altijd hebt geholpen en gesteund waar nodig.

Prof. dr. V.V.A.M Knoers, beste **Nine**, door de loop van de jaren heen ben je steeds meer betrokken geraakt bij mijn promotieonderzoek. Bedankt voor al je advies en academische input waar mogelijk, en bedankt dat je me altijd hebt geholpen en gesteund.

Prof. dr. K.A. Cimprich, dear **Karlene**, thank you very much for our collaboration and for inviting me at your lab in Stanford. It has been a great three months, and I learned a lot! Especially, I want to thank **Joshua** for supervising me at the lab, and I really enjoyed the day trips and coffee trips we made, together with **Julien**, **Stephan** and **Michelle B**: it was great fun! **Caroline**, thanks for your help and company to make me feel at home, and good luck with finishing your PhD! Of course thanks to **Claudia**, **Drew**, **Michelle Z**, **Julie** and **Bobby** as well! You all contributed to an important personal and academic experience!

Beste **Puck**, ik vond het fijn dat jij vanaf het begin betrokken bent geweest bij mijn promotietraject. Ik mocht alles aan je vragen. Bedankt voor je adviezen en supervisie.

The "**Syscilia**" consortium; inspiring researchers who all love cilia. The meetings were intensive, but fantastic! I felt lucky being part of this wonderful consortium! A special thanks to my roommates **Minh** and **Nasrin**. And **Simone**, thanks for everything!

Thanks to all collaborators in **Newcastle, Leeds, Nijmegen, Dublin, Boston, Seattle** and the rest of the world! I hope we keep up the collaborations in the future!

Daphne, bedankt voor je hulp met allerlei regeldingetjes! Fijn dat je altijd klaar stond!

Bedankt aan alle kinderen en collega's voor het doneren van jullie plasjes en/of tandjes. Jullie hebben me heel erg geholpen! **Hester**, **Mandy**, en **Marc** ontzettend bedankt voor jullie samenwerkingen die het voor mij mogelijk hebben gemaakt om met patiëntenmateriaal te werken, en ook bedankt voor jullie klinische input op verschillende onderzoeksprojecten.

Jaap, bedankt voor je vele/leuke kritische vragen tijdens presentaties en de gezelligheid bij congressen en borrels. En **Caroline**, bedankt dat je me nooit heb weggestuurd als ik weer druk in overleg was met Rachel op jullie kamer. De Postdocs **Joost**, **Petra dG** en **Kirsten**, bedankt voor jullie hulp, en leuke gesprekken over wetenschap en van alles en nog wat. En **Bas** (ik weet inmiddels dat de aanwezigheid van alleen jouw naam volstaat).

Het begon eigenlijk allemaal in het verre Oosten. Enkele wijzen waren daar al gehuisvestigd, en ik paste er gelukkig nog bij. **Nynke, Dimitri**, en **Olivier**, ik vond het ontzettend leuk om zo gelijk met elkaar op te gaan tijdens het hele PhD traject en zo van elkaar te leren, elkaar te helpen, lol te hebben, te veel details te delen, elkaar te leren kennen en te veel borrels en bitterballen te consumeren. Daar was **Hendrik** dan gelukkig ook altijd bij aanwezig, en hij zorgde ook voor de nodige (alcoholische) input. Over een tijdje zijn we allemaal echt geen studenten meer... Heel veel succes met de laatste loodjes en ik wens jullie al het beste voor de toekomst! En tja, **Nynke**, ik had ook nooit kunnen voorspellen na het ontbijt in Wageningen dat je nu mijn paranimf bent! Superleuk! Fijn dat we altijd kamergenootjes zijn gebleven door de jaren heen; bedankt dat je er altijd voor me was.

Lieve **Ive** en **P de Bree**, enorm bedankt voor al jullie hulp en alle gezelligheid! Jullie hadden het allebei altijd wel door als ik even een break nodig had! Jaaa fotogenieke **Frans**, altijd gezellig met jou op Q, succes met je gave onderzoek! **Sander**, we hebben twee jaar fijn samengewerkt, en je hebt me een handige erfenis nagelaten toen je het lab verliet; bekendheid bij bijna al je collega's in het Stratenum die me uiteindelijk vaak genoeg hebben geholpen! Bedankt **Livio, Martijn, Rutger, Marten** en anderen! **Krista**, **Frits**, **Adele** en **Diënty** jullie ook heel erg bedankt voor jullie hulp op het lab. Dear **Marijn**, **Nayia**, **Tim**, **Glenn**, **Glen**, **Merle**, **Laura**, **Femke**, **Diana**, **Maarten W**, **Saskia, Rosa, Margreet**, **Priscilla**, **Christian**, **Maarten B** and **Katia** good luck with finishing your PhD thesis! I really enjoyed working with you all! En uiteraard ook bedankt oud-collega's **Arianne**, **Eva**, **Ira** en **Martin**. Ook niet te vergeten, mijn kortstondige collega's **Ka Man**, **Jeroen** en **Zhiyong**, ik vond het erg leuk om een tijdje met jullie te kunnen werken. Ook de andere collega's van de afdeling Nefrologie en de afdeling Medische Genetica bedankt voor jullie samenwerking.

Ook gaat mijn dank uit naar alle collega's van het experimentele Cardio lab. In het bijzonder naar **Arjan** en **Alain**. Het was altijd gezellig met jullie vroeg in de ochtend en bedankt voor jullie hulp en adviezen.

Beste **Lucas**, aan de bar in Doorwerth liggen de roots van onze samenwerking met als resultaat Hoofdstuk 7. Ik wil je enorm bedanken voor deze inspirerende samenwerking waarin we een mooie mix hebben kunnen maken van onze kennis. Prof. dr. R. Goldschmeding, beste **Roel**, en beste **Tri**, ook jullie bedankt voor de samenwerking en acedemische input. Ook bedankt voor de leuke avond in Atlanta!

Ik heb het niet zelf in het leven geroepen, maar Slaats Academy is toch wel een begrip geworden op het lab. Met liefde en plezier ben ik betrokken geweest bij de stages van onder andere **Sven**, **Ludo**, **Khatera**, en **Rachel**. And our Canadian student **Henry**, thanks a lot for the work with the urine cells, this was fun! This all prepared me well for supervising **Miriam**, **Sebastiaan**, and **Veronica.** We spent quite some time together at the lab, which I really enjoyed! Thank you again for the hard work, and the fun we had together! I think we learned from each other and I wish you all the best for the future!

Lieve vrienden en vriendinnen, bedank voor jullie steun, betrokkenheid en gezelligheid! Tijdens bakkies koffie, wijntjes, zumba: waar of in wat voor vorm dan ook! In het bijzonder mijn lieve jaarclubgenootjes **Yvonne**, **Suzan**, **Inge**, **Martine** en **Joke**; we hebben het afgelopen jaar ons 10-jarig jubileum gevierd... ik kijk uit naar de vele gezellige avondjes die nog gaan volgen met de nodige wijntjes en/of likeurtjes. Het is altijd een feest om met jullie te zijn. Een weekendje Keulen ligt in het verschiet!

Tot mijn spijt mogen niet al mijn grootouders deze bijzondere gebeurtenis meemaken, al had ik daar wel op gehoopt. Desalniettemin wil ik de **families Zwart, Slaats** en **Goud** allemaal bedanken voor de interesse die jullie hebben getoond in mijn onderzoek, maar ook dat jullie voor de nodige ontspanning zorgden tijdens feestjes en dergelijke.

Lieve **Thom** en **Joan**, jullie zijn altijd in mijn gedachten en ik ben trots op jullie! Ik hoop dat er voor jullie een mooie toekomst in het verschiet ligt! Ik vind het bijzonder dat jullie me allebei hebben kunnen helpen met de voorbereidingen op mijn promotie, heel erg bedankt dat jullie dit wilden doen!

Lieve **pap** en **mam**, bedankt voor jullie steun en zorg, en voor alles wat jullie me hebben geleerd en meegegeven. Ik bedoel hier niet alleen hard werken, want vooral de afgelopen jaren is gebleken hoe belangrijk doorzettingsvermogen, geduld en liefde zijn. Ik denk niet dat ik meer hoef te zeggen...

Lieve **Joost**, enorm bedankt voor de steun en de vrijheid die je me altijd geeft om mijn studie en werk te kunnen doen. We werken allebei hard aan de toekomst! Ik kijk er naar uit dat onze "villa" af is, zodat we daar samen kunnen gaan genieten en we samen nog vele avonturen mogen beleven. I love you!